RATE EFFECTS IN BULK FORMING

RATE EFFECTS IN BULK FORMING

by

JAMES ALLAM FORSTER, B.Sc., M.Eng.

A Thesis

Submitted to the School of Graduate Studies

in Partial Fulfilment of the Requirements

for the Degree

Doctor of Philosophy

McMaster University

December 1978

To all those "other people",

too numerous to name, without

whom a thesis would never

reach this stage - but especially

to Shawn

DOCTOR OF PHILOSOPHY (1978)
(Mechanical Engineering)

McMASTER UNIVERSITY
Hamilton, Ontario

TITLE: Rate Effects in Bulk Forming

AUTHOR: James Allam Forster, B.Sc. (University of Manchester Institute of Science and Technology)

M.Eng. (McMaster Univesity)

SUPERVISOR: Professor J.L. Duncan

NUMBER OF PAGES: xxi, 319

ABSTRACT

One of the major industrial metalworking processes is extrusion and it is of technological importance to be able to estimate the loads and material flow characteristics within the deforming metal. Hot metals and superplastic materials are particularly sensitive to the speed of the operation although it is difficult to consider this in an analysis of the problem.

This thesis reviews the analytical techniques available to the engineer to determine the loads in bulk forming processes and examines the way in which rate effects have been accommodated. The upper bound method, which is an approximate analytical technique, is reviewed in detail. The concept of a tangential shear zone of constant shear strain rate is introduced and used to enable strain rate effects to be considered within the upper bound technique. The work rate across each discontinuity is shown to be a function of the material strain rate sensitivity, the shear zone width and the tangential velocity change.

A number of tangential velocity fields are proposed for the side extrusion process. These are examined and compared by minimizing the work rate using a computer optimization technique. The optimum solution for a simple tangential velocity discontinuity field is shown to give load estimates which are within 10% of those given by the more exact slip-line field method.

Experiments, performed by the author on the side extrusion of two

materials, which have very different strain rate sensitivities, are reported in detail. A characteristic difference in the extrudate geometry for the two materials is identified and shown to be a result of the difference in the materials strain rate sensitivity index. The experimental extrusion pressures for the two materials at different ram velocities are compared with theoretical values derived using the theory developed earlier in the thesis; the correlation is good.

The shape of the tangential discontinuity between a uniform translational and uniform rotational field is examined and shown to be a circular arc. A number of new tangential velocity discontinuity fields are presented for a variety of common metalworking processes. These fields comprise straight and circular discontinuities and represent a new type of "mixed" field which predicts the rotation of the extrudate.

ACKNOWLEDGEMENTS

The author wishes to express his sincere appreciation to Dr. J.L. Duncan for his continual encouragement, invaluable advice and unending patience during the course of this work.

The discussions and support of Profs. R. Sowerby and D. Embury are also greatfully acknowledged as are the invaluable dialogues with members of the Metal Forming and Physical Metallurgy Groups at McMaster.

The construction of the experimental equipment would not have been possible without the support of the Engineering Workshops, in particular, Jerry De Boer and Arnie Woolvett.

The financial support of the National Research Council is greatly appreciated.

A special word of thanks is happily extended to Pat Dillon of the Word Processing Centre for her expert typing and handling of the authors original scrawl.

Finally, the author takes this opportunity to record his deep appreciation for the continued patience, encouragement and support extended to him by his wife Shawn, to whom this thesis is dedicated.

TABLE OF CONTENTS

TABLE OF CONTENTS (continued)

TABLE OF CONTENTS (continued)

TABLE OF CONTENTS (continued)

TABLE OF CONTENTS (continued)

LIST OF FIGURES

LIST OF FIGURES (continued)

LIST OF FIGURES (continued)

LIST OF FIGURES (continued)

LIST OF FIGURES (continued)

LIST OF FIGURES (continued)

LIST OF FIGURES (continued)

LIST OF FIGURES (continued)

LIST OF FIGURES (continued)

LIST OF FIGURES (continued)

LIST OF TABLES

CHAPTER 1

EXTRUSION

1.1 Introduction

The extrusion of metals is one of the primary forming processes in use today. There are three basic types of process or mechanisms and these are indicated with their associated load/displacement diagrams in Figures 1.1, 1.2 and 1.3. It will be observed that for the more common inverted and direct extrusion methods there is a significant difference between the load/displacement curves. Briefly, for forward extrusion the load increases to a maximum as the billet fills the chamber and then, as the extrusion begins, the load falls steadily. This is due to the reduction of the friction component of the total work as the billet length within the chamber diminishes. With inverted extrusion there is no relative movement between the billet and the chamber and hence the frictional component of the work is virtually zero.

As mentioned, direct and inverted extrusion are industrially the most significant. However hydrostatic extrusion, although not a novel idea, has only attracted the attention of researchers [1-6] in the last 25 years and has been the subject of a recent monograph by Alexander and Lengyel [6].

Perhaps not of immediate industrial significance, the side extrusion process as a continued development of unsymmetric end

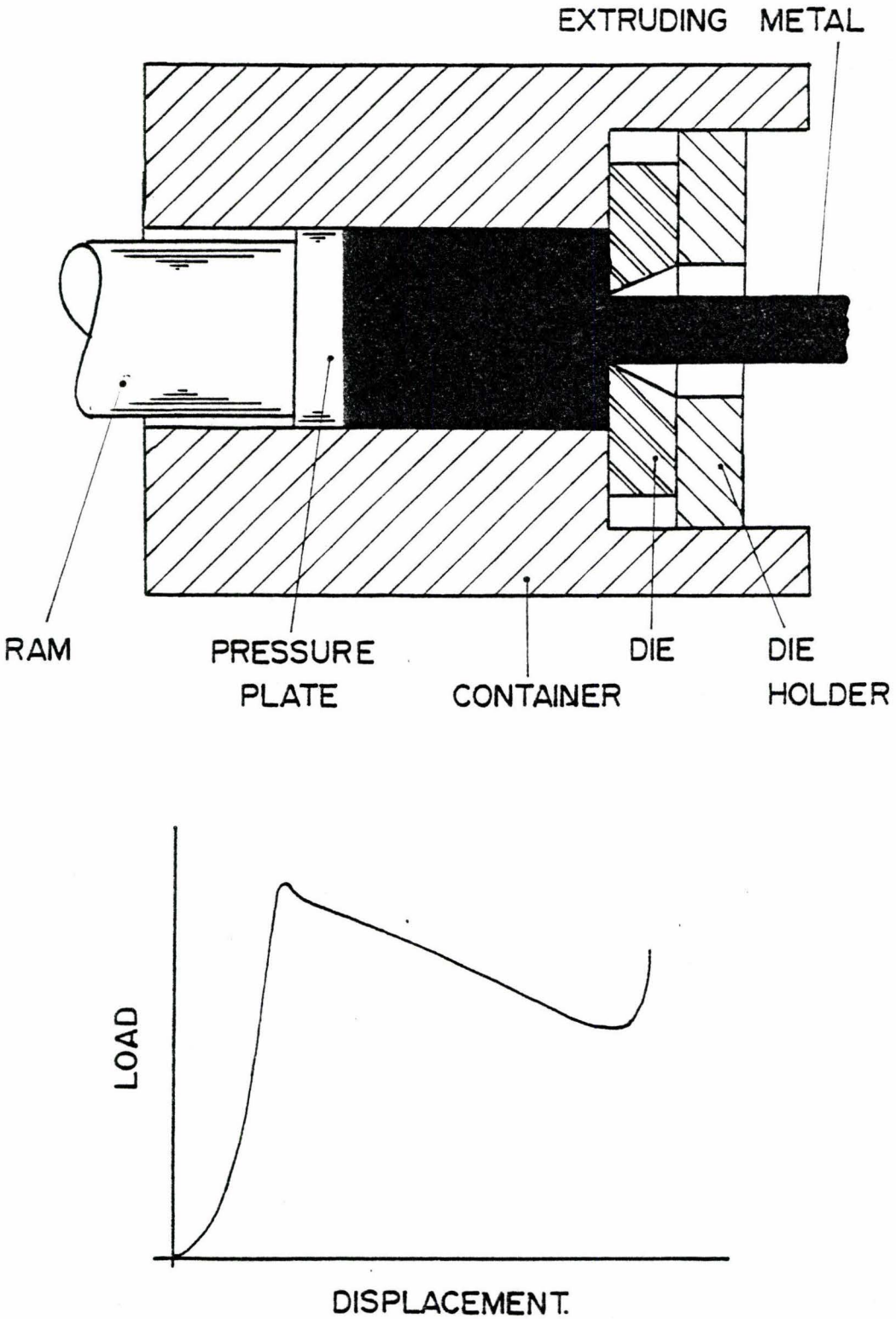

Figure 1.1

Schematic of the direct extrusion process and a typical load/displacement curve

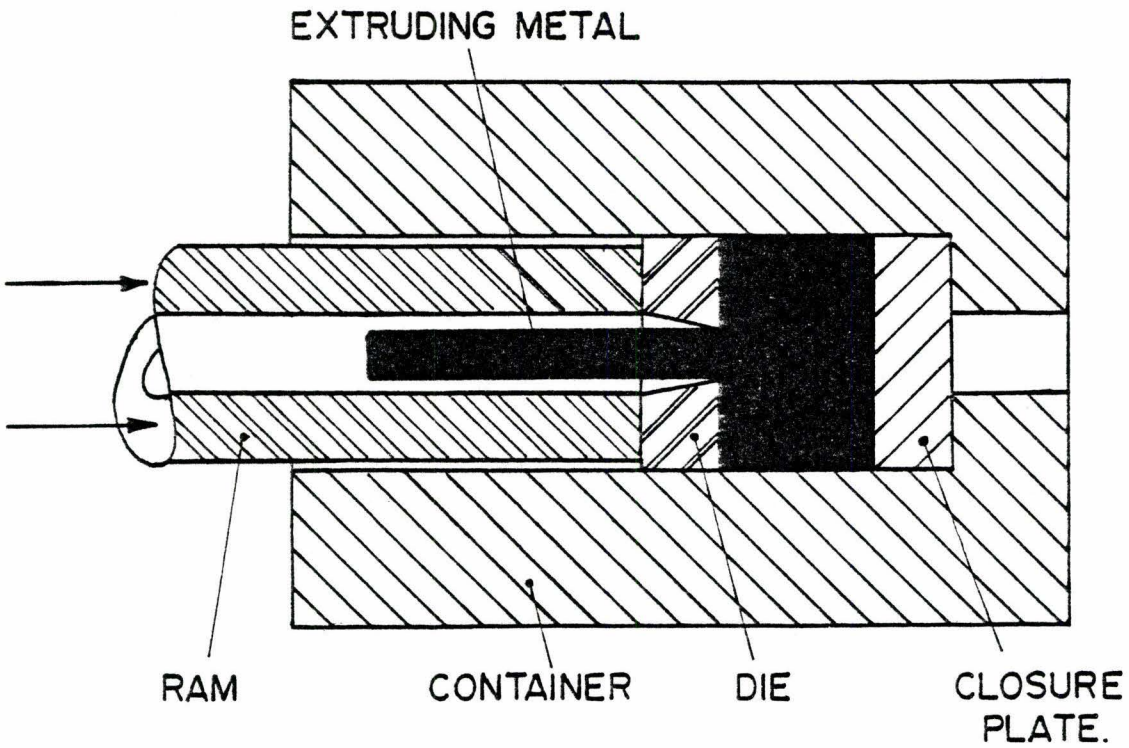

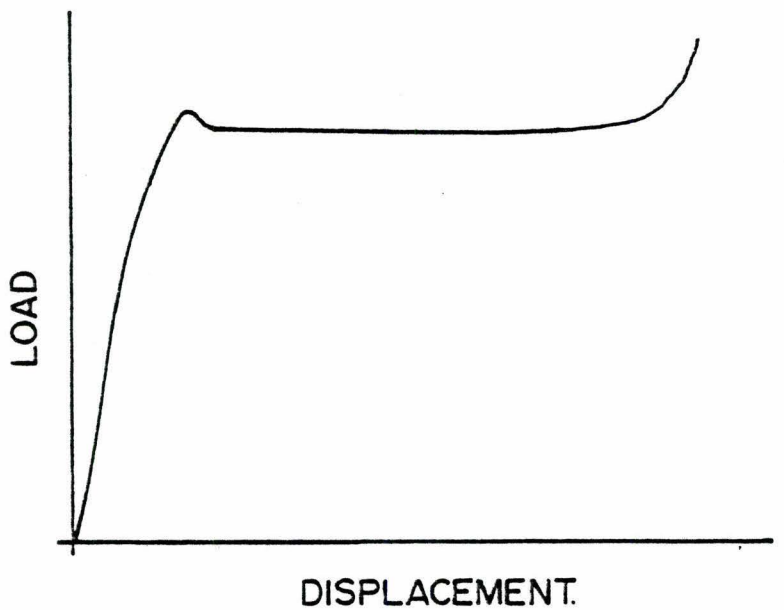

Figure 1.2

Schematic of the indirect extrusion process and a typical load/displacement curve

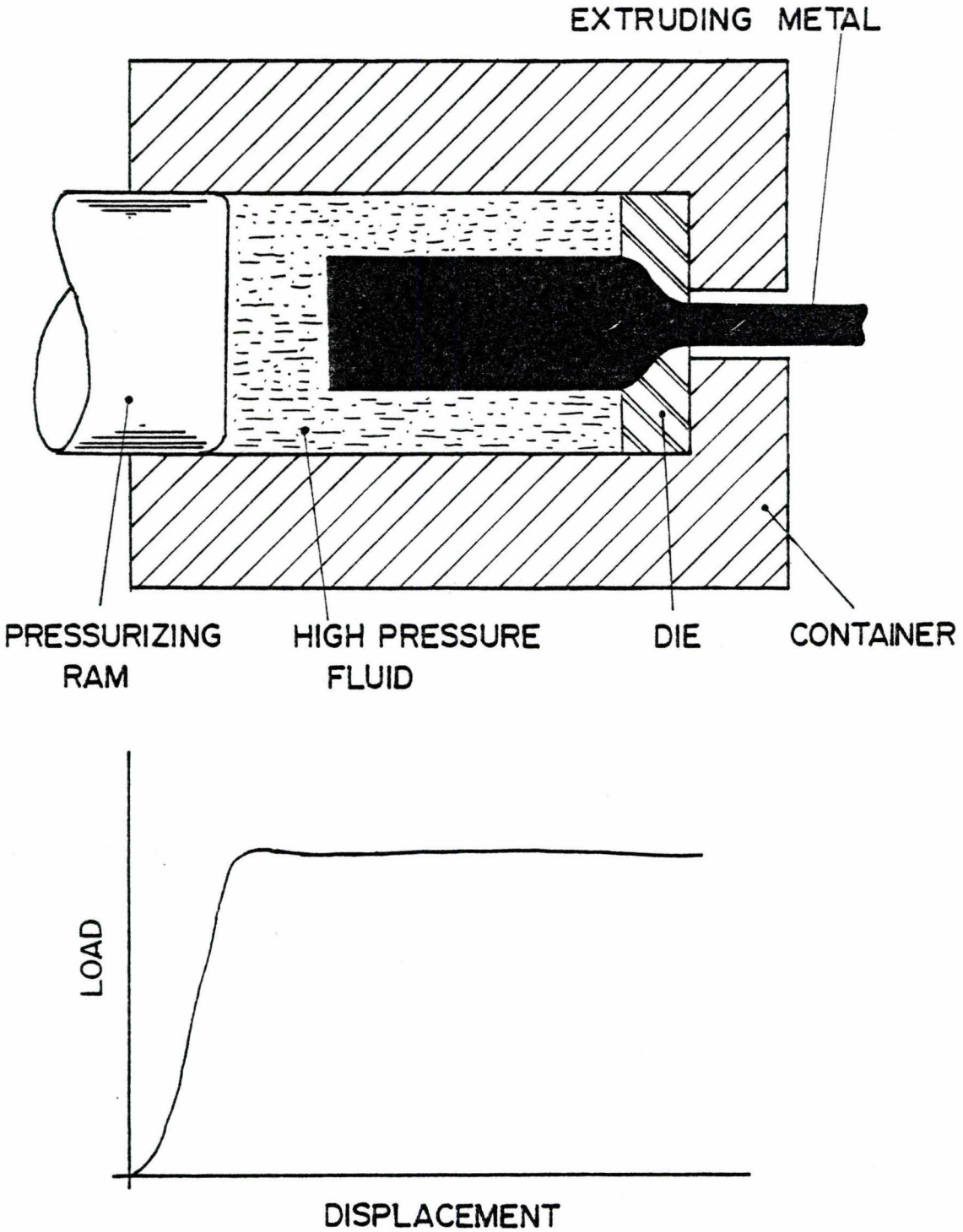

Figure 1.3

Schematic of the hydrostatic extrusion process and a typical load/displacement curve

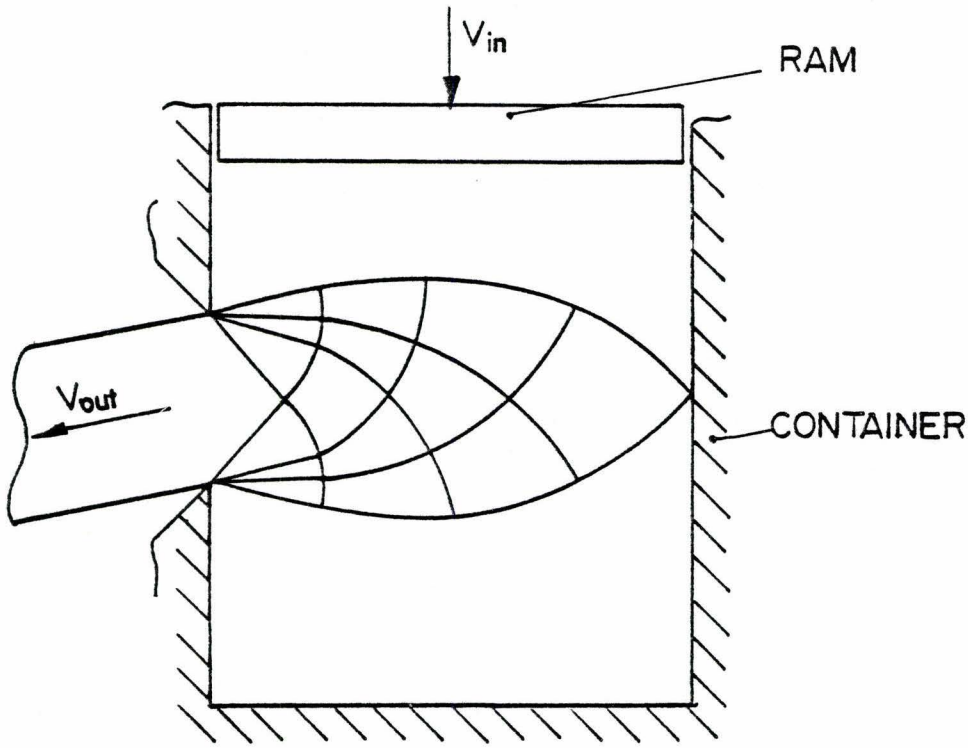

a) PHYSICAL PLANE DIAGRAM

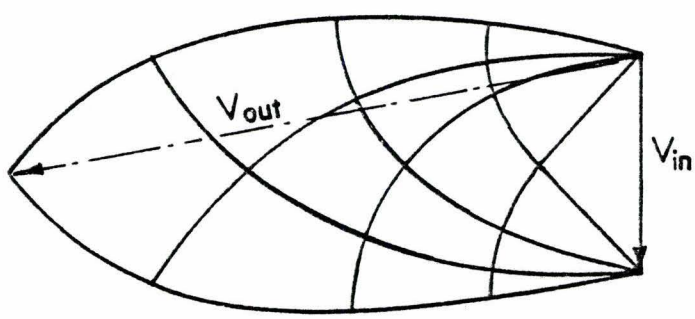

b) HODOGRAPH.

Figure 1.4

Schematic of the side extrusion process after Green [7]

extrusion, was proposed by Green [7] and is illustrated in Figure 1.4. This has subsequently been studied experimentally and theoretically [8, 9, 10] and some of the results utilized in the development of an analytical solution to the backward extrusion of a cup [11].

The majority of the early work in the development of the extrusion industry was performed on lead. Advances in materials technology this century has, however, given the design engineer the necessary materials to deal with the high temperatures and thermal stresses encountered in the hot extrusion of steel and the more useful structural materials. Edgecombe [12] has quoted Fairless, President of the American Iron and Steel Institute, as indicating that within the next century "Extruding will largely have replaced rolling to produce finished products", and has indicated that extrusion presses capable of 4400 tons (39 MN) have been constructed. Many shapes can now be extruded and Figure 1.5 is an illustration of some of the shapes produced in steel [13].

The present annual volume of steel extruded by the major U.S. companies is 60 million pounds (27×10^6 kg) and this represents a significant commercial market. Steel extrusions are used extensively in the manufacture of machines and in the construction industry. In the aluminium industry a much higher proportion of metal is sold as extrusions and these are used in the manufacturing industry and for architectural purposes.

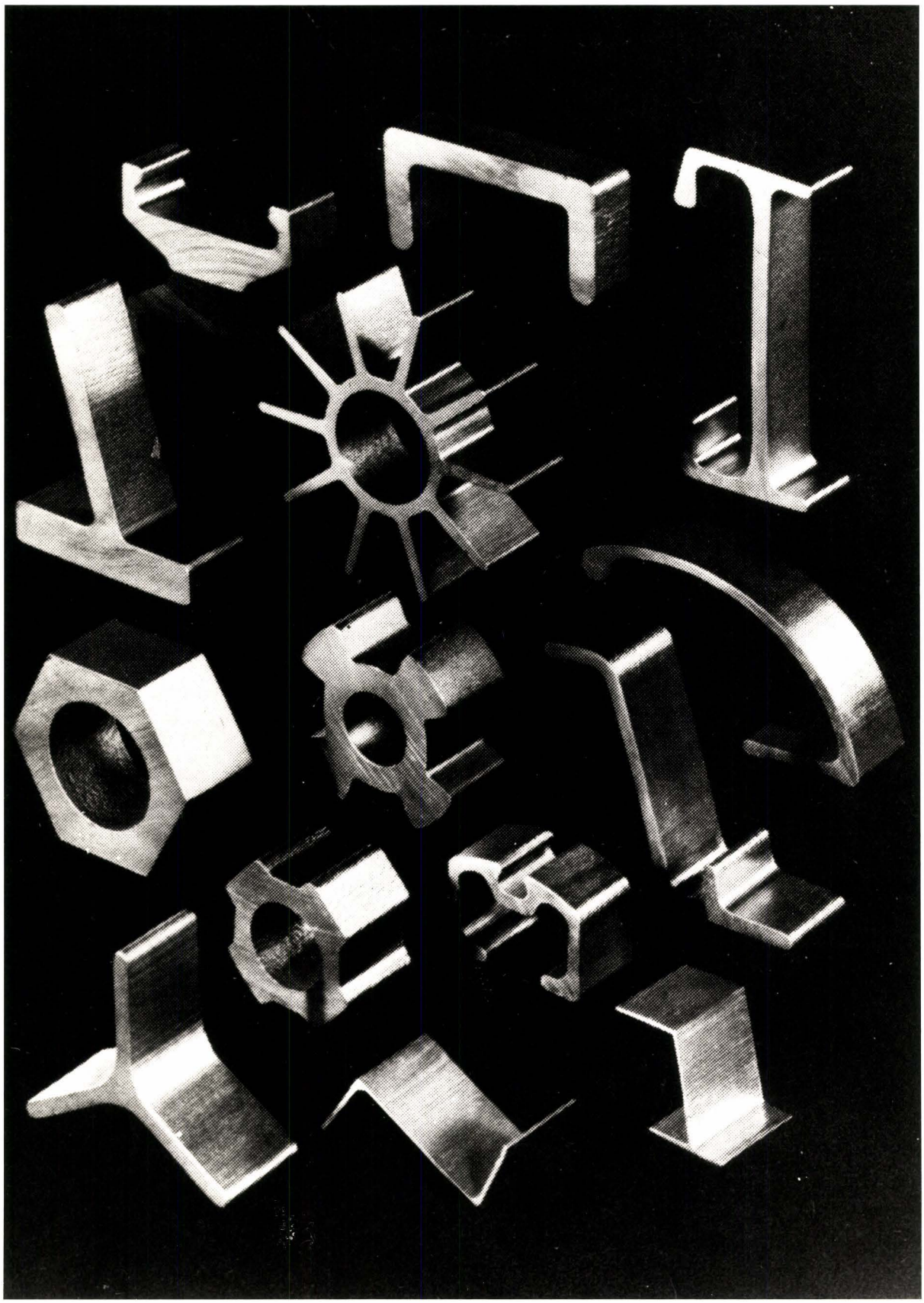

Figure 1.5

Photograph of some typical steel extrusions

1.2 Historical Background

The development of the extrusion industry was primarily around the use of lead and the production of various lead forms. Pearson, [14] in his definitive work on the extrusion of metals, traces the origins of extrusion to Joseph Bramah who was granted a patent in 1797. This patent described a press, Figure 1.6, "For making pipes of lead or other soft metals of all dimensions and for any given length without joints" [14]. Lead was maintained molten in the cavity, a, and was pushed into the die, c, by the pump, b. The molten metal passed through the space between the die and the tapered mandrel, d, and solidified near the exit. Although this idea does not seem to have been utilized it tends to indicate the origins of die casting or continuous casting rather than extrusion.

The first true hydraulic extrusion press was constructed by Thomas Burr, an English plumber, in 1820 and this machine was capable of producing tubing and sheet lead. During the next 30 years the process became fairly well established and minor modifications were made in an attempt to control the uniformity of wall thickness; a problem not unknown today.

Several interesting applications were attempted including the extrusion of tin-lined pipe in a single operation by Shaw in 1863. This was not very successful since the tin sleeve was cast directly into the lead billet prior to extrusion. Hamon made a significant advance in 1867 with the introduction of a press in which the billet was heated by passing hot gases around the extrusion chamber, Figure 1.7.

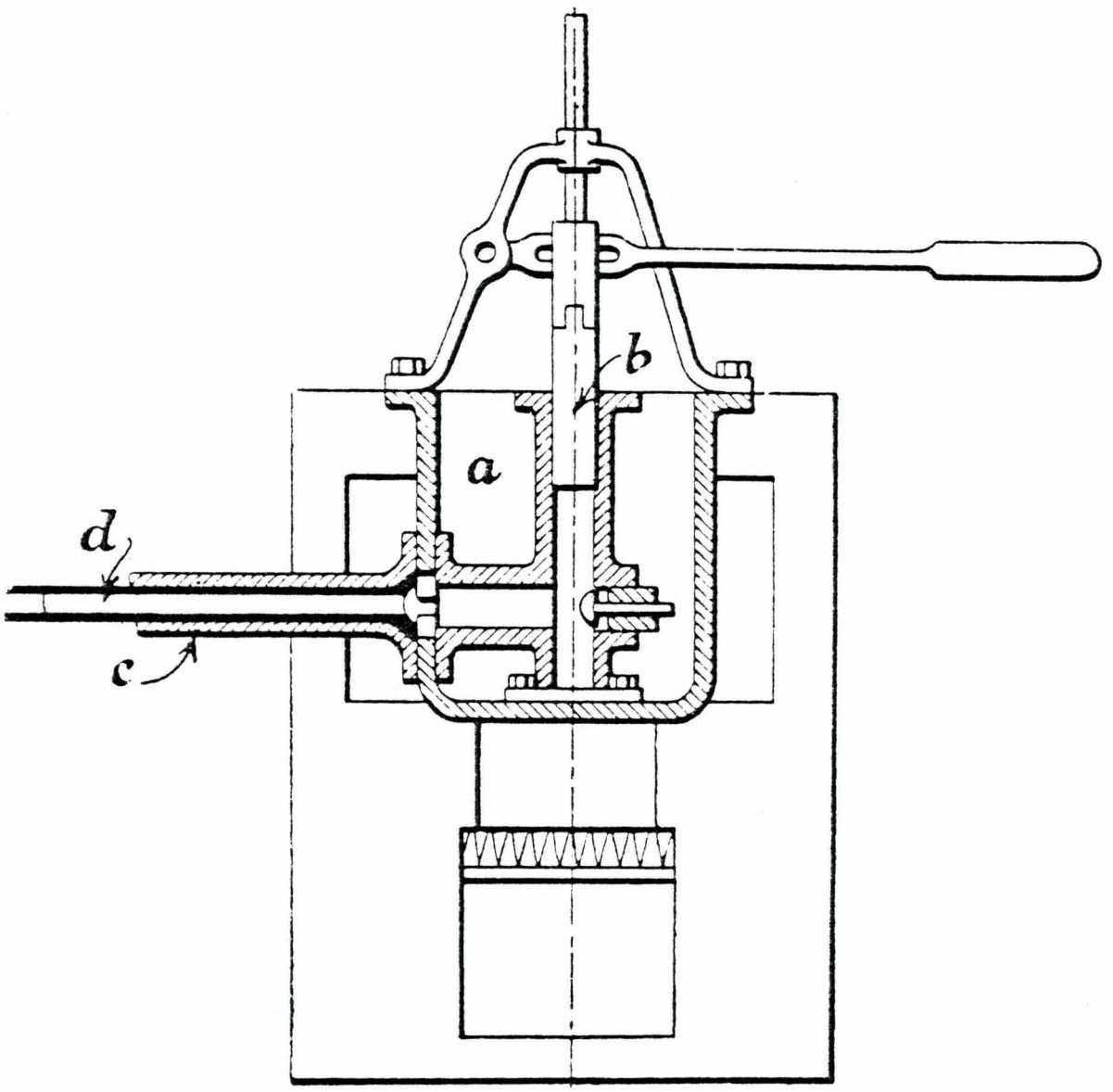

Figure 1.6

Press designed by Joseph Braman in 1797 for extruding lead pipe; from ref. [14]

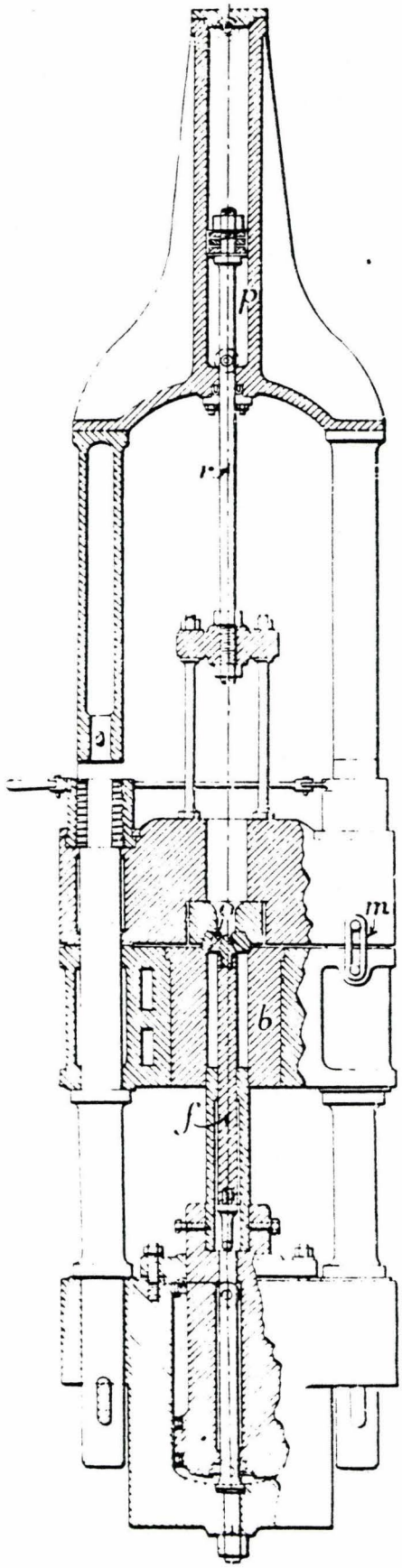

Figure 1.7

Press designed by Hamon in 1867 for warm extrusion;
from ref. [14]

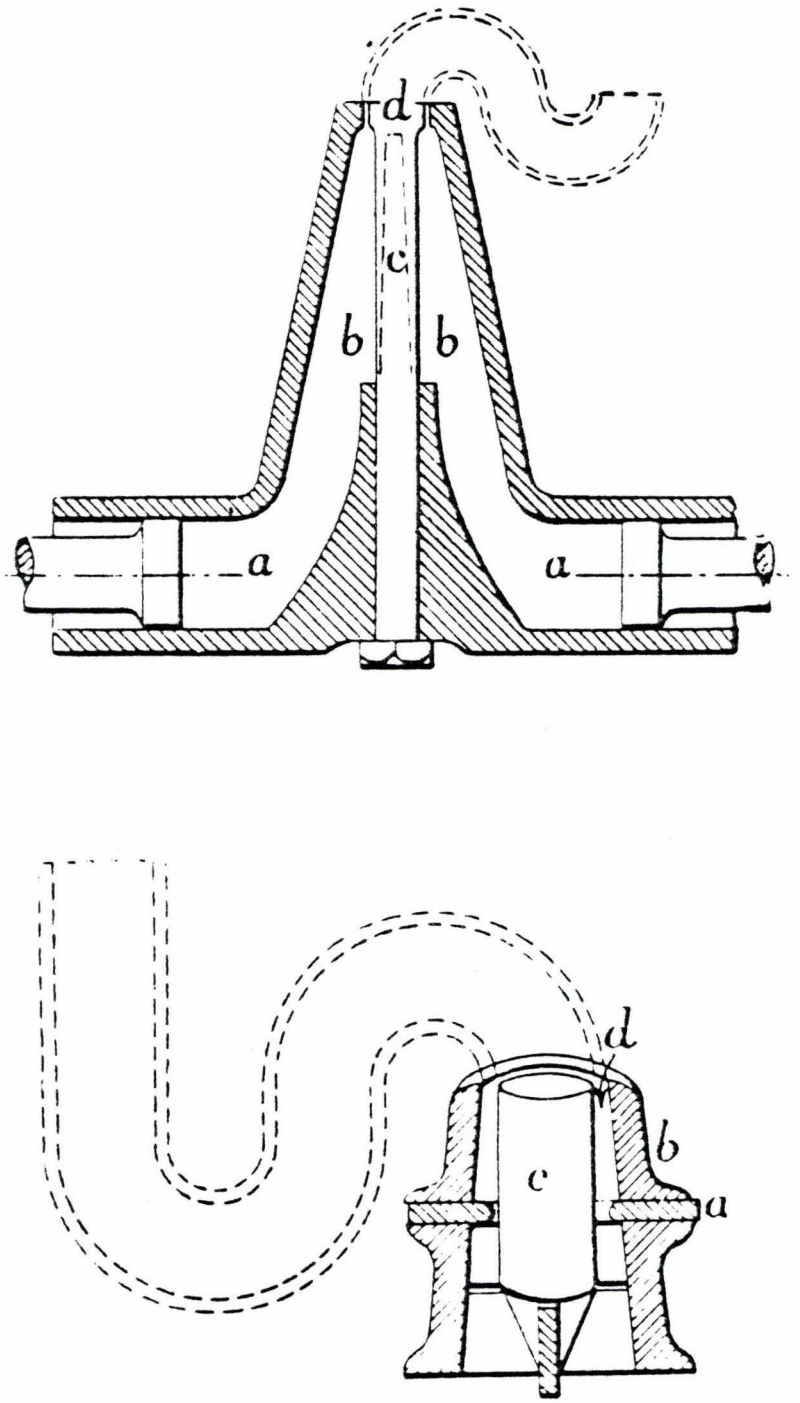

Figure 1.8

Two machines designed to extrude curved pipe;
from ref. [14]

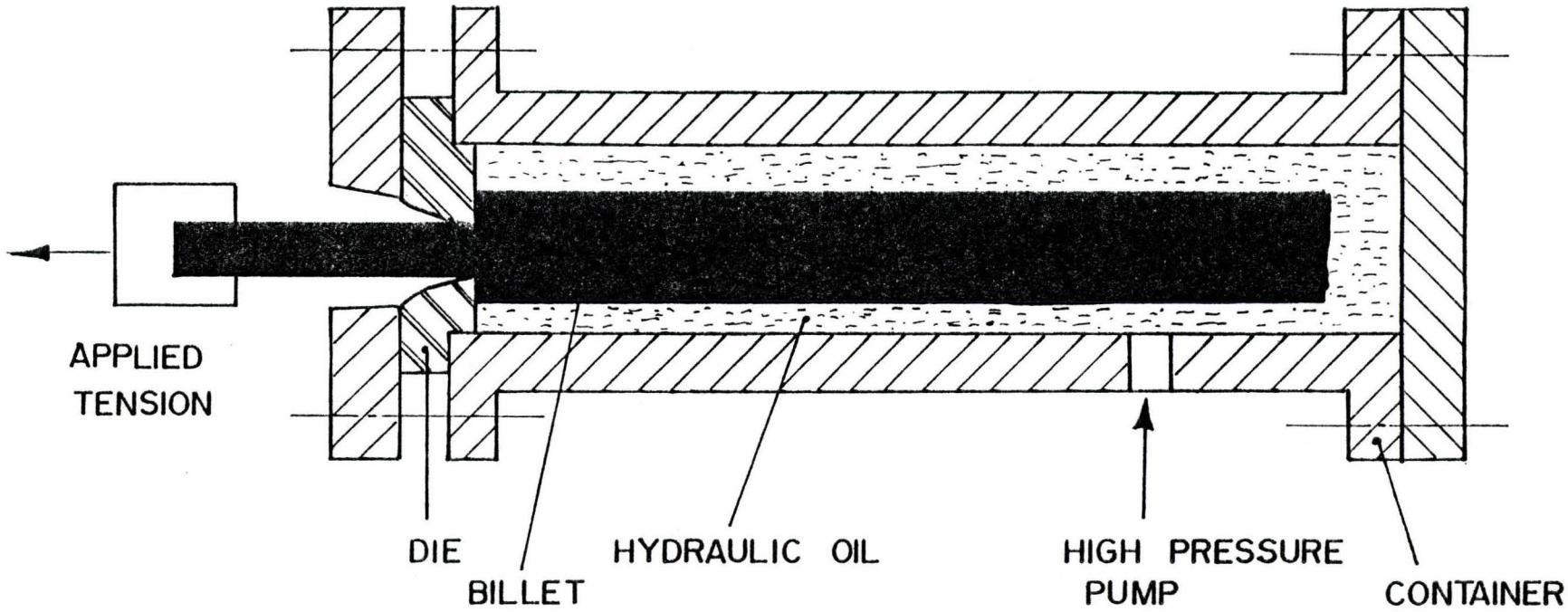

Figure 1.9

Schematic of the hydrostatic press proposed by Robertson in 1893; from ref. [6]

The introduction simultaneously by Haines and Weems of the reverse extrusion method in 1870 was probably the last major technological advance to be made. This method is still used extensively in the processing of the softer metals and in the impact extrusion industry.

The production of lead sheet for roofing, tubing for the plumbing industry, and beading for leaded windows in the late nineteenth century stimulated the industrial development of extrusion presses. A number of interesting machines were produced to extrude curved pipes as shown in Figure 1.8. Continued development lead to the successful design of machines capable of sheathing wire cables with lead. Ultimately this brought about the possibility of rapid communication between continents by telegraph which was accomplished by the laying of the Atlantic and Indian Ocean cables.

A patent issued in 1893 to J. Robertson [15] seems to indicate the beginnings of the hydrostatic extrusion process. Figure 1.9 [6] is a schematic of Robertson's design and includes such refinements as an externally applied drawing load and the rotation of the extruded tube in the die to reduce friction.

The modern concept of extrusion really began in the 1890's with the inventions of Alexander Dick in England and:

> "on his inventive genius has been laid the foundation of the modern extrusion process" [14].

Dick made significant advances in the design of both forward and inverted extrusion equipment. The extent of these advances was such

that modern hot extrusion equipment still embodies the principles discovered by Dick. Development of the process continued, and in the 1920's the Germans began commerical production of carbon steel pipe of approximately 3 inches (76.2 mm) outside diameter on mechanical presses which were rated at 1000 tons [12].

The development of the steel extrusion industry continued and the last major step forward was the introduction of glass lubricants in 1949 by Sejournet [16].

1.3 Recent Developments

A number of extrusion processes, proposed within the last decade, are outlined below. In general these processes have been shown to work on a laboratory scale but are not widely used in industry.

Two processes for the continuous extrusion of wire have recently been proposed by Green [17, 18] and are shown in Figures 1.10 and 1.11. Figure 1.10 indicates the Hydrospin process which is essentially a combination of hydrostatic piercing and the machining process. Initially the billet, which is prevented from rotating, is hydrostatically extruded over the piercing tool to produce a tubular form. A rotating die, which is shaped like a spiral ramp with a step, slides over the piercing tool and presses on the extruding material. The extrusion aperture is located in the face of the step at the end of the ramp. Consequently as the die rotates material is forced along the spiral ramp and through the extrusion die. Extrusion ratios of the order of 2500:1 have been achieved for copper with fluid pressures of

the order of 80,000 lb/in^2 (552 MPa). The major disadvantage of this process is the sealing problem associated with hydrostatic extrusion and that the process is not continuous.

In 1972, Green [18] proposed a simpler method for the continuous extrusion of wire and small sections, Figure 1.11. The principle is based on the frictional grip existing between the workpiece and the extrusion containment. The container is such that it travels with the workpiece towards and over a stationary die. When arranged in the form of a grooved wheel and external shoe the assembly permits continuous extrusion. Successful experiments were reported with aluminium and copper for an extrusion ratio of 4:1. It is anticipated, however, that with suitable equipment the extrusion ratio could be increased to 20:1 and 1000:1 for copper and aluminium respectively.

The concept of continuous extrusion of wire by viscous drag was first proposed by Fuchs [19] in 1971 and is illustrated schematically in Figure 1.12. A rod is centrally located in a chamber and fluid is pumped along the bar. Viscous shear effects against the rod and tube wall result in a pressure drop between inlet and exit and this can be utlized to drag the rod through the container. Figure 1.13 indicates the experimental extruder built by Fuchs who extruded aluminium. Results from these tests provided sufficient information for the proposal for construction of a prototype machine.

Tirosh and Grossman [20] have indicated that, since the reduction in the Fuchs machine is achieved in a single step, the die stresses are extremely high. The extrusion force is obtained by applying the driving

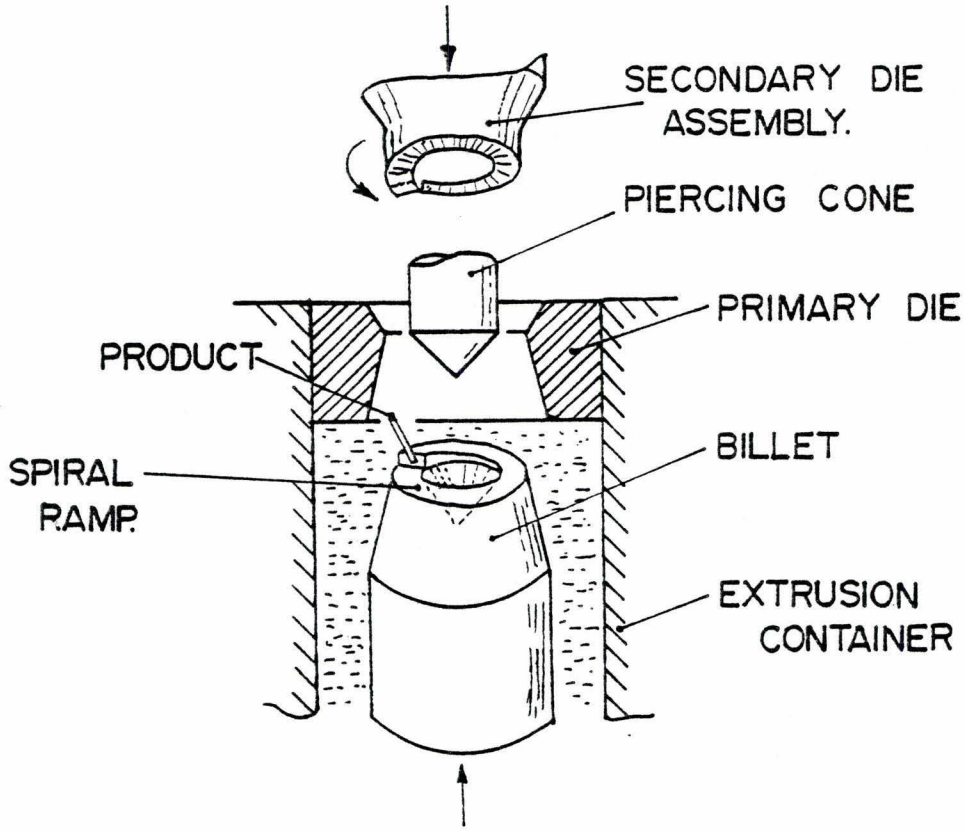

Figure 1.10

The 'Hydrospin' extrusion process for the continuous extrusion of wire proposed by Green [17]

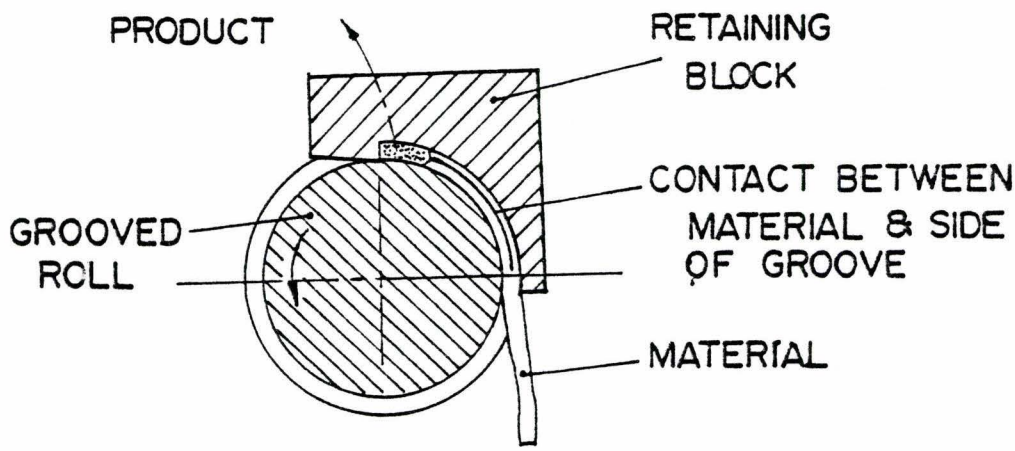

Figure 1.11

Alternative technique for the continuous extrusion of wire proposed by Green [18]

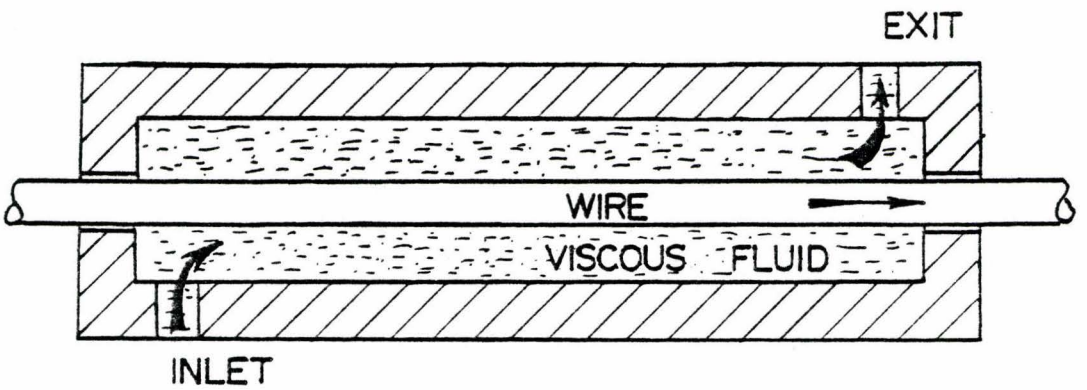

Figure 1.12

Schematic of principle of viscous drag extrusion

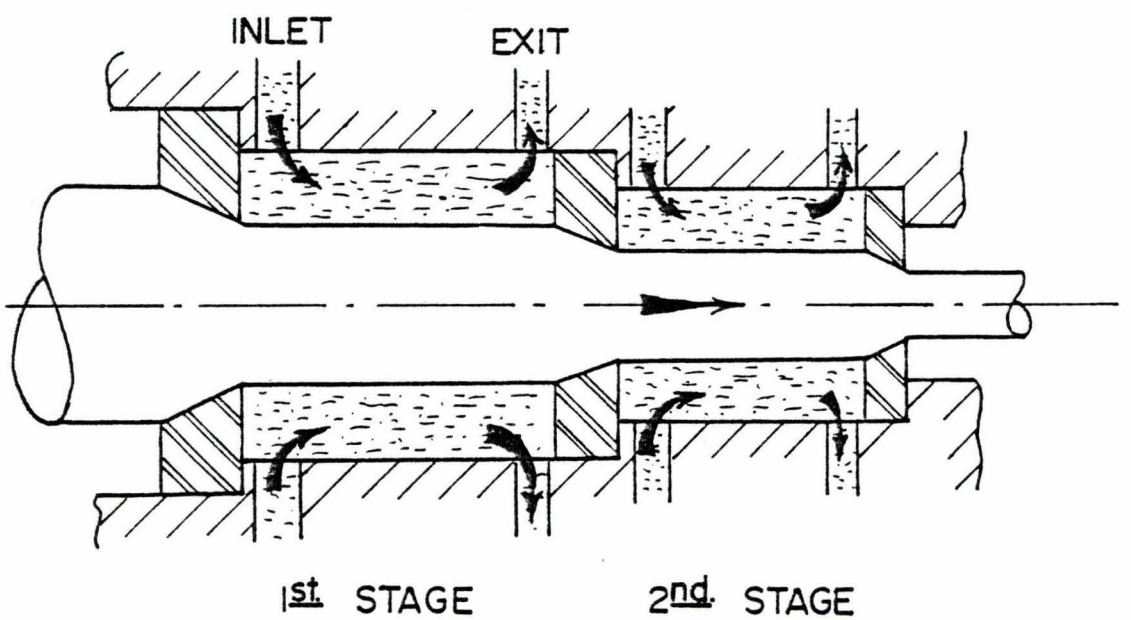

Figure 1.14

Multistage viscous drag extruder proposed by Tirosh and Grossman [20]

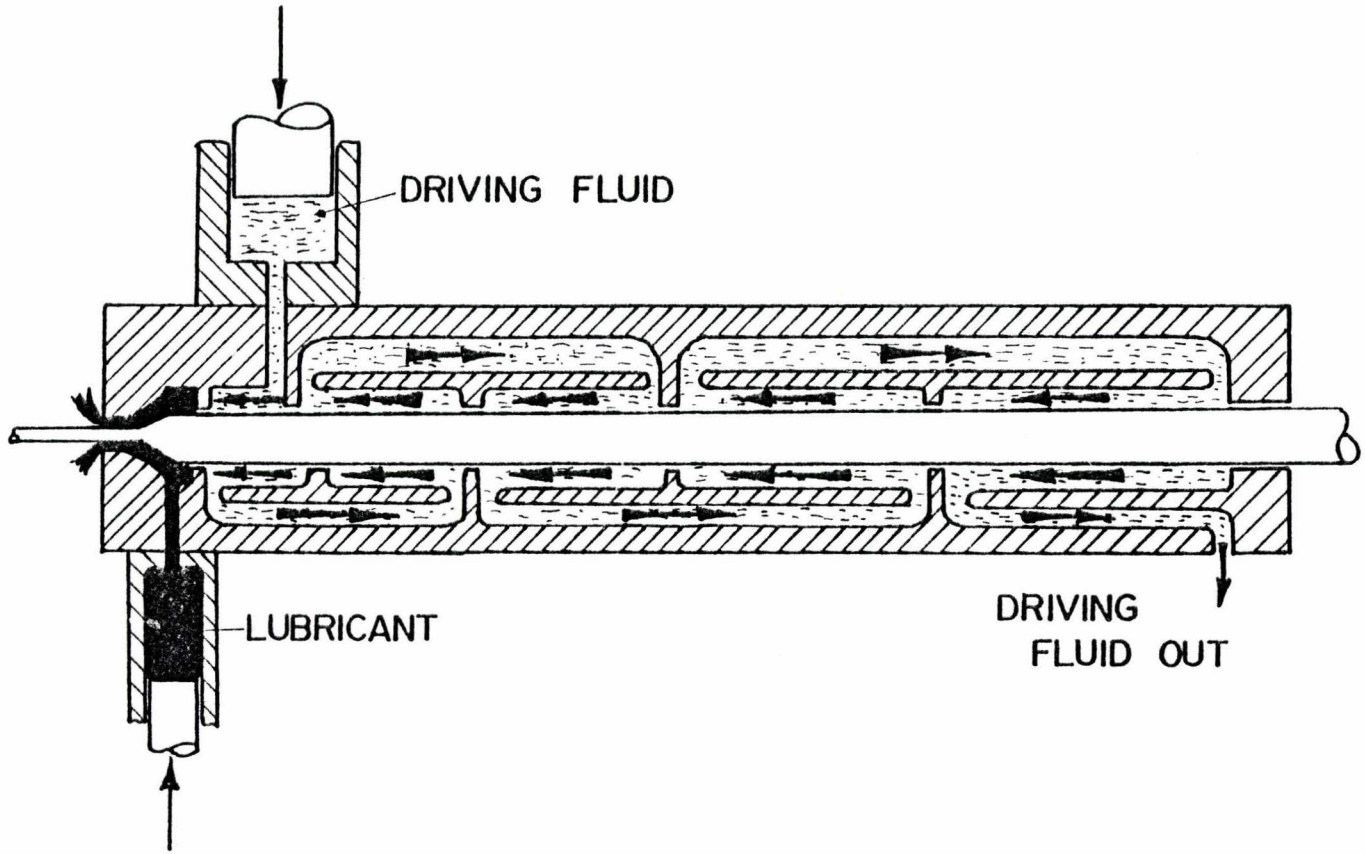

Figure 1.13

Viscous drag extruder with flow reversal cells
proposed by Fuchs [19]

fluid to a relatively long portion of the billet upstream of the die. To prevent buckling of the billet a large number of billet supports are needed which have to be fitted with dynamic seals against the billet, thus complicating the process and adding unnecessary friction. The authors proposed a design which overcomes most of the disadvantages indicated above. The extrusion is performed in a series of dies each separated by extrusion chambers, Figure 1.14. The concept of viscous drag is still utilized to extrude the material but the process is now one of a number of extrusion stages to achieve a given fractional reduction. Experiments were performed for a single stage at zero extrusion ratio to measure the extrusion drag force. Results from these experiments indicate that the theory overestimates the drag force at large flow rates. The authors conclude their paper by indicating the steps which must be followed in the design of a multistage extruder.

The manufacture of helical gears by a cold extrusion process has been patented by Samanta [21, 22]. In this process hollow cylindrical workpieces are placed inside the extrusion chamber and extruded over a mandrel through a gear extrusion die. The ejection of the formed part occurs as successive billets are pushed into the die. The helical gears produced by this method do not require any further machining of the gear teeth although the end faces are turned to remove the axially projecting ends of the individual teeth.

1.4 Analytical Techniques

With the development of the importance of the extrusion process,

academic and industrial research into the mechanisms of flow and the pressure required in the extrusion of a particular product has been of technological importance. Various analytical techniques have been proposed and these are outlined briefly here.

The prime aim of this research was to quantify the effect of temperature, die geometry, ram speed and lubrication on the extrusion load. Experimental and analytical techniques were developed to obtain this information. The standard texts of Pearson [14], Johnson [23], Avitzur [24], Hill [25], Thomsen et al. [26] and Zholobov and Zverev [27] have each given solutions for these problems.

1.4.1 Uniform Work Theorem

The uniform work theorem of Siebel [28] was probably the first analytical approach to this problem but fails to account for the frictional work or the redundant work due to internal shear.

The work done by the extrusion ram is equated to that necessary to cause a similar change in shape in a tensile process assuming that the material has a constant yield shear stress and there is no redundant deformation. Introduction of a correction factor to account for the redundant work gives a better estimate of the extrusion pressure.

The extrusion pressure, given by this analysis, is

$$\bar{p} = c \int_0^{\bar{\varepsilon}} \bar{\sigma}\, d\bar{\varepsilon} \qquad (1.1)$$

where $\bar{\sigma}$ is the material yield shear stress and $\bar{\varepsilon}$ is the finite effective strain and is given by

$$\bar{\varepsilon} = \ln \{\frac{A_o}{A}\} \tag{1.2}$$

c is the redundant work correction factor ($\simeq$ 1.5).

1.4.2 Slip-line Field Solution

The slip-line method was introduced by Henky [29] and is a powerful and well established analytical technique. The application of this technique to engineering problems has been greatly increased by Hill [25], Green [7], Lee [34] and Johnson [23]. A comprehensive monograph [35] has been published in the last decade detailing the work and the solutions achieved with this method.

A slip-line solution is based mathematically on the characteristics of the differential equations of equilibrium. Physically the slip-lines are contours of maximum and minimum shear stress and form an orthogonal network of lines within the plastic zone of a metal. This solution technique assumes that the material behaviour is rigid-perfectly plastic, that is, that material can be divided into two zones, the rigid and the plastic, and that the transition from one to another is across a line boundary. The solution is usually only applied to problems of plane strain, however solutions can be developed for axisymmetric problems. The Haar-Von Karmen hypothesis that the circumferential stress is equal to one of the other principle stresses during plastic deformation is introduced and the Tresca yield criterion

and associated flow law employed as illustrated by Shields [30]. The velocity and stress equations are then hypobolic with identical families of characteristics. Richmond and Morrison [31] examined ideal forming operations and indicated the ideal die profile for axisymmetric plastic flow of an anisotropic perfectly plastic solid. Thomsen [32, 33], however, has obtained good correlation between experimental and theoretical results when the plane strain analysis was applied to some axisymmetric problems.

The exclusion in the formulation of the effects of work hardening and strain rate have only recently been examined in detail. Work hardening has been accommodated within the theory [36, 37] and the effect of strain-rate is now receiving attention [11, 38].

1.4.3 The Visioplasticity Technique

In 1954 Thomsen and his co-workers [39, 40, 41] introduced the concept of visioplasticity where the strain paths are evaluated from experimental observations of distorted grid patterns. Billets of material are split prior to deformation and a grid pattern marked on one half of the billet. The billet is extruded in a step wise fashion with recordings being made between each successive step of the distorted grid. From these experimentally determined grid pattern distortions the velocity vector field, within the deforming material, can be determined and the stresses subsequently calculated. The extrusion loads can be determined for a particular die geometry and flow situation and these compare well with experimentally observed values.

1.4.4 The Upper Bound Technique

The most recent analytical techniques are due to Johnson [42, 43] and Kudo [44, 45] and these can be generally classed as upper bound techniques. In Johnson's analysis a statically admissible velocity field is defined such that the conditions of incompressibility and continuity are satisfied. For the example in Figure 1.15 the load is given by:

$$\bar{p} = \frac{1}{H\sqrt{3}} \sum_{s} \frac{\bar{\sigma} u^*}{V} \, ds \qquad (1.3)$$

where $\bar{\sigma}$ is the mean yield stress and is assumed constant along any discontinuity CA' CB'.

u^* is the change in the tangential velocity component across the discontinuity; obtained from the hodograph.

V the ram velocity.

For a die with H = 1, a ram speed of 1 and $\vartheta = 40^\circ$

$$\bar{p} = 1.01 \left\{\frac{2\bar{\sigma}}{\sqrt{3}}\right\} \qquad (1.4)$$

This compares with a slip-line solution of

$$\bar{p} = 0.95 \left\{\frac{2\bar{\sigma}}{\sqrt{3}}\right\} \qquad (1.5)$$

This is an analytical technique where the smallest answer is closest to the correct solution. Consequently a number of calculations must be performed for different values of ϑ and the minimum value of $\bar{p}$ determined.

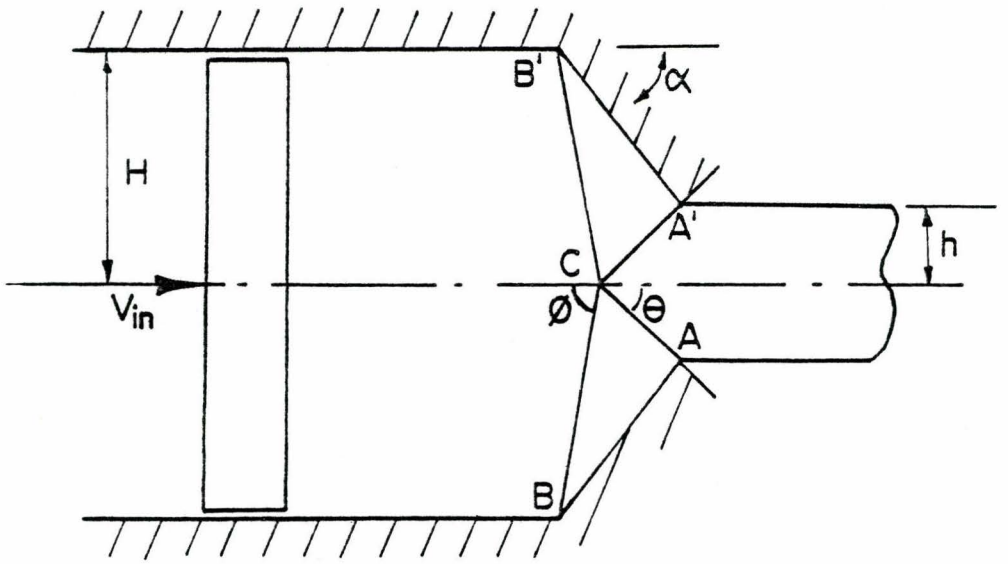

a) PHYSICAL PLANE DIAGRAM.

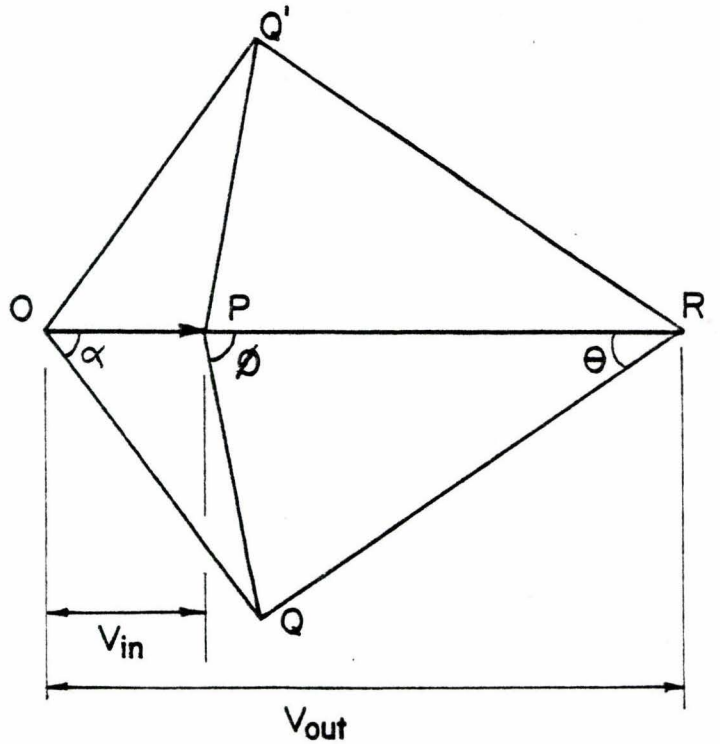

b) HODOGRAPH.

Figure 1.15

Forward extrusion: a) Physical plane diagram illustrating assumed tangential velocity discontinuities, b) Hodograph

1.4.5 Summary of Analytical Techniques

Each of the above methods has been used in an effort to determine the extrusion loads; however, this problem has still not been solved to the complete satisfaction of some investigators. Problems still exist in the complete understanding of the flow systems involved and the effect of extrusion speed.

Table 1.1, from [26], is a comparison of the various methods of calculation for the extrusion of commercially pure aluminium. The billet was 4.3 inch (109 mm) dia. and was extruded into a concentric 1.5 inch (38.1 mm) dia. rod at an extrusion ratio of 8.2. The ram speed was of the order of 0.1 inch/min (0.042 mm/sec) and the steady state extrusion pressure, in the inverted process was 89,500 lb/in^2 (617 MPa).

Thomsen et al. [26] suggested that a possible explanation for the large discrepancy of the extrusion load calculated using the Johnson formula is that the equation for the effective stress which is given by

$$\bar{\sigma} = 31{,}800\ (\bar{\varepsilon})^{0.283} \tag{1.6}$$

is applicable only for low effective strains and that at the larger strains of 4 a more accurate stress/strain curve must be available. Johnson's equation used by Thomsen et al., eqn. (1.7), was developed based on experimental results with lead, tin and aluminium [46]. Johnson indicated that the appropriate values for the constants a and b were 0.8 and 1.5 respectively.

$$\frac{\bar{p}}{\sigma_{ave}} = a + b \ln \left(\frac{A_o}{A_i}\right) \tag{1.7}$$

Method of Calculation	Equation Used	Flow Stress	Maximum Effective Strain	Average Extrusion Pressure
a) Uniform work of deformation	$\bar{p} = c\int_0^{\bar{\varepsilon}} \sigma d\bar{\varepsilon}$	variable $\bar{\sigma} = 31800(\bar{\varepsilon})^{0.283}$	$\bar{\varepsilon} = 2\ell n(D/d) = 2.1$	95200
b) Slab	$\bar{p} = c\int_0^{\bar{\varepsilon}} \sigma d\bar{\varepsilon}$	$\bar{\sigma} = 31800(\bar{\varepsilon})^{0.283}$	$\bar{\varepsilon} = 2\ell n(D/d) = 2.1$	95200
c) Slip Line Analysis	See ref. 26 page 314.	$\bar{\sigma} = 31800(\bar{\varepsilon})^{0.283}$ $= 39,300$	$\bar{\varepsilon} = 2\ell n(D/d)$ $= 2.1$	83500
d) Experimental Pugh and Watkins ref.47	$\bar{p}=14.5[\ell n\frac{A_i}{A_o}+6.9]2240$	—	—	83800
e) Johnson ref. 46	$\bar{p} = \bar{\sigma}_m(1.5\ell n\frac{A_i}{A_o}+0.8)$	$\bar{\sigma}_m=\frac{1}{\bar{\varepsilon}_m}\int_0^{\bar{\varepsilon}_m} \bar{\sigma} d\bar{\varepsilon}$ $= 36000$	$\bar{\varepsilon}_m = 1.5\ell n \frac{A_i}{A_o} + 0.8$ $= 3.96$	145000
f) Visioplasticity		$\bar{\sigma} = 31800(\bar{\varepsilon})^{0.283}$ - variable		95000
g) Experimental Inverted Extrusion	—	—	—	89500

Table 1.1

Comparison of extrusion pressure given by different analyses; from ref. 26.

Pugh and Watkins [47] performed a series of experiments with different materials and it is clear that the values of the constants are functions of the material, the billet temperature, the total strain and the friction conditions.

If, however, we assume that the values for the constants a and b, as given by Johnson are appropriate, then the mean flow stress given by Thomsen et al. [11] may be incorrect. The mean strain for the process is 3.96 and if we use the true stress strain curves given by Johnson [38] the value of the flow stress for aluminium is 20160 lb/in^2 (139 MPa) and the extrusion pressure is 79850 lb/in^2 (550 MPa). This value is certainly more appropraite than that given by Thomsen et al. [26] in Table 1.1. It is not surprising that this value underestimates the extrusion pressure since the flow stress was derived from Johnsons curve for super pure aluminium while the experimental value given by Thomsen was for commercial purity aluminium.

1.5 Effect of Strain-Rate

As mentioned earlier, the prime goal of previous research has been to examine the effect of tool geometry, lubrication, extrusion ratio and ram speed on the extrusion process. Combined experimental and analytical studies have been performed by various workers and the results have proved useful in the design of equipment and press tooling. Little research, however, has been conducted on the effect of strain-rate, although it has been recognized for some time that it could be an important parameter [14]. Figure 1.16, [48] indicates

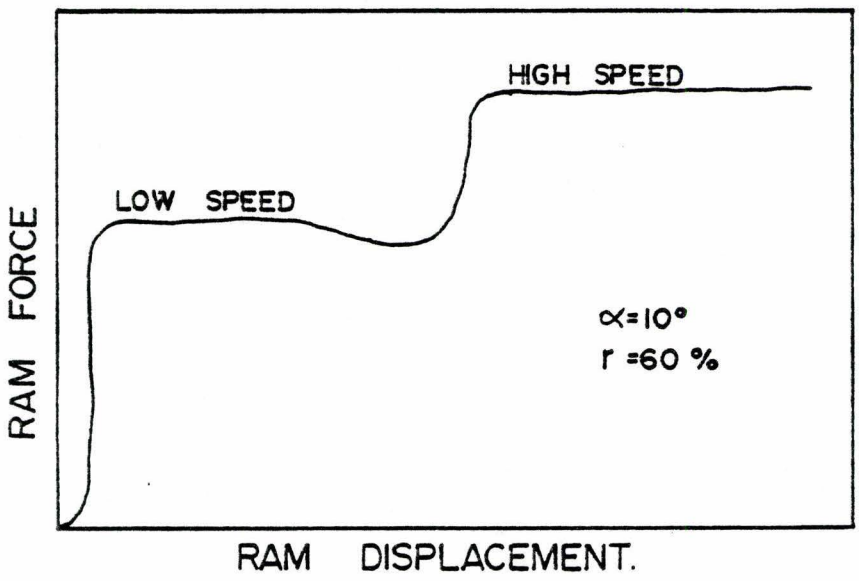

Figure 1.16

Effect of velocity on extrusion pressure; from ref. [48]

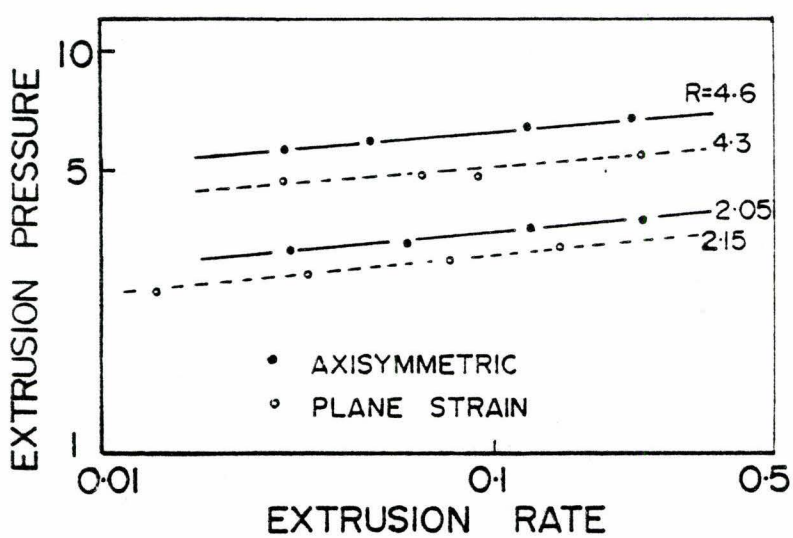

Figure 1.17

Experimentally determined extrusion pressures for lead extruded in plane strain and axial symmetry; from ref. [33]

schematically the rise in extrusion load with increase of ram velocity, while Figure 1.17 [33] indicates the variation of extrusion pressure with extrusion rate and extrusion ratio. It should be noted that in these curves the speed is very slow compared with normal extrusion practice where the extrusion rate is in the range 1 → 10 ins/sec (25→250 mm/sec).

The upper bound technique has been used to predict the pressure for plane strain extrusion of aluminium [49] and has established the effects of die geometry, extrusion ratio, lubrication and strain hardening. However work still continues in this field and new solutions based on experimental observatons are being used to produce design charts for use within the industry [50].

The visioplasticity technique continues to find its proponents [51, 52, 53] and yet becomes more and more complex and expensive with the introduction of elaborate computer programs to analyse the data. This approach, however, often fails to convey a generalised physical concept of the important aspects of the process.

A few papers [54, 55] have been published which deal solely with the problem of obtaining a kinematically admissible velocity field. Once again, however, these analyses although mathematically elegant and contributing to the understanding of the flow mechanisms involved deal with conical dies and small extrusion ratios and hence are not necessarily relevant to industrial problems in which much higher extrusion ratios are common.

1.6 Rate Dependent Materials

In the last decade there has been a revival of interest into problems of stability [56], in particular the instability problems associated with tensile processes. Amongst materials scientists this interest was spurred by a paper by Hart [57] in 1967. Papers in this area have shown the importance of the strain-rate dependence of the flow stress and the way in which it controls the growth of instabilities. The flow stress $\bar{\sigma}$ is related to the strain rate $\dot{\bar{\varepsilon}}$ by an often used equation:

$$\bar{\sigma} = \sigma_o \dot{\bar{\varepsilon}}^m \tag{1.8}$$

where σ_o is a material constant and

m is the strain-rate sensitivity

Research into a particular class of materials, the superplastic alloys, received a great deal of attention in the 1960's with numerous papers being published regarding microscopic flow mechanisms and the industrial significance and opportunities available with this ostensibly new class of alloys. These materials have a constitutive equation of the form indicated above when heated to approximately half their absolute melting points. The processing of these alloys due to the large neck free elongations and the low flow stresses associated with low strain-rates has presented the engineer with some novel metalforming techniques [58→62].

1.6.1 Extrusion of Rate Dependent Materials

The extrusion of highly rate dependent materials although remarkably similar to that of the hot extrusion of metals [63] has received little attention by the theoreticians. Minor mention has been made in a number of papers [24, 64] where a mean strain rate is evaluated for the process.

Jonas et al. [65, 66, 67] have indicated that the mean strain-rate evaluations with respect to time or some displacement parameter can differ by as much as an order of magnitude. Basically however the analyses presented thus far simply apply some form of correction factor to the evaluation of the flow stress to account for the variation of strain-rate during the process. Jonas [64] has derived a constant true strain-rate and used this in an analysis based on the uniform work method of Siebel indicated previously.

Ragab and Duncan [11] examined the slip-line solution for the backward extrusion of a cup and derived a correction factor for the slip-line solution assuming a rigid perfectly plastic material in which the flow stress in a region depended on the strain rate. This analysis is of interest since the authors examined a small area near the corner of the punch, Figure 1.18, and utilized the analysis of a side extrusion process to derive the pressure in this region. Comparison between theoretical and experimental results shows reasonable agreement.

Fenton et al. [38] have proposed a numerical method based on the modified Henky and Geringer equations for solving plane strain metal flow problems of strain rate sensitive materials. The computation,

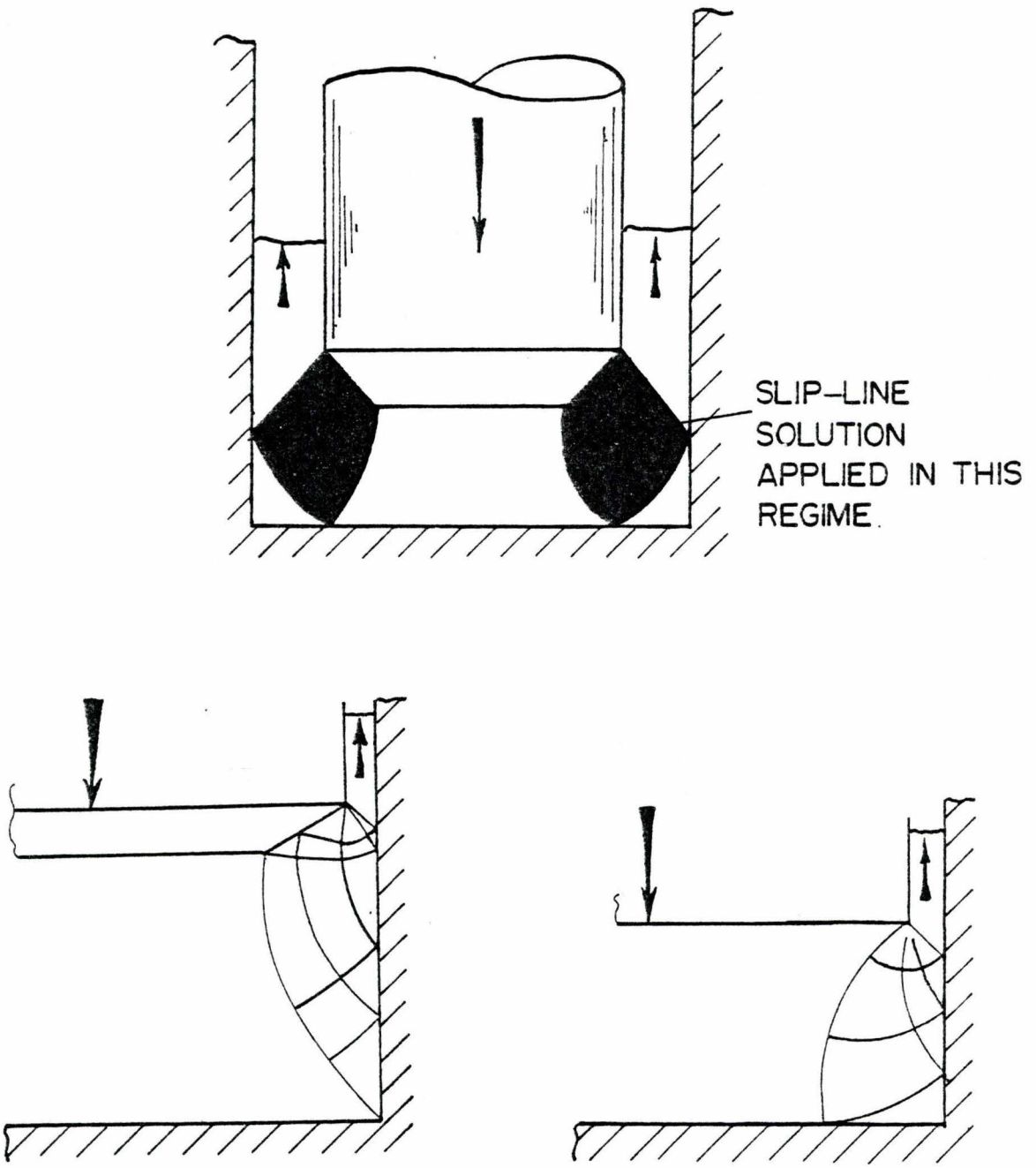

Figure 1.10

Deformation zone indicated by Ragab et al. [11] showing area within which side extrusion is assumed to take place

however, can only proceed if the flow stress distribution is known. The initial flow stress distribution is therefore assumed constant and the slip line field computed. The velocity and strain rate fields can now be evaluated and a new approximation to the flow stress distribution determined based on a flow law of the type indicated in equation 1.8. A new slip-line field can now be generated and the velocity field compared with the previously determined velocity field. Fenton indicated that the process converges after about 5 iterations when the difference between successive solutions is 5% for the velocity field and 1% for the stress field. Computed results are presented for a single case where the rate sensitivity, m, was 0.05. No comparison was made with experimental results available in the literature or any indication given as to the effect of rate sensitivity on the velocity field, stress distribution or extrusion pressure.

Alto and Giorles [68] analysed the extrusion of a rate dependent material by the slab technique and an upper bound approach. The velocity field was determined from experiments performed by Jovane et al. [52]. The authors showed that the slab method generally predicted higher extrusion loads than the upper bound technique and indicated that the method could be considered accurate enough for engineering purposes. In terms of theoretical plasticity it is, however, a lower bound solution.

Jovane et al. [52] conducted a fairly extensive research program on the flow mechanisms in the forward extrusion of superplastic tin-lead (Pb-Sn). This alloy is superplastic at room temperature which makes it

an ideal material for experimental investigations. The authors concluded from a comparison of the flow patterns of lead and the superplastic Pb-Sn that the velocity field was independent of material properties. This invariance of the flow pattern is reasonably demonstrated by their experiments but this does not prove that this is a general principle.

A recent viscoplastic analysis [69] presented by Cristescu examines theoretically the extrusion or drawing of a material with a viscoplastic constitutive equation. Cristescu indicated that the drawing, extrusion, pressure is dependent upon the speed of the operation and that this pressure increase is higher for large extrusion ratios or die angles. The process indicated however is for a conical die and while that might be applicable to hydrostatic extrusion, many industrial extrusion presses are operating with square dies.

1.7 Summary

The extrusion of metals and alloys has been the subject of analysis for some years and fairly well defined techniques are available to determine extrusion pressures. The effect of tool geometry, extrusion ratio and lubrication have been examined in some depth but it is only in the last few years that any serious attempts have been made to examine the effects of strain-rate. With the development of a new group of materials, the superplastic alloys, research into the strain-rate sensitivity of various processing techniques has been stimulated. However, no new analytical technique is

presently available which accounts satisfactorily for the rate-sensitivity of materials.

CHAPTER 2

THE EXTRUSION OF RATE SENSITIVE MATERIALS

2.1 Introduction

In the first chapter the extrusion of rate dependent materials was reviewed briefly. A closer examination is now presented which reviews in detail the literature on the extrusion of rate sensitive materials. The commercial development of the superplastic alloys in the 1960's has led to a re-examination of theories dealing with rate sensitive material properties. This class of alloys exhibit large tensile elongations and are characterized by a material behaviour equation of the form:

$$\bar{\sigma} = \sigma_o \dot{\bar{\varepsilon}}^m \tag{2.1}$$

In the hot working of steels the material behaviour can be characterized by an equation of the form indicated above where m is of the order of 0.1 to 0.15 [63]. The extrusion process has been studied extensively and many papers are available in the scientific and technological literature. However these papers have tended to examine model materials, such as lead, which are non hardening and little has been published in the scientific journals on hot extrusion. With rate dependent materials there is no single forming load but rather a relation between the applied load and the forming speed.

The following is a brief survey of the industrial processes for the forming of highly rate sensitive materials and a summary of the development of analytical methods for dealing with the bulk processing of rate dependent materials. The influence of material properties on the velocity field is discussed and the scope of the present investigation indicated.

2.2 Applications of Superplastic Forming Processes

Superplastic forming technology is now coming of age and the forming of sheet is carried out industrially in a number of centres in Europe and North America. The bulk forming of these alloys is only now receiving attention and has led to some innovative processing techniques.

The sheet forming of superplastic alloys is similar in many ways to the processing techniques used within the plastics industry. The zinc aluminium eutectoid alloy is commerically the most readily available material and has found many practical applications in the areas of enclosures for business machines, instrument and communications equipment, architectural panels [70, 71, 72] and artificial kneecap housings [73].

A promising new material for the sheet forming industry is an aluminium alloy, Supral 150, produced by TI Superform, a British company owned jointly by Tube Investments and British Aluminium [74]. The material is a laminate of a proprietory superplastic aluminium alloy clad on both sides with pure aluminium to improve corrosion resistance and

allow parts to be chemically brightened and anodized using standard techniques. This alloy has found commercial applications in the aircraft industry in the manufacture of components for an ejector seat [75]. Seat backrests for British Rail and heat shields for the exhaust systems of the Lotus sports cars have also provided a market for this material. Perhaps the most promising commercial application, however, is in the production of aluminium body panels for the exotic car manufacturers. The Aston Martin Lagonda [76] is presently being built with a complete set of 17 panels manufactured using the superplastic aluminium. In this market where the annual volume is not large, typically 500-2000 cars, and the traditional methods of manufacture involve the use of highly skilled labour, the superplastic thermoforming process shows great promise. There is little information in the scientific press concerning this alloy but it is probable that the central core is an aluminium copper eutectic which is superplastic at 932°F (500°C). This alloy and other aluminium alloys which can be rendered superplastic have been reviewed in a paper by Grimes et al. [75].

2.2.1 Bulk Forming

a) Forging

Most superplastic alloys are very suitable for hot forging since their fine grain structure apparently reduces any tendency to crack even when the upsetting ratios are large [62]. Sound forgings are produced using the conventional techniques of the non-ferrous industry. If, however, the strain rate in the process is reduced to the region where

the material strain rate sensitivity is high then attractive processing possibilities exist since the forging load is significantly reduced. The disadvantage, however, is that the process is isothermal and that at the appropriate strain rates the process will take some fraction of a minute to complete necessitating the heating of the dies to the appropriate temperature.

Moles [78] examined the forging of a turbine blade in a superplastic tin-lead and indicated that conventional flash gutters were inappropriate for the forging of superplastic materials.

Balliett et al. [79] have recently developed a two stage forging operation designed specifically for the forming of a superplastic alloy by utilizing the rate sensitive properties to advantage. The process consists of a moderately fast stroke to obtain most of the shaping followed by a dwell at constant load. In the latter part of the process material flows slowly at low stresses to fill the die completely and obtain a very precise impression. Figure 2.1 is a photograph showing some of the parts produced by this process at $482^{\circ}F$ ($250^{\circ}C$) in a commercially available Zinc Aluminium eutectoid alloy. The forging pressure was of the order of 30,000 lb/in^2 (207 MPa).

Commercially the zinc aluminium eutectoid alloy, with various additions of alloying elements to improve room temperature properties, is the most readily available superplastic alloy. Stewart [62] has published an extensive study of superplastic forging and the experimental work included the forging of a Zinc Aluminium part having sharp corners and thin webs. Examples of office equipment forged in

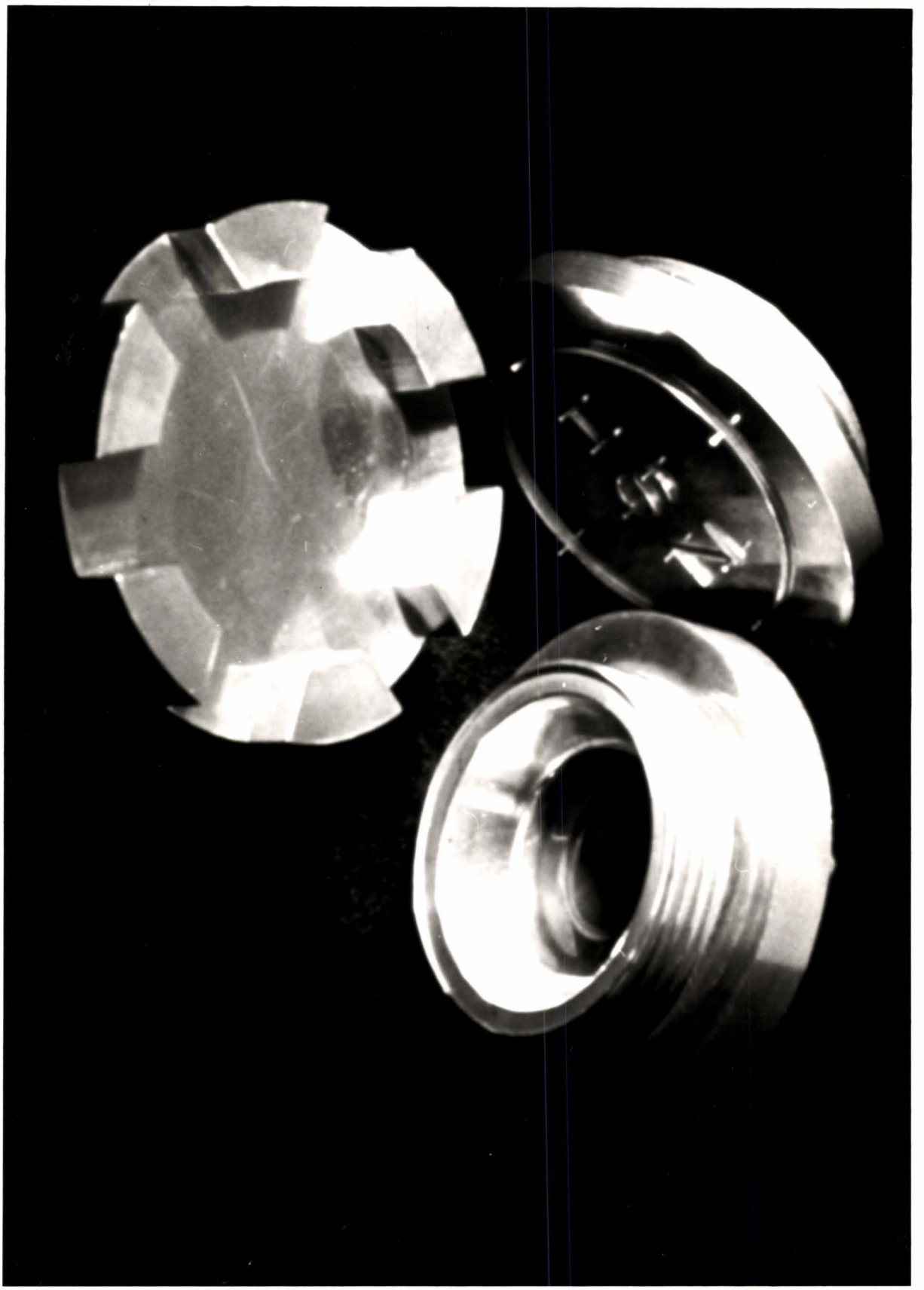

Figure 2.1

Some of the demonstration parts produced by Balliett et al. (79) in a superplastic high strength zinc alloy.

superplastic Zinc Aluminium have been presented by Fields and Stewart [81] while Duncan et al. [82] have mentioned the production of computer memory discs with a superplastic bronze.

Excellent detail can be achieved as demonstrated by the short run coining dies described by Saller et al. [60]. This particular application is of interest in that the ultra fine grain structure associated with the superplastic alloy produces a very high dynamic yield stress at room temperature. Consequently the dies stand up surprisingly well in coining in the drop hammer.

Moles [83] has indicated the economies of superplastic forging for the small industrial concern. Certain dies which are a precision product are normally manufactured by machining and subsequent engraving of the fine detail. In the process developed by Moles the final product is precision forged in Aluminium Bronze at 1200°F (650°C) where use is made of the low flow stress associated with superplastic behaviour [84]. It is anticipated that this process will reduce the cost of the final product significantly. Further investigations are being pursued in the commercial development of the closed die superplastic forging process of the Aluminium Bronze. Cox [85] has discussed the development of a superplastic forging process to 'set' a precision product where uniformity, consistency and repeatability of a prescribed shape are important.

Industrial interest and investment however appears to be directed toward the more exotic titanium alloys used in the aerospace industry [86, 87]. Innovative processing techniques are being developed which

include the simultaneous diffusion bonding and blow molding of sheet titanium [87] to produce hollow structural parts for the areospace industry.

Corti et al. [88] have recently published a study of the modelling of the metal flow during an isothermal superplastic forging process. The tin-lead eutectic, which is superplastic at room temperature, was used to model the material flow in a radial compressor blade which is normally produced by isothermal forging of nickel and titanium. The authors indicated the optimum preform geometry to ensure good die filling and uniformity of the deformation. Through a quantitative analysis of the local strain rates the authors were able to specify the forging press speed schedule to ensure that the strain-rates where within the range necessary for superplastic flow.

Commercial development of the superplastic forging process continues and it is anticipated that this novel technique will be increasingly applied to materials which are difficult to form by conventional methods and to precision applications where the annual volume is not large, Figure 2.2 illustrates some of the parts produced by superplastic forging.

b) Extrusion

Superplastic alloys can be hot extruded in the normal way and consequently there has not been any development of the extrusion process, as such, for this class of alloys. The extrusions of superplastic alloys have been used in interesting processing techniques and these are discussed below.

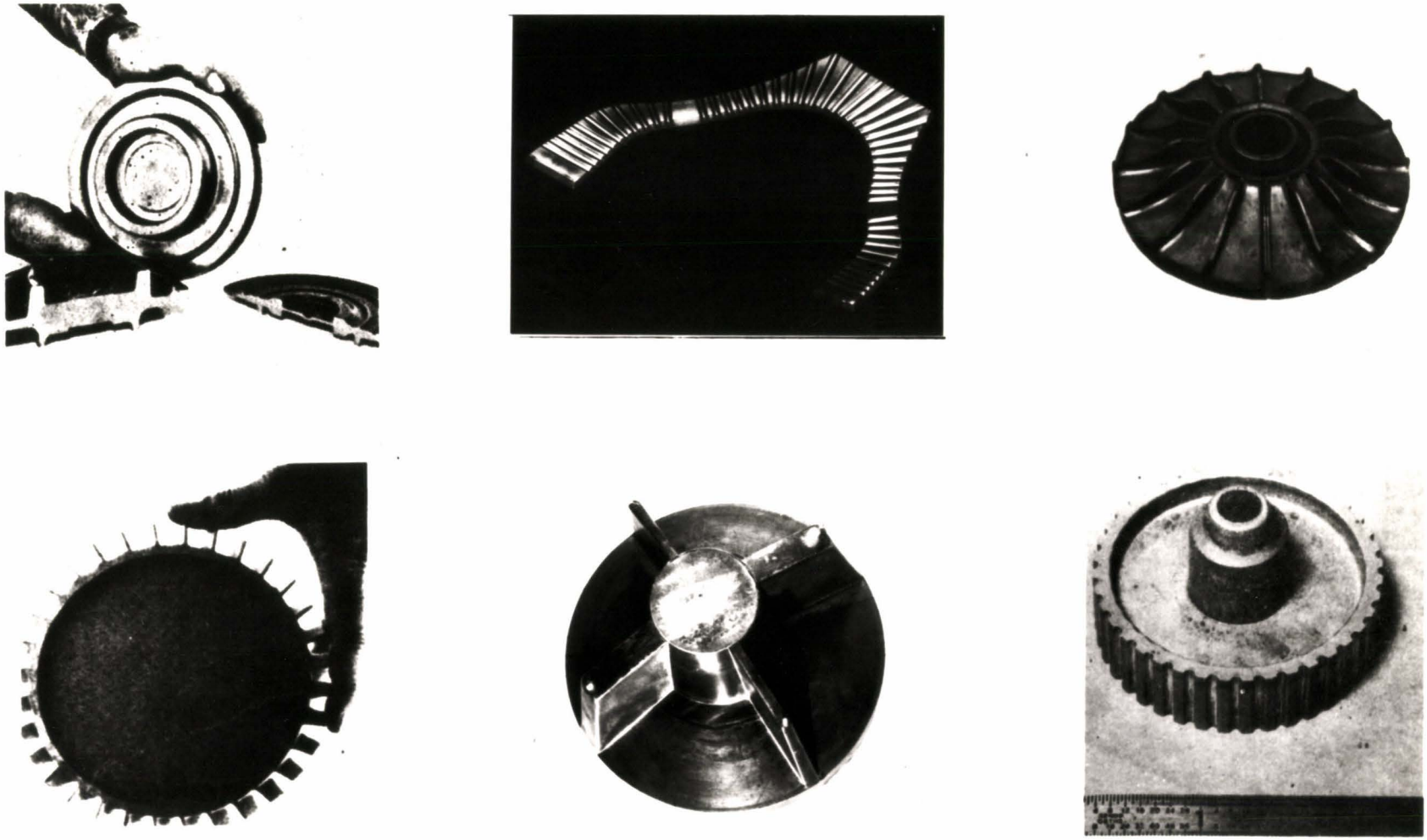

Figure 2.2

An array of parts formed by superplastic forging.

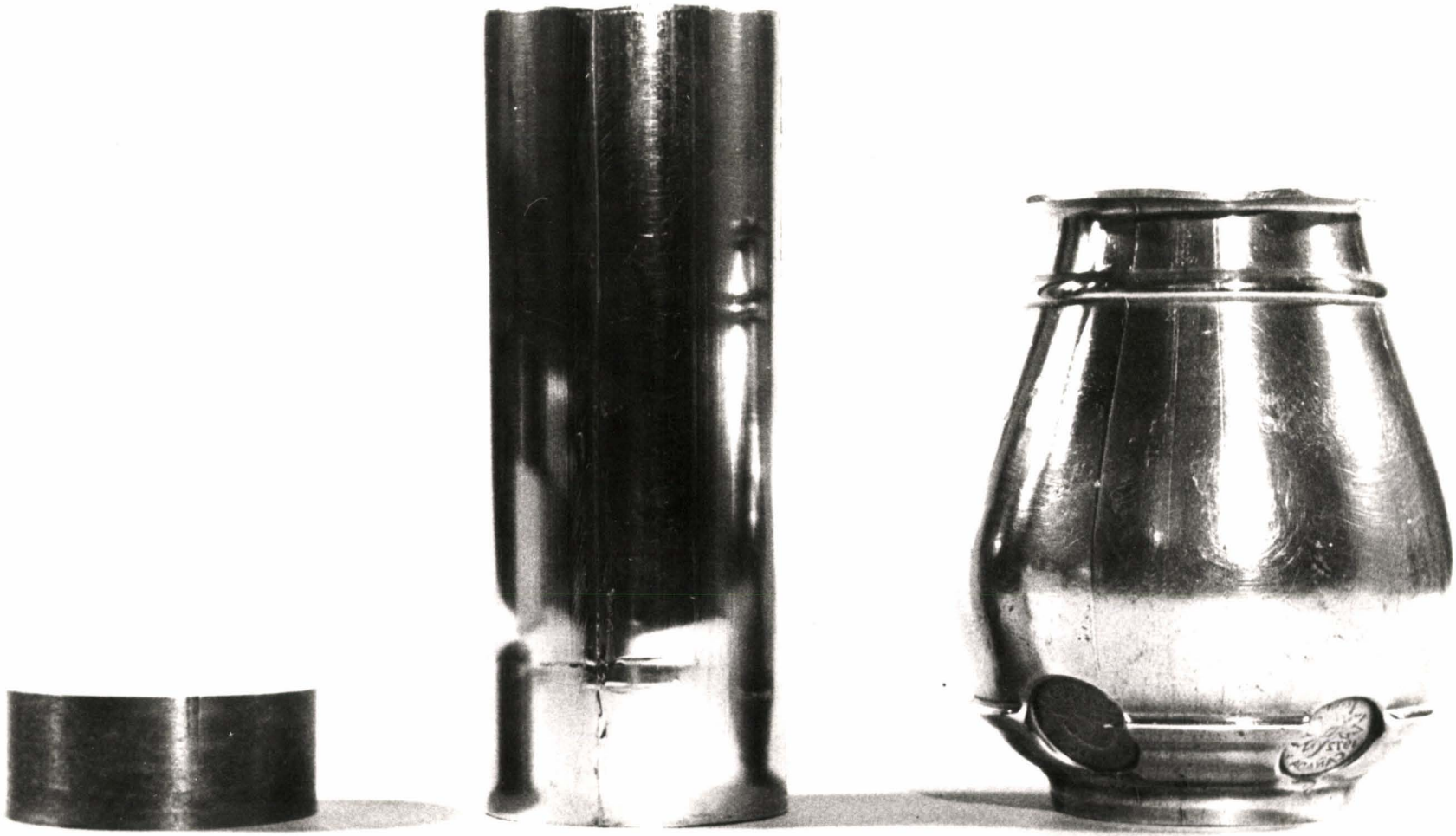

Figure 2.3

Photograph of a) billet, b) backward extruded cup, c) blow molded cup produced by Jain et al. (90)

Back extrusion of small billets has been used to produce cup shaped preforms for subsequent blow molding on a process first demonstrated by Thomsen [89]. Detailed experiments were described by Jain et al. [90, 91] who produced a 2 inch dia. (50.8 mm) Zinc Aluminium cup at a temperature of 482°F (250°C). The 2" dia. 3" deep and 0.07" wall cup (50.8, 76.2, 1.8 mm) was extruded in less than a minute with loads less than 50 tons (445 kN). The cup was subsequently blow molded as shown in Figure 2.3.

2.2.2 Summary of Commercial Applications

The commercial applications of superplasticity have become more than a research and development laboratory curiosity. The forming of superplastic sheet is becoming quite prevalent. The technology is being developed industrially as witnessed by the numerous reports of successful applications appearing in the technical literature. The bulk forming of these alloys has indicated some novel processing techniques especially with regard to forging where advantage can be made of the high strain rate sensitivity at low forging rates. The commercial extrusion of these alloys has not presented the engineer with any significant problems and there has consequently been no need for innovation at this level.

2.3 Survey of Theoretical Work

Extrusion, forging and hot rolling are compressive in nature and the prediction of forming loads is of technological importance. With

rigid, perfectly plastic materials which do not strain harden and in processes which are isothermal a value can be obtained for the forming load by a number of analytical techniques. This is generally expressed in the form of a non-dimensional ratio $\bar{p}/2k$, where $\bar{p}$ is the forming pressure and 2k is the plastic flow stress: k is the yield shear stress. With rate dependent materials however there is no single forming load but rather a relation between the applied load and the forming speed. Comparatively little attention has been given to this forming problem perhaps because in the hot extrusion of metals the material properties are only weakly rate sensitive. The emergence of the superplastic materials has, however, renewed interest into analytical methods capable of predicting the material behaviour for rate sensitive materials. In the work reviewed here the material is considered as a continuum and no attempt is made to examine the deformation in terms of the microscopic structure. The microscopic mechanisms of hot working and rate dependent flow are reviewed by Sellars and Tegart [92] who have examined the effect of strain rate and temperature on the metallurgical aspects of hot working.

The strain rate during the extrusion of conventional alloys was first considered by Feltham [93] who indicated that if Siebel's uniform work principle is accepted and the work done by the extrusion ram is equated to that necessary to cause a similar change of shape in a tensile process then the extrusion pressure is given by:

$$\sigma_{ext} = Y_m \ln (ER) \qquad (2.2)$$

where ER is the extrusion ratio and Y_m is the tensile yield stress and is assumed constant.

For extrusion at high temperatures or for materials which are rate sensitive Y_m is not constant and is a function of strain rate and temperature. Feltham indicated that the average strain rate could be evaluated by dividing the total strain, estimated from the overall change in dimensions of the work piece, by the time an element takes to flow through the deformation region. The shape of the deformation zone was assumed to be the frustum of a cone defind by generators touching the die orifice at 45°. The strain rate is then given by:

$$\dot{\bar{\varepsilon}}_m = \frac{6V}{D} 2 \ln (D/d) \tag{2.3}$$

where the variables are defined in Figure 2.4.

Wilcox and Whitton [94] extended this principle and indicated that a more general mean strain rate is given by:

$$\dot{\bar{\varepsilon}}_m = \frac{6VD^2 \ln (ER)}{\cot \alpha \, (D^3-d^3)} \tag{2.4}$$

where α is the semi-die angle. For dies of large semi angle, a virtual die angle would have to be assumed based on the boundary formed by the dead metal zone. In the analyses of Feltham and Wilcox and Whitton the objective had been to define a mean yield stress at the appropriate temperature and strain rate. Hodierne [95] has pointed out that care must be taken in deciding upon the parameter with respect to which the mean is to be taken. He considered the mean strain rate with respect to displacement through the deformation zone to be more appropriate, i.e.

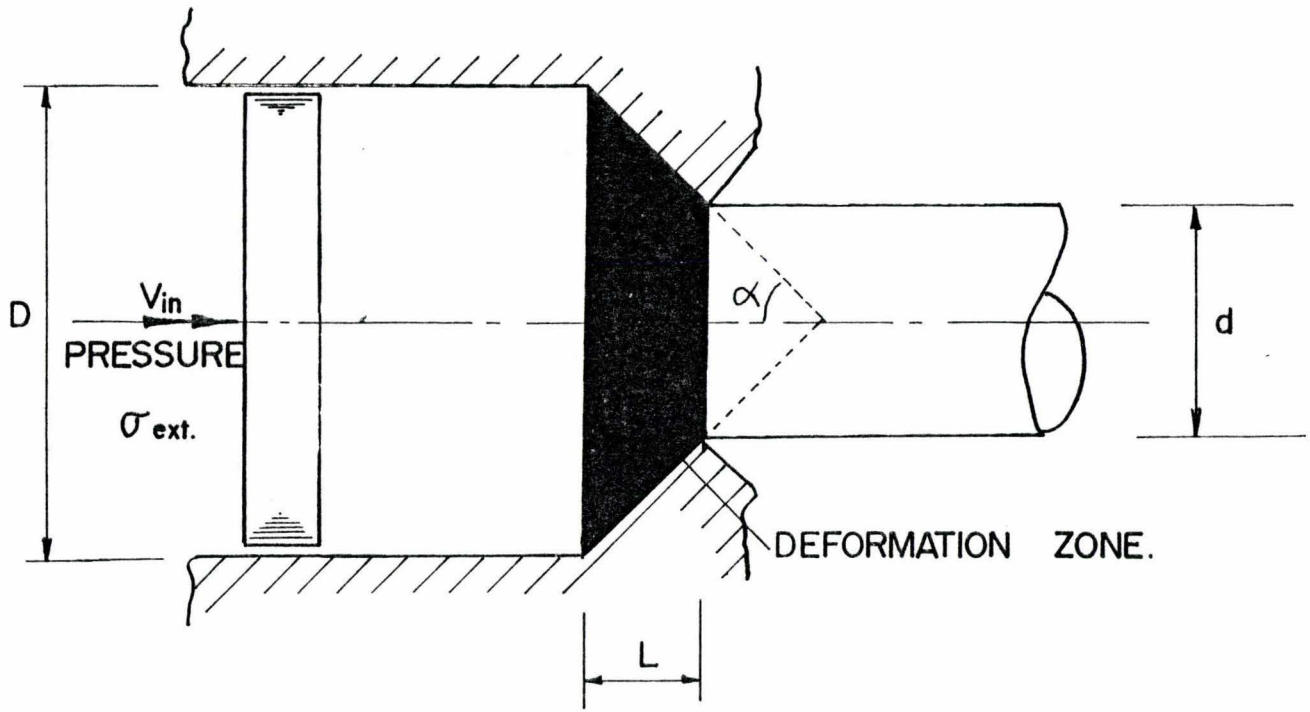

Figure 2.4

Deformation zone geometry defined by Feltham [93]
indicating variables

$$\dot{\bar{\varepsilon}}_m = \frac{1}{x} \int_0^x \dot{\varepsilon}\, dx \tag{2.5}$$

where x is the axial distance through the die zone. For axisymmetric extrusion of a bar the mean is given by:

$$\dot{\bar{\varepsilon}}_m = \frac{2V\,(D+d)\,\tan\,\alpha}{d^2} \tag{2.6}$$

where the symbols have the usual meaning.

For the case of extrusion with large reductions Hodierne's estimate, eqn. (2.6), can give strain rates an order of magnitude greater than those averaged with respect to time given by Feltham et al. Hodierne's averaging technique is further supported by Blazynski [96] who studied tube making and wire drawing, and Atkins [97] who examined sheet and wire drawing.

The discussion of an appropriate mean strain rate was continued by Chandra and Jonas [65] who introduced a mean strain rate which was derived from a material constitutive equation of the form given by eqn. (2.1). Their relation for the mean strain rate is,

$$\dot{\bar{\varepsilon}}_m = 4VD^2 \tan\,\alpha \left\{ \frac{2}{3m\,\ln(ER)} \left[\left\{ \frac{1}{d} \right\}^{3m} - \left\{ \frac{1}{D} \right\}^{3m} \right] \right\}^{1/m} \tag{2.7}$$

This equation gave values of the strain rate three orders of magnitude higher than those indicated by Wilcox and Whitton. Strain rates were calculated and compared with equivalent values given by the Wilcox and Whitton formula. For the extrusion of ice at $14^{\circ}F$ ($-10^{\circ}C$) it was shown that the extrusion pressure was from 4 to 58% higher if the

rate sensitivity of the material was considered in the analysis. Equation (2.7) was derived from a consideration of the uniform work method which gives the homogeneous extrusion pressure. To account for the redundant work it has been accepted that a "shear factor" or "efficiency" is introduced into equation (2.2) which is normally of the order of 1.5. Chandra and Jonas consider that this factor may in fact represent two corrections: a minor component due to the extra shear strain associated with the redundant work and a major one which is related to the rate sensitivity.

Atkins [97] has presented an analysis based on the determination of forces where an empirical equation of a more general form is used, i.e.

$$\bar{\sigma} = A\ \varepsilon^{n}\ \dot{\varepsilon}^{m} \tag{2.8}$$

In this paper Atkins confined his examination to the cold working of metals and assumed that temperature effects are neglible. The results were presented in the form of a correction factor dependent upon the material, the extrusion ratio, the semi die angle and the ram velocity. However, no comparison of predicted and experimentally determined forces was presented. Atkins did indicate, however, that the rate sensitivity of material behaviour may not be limited to the case of hot working where recrystalization reduces the effect of work hardening, but must be considered in the analysis of cold working process. One of the processes Atkins examined was wire drawing and the mean strain rate, taken with respect to distance through the die, is given by

$$\dot{\bar{\varepsilon}}_m = \frac{2V \tan \alpha}{D}\left[1 + \left\{1 - \frac{1}{ER}\right\}^{1/2}\right] \tag{2.9}$$

Ragab and Duncan [11] examined the unsteady transient backward extrusion of a rate sensitive material. The slip line field for a rigid plastic material was assumed to remain unchanged due to the rate sensitivity of the material and was used to define the velocity field and hence the volume of deformation. The time taken for unit volume to flow through this deformation zone was determined and a mean strain rate identified as:

$$\dot{\bar{\varepsilon}}_m = \frac{\bar{p}}{2k} \cdot \frac{\dot{Q}}{Q_D} \tag{2.10a}$$

where $\bar{p}$ is the extrusion pressure

k the yield shear stress

$\dot{Q}$ the volume flow rate

Q_D the volume of the deformation zone.

and the value of $(\bar{p}/2k)$ was determined, as for a rigid perfectly plastic material, by the slip-line field analysis. Consideration of the equilibrium of the process led to the derivation of a non-dimensional rate sensitive extrusion parameter of the form:

$$\frac{\bar{p}}{\sigma_o (v/h)^m} \tag{2.10b}$$

It was shown that this parameter was a function of a geometric factor and the strain rate sensitivity index m. The variation of the load in the backward extrusion process as the ram moved in the die was

considered and the analysis provided an explanation for the apparent steady state observed for the extrusion of rate sensitive materials. Using the analysis presented design charts could be constructed to give the extrusion parameter, defined by eqn. (2.10(b)), for a given geometry and strain rate sensitivity. Good correlation was obtained between experimental and theoretical curves for the backward extrusion of cups in the zinc aluminium eutectic alloy at 482°F (250°C).

Fenton et al. [38, 98, 99] have presented a number of solutions which pertain to the determination of loads in the extrusion of rate-sensitive materials. In an early analysis [38] a numerical method was proposed based on the modified Henky and Geringer equations for solving plane strain flow problems. The computation, however, can only proceed if the flow stress distribution is known. The initial flow stress distribution is therefore assumed constant and the slip-line field computed. The velocity and strain rate fields are re-evaluated and a new approximation to the flow stress distribution determined based on the flow law,

$$\bar{\sigma} = \sigma_o \, (1 + C \, \dot{\bar{\varepsilon}})^{0.05} \qquad (2.11)$$

A new slip-line field is generated based on the new flow stress distribution and the iterative process continued until the difference between successive solutions is less than 5% for the velocity field and 1% for the stress field. Computed results for the extrusion pressure were presented but no comparison was made with experimental results or any indication given as to the effect of rate sensitivity on the

velocity field, stress distribution or extrusion pressure.

In a further paper Fenton [98] used the upper bound technique to determine the load in the forward extrusion process. The concept of a thin deformation zone was introduced across which the tangential velocity changed thus enabling the strain rate to be evaluated. The strain rate was used to determine the constants for substitution into a flow stress equation first suggested by Swift [100], i.e.

$$\bar{\sigma} = \sigma' \bar{\dot{\varepsilon}}^{n} \tag{2.12}$$

The coefficient σ' and exponent n are functions of the strain rate. The experimental work of Bailey and Singer [101] and Alder and Phillips [102] was used to determine the values of functional relationships for σ' and n for pure lead and aluminium.

For lead

$$n = \log 1.67\, \bar{\dot{\varepsilon}}^{0.011} \qquad \sigma' = 3225\, \bar{\dot{\varepsilon}}^{0.0503}$$

For aluminium (2.13)

$$n = \log 1.655\, \bar{\dot{\varepsilon}}^{0.00855} \qquad \sigma' = 24000\, \bar{\dot{\varepsilon}}^{0.02155}$$

Fenton used the concept of a finite shear zone width to determine the strain rate associated with each discontinuity and then evaluated appropriate values for n and σ'. The results of the computation were compared with experimental results reported in the literature and shown to be in good agreement. However, the materials considered are only very midly rate sensitive and no indication was given of the variation of the extrusion pressure for superplastic materials; i.e. materials with a strain rate sensitivity greater than 0.3.

Tang [103] has developed a three dimensional theory of superplasticity based on the Parker-Sherby flow law, i.e.

$$\dot{\varepsilon} = \frac{A\,\sigma^2}{L} + B\,\sigma^2 \sinh\,(C\sigma^{2.5}) \tag{2.14}$$

where $\dot{\varepsilon}$ is the true strain rate, σ the true stress, L the grain size and A, B and C material constants at a given temperature. An analysis for the flow through a rectangular and circular orifice was presented and the steady state velocity profile at the orifice for the flow of a superplastic tin-lead eutectic determined for different steady state pressures. The drawing and extrusion of a rate sensitive material through cone-shaped dies has also been examined by Tang [104]. The flow is assumed to be radial towards the apex of the conical die and stress and die pressure distributions determined for extruding with coulomb friction. No experimental data was presented or any attempt made to correlate the results with data available in the literature.

The plastic flow through conical dies for a material with a viscoplastic constitutive equation has been examined by Cristescu [69]. The extrusion of a material with a Bingham-type constitutive equation of the form:

$$\dot{\bar{\varepsilon}} = \frac{1}{\eta} f\,(\bar{\sigma}) \tag{2.15}$$

was examined where η is the viscosity. The theory developed depends essentially on the speed of the process and Cristescu indicated that the extrusion pressure increases with working speed or with an increase in fractional reduction. The increase was more significant for high

reductions and semi-cone angles.

Wong and Jonas [105] have presented an analysis for the extrusion of aluminium which is based on the metallurgical mechanisms of deformation. The velocity, temperature and pressure are related by an equation of the form

$$V = A\,[\sinh(\alpha\,\bar{p})]^{n} \exp\frac{-\Delta H}{RT} \qquad (2.16)$$

where A, α n are constants determined experimentally, ΔH is the activation enthalpy determined experimentally in a similar process, R is the universal gas constant, T the absolute temperature and V the ram velocity.

While equations of this form have been used extensively to correlate creep data [106], results from hot torsion tests [107] and extrusion results [108], the basis is essentially an experimental one. The application of this form of correlation has been successful and a number of papers are available in the literature especially with regard to the aluminium alloys [107-110]. However, this type of analysis, since it is essentially one of curve fitting can be applied to any material.

Tomita et al. [111, 112] have developed an approximate numerical scheme, using the finite element technique, for analysing the deformation of materials obeying eqn. (2.1). Plane stress and plane strain problems were considered and results presented for the velocity, strain rate and stress distributions. The side extrusion process was examined as an example of a plane strain process. The flow patterns and

representative strain rate distribution for a number of billet heights were presented and Tomita indicated the form of the pressure variation as the ram moved into the die. Friction was incorporated into the analysis by assuming a frictional stress which was a constant fraction of the current shear stress of the material. No comparison of the theoretical results with experimental data was presented.

The direct extrusion of a rate sensitive material through conical dies has been considered by Ragab and Baudelet [180]. The slab technique was utilized to estimate the force required to extrude a material whose mechanical behaviour is described by an equation of the form

$$\sigma = \sigma_o \sinh^{-1} (\dot{\varepsilon}/\dot{\varepsilon}_o) \qquad (2.17)$$

The analysis is similar to that presented by Chandra and Jonas [65] and an identical expression for the mean strain rate is obtained if a constitutive equation of the form of eqn. (2.1) is assumed.

The effect of friction was considered and experimental results for the extrusion of a superplastic tin lead alloy agreed well with the theoretical predictions.

The following analyses do not deal with rate sensitive materials in particular however similar methods could be used for any group of alloys. Hirst and Ursell [113] have presented design charts for the extrusion process which are a function of the extrusion ratio and the billet preheat temperature. Limitations on the extrusion ratio imposed by the geometry and preheat temperature of the billet are expressed in the form of a family of curves. The maximum reduction is restricted by

an unacceptable temperature rise due to the heat generated during plastic deformation and this can also be expressed by a family of curves. An enclosed area is thus defined on a graph of extrusion ratio against preheat temperature within which extrusion is possible for any given conditions. Based on empirical laws and data from compression tests, curves were produced which compared well with experimental data. It should be noted that these curves are generated for use within the extrusion shop to indicate the maximum speed, for a given extrusion ratio, which will produce a satisfactory product. The diagram, itself does not indicate the extrusion pressure or the flow geometry within the extrusion die. Meadows and Cutler [114] produced a similar skeleton diagram for Al-Mg-Si alloys and indicated good correlation with industrial results.

Farmer and Pirog [50] examined the forward extrusion of aluminium and investigated the effects of extrusion ratio, die angle and billet length to billet diameter ratio on the extrusion pressure. A design chart was presented which consists of a basic extrusion pressure curve at a given set of conditions and a series of correction factor curves, based on the initial conditions, to determine the effect of each of the variables. The extrusion pressure is thus obtained by determining the basic extrusion pressure for the given extrusion ratio and material through a 180° die with a billet length to diameter ratio of 1. Corrections are then made according to the actual die angle, the initial billet to length ratio, and the friction conditions.

2.3.1 Summary of Theoretical Studies

The effect of strain rate on the extrusion pressure has been known for some time. It has been accomodated within the simpler theories of metal deformation by the evaluation of a convenient mean strain rate for the process or the addition of an efficiency or redundant work term. The development of the superplastic alloys has stimulated further research into the mechanics of hot deformation processes and the effects of strain rate. The theories developed by Tang, Cristescu and Chandra have not been supported by extensive experimental work and may be too complex for application in the industrial situation.

The work of Hirst and Ursell, and Meadows and Cutler tends towards fulfilling the industrial need for simple diagrams indicating the limiting factors affecting the process. The work of Farmer and Pirog while being essentially a series of corrections for each variable is again a useful tool for the commercial extrusion shop. However, the major disadvantage of these methods is that they do not convey an appreciation of the essences of the extrusion process and must be evaluated and documented for each material requiring the investment of a large amount of time and money.

2.4 Experimental Work

There is a dearth of knowledge in the literature on the extrusion of highly rate sensitive materials and the variation of extrusion pressure with rate sensitivity and velocity.

Jovane et al. [52] investigated the extrusion of the tin-lead eutectic in the as-cast and superplastic conditions and compared the velocity fields with those obtained for lead. The visioplasticity technique [115] was utilized and the velocity fields determined through a 45° conical die at extrusion ratios of 2 and 4 and a ram velocity of 0.003 ins/min. (.00127 mm/sec). The small differences observed in the flow geometry were attribued to differences in the boundary friction and Jovane concluded that the experiments supported the thesis that the flow field, within a plastically deforming material is essentially unique for identical boundary conditions.

Shabaik and Virani [63] used the superplastic eutectic tin-lead alloy as a model material for the hot extrusion of steel and showed that the flow patterns were identical if dynamic similarity were achieved. The flow lines, flow function and velocity components were compared, using the results of a visioplastic analysis of the deformed grids, for the hot extrusion of steel at $1800^{\circ}F$ ($982^{\circ}C$) and 10 inch/sec (254 mm/sec), and the superplastic eutectic of tin lead at room temperature and 0.088 inch/min (.037 mm/sec). At the conditions inidicated above the stress strain rate behaviour for the two materials is characterized by an equation of the form of eqn. (2.1).

Recall $\bar{\sigma} = \sigma_o \dot{\bar{\varepsilon}}^m$

For the steel $\sigma_o = 15400$ lb/in^2 sec^m $m = 0.145$

$\sigma_o = 106$ MPa sec^m

For the tin lead $\sigma_o = 17100$ lb/in^2 sec^m $m = 0.15$

$\sigma_o = 118$ MPa sec^m.

Shabaik and Virani concluded that for dynamic similarity of the flow fields dynamic similarity of the mechanical properties is necessary in the form of identical strain rate sensitivities.

Chandra and Jonas [66] have described experiments in which ice was extruded by the indirect process through a 45^o conical die and extrusion ratios in the range

$$4 < ER < 144$$

Two series of extrusion tests were conducted. In the first the crosshead velocity was determined such that the mean strain rate, as defined by the Wilcox and Whitton formula, eqn. (2.4), was equal to 1.1 * 10^{-3} per sec. The crosshead velocity in the second series of experiments was determined using the Chandra and Jonas formula, eqn. (2.7), such that the mean strain rate was again 1.1 * 10^{-3} per sec.

The strain rate sensitivity assumed for the ice was 0.2. No information, however, was given regarding the flow stress constant, σ_o, or the determination of the material properties. Comparison of the theoretical and experimental curves indicated that the Wilcox and Whitton formula for the mean strain rate underestimated the flow stress by between 4 and 54%. The mean strain rate however, as developed by

Chandra and Jonas, gave excellent correlation between experimental and theoretical curves, especially at the higher extrusion ratios.

Shabaik and Thomsen [117] have presented a visioplastic analysis of the axisymmetric forward extrusion of lead. Small die angles and extrusion ratios were used and the velocity field determined experimentally. Two different material behaviour equations, namely:

$$\bar{\sigma} = \sigma_o \dot{\bar{\varepsilon}}^m$$
$$\bar{\sigma} = \sigma_o \bar{\varepsilon}^n \qquad (2.18)$$

were examined and the effect of material properties on the stress distribution determined. The authors concluded that the effect of material properties on the stress distribution appeared to be of minor consequence.

The reverse extrusion and blow molding of a eutectoid zinc aluminium alloy was studied by Jain et al. [58, 90]. Reverse extrusion is a transient unsteady process however Jain indicated a relationship between the extrusion velocity and pressure which was identical to that for the material stress strain rate properties, i.e.

$$\bar{p}_{ext} = A\, V^{m'} \qquad (2.19)$$

where A and m' are constants, V is the ram velocity and $\bar{p}_{ext}$ is the extrusion pressure. The value for the velocity sensitivity index however, was not identical to that in the material property equation; Table 2.1 summarizes the results obtained by Jain. The effect of ram profile geometry was investigated and it was concluded that the shape of

the ram corner had a signficant effect on the ram load. A chamfer in the range 45^{o} to 50^{o} was considered to be an optimum.

Material and condition	Material behaviour $\sigma = \sigma_o \dot{\bar{\varepsilon}}^m$	Ext. Ratio	Material extrusion behaviour $\bar{p} = AU^{m'}$
Zn-Al As Cast	σ_o = 12000 lb/in^2.sec^m		A = 300 x 10^3 lb/in^2.sec^m
		8.3	A = 2065 MPa sec^m
	σ_o = 82.7 MPa sec^m		m' = 0.28
	m = 0.18		A = 278 x 10^3 .b/in^2.sec^m
		20	A = 1917 MPa sec^m
			m' = 0.16
Zn-Al Superplastic	σ_o = 13000 lb/in^2.sec^m		A = 138 x 10^3 lb/in^2 sec^m
		8.3	A = 952 MPa sec^m
	σ_o = 89.6 MPa sec^m		m' = 0.28
	m = 0.39		A = 342 x 10^3 lb/in^2 sec^m
		20	A = 2356 MPa sec^m
			m' = 0.3

TABLE 2.1

Material property constant and inverted extrusion constants for reverse extrusion of Zn-Al at 250^{o}C.

2.4.1 Summary of Experimental Work

The extrusion of rate sensitive alloys has not been studied extensively. The work of Jovane et al. [52], Ragab [11], Jain [58, 90] and Shabaik [63] have each examined a single alloy at particular extrusion ratios and speeds. A comprehensive study of the extrusion of these alloys has not, to the authors knowledge, been undertaken or published.

The work of Chandra and Jonas [66], while indicating the care with which the mean strain rate must be selected, compared results for ice which is only marginally rate sensitive with a reported value of m = 0.2. No data was published concerning the constants in the flow stress equation and it is difficult to compare the results with other thoeries. The work of Shabaik and Thomsen [117] used lead to define the flow field and then proceeded to use different material behaviour laws to predict the stress distribution. The fact that different material behaviour equations produce nearly identical stress distributions led Shabaik and Thomsen to conclude that the stress distribution is independent of material properties and is only a function of the geometry of the process. This conclusion however, is based on the flow field determined for a non-hardening rate insensitive material, and consequently, the authors are in error in applying formula for different material behaviour. They assume, implicitly, that the flow geometry is independent of material properties and this, although intimated by Jovane et al. [52], is not valid and is discussed in the next section.

2.5 The Effect of Material Properties on the Velocity Field and the Deformation Zone

In the preceeding section it was indicated that a number of researchers have assumed the invariance of the velocity field and deformation zone geometry with respect to velocity and material properties. In the following section this assumption is examined and information reported in the literature, for a variety of materials

extruded commercially, is reviewed and discussed.

The effect of velocity and material properties in any deformation process is a complex one involving the combined effects and interactions of the velocity on each of the following:

1) the variation of the flow stress with strain-rate.
2) the variation of flow geometry with velocity and material properties.
3) the variation of temperature within the deformation zone and its effect on 1) and 2)

2.5.1 The Variation of the Flow Stress with Strain Rate

The effect of velocity or strain rate is dependent on the testing temperature, the particular strain rate regime and the class of alloys. For the hot isothermal working of materials and the superplastic deformation of certain alloys the flow stress and strain rate can be expressed by equation (2.1). Recall

$$\bar{\sigma} = \sigma_o \dot{\bar{\varepsilon}}^m$$

Values of the strain rate sensitivity for some alloys and the temperature at which they apply are indicated in Table 2.2. For superplastic alloys at a processing temperature of approximately half the absolute melting point the rate sensitivity is typically in the range:

$$0.3 < m < 0.7$$

Material	Temperature °F	Strain rate sensitivity
Pb Sn eutectic	70 (20°C)	0.5
Zn-Al eutectic	480 (250°C)	0.5
Mg - 6% Zn - 0.5% Zr	520 (270°C)	0.6
Al-Cu eutectic	960 (500°C)	0.9
low alloy steels	1470 (800°C)	0.65
Ti - 6% Al - 4% V	1830 (1000°C)	0.85

TABLE 2.2

Some alloys and the values of the strain rate sensitivity for particular temperature when the material behaviour is characterized by $\sigma = \sigma_o \dot{\varepsilon}^m$.

2.5.2 The Variation of Flow Geometry with Velocity and Material Properties

The literature concerning the effects of velocity on the flow geometry in the extrusion process is contradictory. Firsch and Thomsen [40] examined the indirect extrusion of lead at room temperature with ram velocities of 0.1, 0.74 and 5.15 inch/min (.042, 0.313, 2.18 mm/sec). The flow geometry was determined using the visioplasticity technique and it was concluded that the flow geometry was invariable with respect to the velocity.

Thomsen and Firsch [116] also determined the velocity field, using the visioplasticity technique, for the axisymmetric inverted extrusion of aluminium at room temperature through a square die. The extrusion ratio was 8.25 and the ram velocity 0.045 inch/min (0.019 mm/sec). The flow patterns obtained were compared with those for lead [40] and found to be identical. The extrusion studies by Jovane et al.

[52] also indicated the invarience of the flow pattern for a super-plastic tin lead eutectic and pure lead at small extrusion ratios and through a 45° conical die at very slow speeds.

Shabaik and Thomsen [117] examined the direct extrusion of lead and confirmed that the steady state flow field did not change when the ram speed was varied. However, whilst this work does indicate a further application of the visioplasticity technique the conclusion of the invarience of the velocity field with ram speed and material properties is questionable. The visioplasticity technique uses experimentally determined grid distortions to define the flow function and hence the strain rate field. The material used by the investigators was pure lead a non-hardening, rate insensitive material in a direct extrusion process with conical dies of 25, 35 and 45 semi-die angle through extrusion ratios of 2, 3 and 4. These conditions are not very severe and one would not expect significant changes in the velocity distribution. The same comment is equally applicable to the work of Frisch and Thomsen [40] mentioned above.

The hot extrusion of copper at 800°F (427°C) and steel at 1800°F (982°C) through conical dies was investigated by Altan et al. [118]. Comparisons of the effective strain distributions for the two materials led the authors to conclude that the effect of ram velocity was neglible. Small variations in the deformation patterns for steel and copper extruded under identical conditions was attributed to the geometry of the process.

There is evidence in the literature which indicates that the

deformation zone geometry is not independent of material properties and this is now reviewed. The effects of temperature and speed on the warm extrusion of steel led Singh et al. [119] to conclude that at higher velocities the deformation in the extruded product was more uniform. This conclusion was not substantiated by experimentally determined flow fields but was based on a qualitative assessment of distorted grid patterns.

Medrano et al. [53] and Hinesley and Conrad [108] have both examined the occurance of a double maxima flow pattern observed in the extrusion of some aluminium alloys. Two flow patterns are observed as shown in Figure 2.5, one with the more commonly observed single maximum and the other, less common type, where two maxima occur symmetrically about the extrusion axis separated by a minimum at the axis. Medrano et al. [53] concluded that the deformation zone geometries were quite different for the two cases, as shown in Figure 2.6, and that the geometry of flow was dependent on:

a) the temperature and ram speed

and b) that friction was a secondary effect.

Hinesley and Conrad [108], examining the same phenomenon, indicated that the change of the deformed grid from a single to a double maximum pattern occured at approximately a constant value of the Zener-Holloman parameter. They concluded that the very appreciable changes in the flow pattern are mainly related to the material plastic flow behaviour.

Farag and Sellars [120] also conducted a visioplastic analysis of

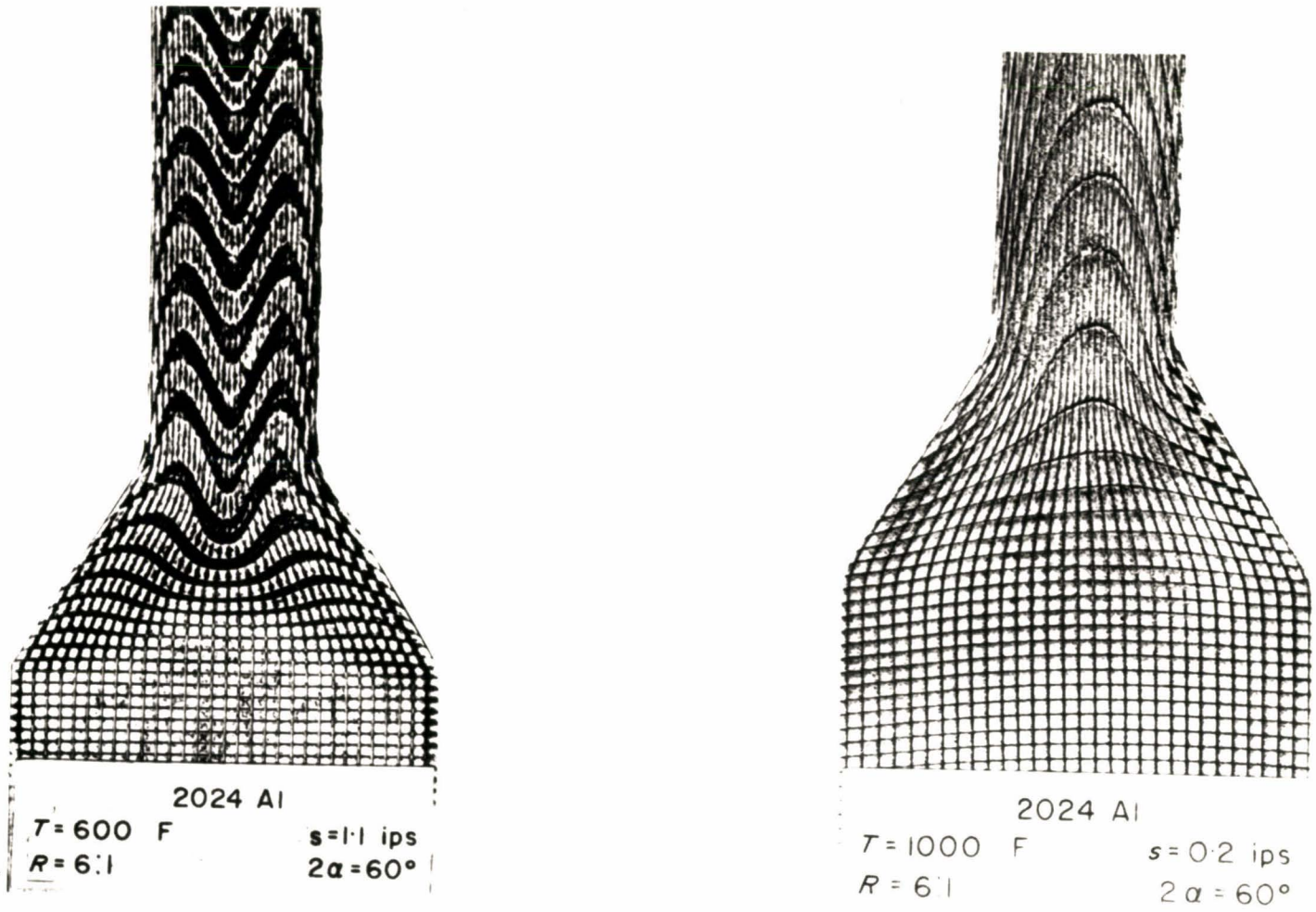

Figure 2.5

Grid distortions obtained with aluminium alloys showing single and double maxima flow patterns: from ref. [53]

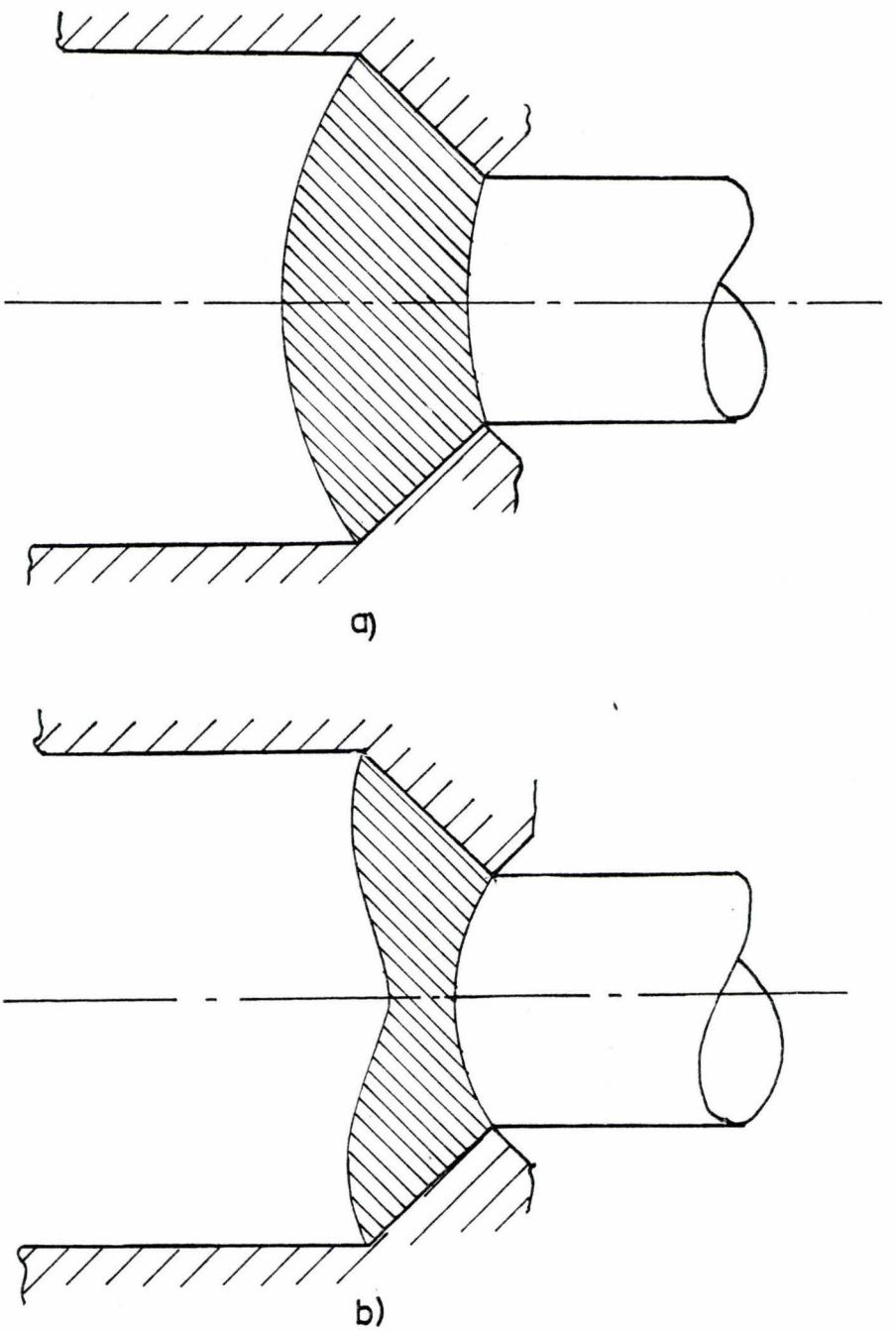

Figure 2.6

Deformation zone geometries for the formation of the different flow patterns

the deformation of an aluminium alloy which exhibited the double maxima flow pattern and concluded that

a) the patterns were more pronounced at higher speeds.

b) that while the phenomena occured in the silicon, magnesium, manganese alloy tested it did not occur in pure aluminium and that consequently the flow is related to the negative strain hardening characteristic of the alloys studied.

c) agreed with the concept of a change in the flow geometry at a particular value of the Zener Holloman parameter as proposed by Hinesley and Conrad [108].

It is interesting to note that Zimmerman and Avitzur [121] and Lambert and Kobayashi [54] have predicted similar changes to the geometry of the plastic zone due to changes in the interfacial friction. Figure 2.7 indicates the plastic zone boundaries presented by both authors for low and high friction conditions. Gurney and De Pierre [122] investigated the effects of friction on the plastic zone geometry and its effect on the production of the central bursting defect. They indicated that for low frictional restraint the central burst defect was likely to occur. High interface friction however increased the compressive state in the deformation zone and thus reduced the tendancy for tensile failures. Gurney and De Pierre concluded that the shape of the plastic zone is dependent on the ratio of the interfacial restraint to the flow stress of the material.

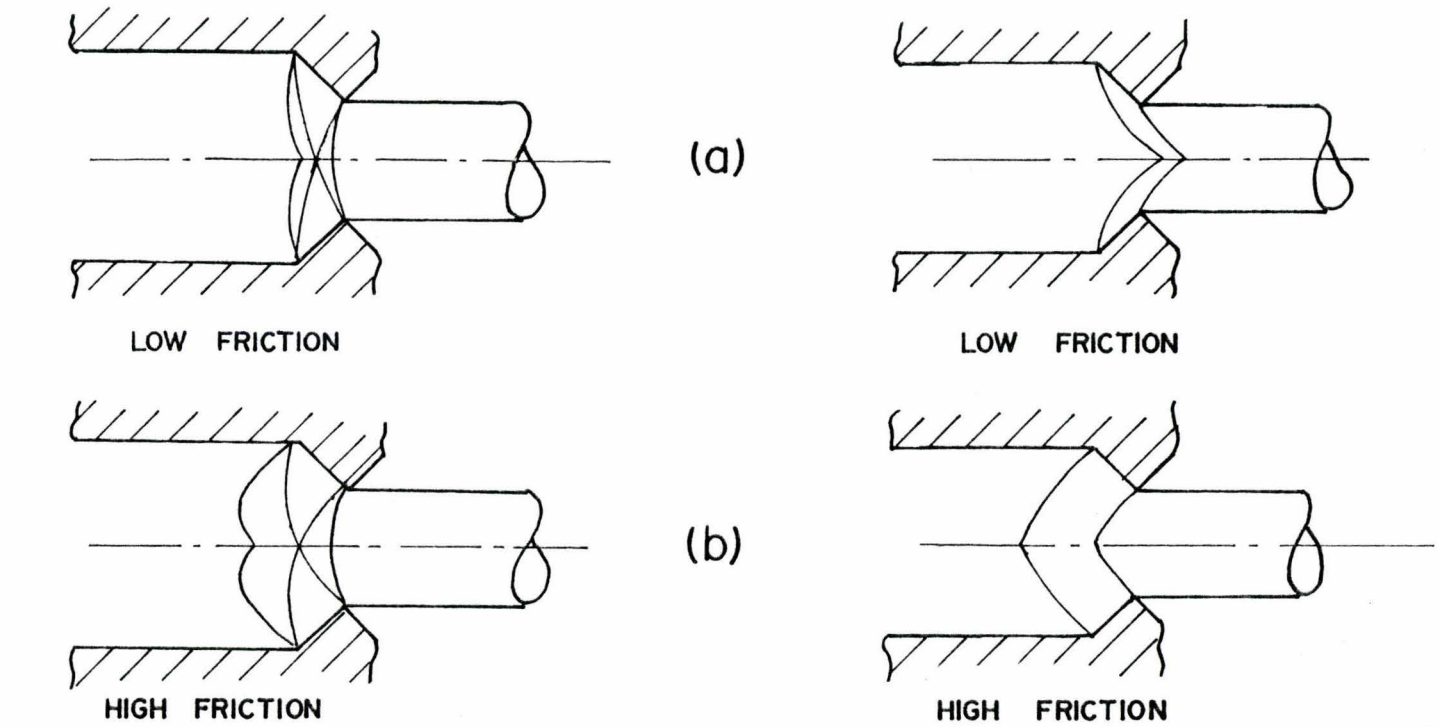

Figure 2.7

Plastic zone geometries proposed by Lambert and Koboyashi [54] and Zimmerman and Auitzur [121] for extrusion through conical dies with a) low interfacial friction b) high interfacial friction

2.5.3 The Variation of Temperature within the Deformation Zone and its Effect on Material Properties and Flow Geometry

The variation of material properties with temperature is well known, however the point to point variations of temperature within a plastically deforming material is not well defined. The problem is a complex one of heat generation, and conduction within a moving body. Analyses have been presented for the evaluation of the temperature and the temperature distribution in steady state and unsteady flow conditions but they will not be reviewed here.

The variation of the deformation zone geometry with temperature, has not, to the authors knowledge, been examined in any depth.

2.6 Summary and Conclusions

The effects of material properties and ram velocity on the plastic zone geometry have been reviewed and conflicting evidence presented. It is clear that, while for some materials it appears that the flow geometry is identical, it has not been proved that it is a unique function of the geometry of the process.

The work of Gurney and De Pierre has shown the effect of friction on the geometry of the deformation zone and it may appear that this could be the primary cause for the double maxima pattern observed with aluminium alloys. Medrano et al., however addressed themselves to this particular problem and indicated that the frictional restraint was of secondary importance to the effects of temperature and ram speed. However, increasing the frictional restraint did enhance the production

of the double maxima flow pattern.

The experimental and theoretical work published in the literature on the extrusion of rate sensitive materials has been reviewed. It has been indicated that there has, and continues to be, a general dicussion of the appropriate mean strain-rate which should be utilized in a particular instance, especially with regard to rate sensitive materials. Table 2.3 lists some of the mean strain rates reported in the literature for the direct extrusion of a superplastic tin-lead. Theoretical predictions for the extrusion load are compared with experimental data reported by Jovane. It is clear that the analyses give vastly different solutions and that all underestimate the experimental result. However, it is encouraging to note that Chandra's solution, which is the only formula to consider the rate sensitivity index, gives the theoretical solution which is closest to the experimental extrusion load.

In conclusion it is clear that for rate sensitive materials the extrusion pressure is a function of the ram velocity and that this has been incorporated into theories in only the most rudimentary way. The deformation zone geometry has been examined in the literature for simple die geometries and it has been shown that the velocity fields are not very different, however the interface friction does have a significant effect. The variation of flow patterns in aluminium has indicated that the shape of the velocity field is a function of the material properties.

Researcher	Formula	Eqn.	$\dot{\bar{\varepsilon}}_m$	$\bar{\sigma}_m$ lb/in^2	σ_t lb/in^2	F_t lb	F_t/F_e
Fetham [93]	$\dot{\varepsilon}_m = \frac{6U}{D} 2\ell n(\frac{D}{d})$	2.3	0.000416	1505	2086	1639	0.41
Wilcox and Whitton [64]	$\dot{\varepsilon}_m = \frac{6UD^2 \ell nR}{\cot\alpha(D^3-d^3)}$	2.4	0.0000857	739	1025	805	0.20
Hodierne [95]	$\dot{\varepsilon}_m = \frac{2U(D+d)\tan\alpha}{d^2}$	2.6	0.0006	1775	2460	1932	0.48
Chandra and Jonas [65]	$\dot{\varepsilon}_m = 4UD^2\tan\alpha\{\frac{2}{3m}\ell nR [(\frac{1}{d})^{3m} - (\frac{1}{D})^{3m}]\}^{1/m}$	2.7	0.00169	2833	3927	3084	0.77
Atkins [97]	$\dot{\varepsilon}_m = \frac{2U\tan\alpha}{D}\{1+\{1-\frac{1}{ER}\}^{\frac{1}{2}}\}$	2.9	0.00019	1049	1455	1142	0.29

Table 2.3

Comparison of mean strain rates and extrusion loads predicted by various authors for extrusion of tin lead.

Experimental work from Jovane et al [52]. Material behaviour characterized by:

$\sigma = 15000\ \dot{\varepsilon}^{0.2}$ For $\dot{\varepsilon} > 0.01$ $\sigma = 50000\ \dot{\varepsilon}^{0.45}$ For $\dot{\varepsilon} < 0.01$

2.7 Scope of Present Study

The purpose of the present study is to examine the effects of ram velocity and strain-rate sensitivity on the velocity field and to try to establish the invariance, or otherwise, of the flow geometry. An attempt will be made to incorporate the effects of strain rate sensitivity into the upper bound technique and to compare theoretical and experimental velocity fields and pressures.

In forward and indirect extrusion the product and velocity field are heavily constrained by the physical geometry of the process. The side extrusion process, indicated schematically in Figure 1.4, has been examined theoretically and experimentally previously and it is clear that the angle of the emergent extrudate is dependent on the velocity field. This provides a convenient way to observe changes in the velocity field whether they are due to changes in material properties, ram speed or friction. The side extrusion process and the work presented by previous investigators is reviewed in the following chapter.

CHAPTER 3

SIDE EXTRUSION - A REVIEW OF THE LITERATURE

3.1 Introduction

Many alloys are extruded either hot or cold by both the direct and indirect processes indicated previously. The mechanical properties of the extruded product are dependent on the amount of strain undergone by each element as it passes through the deformation zone. Consequently attempts are made to obtain uniformity of flow and in some unsymmetric shapes it has been found necessary to place a further hole in the die to achieve this as shown in Figure 3.1. An additional advantage of this extra aperture is that the total extrusion ratio is reduced and consequently the extrusion pressure will be reduced.

The flow of materials through non-symmetrical dies of complex shape has provided the incentive for the consideration of basically different extrusion arrangements. The first major study of non-symmetrical extrusion is attributed to Green [7] who proposed slip line field solutions for plane strain extrusion through a square die situated at the end and in the side of the container. It would seem that this is one of the first mentions of a side-extrusion process although it might be argued that the early production machines for extruding curved lead pipes utilized this principle; see Figure 1.8. Subsequent theoretical investigations have indicated some novel ideas

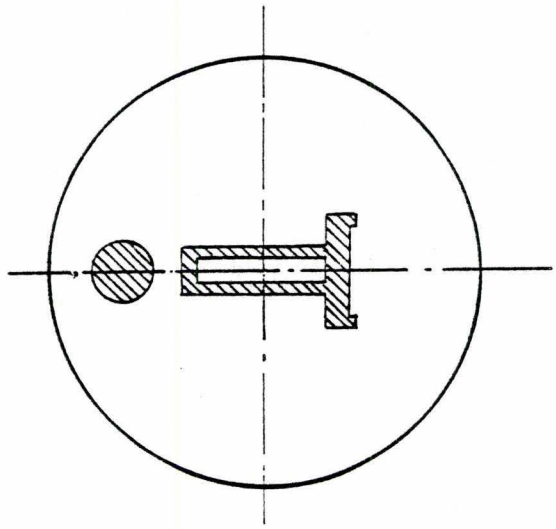

Figure 3.1

Die made with an additional aperture to balance material flow when extruding a section of unsymmetrical shape; from ref. [14]

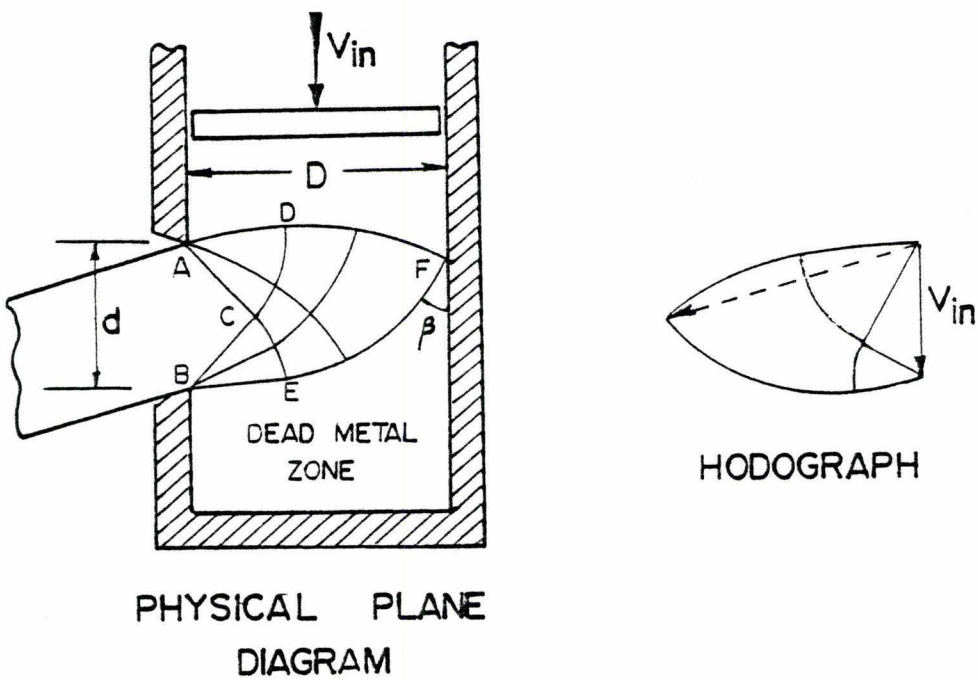

Figure 3.2

Diagram of the side extrusion process and the slip line field and hodograph suggested by Green [7]

for producing corrugated plate [128] and bimetallic laminated sheet [123]. The following is a summary of the salient features of the work presented in the literature on these processes.

3.2 Side-extrusion

The side extrusion process is indicated schematically in Figure 3.2 where material is extruded perpendicular to the direction of the applied ram force. In the work by Green [7] plane strain side extrusion was considered as an extension of the general problem of unsymmetric plane strain extrusion; experiments were performed using plasticine as a model material and indicated the validity of the slip-line fields chosen. The slip-line field developed is shown in Figure 3.2 with the associated hodograph. If the process is assumed to be frictionless then the slip-line BEF intersects the wall at an angle $\beta = \pi/4$ and the field is symmetric about CF. If friction is included then the point F moves up the wall and if the wall is perfectly rough, $\beta = 0$.

Unsymmetric end extrusion illustrates dramatically the effect of lubrication on the size and shape of the dead metal zone as shown in Figures 3.3 and 3.4. It will be observed that if the die opening is not central then a larger dead metal region exists under the side of greatest length with the result that flow is more restrained on that side. This effect is more clearly demonstrated if the container has smooth walls, as in Figure 3.4, where material under the short side of the die flows so easily that the extruded product tends to rotate as it emerges from the die.

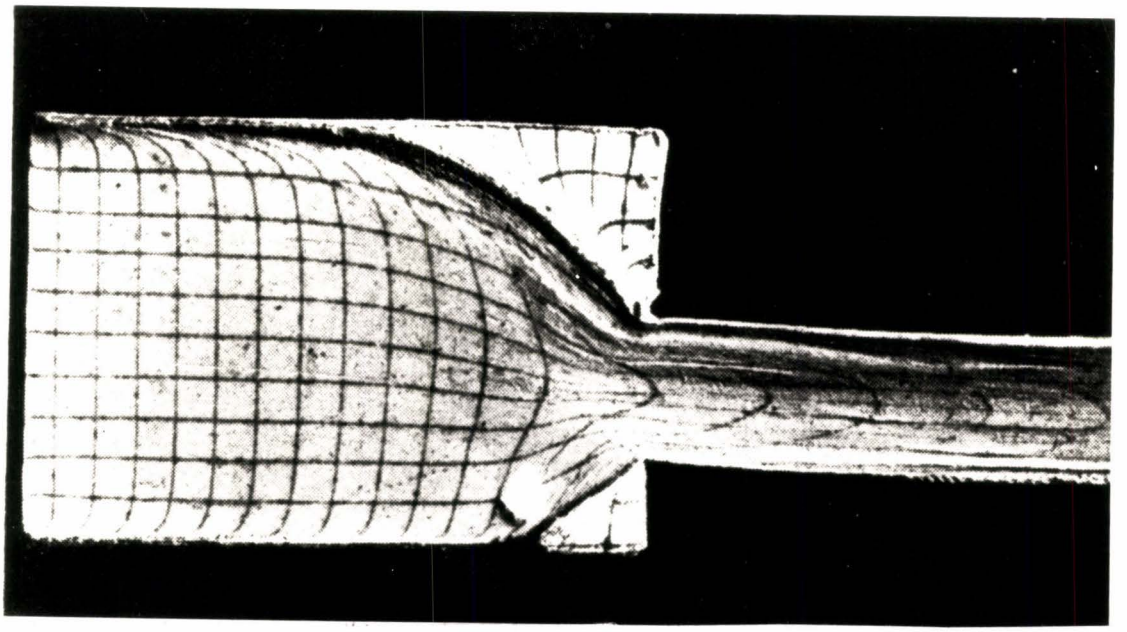

Figure 3.3

Unsymmetrical end extrusion of plasticine with rough container walls; from ref. [7]

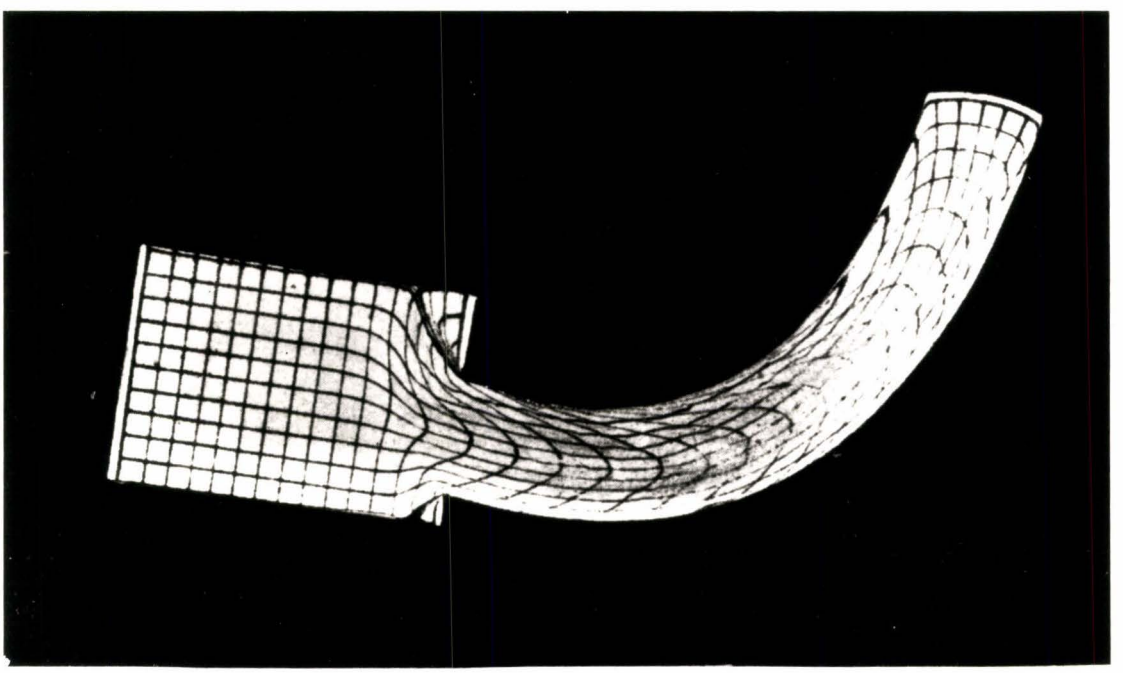

Figure 3.4

Unsymmetrical end extrusion of plasticine with smooth container walls; from ref. [7]

The rotation of the extruded product demonstrated so dramatically in Figure 3.4 for the unsymmetric end extrusion is, however, not predicted or reported in the side extrusion case. In all cases the exit velocity is assumed to be constant across the die aperture. Consequently, the theory predicts that the product will be extruded straight at some angle θ which, for the frictionless condition, is given by equation (3.1)

$$\theta = \tan^{-1} \{\frac{2D}{d}\} \tag{3.1}$$

where D is the width of the die and d the aperture. There is no simple expression, however, for the case when friction is acting.

Johnson [10] determined theoretically the effect of geometric variables on the extrusion parameter ($\bar{p}/2k$) for the partial sideways extrusion process indicated in Figure 3.5(a). This is similar to the problem of extrusion through square dies, the two halves being staggered; Figure 3.5(b). The slip-line field analysis was employed and indicated that the extrusion pressure for the unstaggered square die is always less than that for the oblique die, no matter what the eccentricity. This might suggest that the extrusion pressure for sideways extrusion, which is a special case of partial sideways extrusion, would be greater than the forward extrusion pressure for the same extrusion ratio. However, Johnson and Kudo [23] have indicated, Figure 3.6, that for a reduction ratio r, in the range,

$$0.45 < r < 0.9$$

the extrusion pressure for sideways extrusion from a smooth container is

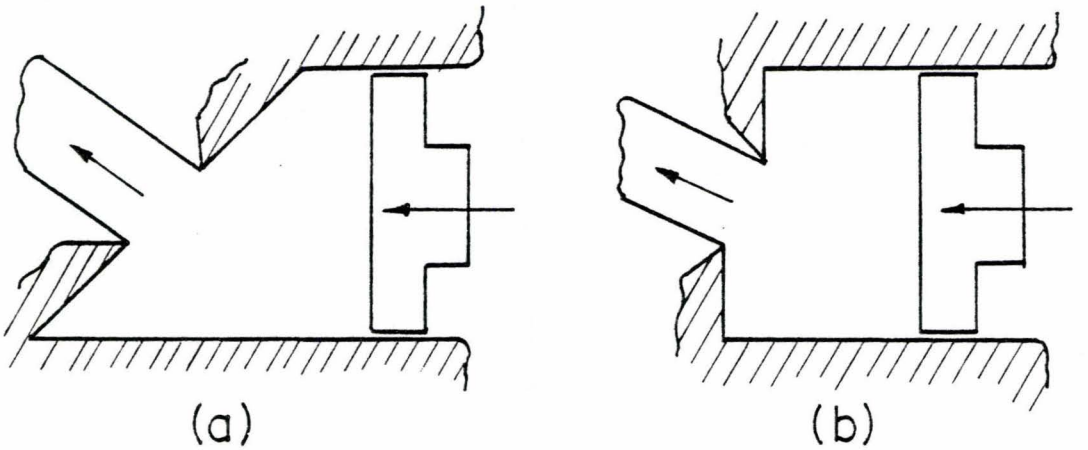

Figure 3.5

Schematic diagram of partial sideways extrusion, (a), and extrusion through a square staggered die, (b); from ref. [10]

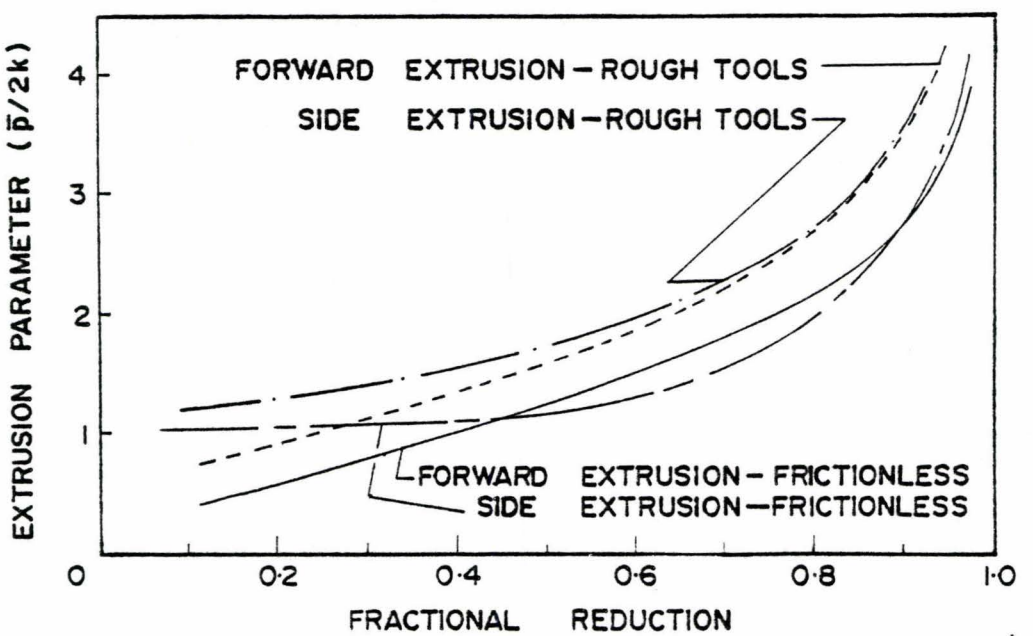

Figure 3.6

Comparison of steady extrusion pressures for side extrusion and end extrusion; from ref. [23]

less than that for forward extrusion. A brief survey of the literature on side extrusion was given and indicated the form of slip-line fields which have been used. The analogy between sideways extrusion and the identation of a flat plate of finite thickness was made and the slip-line fields shown to be the same. For large reductions the authors indicated that under certain circumstances the results of Ross [124], for the compression of insert blocks, are applicable.

Johnson et al. [125] have calculated the sideways extrusion pressure for both rough and smooth containers and have suggested a number of possible die configurations as shown in Figure 3.7. Also presented is the unusual case of a single orifice which is wider than the original thickness of the slug. However, it is probable either that cavitities would form, or that the material would buckle.

An upper bound solution for sideways extrusion has been given by Johnson [42] where the velocity field chosen was based on the slip line field. For an extrusion ratio of less than one it was shown that the upper bound solution for $\bar{p}/2k$ was very close to that given by the slip-line field analysis; 1.26 and 1.20 respectively.

The work reviewed up to this point was for the plane strain extrusion of rigid perfectly plastic, non-hardening isotropic materials. The only experimental results available were those by Green [7] who used plasticine as a model material to indicate the deformation field and to check the validity of the slip-line fields chosen. In 1966, Duncan et

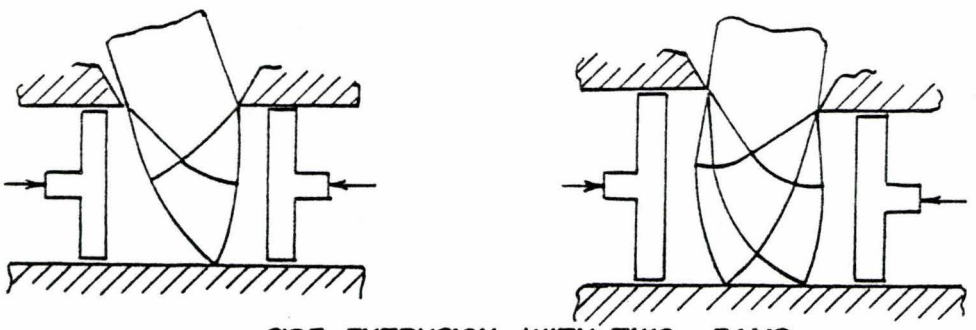

SIDE EXTRUSION WITH TWO RAMS

a) SYMMETRIC DIE b) INCLINED ORIFICE

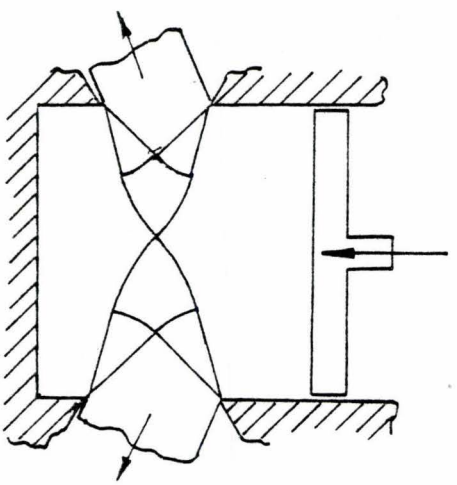

SIDE EXTRUSION THROUGH OPPOSITE HOLES

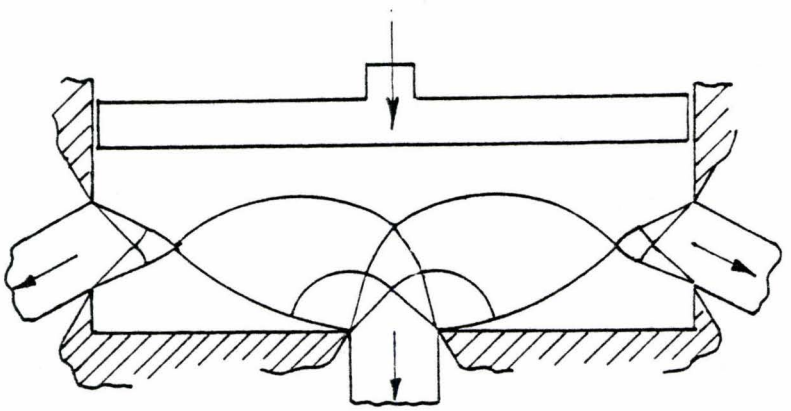

COMBINED SIDE AND END EXTRUSION.

Figure 3.7

Some die configurations considered by Johnson et al. [125]

al. [8, 9] presented theoretical and experimental papers* dealing with the effect of tool geometry on the extrusion pressure in side extrusion. The first paper [8] investigated a number of new die and container configurations using the slip-line method as indicated in Figure 3.8. Experiments were performed with pure lead to examine the theoretical predictions of the extrusion pressures for the cases shown in Figure 3.8(a) and (b). In both cases the experimental pressures were 50% higher than those obtained from the slip-line analysis. However, the proportional change in pressure, for different base inclinations, was very nearly the same as that predicted.

Plane strain double orifice extrusions similar to the type indicated in Figure 3.8 (J) were attempted to determine the limiting eccentricity. Dies of different extrusion ratio were used and it was found that if the smaller orifice was placed in the upper position then the length of strip, extruded through this die, was 10% or less than that through the larger die. If the position of the dies were reversed no metal was extruded through the smaller orifice.

Further experimental work by Duncan et al. [9] determined, in detail, the material properties for pure lead and tellurium lead and attempted to take account of strain-rate effects. Compression tests were conducted at different velocities to determine the rate dependence of the flow stress. An equivalent flow stress for the side extrusion

---

* Prof. W. Johnson [126] has indicated that the first experiments performed on the side extrusion of metals were by Basu [126a] in 1963. The results of this work however were not published otherwise in the scientific literature.

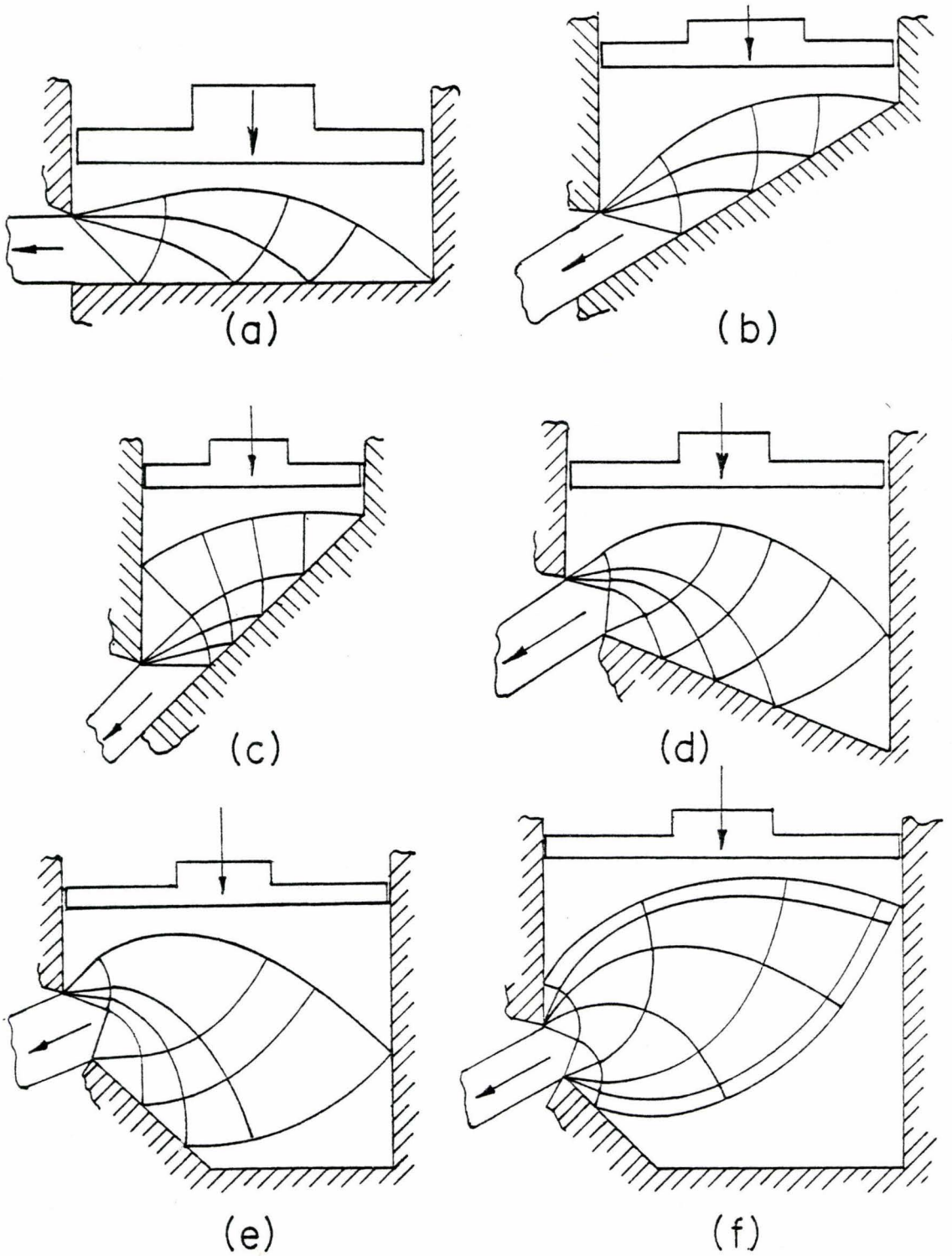

Figure 3.8

Some die configurations considered by Duncan et al. [8]

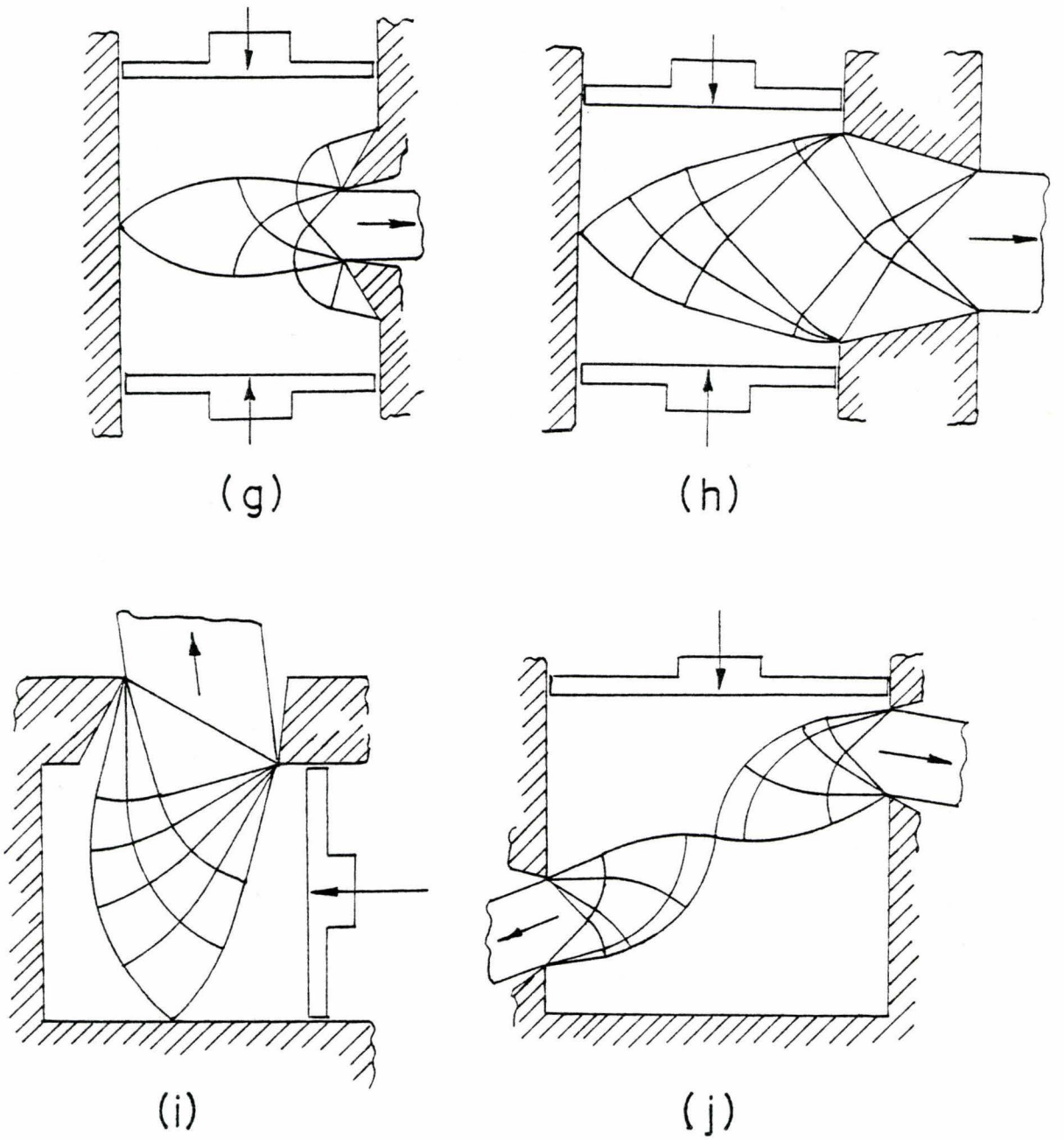

Figure 3.8 (cont.)

Some die configurations considered by Duncan et al. [8]

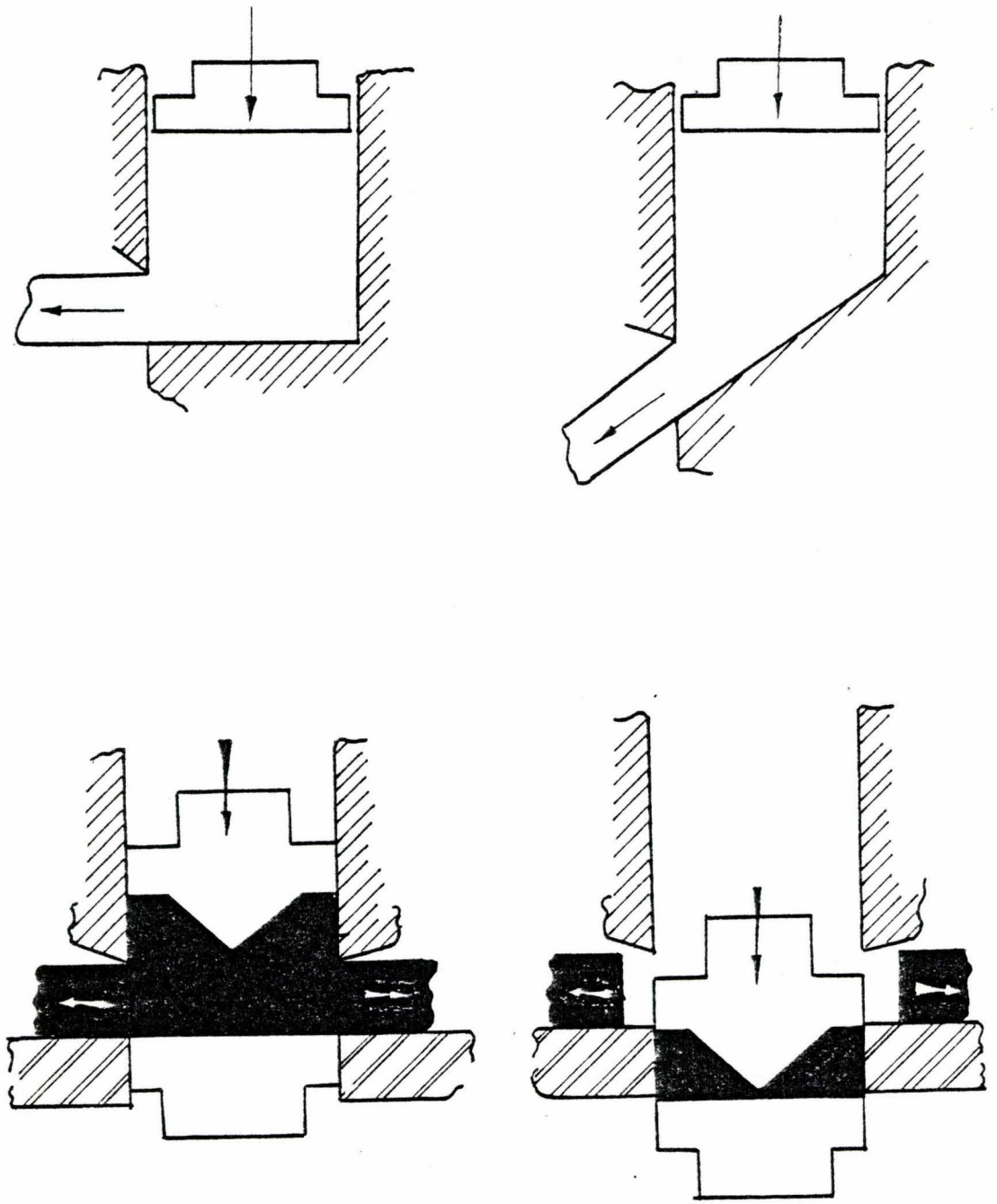

Figure 3.9

Some possible container configurations for side extrusion suggested by Duncan et al. [9]

process was proposed based on the equivalent strain and the time taken to extrude unit volume. The equation given in this paper is, however, incorrect since it is not dimensionally consistent. An important aspect of this paper is that the authors indicated some of the possible technological aspects of this process. Figure 3.9 is reproduced from reference 9 and indicates some novel container configurations for side extrusion. Also shown is an arrangement to reduce cycle times and simplify the ejection of the unextruded billet.

Quenzi et al. [128] and Masura et al. [129] have examined the symmetrical lateral extrusion of aluminium where the product flow is normal to the direction of two co-axially opposed rams moving with equal speed; Figure 3.10. Quenzi et al. utilized the slip-line theory and analysed the material flow, product strength and extrusion force. In this example the process is three dimensional, however, the flow in the plane of the die parting line is assumed to be plane strain. Experimental results were obtained by converting the results of a microhardness traverse across the central plane and compared with the theoretical results; the agreement was very good and is shown in Figure 3.11. The theoretical extrusion force was determined from the slip line field and summed with a frictional force term evaluated from the mean billet pressures given by the slip line solution. For the two geometries considered the agreement between the theoretical extrusion force and the average experimental extrusion force was good.

Masura et al. [129] examined the same process as Quenzi et al. but confined their study to the formation of defects in the aluminium

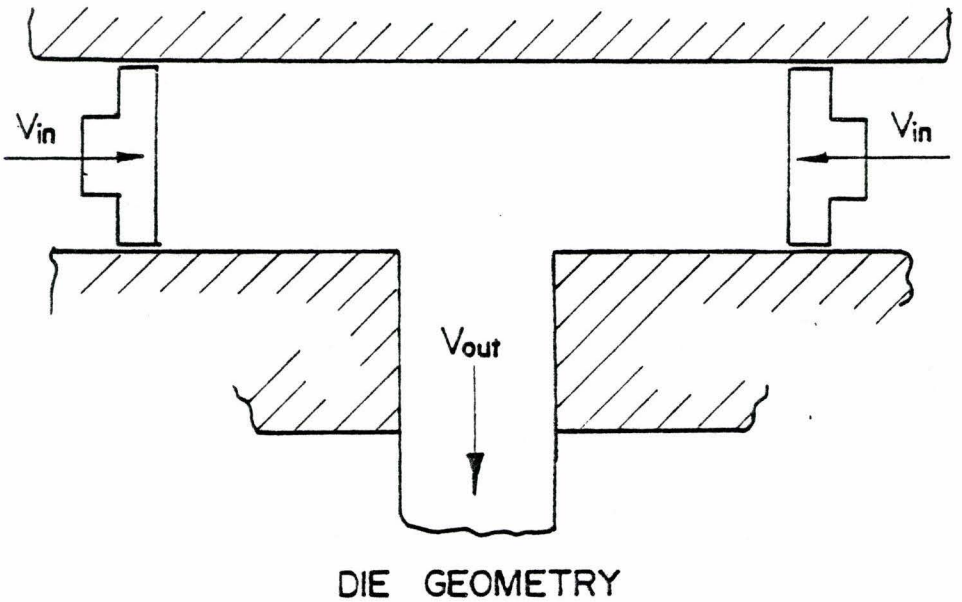

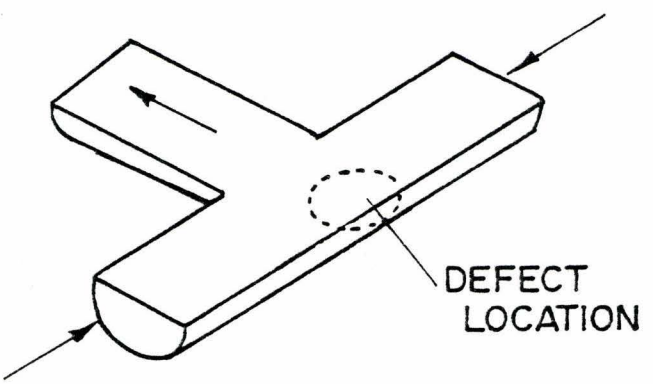

Figure 3.10

Lateral extrusion process examined by Quenzi et al. [128] and Masura et al. [129]

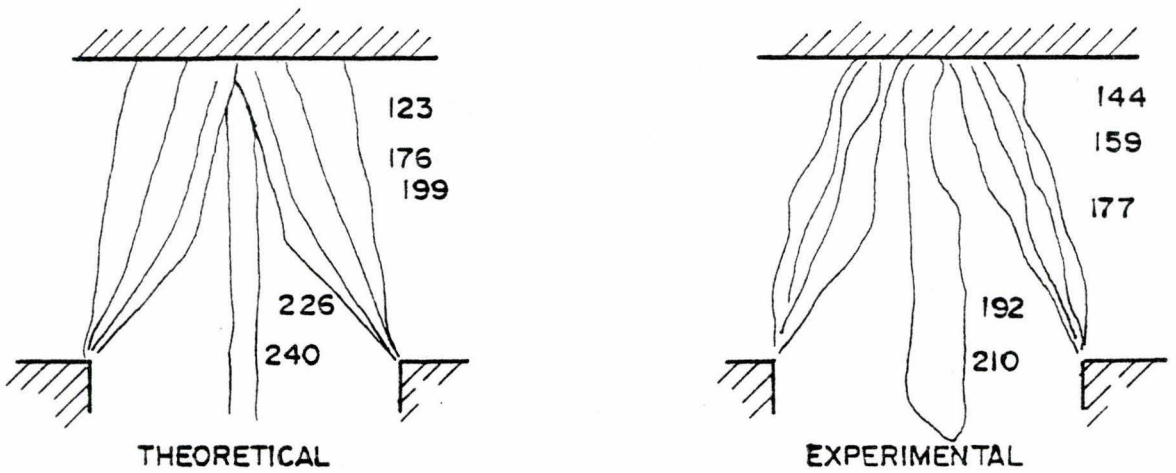

Figure 3.11

Theoretical and experimental material strength distribution throughout flow field; from ref. [128]

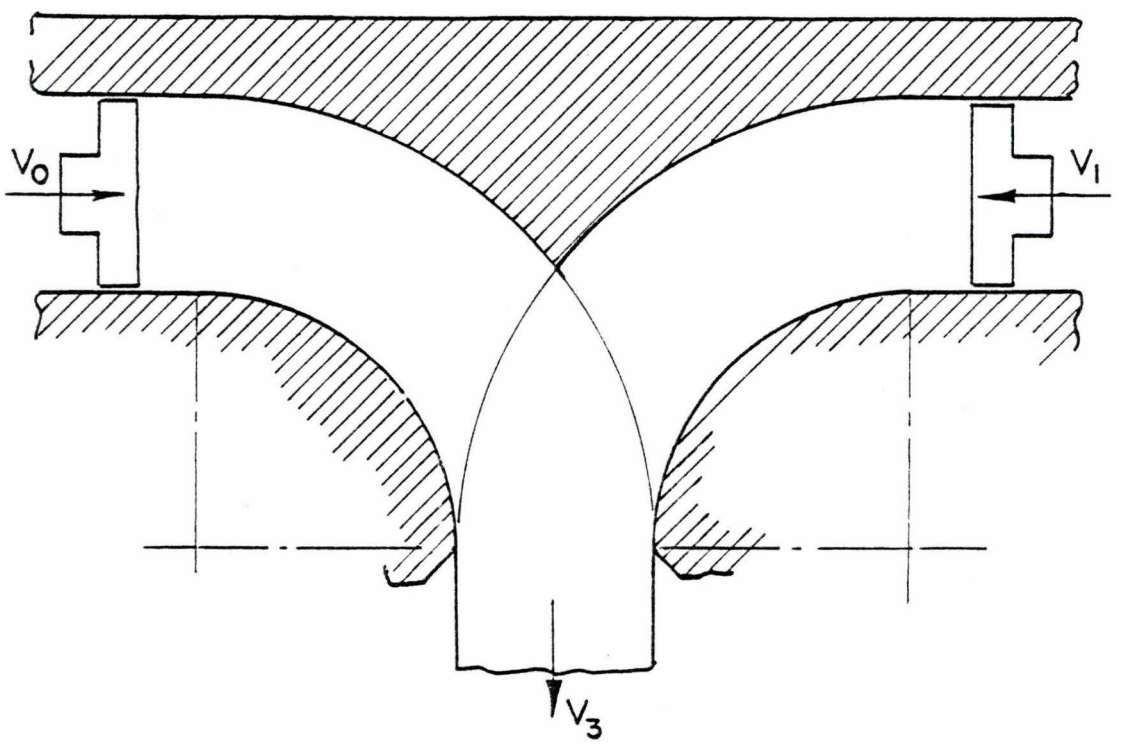

Figure 3.12

Side extrusion of bimetallic strip by Alexander and Whitlock [123]

billet close to the die wall opposite the extrusion aperture, as shown in Figure 3.10. The development of the defect was examined microscopically at different stages during the extrusion process for different lubricants. The results indicated that for dry friction there was neglible defect formation whilst the defect growth increased significantly with lubrication. The authors concluded that if a defect free product was required then hot extrusion without lubrication was recommended.

An interesting application of the side extrusion process presented by Alexander and Whitlock [123] is shown in Figure 3.12. Two billets of different materials are extruded simultaneously to produce bimetallic strip. The ratio between the ram speeds determines the material thickness ratio of the product. The pressure generated at the interface is assumed to be large enough to cause pressure welding. Model tests were conducted using plasticine and deformed grid patterns indicated the validity of the slip-line field chosen in the analysis. The proposed slip-line field solutions are incomplete however since they relate only to the deforming material within the die. Ram speed ratios up to 10 were attempted and shown to be possible although satisfactory theoretical solutions were not found for ram speed ratios greater than 1.5. No experimental results were reported for metals.

Johnson and Chitkara [128] have indicated how the side extrusion process might be used to produce corrugated sheet. The process involves side extrusion with two co-axial rams moving at different speeds. this is essentially the same process as that indicated by Johnson et al.

[125] and shown in Figure 3.7(a). The authors analysed the effect of differential ram velocities on the exit velocity and direction using the slip-line field suggested previously. Programs of the relationship between the two ram velocities were presented which, it was suggested, would produce corrugated sheet. It is interesting to note that this technique of differential ram velocities was used in the late ninetenth century to produce curved lead pipes for the plumbing industry; see Figure 1.8.

Johnson and Mamalis [131] have presented a force plane diagram for the side extrusion of a rigid plastic material. This diagram, Figure 3.13, is determined from a consideration of the equilibrium of the system using a known slip-line field. In the example shown the shear stress, and hence shear force, on the face IC is known and the normal force on this face can be found. The construction of the remainder of the diagram is relatively simple based on the slip-line field. Johnson and Mamalis have presented diagrams for a number of common metalworking problems where the slip line field has been well established.

Recent work by Das et al. [132] and Chitkara et al. [133] has indicated theoretical and experimental results respectively for unsymmetric end extrusion. Das et al. presented slip-line field solutions for plane strain unsymmetric end extrusion. Two families of slip-line fields, which were originally proposed by Green [7], Figure 3.14, were solved. The exit slip-lines are curved and the solution of problems of this nature, altough extremely complex, can be attempted

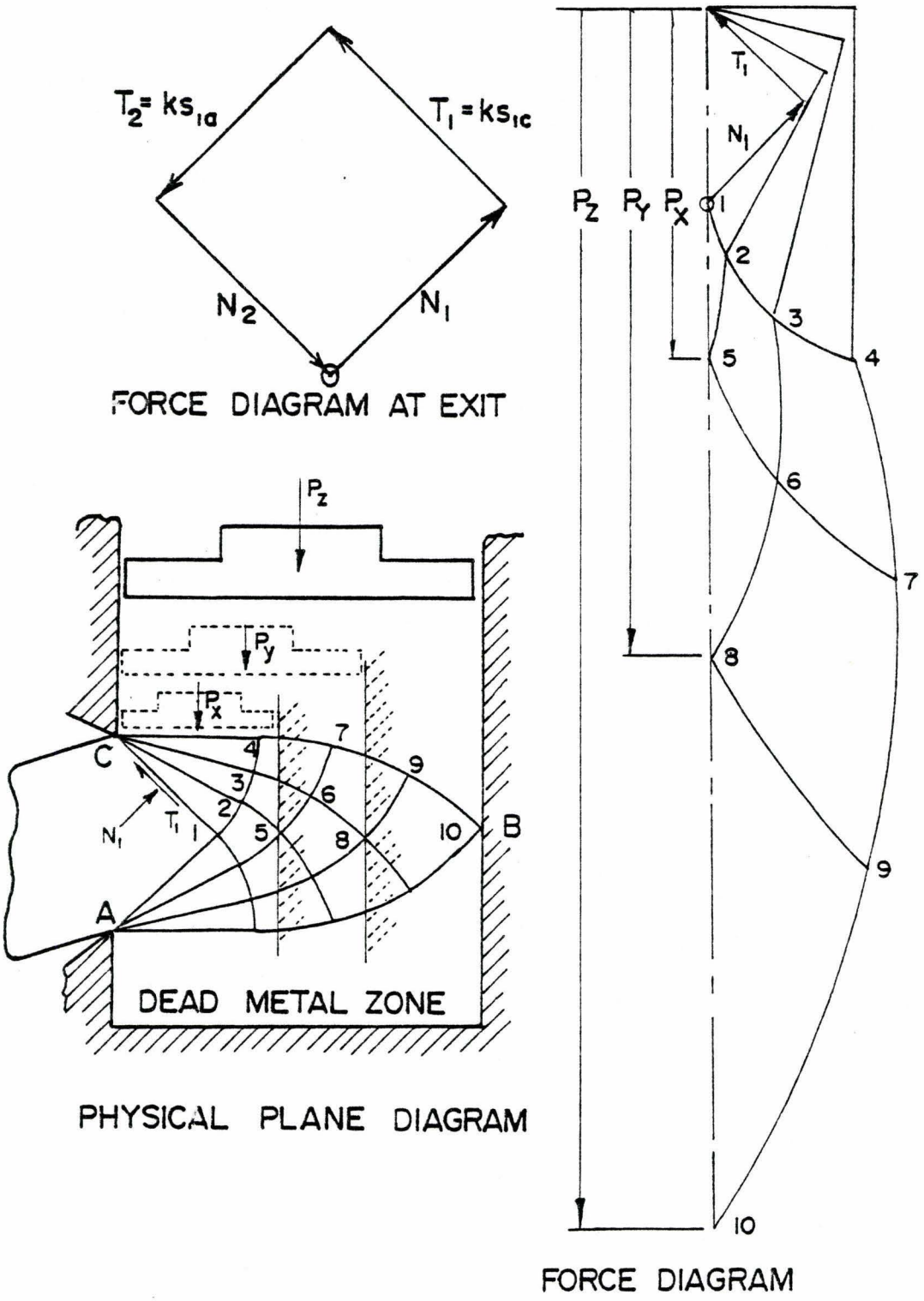

Figure 3.13

Slip line field and force plane diagram presented by Johnson and Mamalis [131]

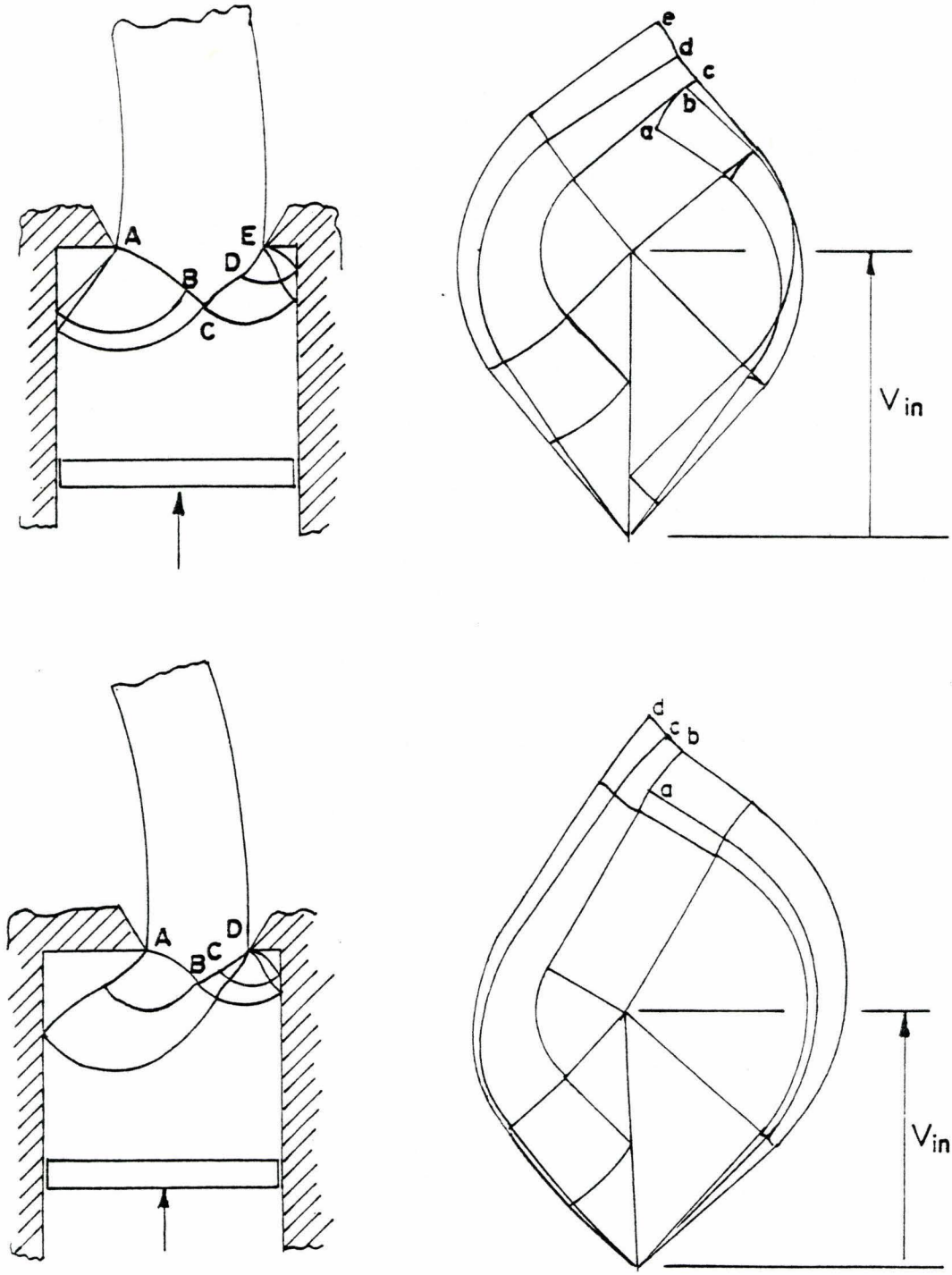

Figure 3.14

Slip line fields for unsymmetric end extrusion suggested by Green [7] to account for rotation of extruded product

using the computation techniques developed by Dewhurst and Collins [134]. This technique involves the non-linear optimization of a set of algebraic equations representing the slip-line field and hodograph geometry. The curved exit slip-lines predict that the product will rotate, with constant curvature, towards the die with the largest dead metal region. The plasticine experiments by Green [7] had shown this to be qualitatively correct. It would appear that the work of Das et al. is the first to predict, quantitively, the rotation of the product*. However no theoretical curves were presented to indicate the variation of the exit geometry based on the analysis.

Experimental results for unsymmetric end extrusion are described by Chitkara et al. [133] and compared with the results of Das et al. Tellurium lead and commercial by pure aluminium were used to determine the variation of the extrusion pressure and radius of curvature of the extruded product with reduction and die eccentricity. Chitkara concluded that the agreement between the theoretical and experimental values for the extrusion pressure was within 10%. However the theoretical solution was only applicable when the excentricity is low. The extrusion pressure increases with increasing excentricity as anticipated but for reductions below 45% is unaffected by eccentricity.

---

* A paper by Johnson [133] on the application of the upper bound technique to extrusion through curved dies indicates that the product will rotate towards the die with the smallest radius of curvature. If one assumes that the curved die is the boundary of the dead metal zone then this paper represents the first theoretical evaluation of the radius of curvature of the product. The curvature however is in the wrong sense to that observed with plasticine.

The correlation between the measured radius of curvature and that predicted by the theory was not good. This is probably due to the technique used to evaluate the radius of curvature and also to the small billet sizes used.

A number of papers have recently been presented in the scientific literature which warrant mention in this chapter. Extrusion cutting, which is shown schematically in Figure 3.15, can be described as:

> ".... geometrically restrained orthogonal cutting where the deformation is fully determined by the tool and not, as in the casee of conventional cutting, also by the properties of the material being cut". [181]

De Chiffre described experiments wtih wax and brass and indicated that the agreement between experimental and theoretical results was good. The similarity between extrusion cutting and side extrusion with an inclined base was recognised and an upper bound analysis presented based on the slip-line field. The quality of the "chip" produced by this process was excellent and it was proposed that this method might be used to manufacture small items such as strips and wires of various sections.

An interesting method of cold pressure welding presented by Kudo et al. [182] is shown schematically in Figure 3.16. The two billets to be welded are placed face to face in a container and then laterally extruded by two opposed punches. As the material extrudes the pressure generated at the interface is sufficient to ensure an excellent bond. Experiments were described for the plane strain extrusion of aluminium

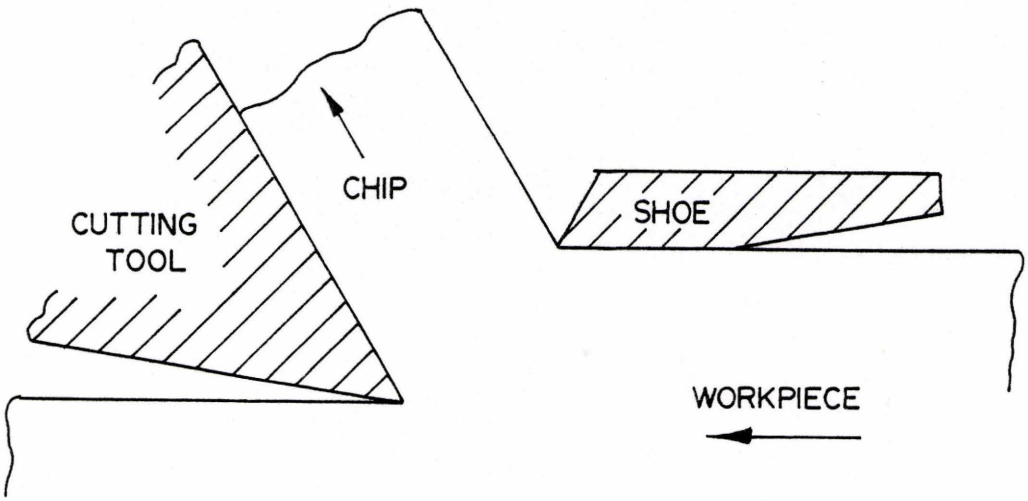

Figure 3.15

Schematic diagram of extrusion cutting process proposed by De Chiffre; from ref. [181]

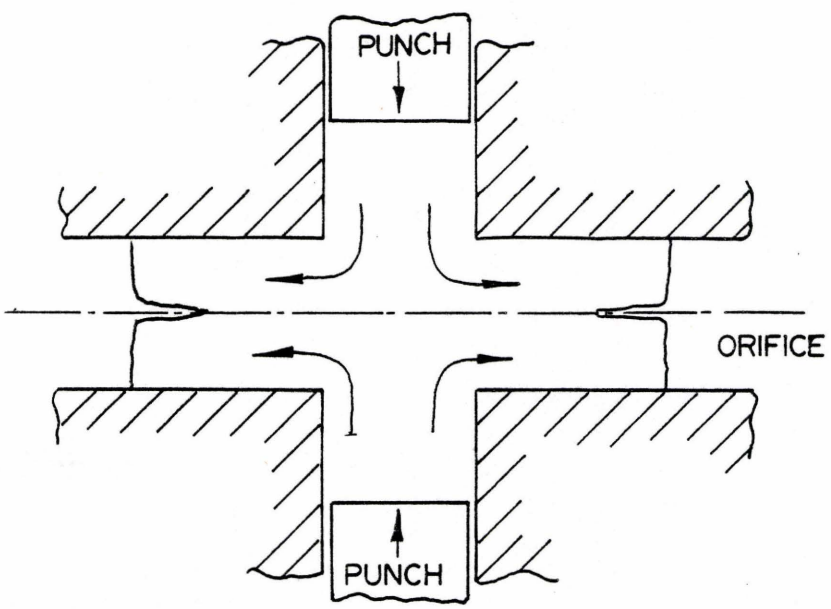

Figure 3.16

Schematic of cold pressure welding process proposed by Kudo et al.; from ref. [182].

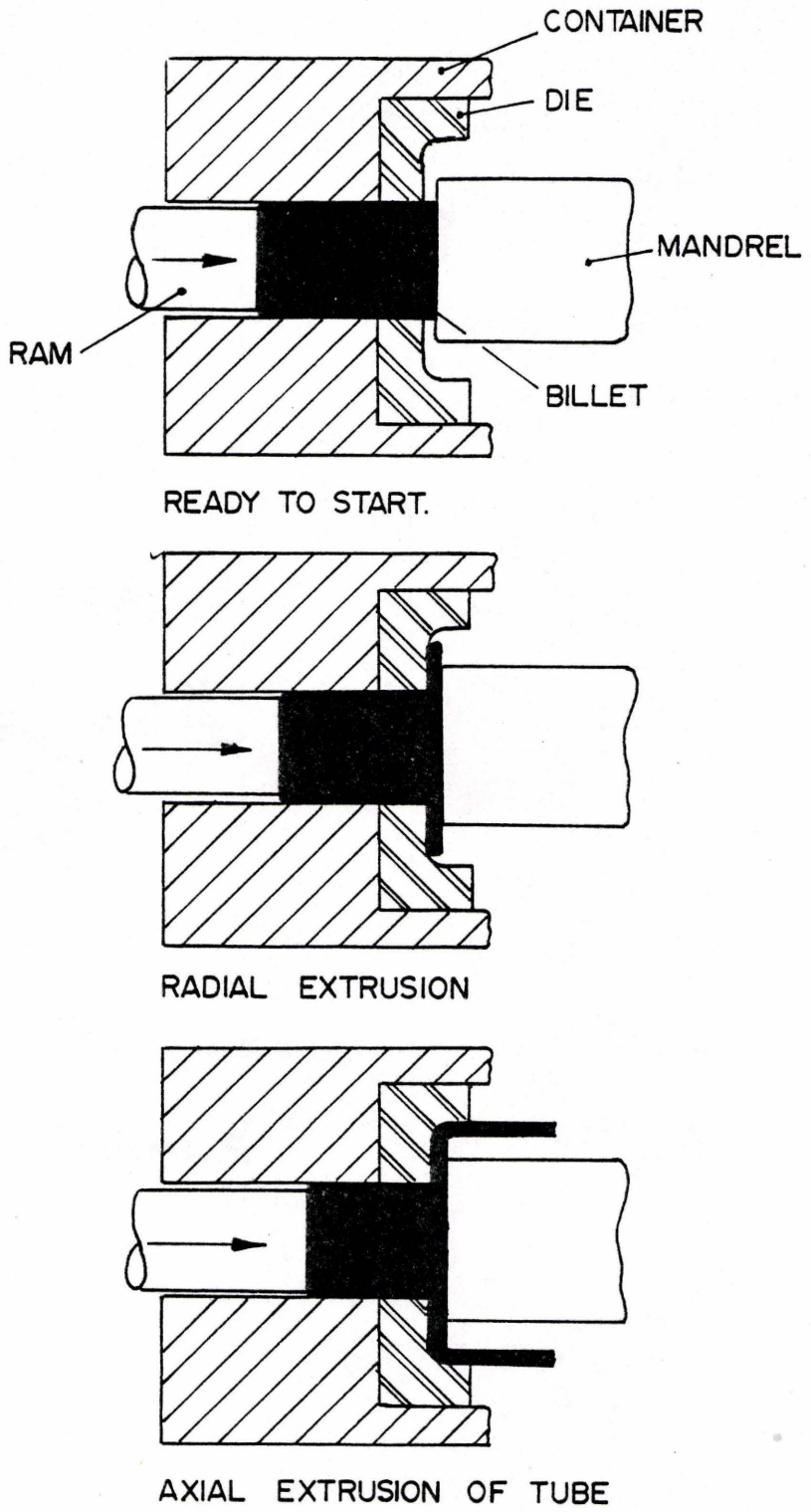

Figure 3.17

Schematic of Raflo extrusion process proposed by Rowell; [183].

which showed that the entegrity of the bond was excellent even when the mating surfaces were deliberately contaminated with oil. Shear and tensile tests indicated that the weld was as strong as the mother material provided that sufficient material was extruded to ensure a good weld.

The production of bimetallic strip, by pressure welding dissimilar metals, was proposed although no experiments were performed. The die geometry is simpler than that proposed by Alexander and Whitlock [123] and it would be interesting if this work were continued.

Rowell [183, 184] has described the production of large diameter tube from a billet of smaller diameter. The radial extrusion or Raflo process is shown schematically in Figure 3.17. Material is extruded laterally at the end of the extrusion chamber and then "turned" to produce a tubular form. A major advantage of the process is that the extrusion load is greatly reduced since the effective extrusion ratio is reduced. Initially experiments were performed on a laboratory press to determine the feasibility of the process and the important die variables. The success of the initial phase led to the conversion of an extrusion press, due to be scrapped, to attempt a few "industrial" experiments. Following the conversion a 10 inch diameter (254 mm) brass tube with a 0.187 inch (4.76 mm) wall was sucessfully produced from a 5 inch diameter (127 mm). The extrusion load was 370 tons (3.3 MN) which compares with a value of 8750 tons (78.3 MN) if the tube were produced by conventional extrusion. The advantages of such a process are clear, however, the extrusion industry seems to be slow in investigating the

use of this method [185].

3.3 Summary

The side extrusion process, as a special case of unsymmetric end extrusion, has been the subject of a number of theoretical papers. The only quantitative experimental work reported in the literature is that by Duncan et al. which indicated that the theoretical extrusion pressure, calculated using the slip-line method, underestimated the experimental values by some 40%. Although a number of interesting technological applications have been suggested, these have not been exploited industrially. It is doubtful whether side extrusion will be used industrially since the complexities of the process seem prohibitive. However, side extrusion is a useful process to study in the research laboratory as the effects of tool geometry and material behaviour can be readily observed. The exit angle is dependent on the deformation zone geometry and could therefore be used to measure the effect of process variables on the deformation zone. Any changes in the internal flow field will produce different exit directions and this quantity can be used as an indication of the internal flow field.

CHAPTER 4

AN UPPER BOUND SOLUTION FOR THE BULK DEFORMATION OF RATE SENSITIVE MATERIALS WITH PARTICULAR REFERENCE TO THE SIDE EXTRUSION PROCESS

4.1 Introduction

This chapter presents a brief introduction to the upper bound technique and the way in which the effects of strain hardening and strain rate sensitivity have been accommodated. The side extrusion process and the analytical and experimental work presented to date was reviewed in Chapter 3. It was suggested that changes in the velocity field would be apparent by changes in the exit geometry of the extruded product and that this might be a reasonable way in which to measure or observe the effects of material properties on the velocity field. Three velocity discontinuity fields for the side extrusion process are presented and compared using the upper bound technique for rigid perfectly plastic materials.

A new technique is presented for the analysis of bulk deformation problems which gives an upper bound solution. This analytical method introduces the concept of a thin shear zone of constant shear strain rate and a tangential shear strain rate discontinuity. The technique is applied to the side extrusion process and indicates that the geometry of the velocity field is a function of the strain rate sensitivity index.

A short discussion then follows on the application of the analytical method to real materials and a brief comparison is made with previous work on the mechanics of metal cutting. The concept of a thin shear zone is not new in the analysis of orthogonal cutting and a short review is presented of the work associated with the determination of the shear zone size. It is concluded from this review that it is appropriate to assume a shear zone thickness to length ratio and this is done in later chapters when results are generated, using the rate-sensitive upper bound technique, for particular materials.

4.2 The Upper Bound Technique

The determination of loads in metalworking problems is of technological importance and since no exact solutions are available a number of approximate solutions have been proposed. These solution techniques can be clearly separated into two classes; those which overestimate the load, the upper bound*, and those which underestimate the load, the lower bound. For design purposes the engineer is concerned with ensuring a safe design and consequently tends to use upper bound techniques. The essential difference between the two bounding

---

* It should be pointed out that an upper bound analysis will only overestimate forces if all other assumptions in the analysis are valid. In actual examples simplifying assumptions must be made about material behaviour, friction and thermal effects and in an engineering rather than a mathematical sense it may not be easy to determine whether or not the solution will overestimate actual loads.

techniques is that for an upper bound solution we are concerned with finding a valid velocity field in order that the continuity of material flow is satisfied: no attention is paid to the equilibrium of the system. In the lower bound technique the situation is reversed and the equilibrium conditions for the system are satisfied while the continuity conditions can go unsatisfied. For a detailed proof of the bounding techniques the reader is referred to the texts by Hill [25], Johnson and Mellor [43] and Thomsen et al [26]. In this study we will restrict our attention to the upper bound technique. It should be noted that while any kinematically admissible velocity field will give a valid upper bound solution the field which gives the minimum work rate will be closest to the exact solution.

A considerable amount of work has been presented in the literature on plane strain problems [23, 42, 44] although this technique is equally applicable to axisymmetric problems [130, 131, 135]. Materials are assumed to be rigid, perfectly plastic with a constant yield stress. Halling and Mitchell [49] have presented an analysis which deals with a material which is strain hardening. Fenton [98] has included the effects of strain rate sensitivity in the determination of the material constants for a material which strain hardens as indicated previously in Chapter 2.

4.2.1 Rigid Perfectly Plastic Materials

We assume plane strain conditions and a material whose behaviour could be defined by a constant uniaxial yield stress, i.e.:

$$\sigma = Y \tag{4.1a}$$

as shown schematically in Figure 4.1. In this case we must also select a yield criterion to obtain a relation between Y and the yield shear stress k. Alternatively we may describe the material behaviour in terms of a constant shear stress i.e.

$$\tau_{max} = k = \text{constant} \tag{4.1b}$$

We examine an element of material ABCD and suppose that it undergoes a shock or instantaneous change in tangential velocity as shown in Figure 4.2. The normal component of the velocity is unchanged across the discontinuity, thus ensuring that the conditions of incompressibility and continuity are satisfied. The rate at which plastic work is dissipated over a length of discontinuity s and for unit depth is:

$$\dot{W} = ksv^* \tag{4.2}$$

where k is the yield shear stress

v* is the change in the tangential velocity.

If a series of discontinuities is assumed and the velocity diagram or hodograph obtained, then the total power dissipated across all discontinuities can be obtained. This must be equal to the external power input and can be equated to give the applied load.

The discontinuity pattern for a particular operation is chosen intuitively and the best field is that which gives the lowest value of the extrusion pressure. A few velocity fields for extrusion and their associated hodogrpahs are shown in Figure 4.3.

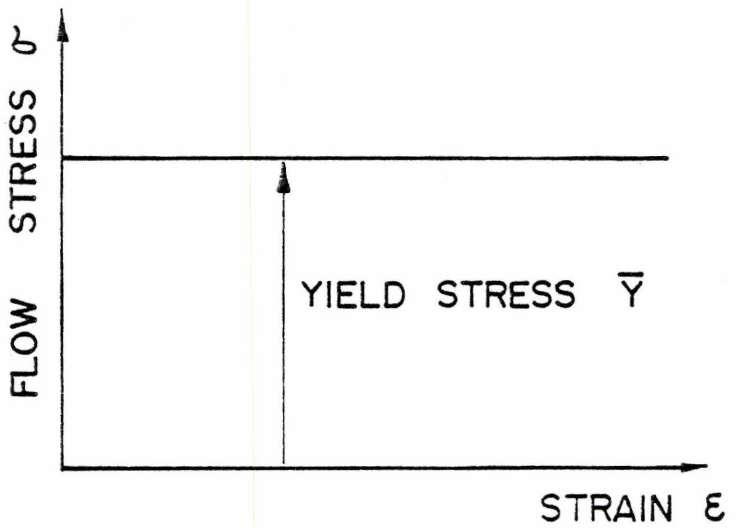

Figure 4.1

Schematic representation of a rigid perfectly plastic material with constant yield stress

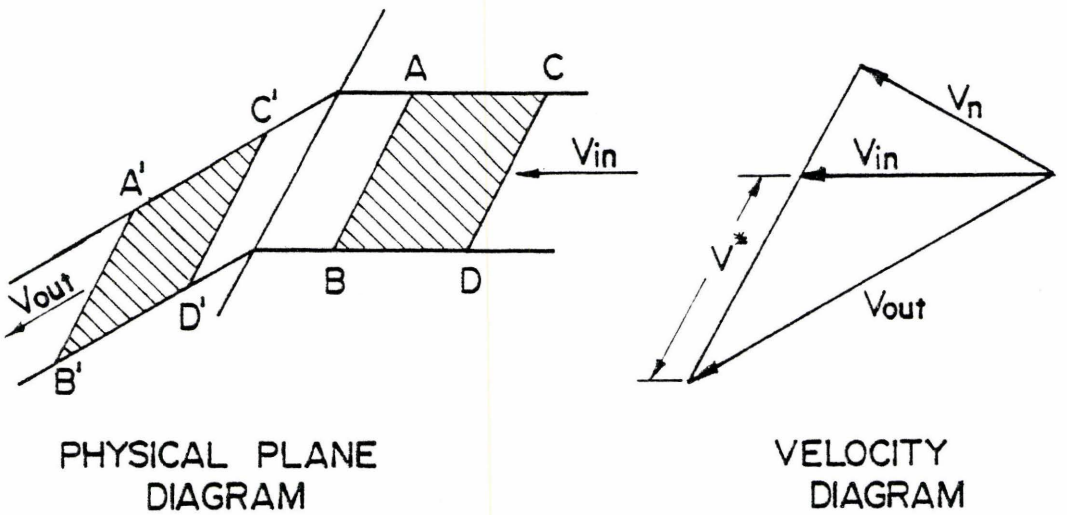

Figure 4.2

Element of material crossing a discontinuity and the associated hodograph

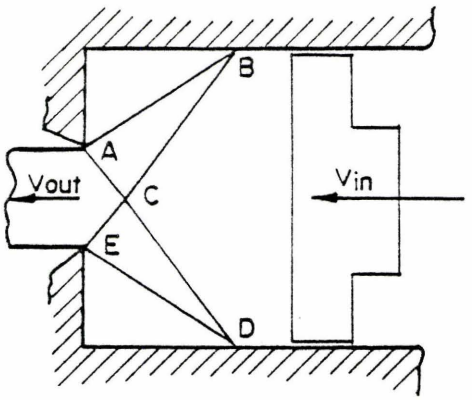

PHYSICAL PLANE DIAGRAM

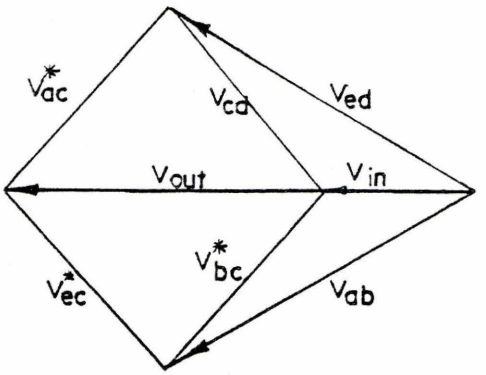

HODOGRAPH

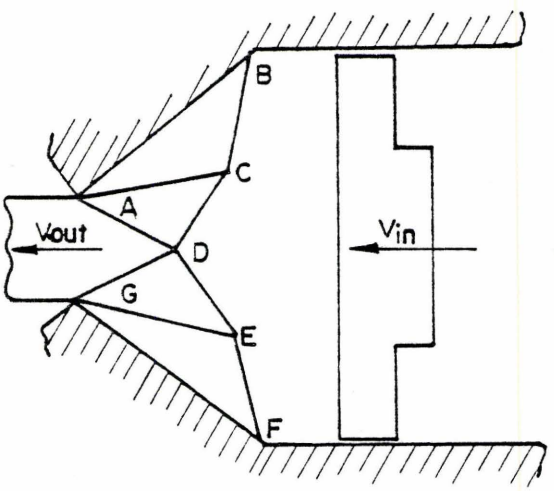

PHYSICAL PLANE DIAGRAM

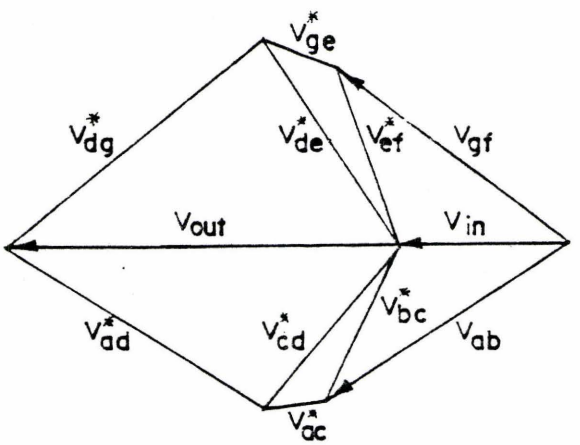

HODOGRAPH

Figure 4.3

Some velocity discontinuity patterns for the forward extrusion process

4.2.2 Upper Bound Solutions by Force Polygons

A recent paper by Johnson and Mamalis [137] has indicated that the force and pressure distributions in metal forming processes can be determined from a valid tangential velocity discontinuity pattern for plane strain problems. This work was a continuation of a series of papers [138, 139, 140] which were initiated by the work of Westwood and Wallace [138]. A force diagram is constructed by initially determining a known force and then completing the diagram. For example, in the forward extrusion case, Figure 4.4a, the tangential and normal forces at the exit discontinuity AB can be determined since

1) The tangential force per unit depth is given by

$$T_1 = ks_{AB}$$

where k is the yield shear stress and s_{AB} is the length of the discontinuity.

2) The boundary conditions specify that the sum of the forces along AB in the forward direction should be zero, i.e.

$$(\Sigma F_x)_{AB} = 0$$

The normal force along AB can therefore be determined. The magnitude of the tangential force along any discontinuity is defined by

$$T_i = k\, s_i$$

and the direction of the normal forces is implicit. Consequently, the solution becomes a process of systematically determining the value of the normal forces acting on each element within the velocity field. The

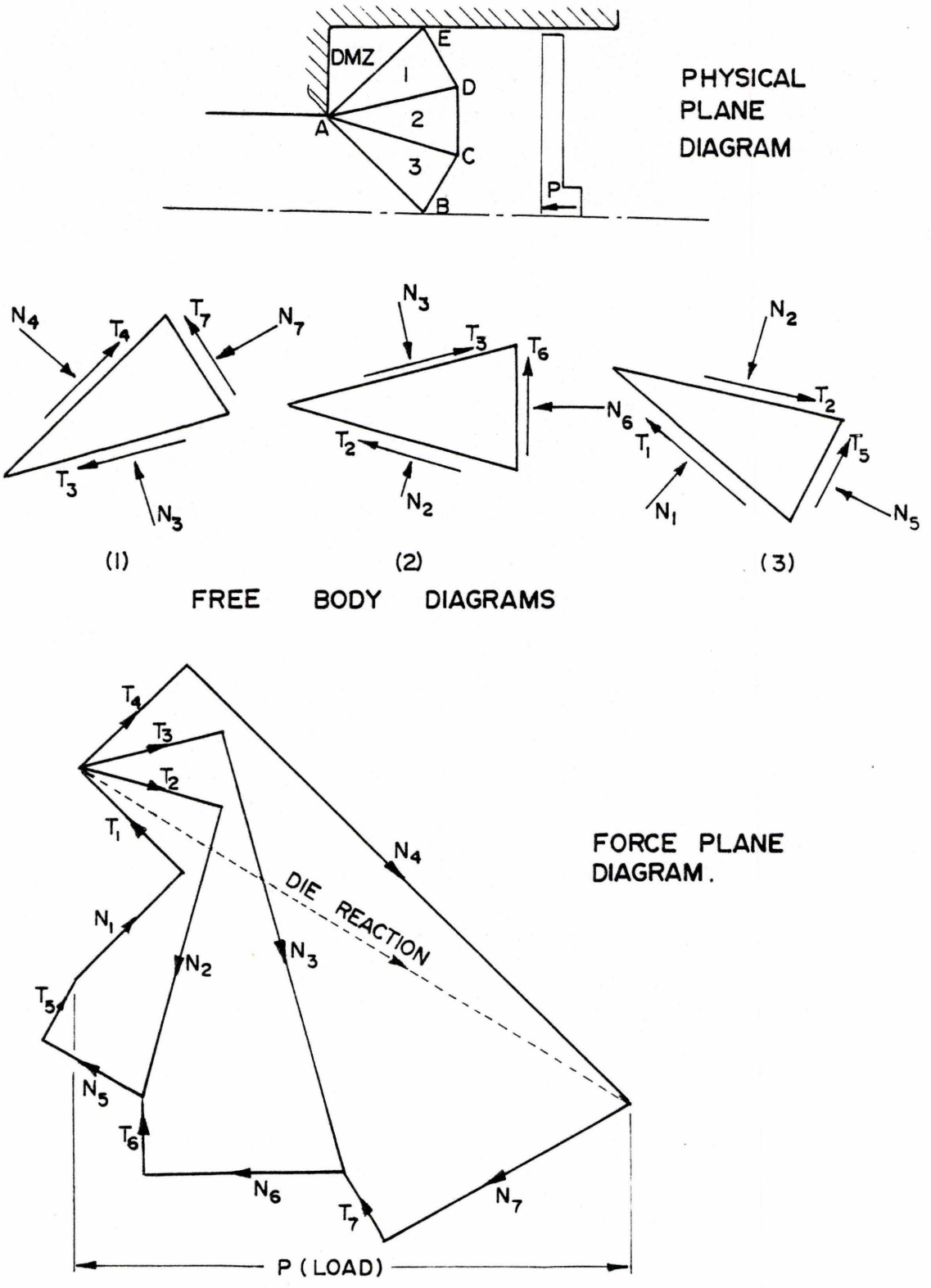

Figure 4.4(a)

Tangential velocity discontinuity field and force plane diagram for forward extrusion; from ref. [137].

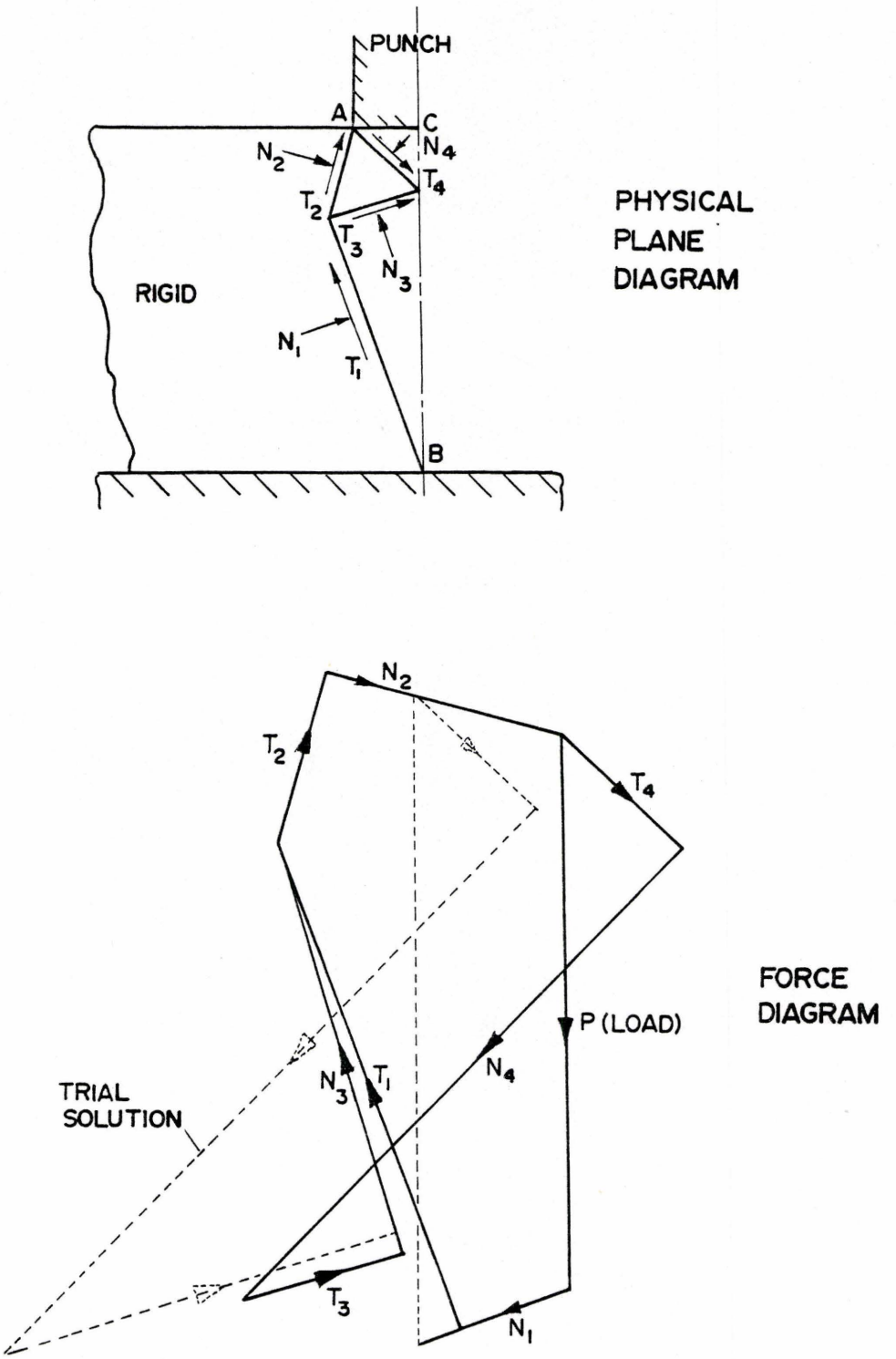

Figure 4.4(b)

Velocity discontinuity field and force plane diagram for indentation; from ref. [137].

free body diagrams for the three triangular elements in Figure 4.4 are shown and the complete "associated" force diagram is also given. The extrusion force is defined by the resultant 'x' component P.

In the original paper by Westwood and Wallace [138] plane strain extrusion, drawing, tube ironing and compression were examined and force polygons presented for each of these cases. Theoretical curves were presented for the variation of the extrusion parameter (p/2k) with extrusion ratio and frictional condition. Johnson and Mamalis [137] examined extrusion rolling, indenting and machining and indicated solutions for these processes. Figure 4.4b illustrates the solution for indenting which can be considered as a second type of solution. In the first type of solution, illustrated in Figure 4.4a, the starting point was a boundary of the plastic deformation zone where the direction of a force was known; recall that the boundary condition was that the force to the left of AB in the 'x' direction was zero. For problems, such as indenting there are two shear planes at the exit plane where the boundary conditions are known. Consequently, while the tangential forces on AB and BC are known the value of the normal forces cannot be determined explicitly for the boundary condition that the resultant force acting parallel to the base is zero; a trial and error procedure is therefore adopted. The solution given in Figure 4.4b is taken from Johnsons' paper [137] and iit should be noted that the normal force N_1 is a tensile force. Clearly the extrusion load could have been determined more simply using the standard upper bound sliding block technique after drawing the hodograph.

It is clear that, whilst the force polygon method is simpler and more direct than the traditional velocity discontinuity and hodograph method, it can be less accurate and more time consuming. The solution for processes which involve more than a single shear plane at a position where the boundary conditions are known, gives rise to a tedious trial and error procedure and, although possible, is not recommended. The major advantage of the method is that the force on a given plane can be determined directly.

4.2.3 Effect of Strain Hardening

Halling and Mitchell [49] have extended the original upper bound analysis to accommodate the strain hardening characteristics of real materials. Figure 4.5 indicates schematically the stress strain curve for a typical strain hardening material with a constitutive law of the kind,

$$\bar{\sigma} = \sigma_0 (\varepsilon_0 + \bar{\varepsilon})^n \tag{4.3}$$

The work per unit volume, indicated by the shaded portion in Figure 4.5 is given by:

$$W = \int_{\varepsilon_1}^{\varepsilon_2} \bar{\sigma} d\bar{\varepsilon} \tag{4.4}$$

Assuming a mean equivalent stress σ_m,

$$W = \bar{\sigma}_m (\varepsilon_2 - \varepsilon_1) \tag{4.5}$$

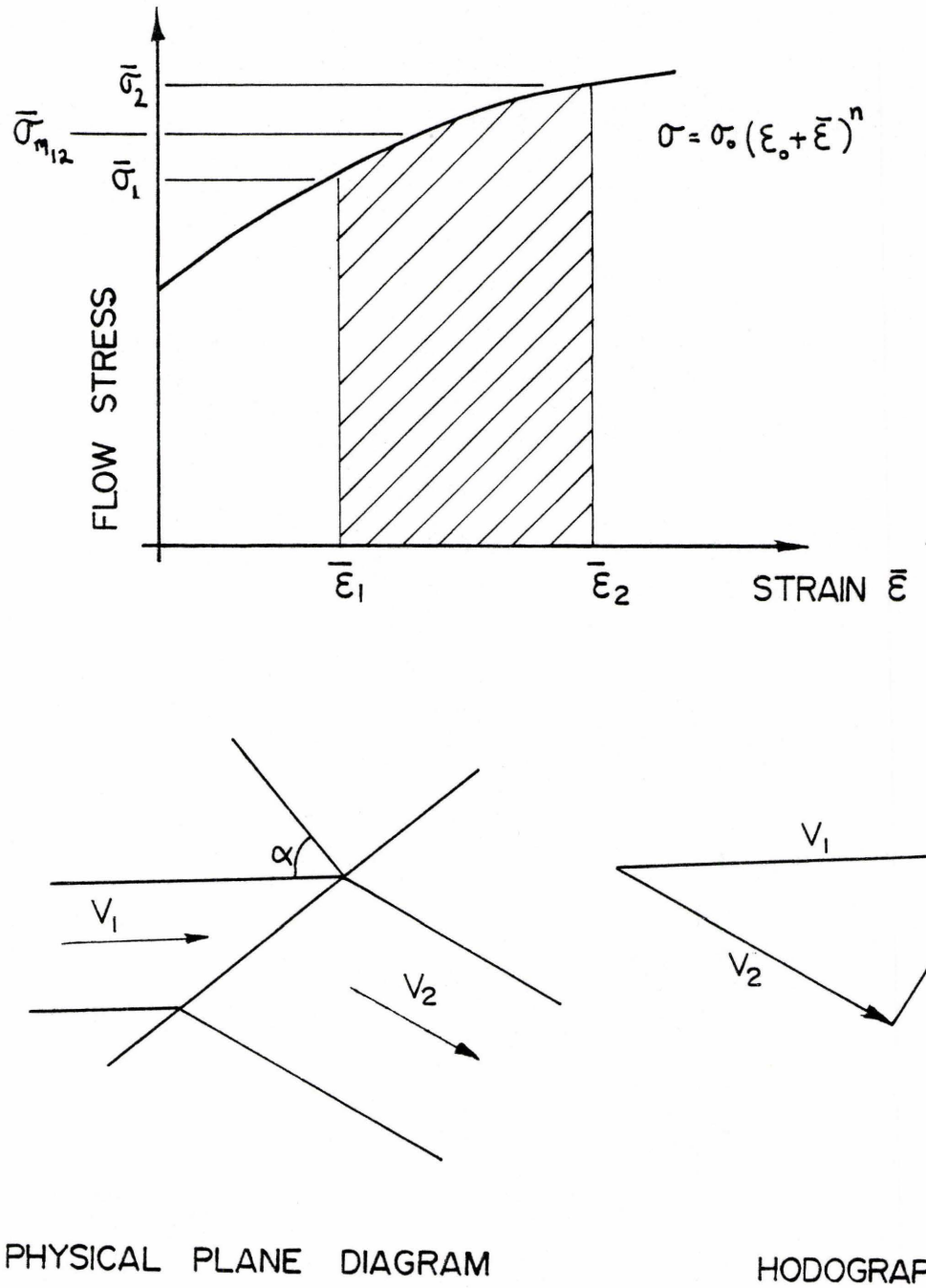

Figure 4.5

Schematic representation of a stress strain curve for a typical strain hardening material indicating work done in crossing a discontinuity from 1 to 2

If the Von Mises yield criterion is assumed, then the yield stress is given by:

$$k_c = \bar{\sigma}/\sqrt{3} \tag{4.6}$$

where k_c is the current yield shear stress. Halling and Mitchell introduced a mean yield shear stress which, by equating the work equations, defined the strain across the tangential velocity discontinuity in terms of the velocities, i.e.

Across any discontinuity the work rate, per unit depth, is obtained from Eqn. (4.5)

$$\dot{\omega} = \sigma_m (\varepsilon_2 - \varepsilon_1)\, sv_n \tag{4.7a}$$

where s is the length of the discontinuity and

v_n is the velocity normal to the discontinuity.

Recall Eqn. (4.2)

$$\dot{w} = k\, v^*\, s$$

substituting for the yield shear stress, Eqn. (4.6)

$$\dot{w} = \frac{\bar{\sigma}_m}{\sqrt{3}}\, v^*\, s$$

and equating to Eqn. (4.7) we obtain

$$\varepsilon_2 - \varepsilon_1 = \frac{v^*_{12}}{v_n \sqrt{3}} \tag{4.7b}$$

The strain across each discontinuity can be determined from the hodograph and used to compute the total work. The pressure derived

using this analysis is not significantly different than that given by the rigid perfectly plastic solution assuming a mean strain. However, this solution enables a theoretical prediction of the hardness distribution across the extruded product to be made. Halling and Mitchell analysed the forward extrusion process using a velocity field proposed by Johnson and indicated that the theory yielded information which was in agreement with known physical behaviour.

4.2.4 Effect of Rate-sensitivity

The effect of velocity or strain rate cannot be handled in any explicit manner by the upper bound technique as discussed this far. The tangential velocity is assumed to make an instantaneous change across any discontinuity and consequently the strain rate is infinite. The variation of properties with strain or strain-rate is usually handled by defining a mean flow stress associated with a mean strain or strain rate as appropriate.

Recently Fenton [98], as discussed in Chapter 2, has approached the analysis from the view point of a tangential shear zone. Although this solution is correct along a shear zone, continuity and incompressibility conditions are not satisfied when two tangential velocity discontinuities meet and overlap. The velocity field is defined as usual but the discontinuities are considered to have finite width. The strain rate within the shear zones can thus be defined and the flow stress evaluated accordingly. Fenton's analysis defined an effective strain rate and determined this in terms of the zone width and the die

geometry as shown in Figure 4.6. The expression for the strain rate within AC is:

$$\dot{\varepsilon}_{AC} = \frac{1}{\sqrt{3}} \frac{H\ u\ \mathrm{Sin}\ \alpha}{h\ \Delta S\ \mathrm{Sin}\ (\alpha+\theta)} \tag{4.8}$$

An equivalent strain rate was defined and used to determine the flow stress based on an empirical flow stress relationship; i.e.

$$\bar{\sigma} = \sigma' \bar{\varepsilon}^{n} \tag{4.9}$$

where σ' and the exponent n are functions of the strain rate. A constant ratio of the shear zone width to the shear zone length was assumed and extrusion pressures calculated. The calculated values were compared with experimental results available in the literature for lead and aluminium and the correlation shown to be good. The value of the length to width ratio of the shear zone was varied and it was indicated that this ratio made only a small difference on the value of the predicted extrusion pressures. This is not surprising since the strain rate sensitivity of the materials chosen was very small; less than 0.1. The concept of a thin shear zone has its origin in the mechanics of metal cutting and one finds that researchers in the metal cutting area have been using a form of the upper bound solution for some time although not discussed as such. This topic is dicsussed in more detail in a later section of this chapter.

The work of Fenton is the only analysis, to the author's knowledge, which incorporates the effects of the rate sensitive material properties into the upper bound technique. However, since a strain

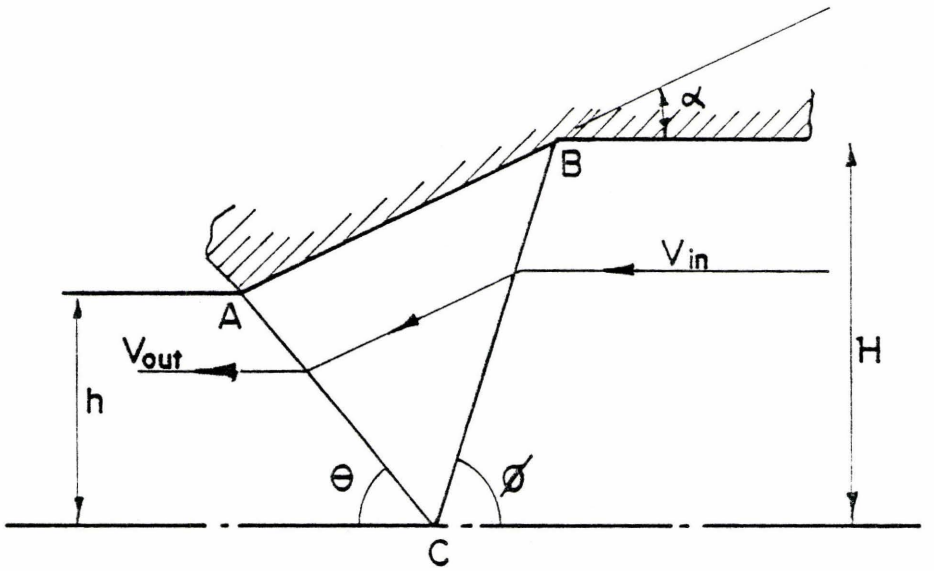

PHYSICAL PLANE DIAGRAM

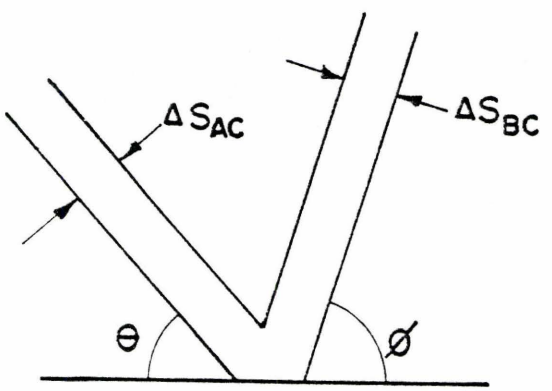

SHEAR ZONE GEOMETRY
AT C

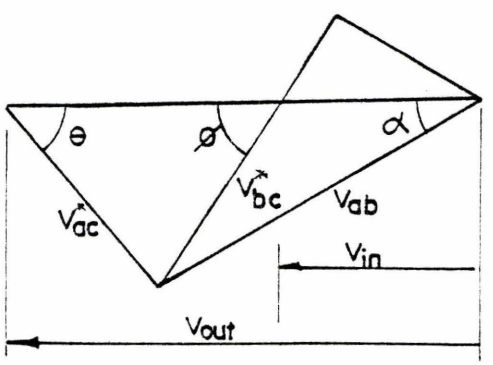

HODOGRAPH.

Figure 4.6

Diagram indicating die and shear zone geometry used by Fenton [96]

hardening constitutive equation was used it is difficult to differentiate between the effects of strain hardening and strain rate sensitivity.

4.3 Upper Bound Solution for Rate Dependent Materials - a New Analysis

Consider plane strain conditions with unit depth and assume that material shears in a narrow band at constant strain rate; outside this band material is rigid. The material behaviour can be characterized by a constituitive equation of the form:

$$\bar{\sigma} = \sigma_o \dot{\bar{\varepsilon}}^m \qquad (4.10)$$

or $$\tau = k' \dot{\gamma}^m$$

We examine a small element ABCD within the band a distance 'x' from the boundary as shown in Figure 4.7. A point such as 'A' has components of velocity v_T and v_n as indicated in the hodograph.

By definition, the shear strain rate is:

$$\dot{\gamma} = \frac{dv_T}{dx} + \frac{dv_n}{dy} \qquad (4.11)$$

but v_n is constant and as v_T is a function of 'x' only equation (4.11) can be written as:

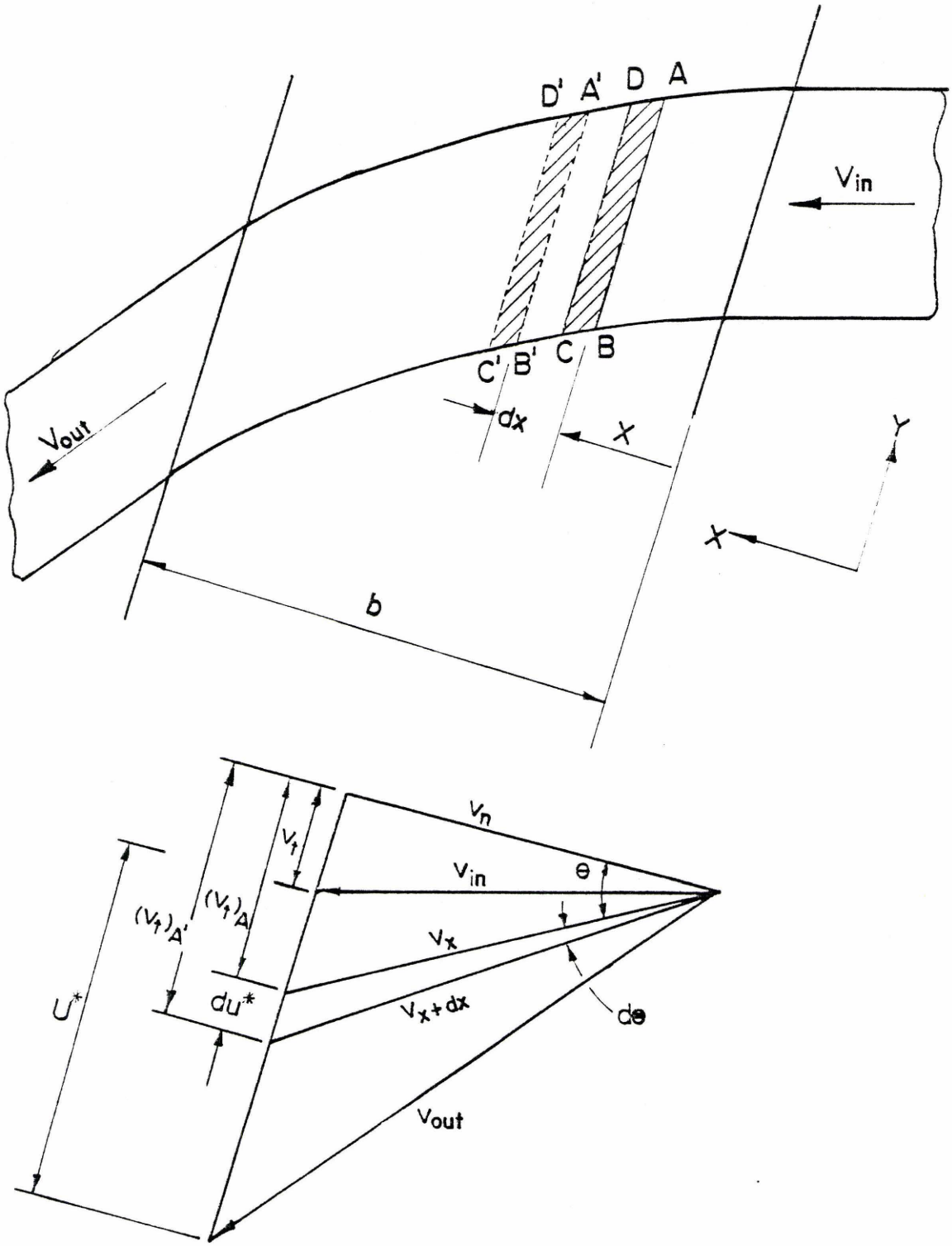

Figure 4.7

Geometry of shear zone and hodograph used in analysis

$$\dot{\gamma} = \frac{dv_T}{dx} = \frac{dv^*}{dx} \tag{4.12}$$

where dv^* is the change in tangential velocity. It is prescribed that $\dot{\gamma}$ is constant within the band and hence as dv^*/dx is constant, we obtain

$$\dot{\gamma} = \frac{v^*}{b} \tag{4.13}$$

where v^* is the total tangential velocity change and b the band width.

From the geometry of the hodograph

$$dv^* = \frac{v_n d\theta}{\cos^2\theta} \tag{4.14}$$

and as dv^*/dx is a constant, the shape of the streamline is defined by the condition

$$\frac{1}{\cos^2\theta}\frac{d\theta}{dx} = \text{constant} \tag{4.15}$$

An upper bound on the shear stress acting on the face AB may be taken as

$$\tau = k'\{\frac{v^*}{b}\}^m \tag{4.16}$$

and the rate of doing work during the displacement dx is

$$d\dot{W} = \tau dv^* ds \tag{4.17}$$

where ds is the length along the band, namely AB. Substituting equation (4.12) into equation (4.17) and integrating, we obtain

$$\dot{W} = \tau\dot{\gamma}bds \tag{4.18}$$

substituting for τ and $\dot{\gamma}$

$$\dot{W} = k' \frac{v^{*m+1}}{b^m} \quad ds \tag{4.19}$$

In analysing any process we establish an upper bound field as for a rigid perfectly plastic material but consider that each discontinuity is a band of finite width b. The total power dissipated by the process is thus

$$\dot{W} = \sum_{i=1}^{n} \frac{k' u_i^{*m+1}}{b^m} s_i \tag{4.20}$$

where s_i is the length of each band.

Considering frictional faces: An upper bound on the frictional component of the work rate can be determined by assuming that material shears at the boundaries with a shear stress equal to the local yield shear stress. That is that the Coulomb friction coefficient, μ, at the tooling interface fulfills the condition that

$$\mu > \frac{k'}{p_Q} \frac{v_Q}{b}^m \tag{4.21}$$

where p_Q is the normal pressure on the interface.

At a shearing tool face Q the shear strain rate is then given by:

$$\dot{\gamma}_Q = \frac{v_Q}{b} \tag{4.22}$$

and the working rate is

$$\dot{W}_Q = \frac{k'}{(b)^m} u_Q^{1+m} s_Q \tag{4.23}$$

If appropriate this term is added to the summation in equation (4.20).

4.3.1 Dimensionless extrusion parameter for rate sensitive materials

A dimensionless parameter can be recognized of the form:

$$\frac{\bar{p}}{k'} \{\frac{b}{V_{in}}\}^m \tag{4.24}$$

The similarity between this parameter and the rigid plastic extrusion parameter ($\bar{p}/2k$) is clear. In the analysis given below, this parameter will be used to indicate the effect of the rate sensitivity on the extrusion pressure and the velocity field.

Rewriting equation (4.21) for the work rate and equating it to the external work rate then

$$\bar{p} * D * V_{in} = \frac{k'}{(b)^m} \sum v_i^{*(m+1)} s_i \tag{4.25}$$

$$\frac{\bar{p}}{k'}\left\{\frac{b}{V_{in}}\right\}^{m} = \frac{1}{DV_{in}^{(m+1)}}\sum v_i^{*(m+1)}\, s_i \qquad (4.26)$$

It is apparent that the extrusion parameter is a function of the die geometry, the ram velocity and the tangential velocity change. If m=0 then equation (4.26) reduces to the more familiar form given by the rigid plastic upper bound technique. The extrusion parameter presented above can be considered to be made up of two components; a component due to the rigid plastic work and a component due to the materials rate sensitivity.

4.3.2 Summary of the Rate Sensitive Upper Bound Technique

A contribution has been made in the form of a solution for bulk deformation problems which is an extension of the upper bound technique. The concept of a shear zone of constant shear strain rate was introduced and equations developed for the work rate across the shear zone. The value of the shear zone width is initially assumed constant and a dimensionless extrusion parameter was recognized as shown in equation (4.26). The value of the shear zone width and the choice of a appropriate value is discussed in detail in section 4.5. If the strain rate sensitivity index in equation (4.26) is equated to zero then the solution is identical to that given by the rigid perfectly plastic analysis.

4.4 Application of Upper Bound Solutions

The side extrusion process, as described in Chapter 3, is used in the present study to evaluate the effect of material properties on the velocity field. Many slip-line fields have been proposed for various geometries of the side-extrusion process and were indicated in Chapter 3, as for example Figure 3.8. Thus far the upper bound technique has been used only once in the analysis of the side extrusion process [42]. Intuitively one chooses tangential velocity diagrams which are approximations to the slip-line field solution and in this section three tangential velocity fields are proposed and compared using the upper bound technique assuming rigid perfectly plastic material behaviour.

4.4.1 Rigid-plastic Solution: Model #1

The first model of velocity discontinuities is shown in Figure 4.8 and is similar to that suggested by Johnson [42]. This model is a simple velocity field derived from the slip-line field presented by Green [7]. The material below BDF is considered to be rigid and is accordingly a dead metal zone. The bottom of the die is assumed to be far away and does not interact with the deformation zone. The process is assumed to be frictionless and the discontinuities EF and DF supposed to intersect the die wall at 45^{o}. The algebraic expressions for the lengths of the discontinuities and the velocities are presented in detail in Appendix 1. Briefly the work rate is a function of the extrusion ratio and the distance 'x' indicated in Figure 4.8. The optimum value of 'x' can be determined explicitly by considering the

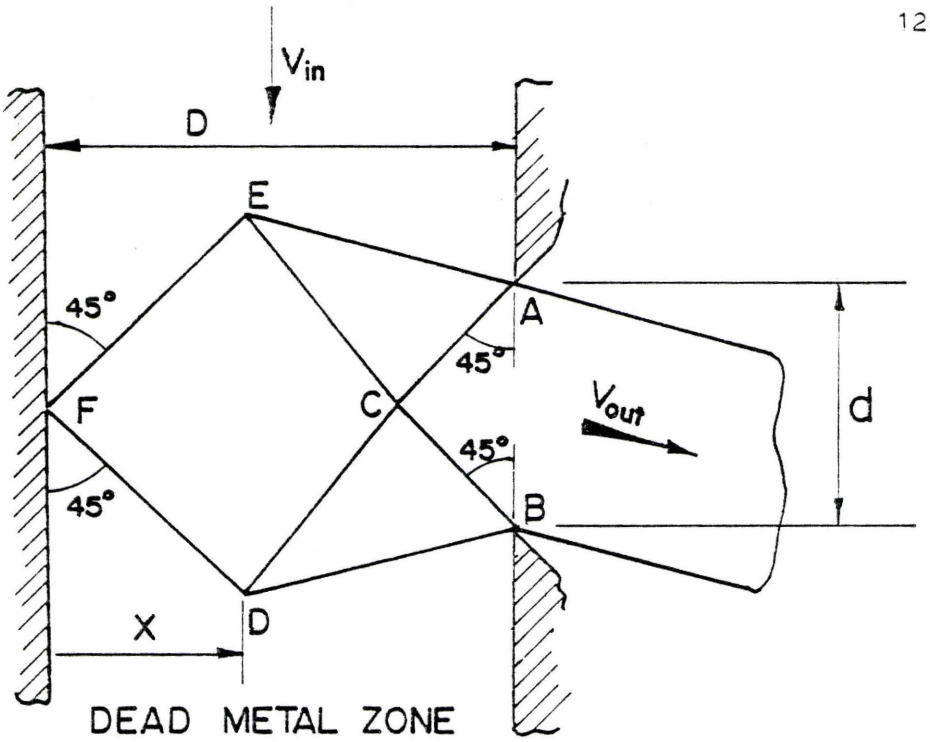

a) PHYSICAL PLANE DIAGRAM

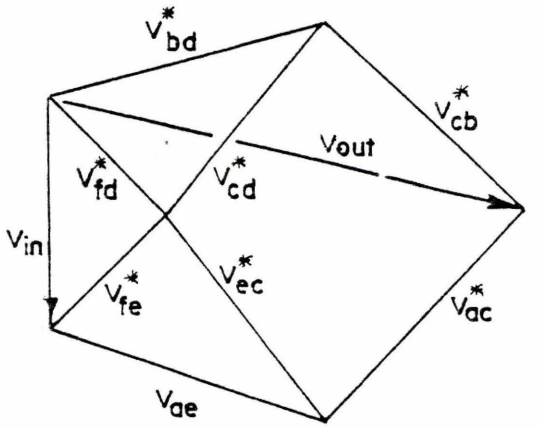

b) HODOGRAPH

Figure 4.8

Tangential velocity discontinuity field and hodograph; Model #1

work rate and minimizing this function. The analysis is presented in Appendix 1 where it is found that the optimum value of 'x' is given by

$$x = \{\frac{2D-d}{4}\} \qquad (4.27)$$

where D is the width of the billet

and d the die aperture.

The values of the extrusion parameter ($\bar{p}/2k$) given by this model for various extrusion ratios is given in Table 4.1.

Fractional Red.	0.5	0.6	0.67	0.75	0.8	0.9	0.95
Extrusion Ratio	2	2.5	3	4	5	10	20
($\bar{p}/2k$)	2.13	2.6	3.08	4.06	5.05	10.03	20.01
$(\bar{p}/2k)_{slf}$	1.75	2.0	2.18	2.48	2.73	-	-

TABLE 4.1

Variation of extrusion parameter with fractional reduction: Model #1

4.4.2 Rigid Plastic Solution: Model #2

In the first model the intersection of the discontinuities with the die wall was set at 45° which is the boundary condition, in the slip-line field solution, if the process is assumed frictionless. This limited the field to a single degree of freedom. In this model no constraint is exercised with regard to the intersection of the discontinuities as shown in Figure 4.9. The field has a total of three degrees of freedom as defined by the angles θ, ψ, ξ. Algebraic expression have been determined for the tangential velocity changes and the lengths of the discontinuities and are presented in Appendix 2. The

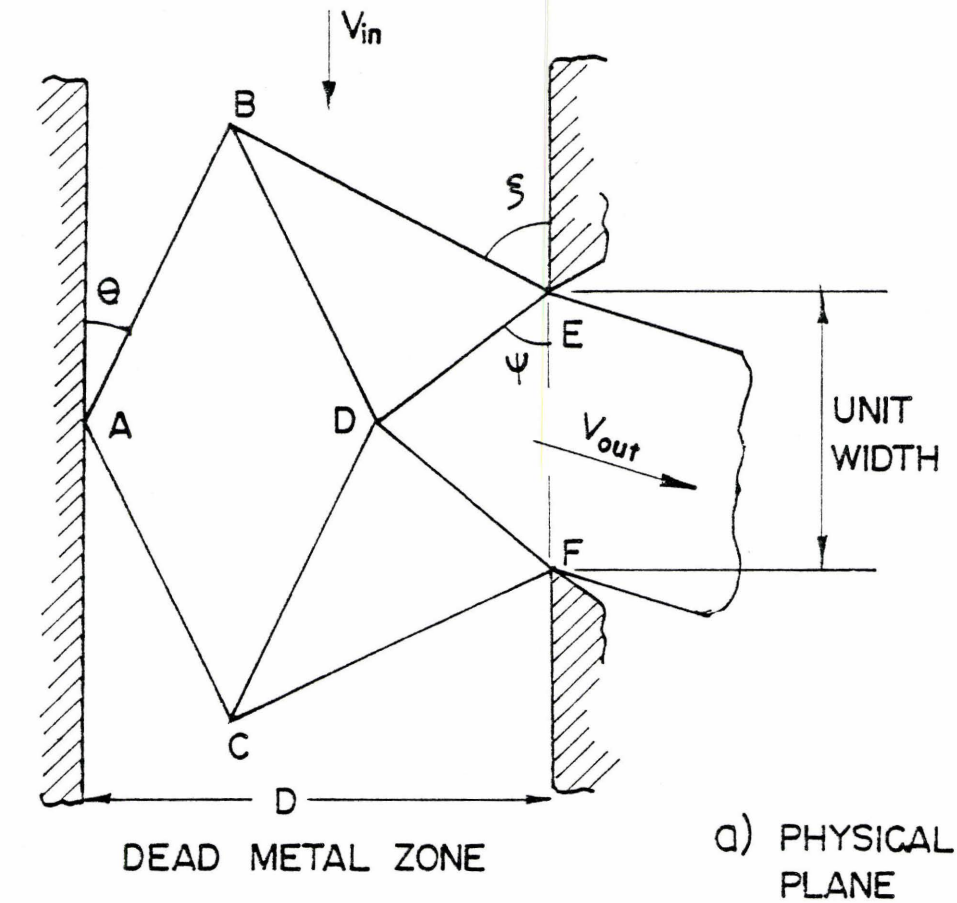

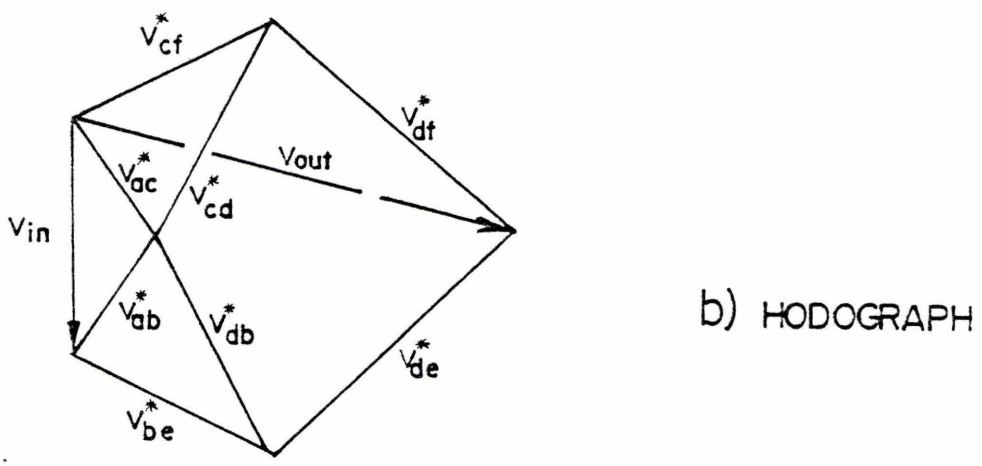

Figure 4.9

Tangential velocity discontinuity field and hodograph; Model #2

optimum solution is again given by that field which minimizes the work. With three variables, however, there is no simple explicit solution to minimize the work equation and one must resort to numerical computation. The optimization programs by Siddall [141, 142] in the 'OPTISEP' package have been used to generate the optimum solutions for different extrusion ratios. The solution presents the optimum field geometry and the extrusion parameter ($\bar{p}/2k$).

The 'OPTISEP' package is a computer program package which comprises a number of routines which permit the use of several methods of optimization without a detailed knowledge of optimization theory. In all the programs an objective function is minimized subject to certain constraints. The objective function in this example is the work rate and the constraints which are geometrical, are derived from the physical plane diagram. For the work reported here, two algorithms were used; SEEKI and DAVID and they are outlined briefly below.

SEEKI - This algorithm incorporates a direct search for the optimum followed by a random search to check the solution. Starting from an initial base point, a variable is incremented. If the objective function is minimized and the constraints are satisfied, then the variable is incremented further. If a move does not improve the solution then the variable is returned to its previous value. Each variable is checked in this manner and if no move improves the solution then the step length is halved and the search repeated. This process continues until the step length is smaller than a user defined value or until a maximum number of cycles, again user defined, have been

exceeded.

It is possible for this type of method to hang up on a constraint or to achieve a local rather than global optimum. For this reason the final optimum is checked by generating a number of random values within the vicinity of the assumed optimum. If an improved point is found; indicating that the optimum was only local, then the direct search is repeated.

DAVID - Subroutine DAVID uses the Davidson-Fletcher-Powell gradient method of search. At any step the value of the variable is a function of the previous value and the partial derivatives of the previous step. The program proceeds until two successive values of the optimization function are less than a user defined convergence criterion or the number of iterations exceeds another user defined variable.

In the work described here the solution was generated using both methods and a number of different starting points. In each case the solution generated was the same. The philosphy of optimization techniques and methods are discussed in detail by Siddall [141] and details of the programs used are given in the 'OPTISEP' user's manual [142].

Table 4.2 gives the variation of the extrusion parameter with the fractional reduction for the appropriate optimum field. The variation of the optimum field geometry generated by the the program, for changing fractional reduction is presented in Figure 4.10. The optimum field geometry for two different extrusion ratios is compared with the frictionless slip-line field solution in Figure 4.11.

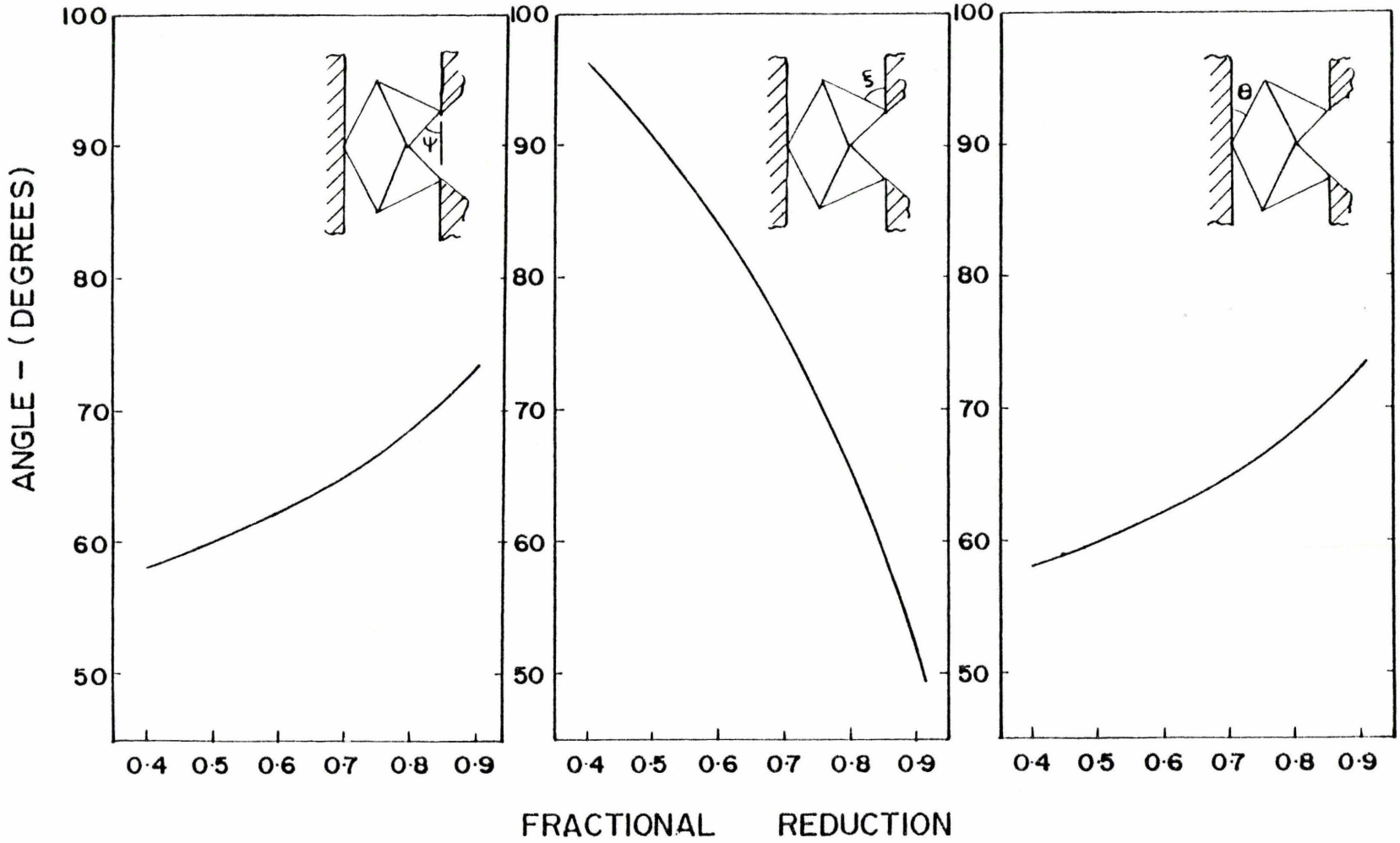

Figure 4.10

Variation of optimum field geometry with fractional reduction for model #2

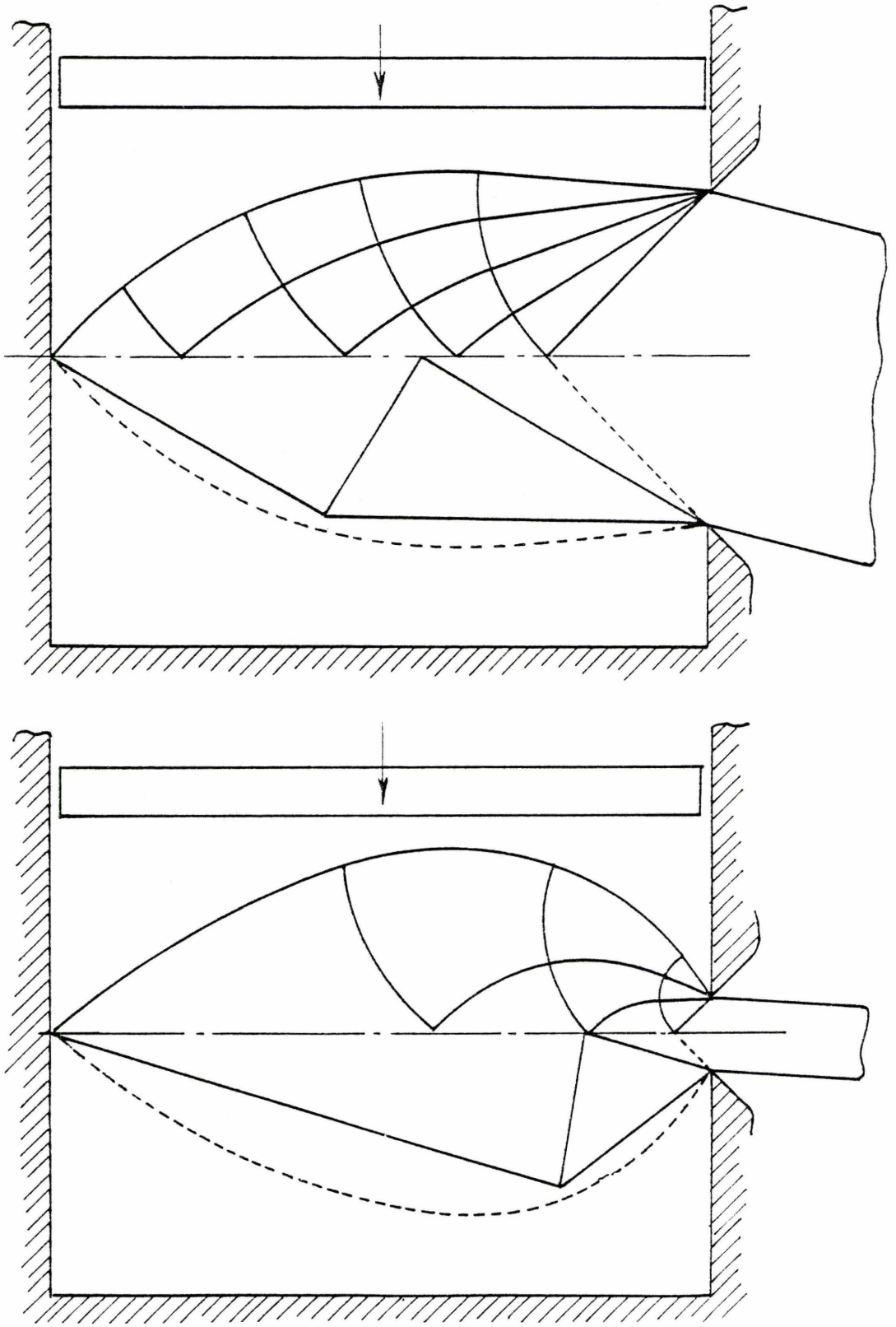

Figure 4.11

Comparison of optimum tangential velocity discontinuity fields with the slip-line field for two extrusion ratios; Model #2

Fractional Red.	0.4	0.5	0.6	0.7	0.8	0.9	0.95
Extrusion Ratio	1.67	2	2.5	3.33	5.0	10.0	20
$(\bar{p}/2k)$	1.62	1.80	2.06	2.42	3.01	4.22	5.71
$(\bar{p}/2k)_{slf}$	1.62	1.75	2.0	2.30	2.73	-	-

TABLE 4.2

Variation of extrusion parameter with fractional reduction: Model #2

4.4.3 Rigid Plastic Solution: Model #3

The previous model was extended in the search for a better solution. Figure 4.12 illustrates the third proposed velocity field. This is a more elaborate discontinuity model than Model #2 with five degrees of freedom as expressed by the angle θ, ψ, ξ, α and β. The 'OPTISEP' package was used to minimize the work equation based on the algebraic expressions for the geometry of the discontinuity diagram and the hodograph as presented in Appendix 3. The variation of the optimum field geometry with fractional reduction is presented in Figure 4.13.

Figure 4.14 illustrates the optimum fields generated by the computer programs for very different extrusion ratios and compares them with the slip-line field. A comparison of the optimum velocity fields for models 2 and 3 for an extrusion ratio of 2 is given in Figure 4.15. The value of the extrusion parameter $(\bar{p}/2k)$ for different fractional reductions is given in Table 4.3.

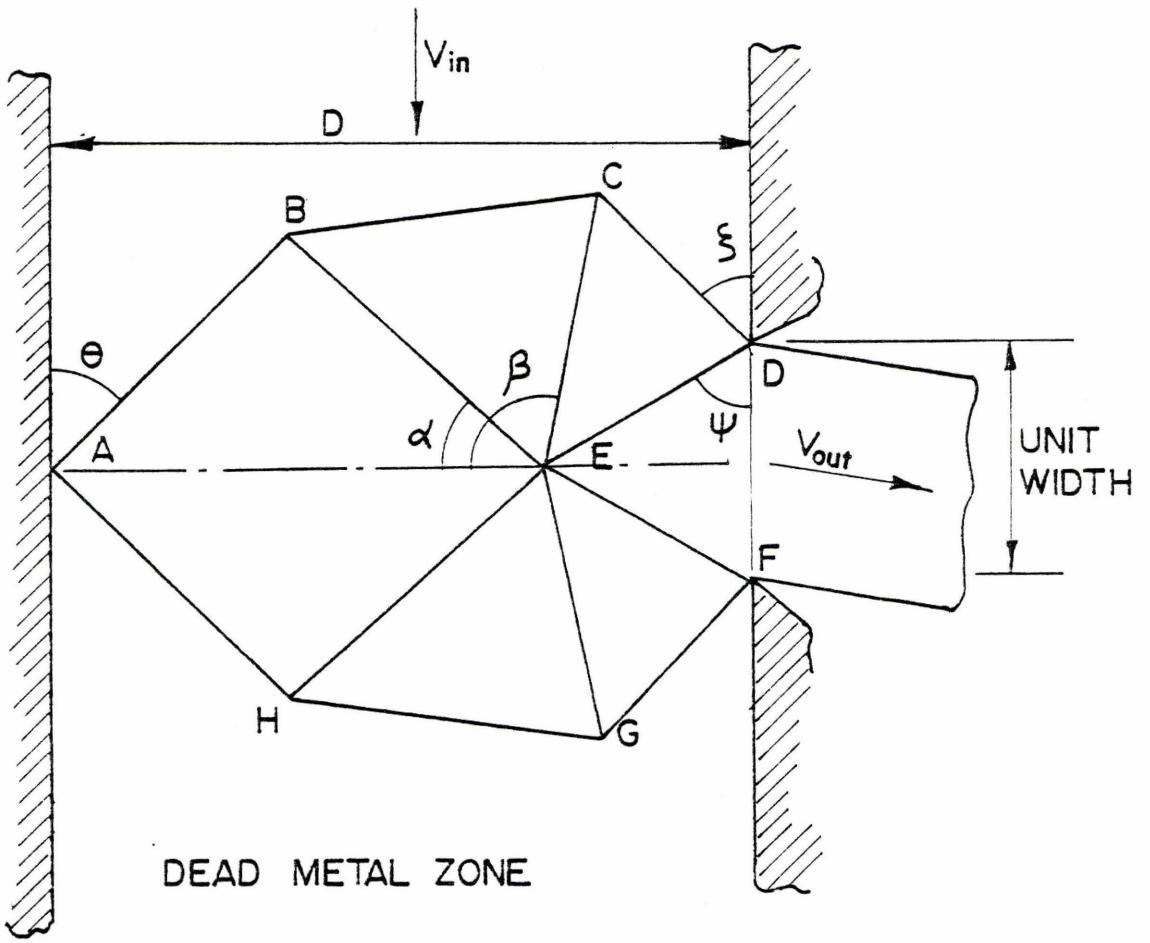

a) PHYSICAL PLANE DIAGRAM

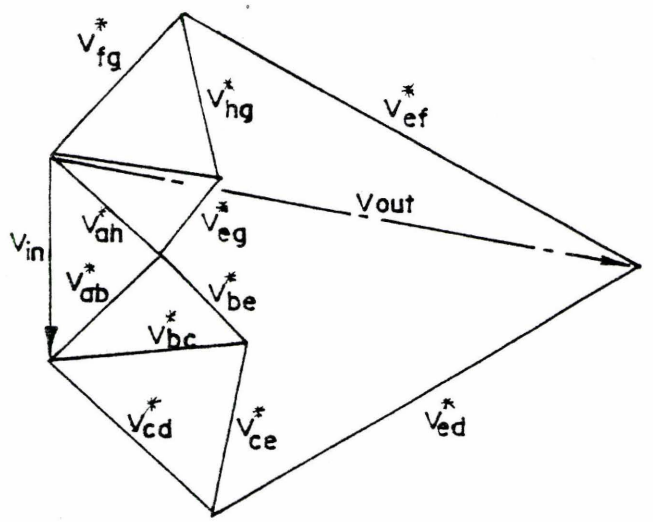

b) HODOGRAPH

Figure 4.12

Tangential velocity discontinuity field and hodograph; Model #3

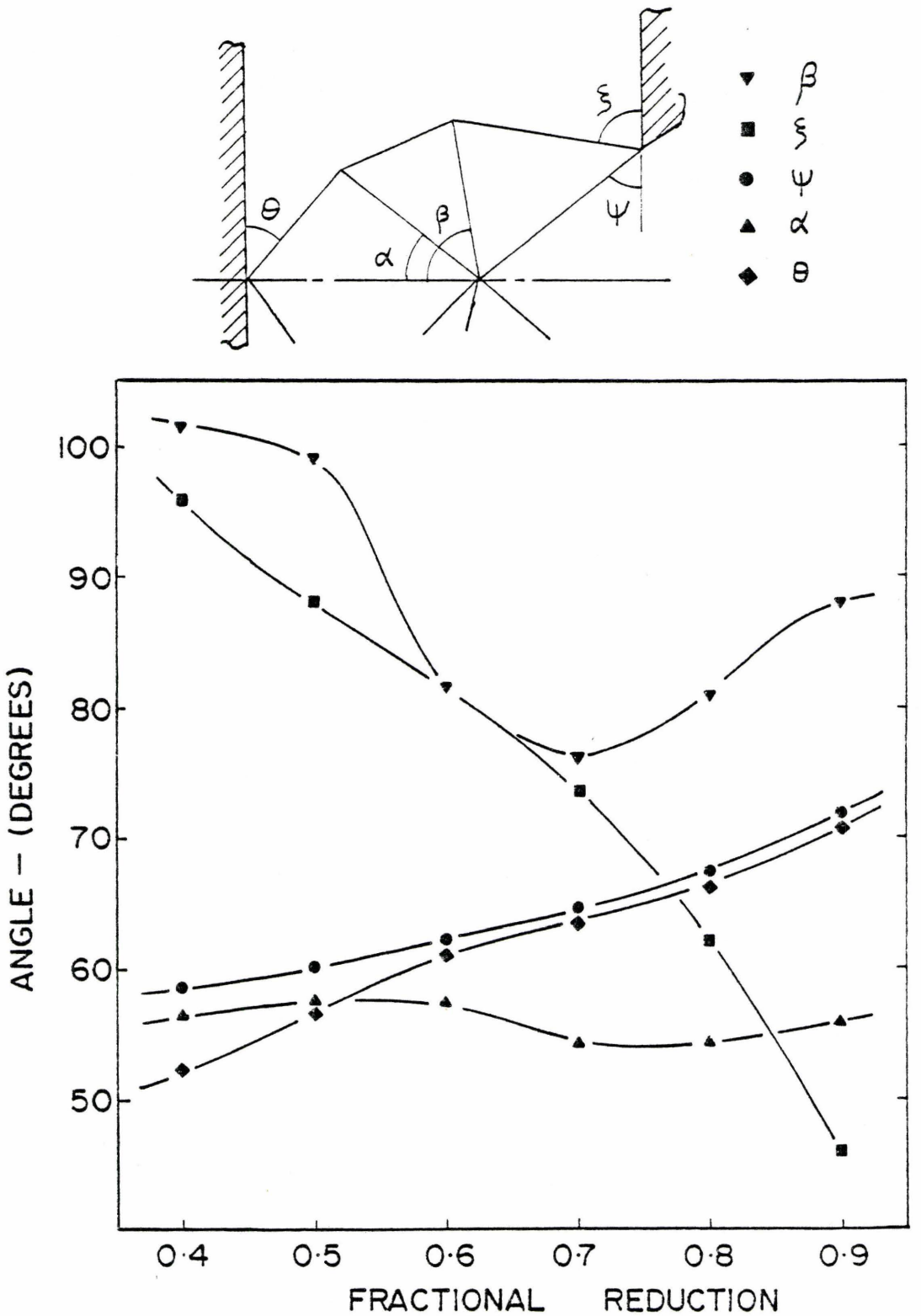

Figure 4.1

Variation of velocity field geometry with fractional reduction; Model W3

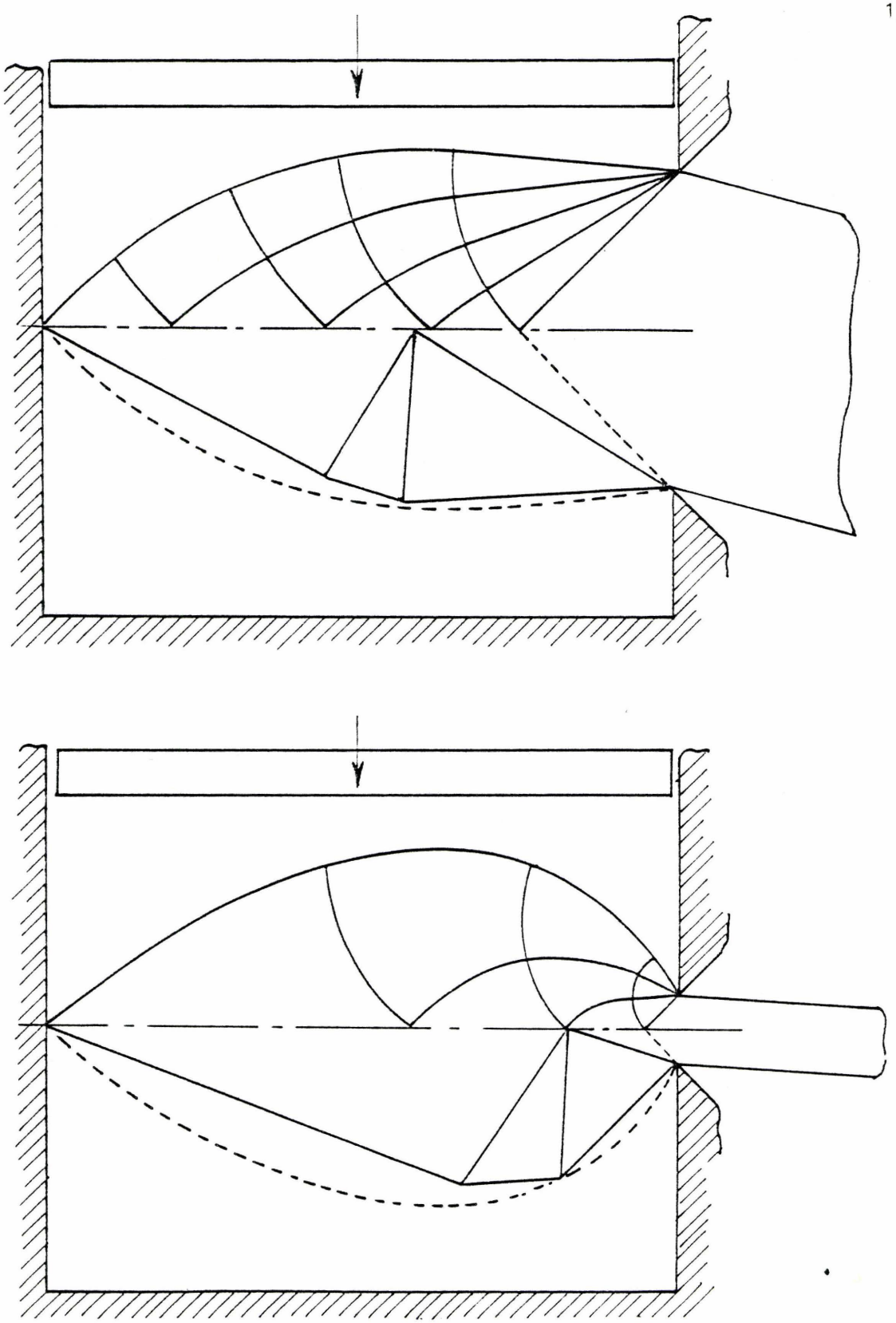

Figure 4.14

Comparison of optimum tangential velocity discontinuity fields with the slip line field for two extrusion ratios; Model #3

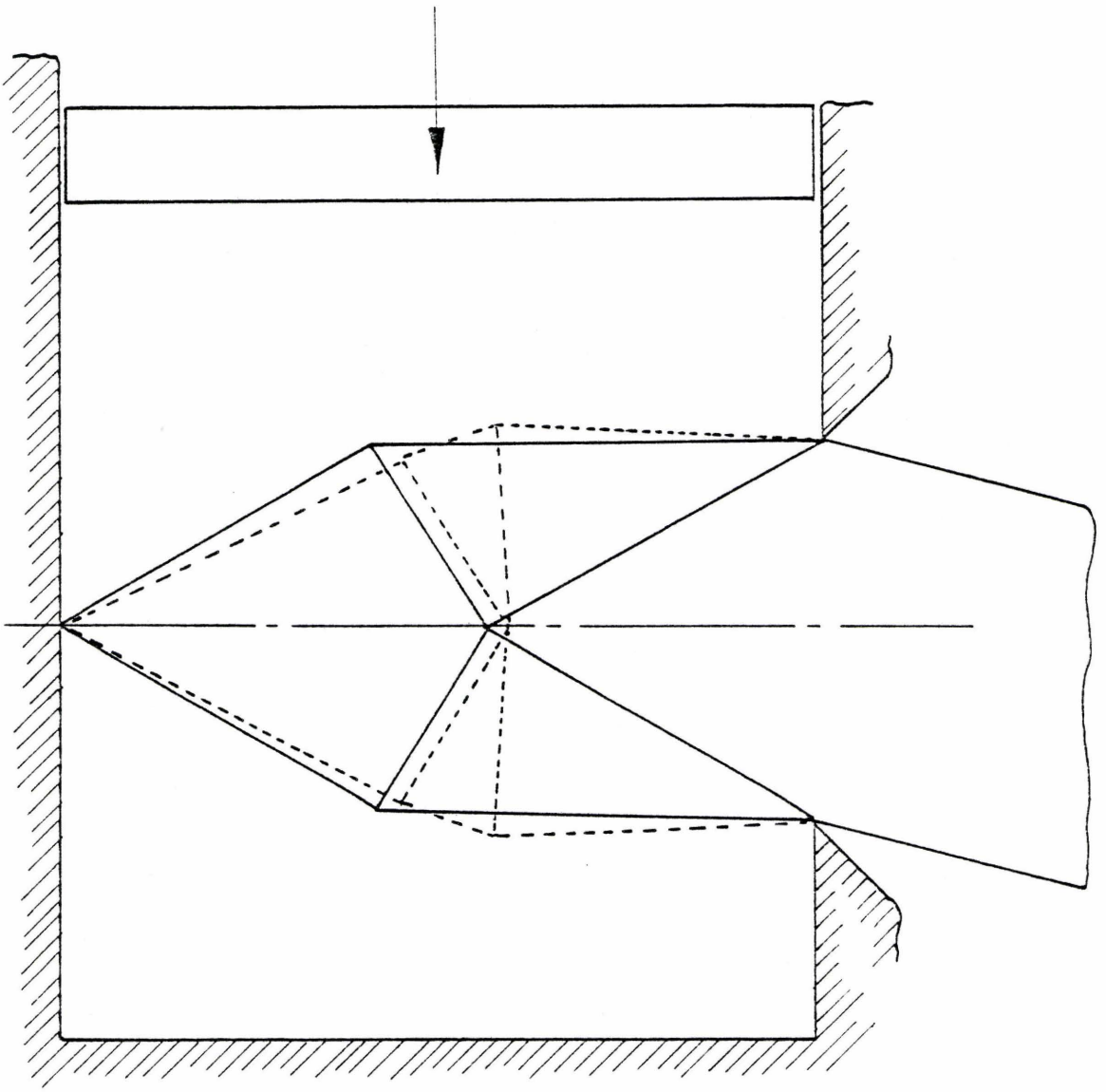

Figure 4.15

Comparison of optimum velocity fields for models 2 and 3 for an extrusion ratio of 2

Fractional Red.	0.4	0.5	0.6	0.7	0.8	0.9	0.95
Extrusion Ratio	1.67	2	2.5	3.33	5	10	20
$(\bar{p}/2k)$	1.63	1.81	2.05	2.4	2.97	4.10	5.44
$(\bar{p}/2k)_{slf}$	1.62	1.75	2.0	2.30	2.73	-	-

TABLE 4.3

Variation of extrusion parameter with fractional reduction: Model #3

4.4.4 Summary of Models for Rigid Plastic Materials

Three tangential velocity discontinuity fields have been presented for the frictionless plane strain side extrusion of a rigid plastic material. The variation of the extrusion prameter $(\bar{p}/2k)$ with fractional reduction for each of the models is compared, in Figure 4.16, with the solution generated using the slip-line field method. It is evident that models 2 and 3 are far superior to model 1 in that the solutions for the extrusion parameter are smaller and closer to the slip line field solution. There is, however, little difference between the values of $(\bar{p}/2k)$ for the second and third models which even at high fractional reductions give solutions which are within 10% of those given by the slip line field analysis. The difficulty of determining an optimum solution is a function of the number of independent variables and the computational time increases dramatically. Consequently, the second model will be used in any further analysis.

4.5 Rate Sensitive Solution: Model #2

In section 4.3 an upper bound analytical technique was developed to handle materials which are rate sensitive. The upper bound solution

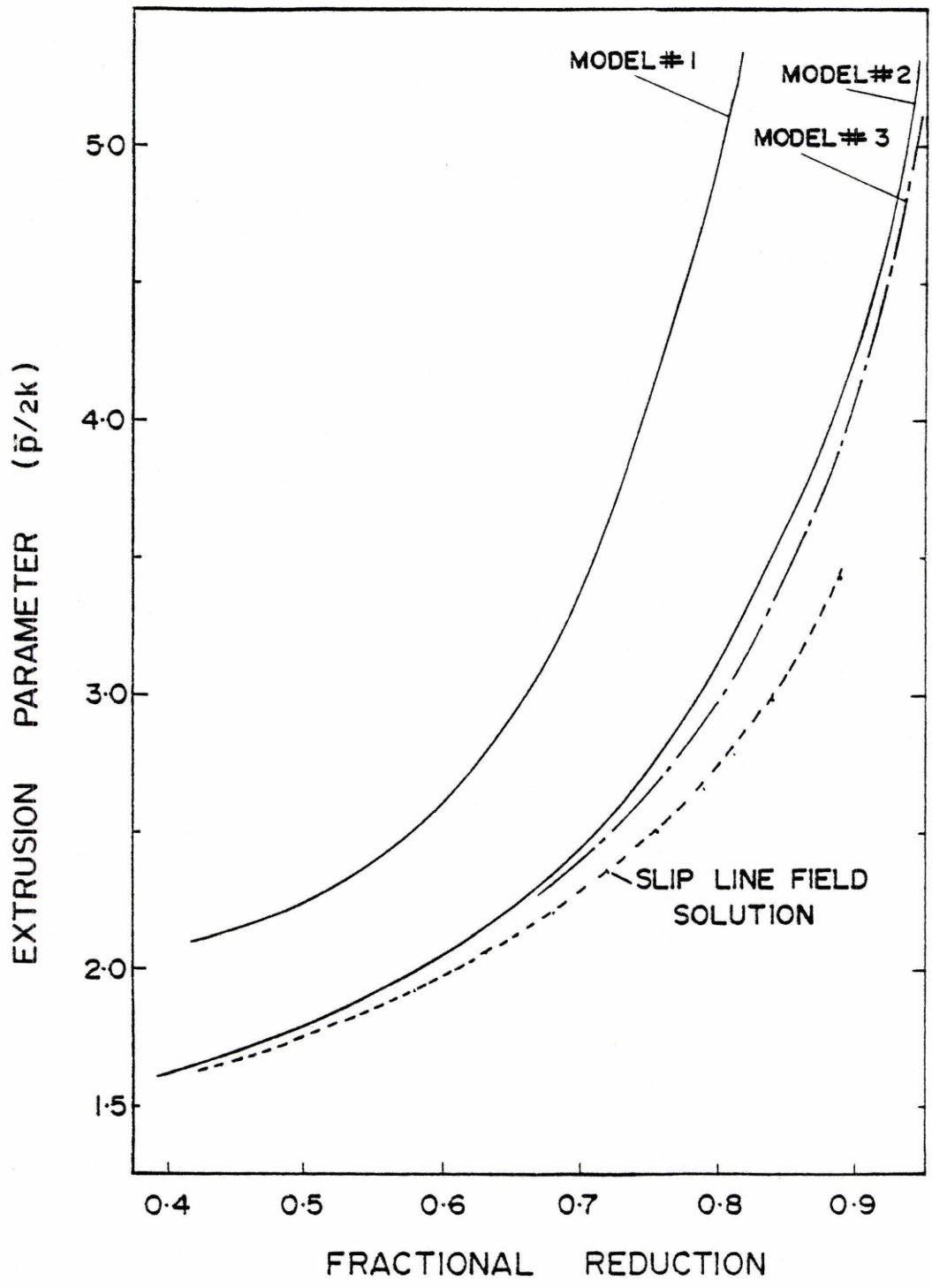

Figure 4.16

Comparison of the variation of the extrusion parameter ($\bar{p}/2k$) with fractional reduction for each model

for the sideways extrusion process was examined and three tangential velocity fields examined in detail for the extrusion of a rigid plastic material. It was evident that the second and third models proposed predicted loads which were very similar and substantially smaller than those predicted by the first model. Due to the savings in complexity and computational time it was decided to use the second model when applying the rate sensitive analysis presented in section 4.3.

A computer program was written using the algebraic expressions developed in Appendix 2 and the 'Optisep' optimization package to minimize the dimensionless parameter identified in the analysis, equation (4.24). The results of the program indicate that:

a) the geometry of the velocity field is a function of the strain rate sensitivity as shown in Figure 4.17

and that

b) the variation of the extrusion parameter with fractional reduction is a function of the strain rate sensitivty as shown in Figure 4.18.

These results are for a material whose mechanical properties are described by an equation of the form indicated by equation (4.10). Recall

$$\sigma = \sigma_o \dot{\bar{\varepsilon}}^m$$

Materials which are highly rate sensitive have a stress, strain-rate curve which is sigmoidal as shown schematically in Figure 4.19 and the material properties are characterized by equation (4.10) only within a

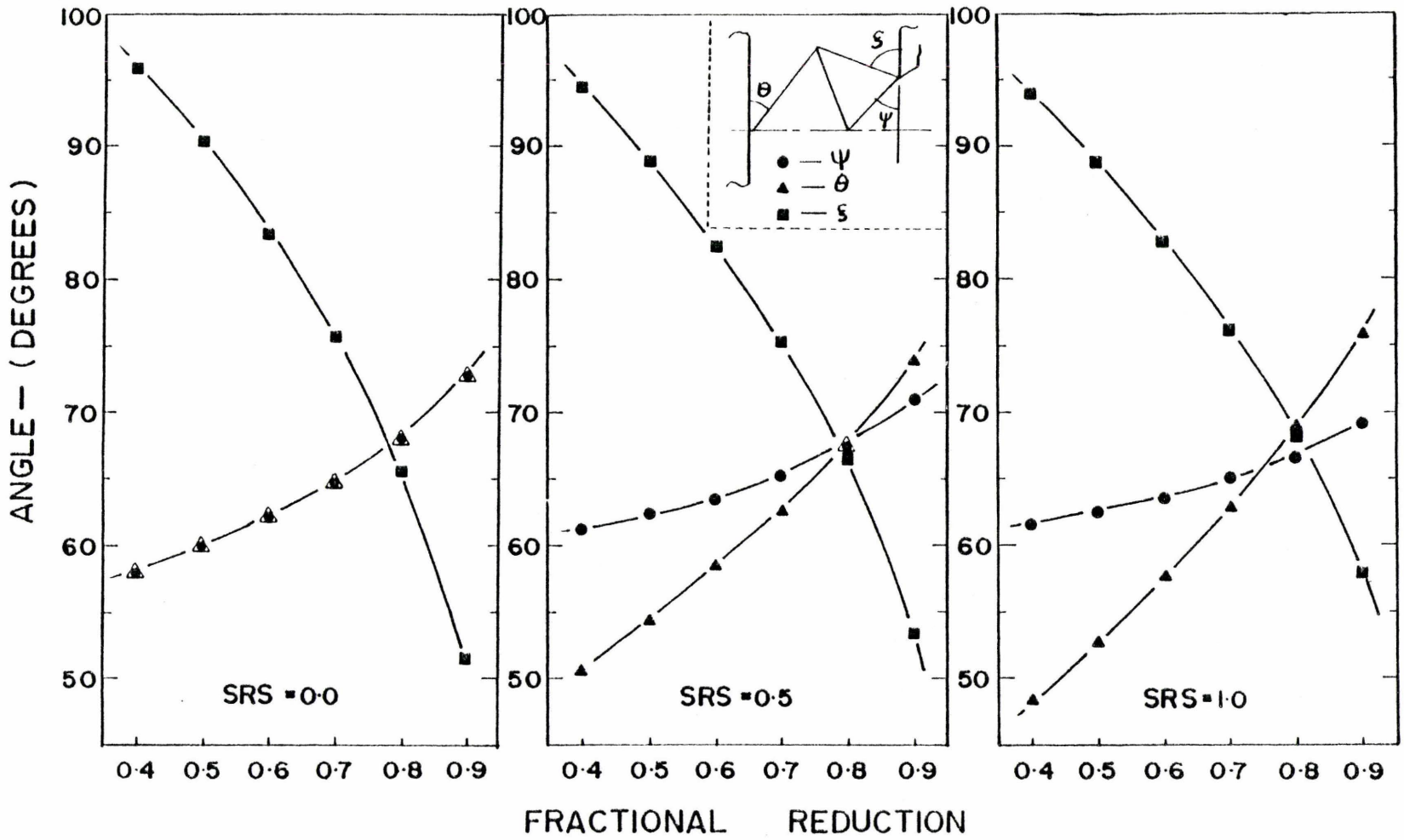

Figure 4.17

Variation of tangential velocity discontinuity field geometry with fractional reduction for different strain rate sensitivities; Model #2

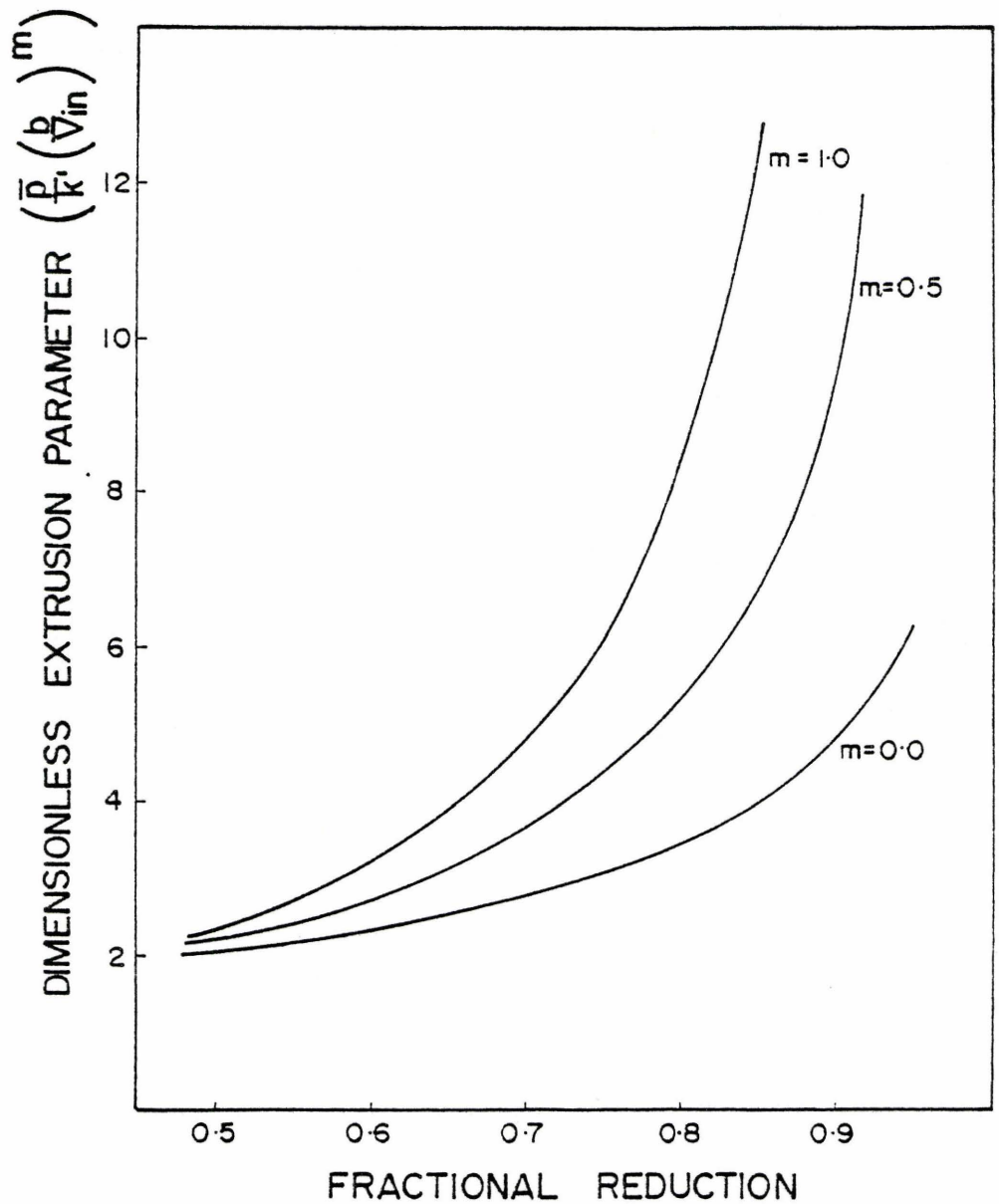

Figure 4.18

Dimensionless extrusion parameter $\bar{p}/k \cdot (b/v_{in})^m$ as a function of fractional reduction and strain rate sensitivity; Model #2

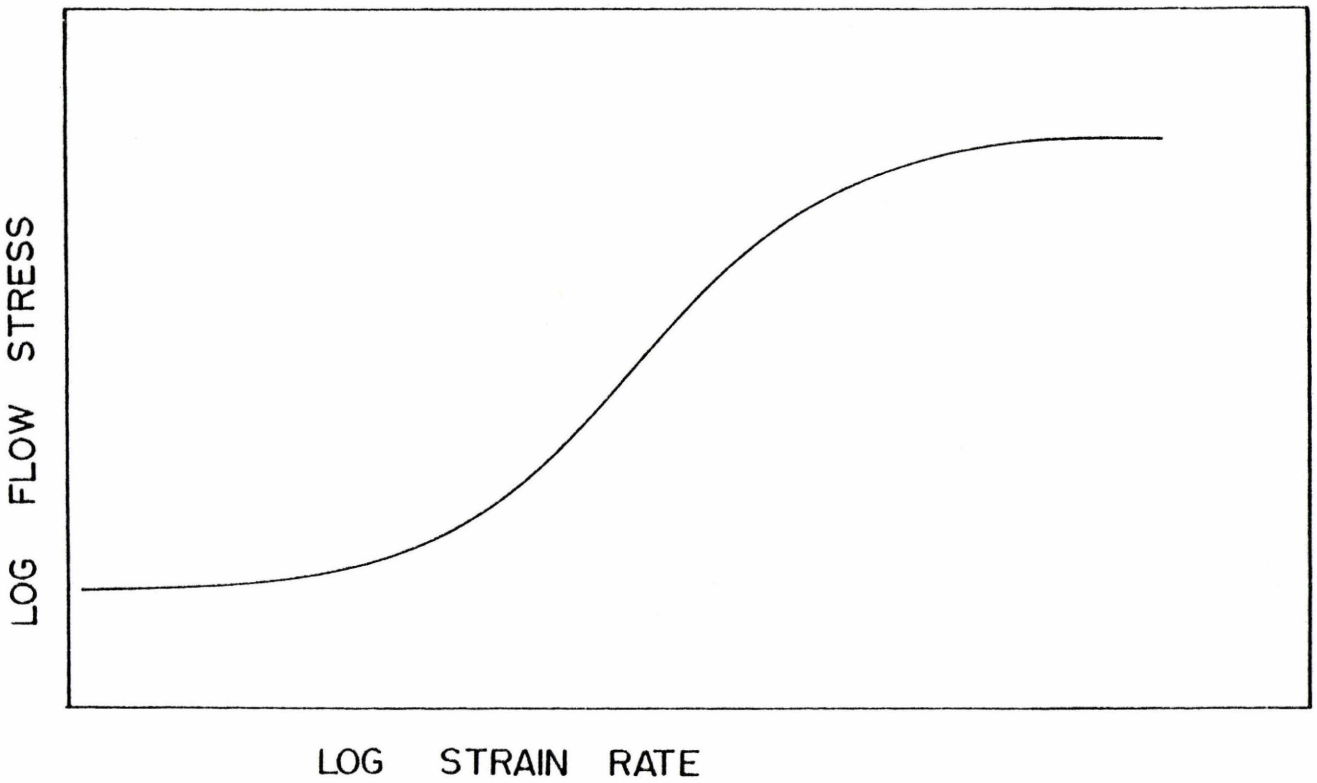

Figure 4.19

Schematic of typical stress, strain rate curve for a rate sensitive material

specified strain rate regime. Outside this regime equation (4.10) is not applicable. The application of the rate sensitive model to real materials is discussed in the following section. The usefulness of examining the variation of the dimensionless extrusion parameter is that it clearly indicates the effect of the strain rate sensitivity on the flow geometry and extrusion pressure.

4.5.1 Application of Rate Sensitive Upper Bound Technique to Real Materials

Figures 4.17 and 4.18 are indications of the effect of the strain rate sensitivity on the velocity field. It is evident that the determination of the extrusion pressure from the dimensionless extrusion parameter requires a knowledge of the material shear strain rate coefficient k', the strain rate sensitivity m, the ram velocity V_{in}, and the shear zone width b.

Engineering materials which are highly strain rate sensitive, that is $m>0.3$, typically have a flow stress, strain rate curve which is sigmoidal in shape as shown in Figure 4.19. The material properties are only rate sensitive within a certain range of strain rates. Outside this range the material behaviour can be considered to be strain rate insensitive. In the analysis presented, the value of the strain rate within the shear zone was evaluated, however the applicability of the material behaviour equation is not considered. In the work presented in later chapters the numerical value of the strain rate, generated by the computer program in its search for an optimum solution, will be used in

conjuction with an appropriate material behaviour equation, to determine the shear flow stress.

The material constant in the dimensionless parameter is the shear strain rate coefficient, k', given by equation (4.16). It is difficult to determine this constant experimentally however, a relationship can be found for the strain rate coefficients σ_o and k': recall

Equation 4.10 $\quad \sigma = \sigma_o \dot{\varepsilon}^m$

Equation 4.16 $\quad \tau = k'\dot{\gamma}^m$

Using the representative stress and strain relationships, it can be shown that, (see Appendix 4):

$$k' = \frac{\sigma_o}{\sqrt{3}} \left\{\frac{2}{\sqrt{3}}\right\}^m \qquad (4.28)$$

Since σ_o is readily determined from uniaxial tension or compression tests then k' can be determined.

An optimum solution in the true sense cannot be found since the optimum value of b, the shear zone width, would be infinite. An arbitrary value must therefore, be given to b. A number of possible values for b suggest themselves for consideration: b is a function of:

a) the ram velocity

b) the extrusion ratio

c) the total strain

d) the strain across each discontinuity

e) the length of the discontinuity

f) the material properties.

When considering the value for an assumed condition one searches

the field of interest and examines processes which, although different in nature, contain a number of similar concepts. The machining of metals is a shear deformation process in which material shears, to a first approximation, across a straight line from the tip of the tool to the free surface. Although the strain rates in the machining process are much higher than those normally encountered in extrusion, it would be appropriate to examine this area. Extensive research has been performed on many aspects of the shear process in machining. The results of this work are examined in the following section with the purpose of indicating the nature of the shear zone and the important parameters effecting its size and shape. Utilizing the results of this work, a decision can be made on an appropriate value for the shear zone width, b, introduced in the analysis.

4.6 The Mechanics of Metal Cutting - The Thin Shear Zone Model

Research in the field of metal cutting has attempted to develop a theory and understanding of the mechanics of metal cutting to enable the prediction of important cutting parameters. Most cutting operations are extremely complex and researchers have tended to examine only the simpler case of orthogonal machining to obtain a clear understanding of the mechanisms involved in the cutting process.

In orthogonal machining the cutting edge is perpendicular to the cutting direction and parallel to the work surface; provided that the width is much greater than the depth of cut, $w/d>20$, then the chip is formed under approximately plane strain conditions. Ernst [143]

recognized that there exists three types of cutting process and that these are dependent upon the mechanism of chip production. We shall limit our consideration to the case when a continuous chip is formed by plastic deformation without fracture.

A shear model was proposed by Merchant* [144] who assumed that material sheared across a plane AB at infinite strain rate as shown in Figure 4.20. The cutting forces can be determined from the geometry of the shear plane model and the principle of minimum work. The theoretical and experimental values, however, do not show good quantitative agreement and it is customary to introduce an effectiveness parameter.

Palmer and Oxley [147] proposed a thick shear zone model, Figure 4.21, following experiments where they observed the movement of individual grains through the deformation zone with cine film. The slip-line theory was used in the analysis, however, the field chosen indicated that the hydrostatic stress distribution varied from compression at the outer free surface to tension near the cutting edge. The major criticism of this paper was that the cutting mechanism, proposed to explain the tensile hydrostatic stress distribution, indicated that the tool and chip were not in contact at the tool point, as shown in Figure 4.23.

---

* Historically Briks [145] is credited with being the first to realize that plastic deformation is involved in metal cutting in a paper published in 1896. The interested reader is referred to an excellent paper by Finnie [146] which traces the early history of the analysis of metal cutting.

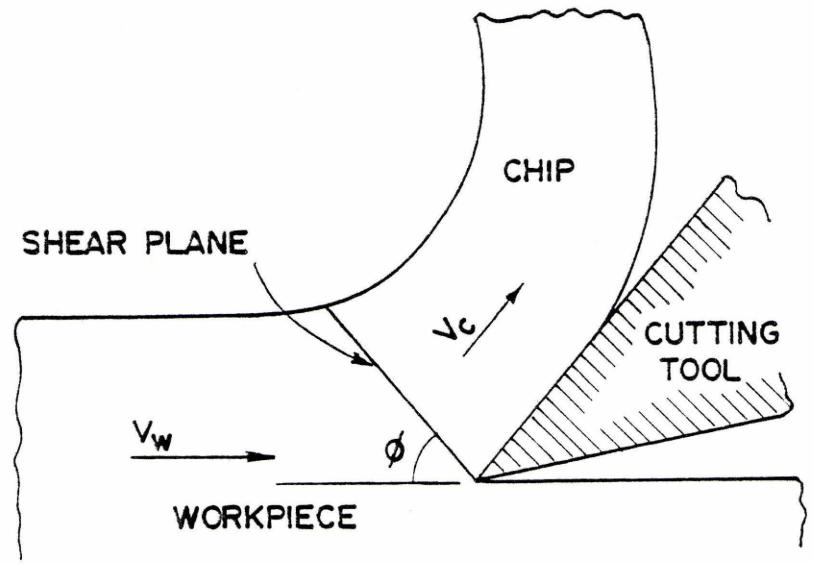

a) GEOMETRY

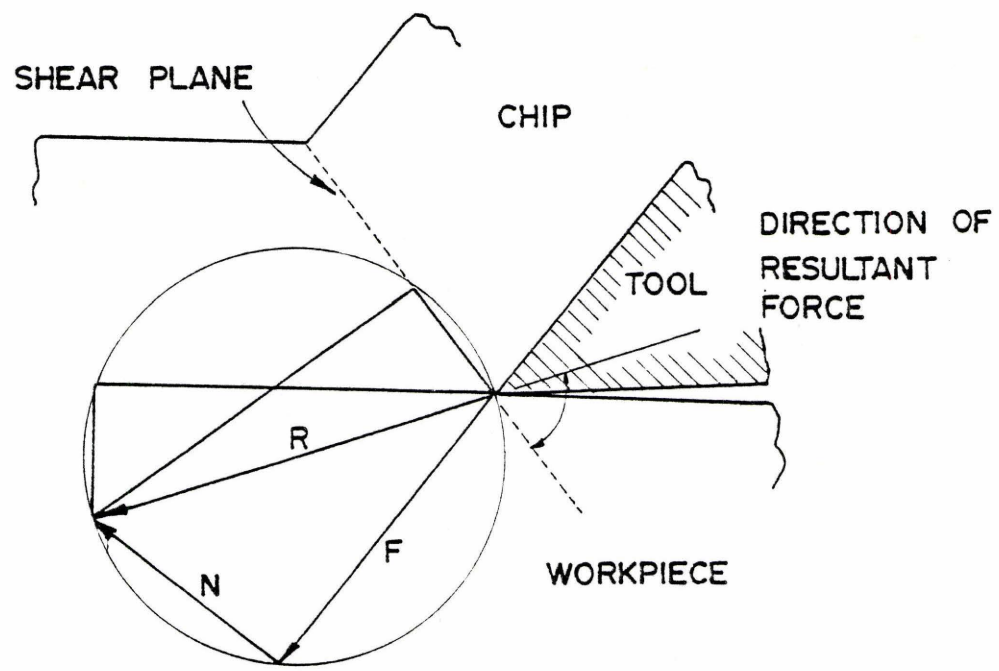

b) FORCE DIAGRAM

Figure 4.20

Shear plane model and force diagram for orthogonal machining proposed by Merchant. [144]

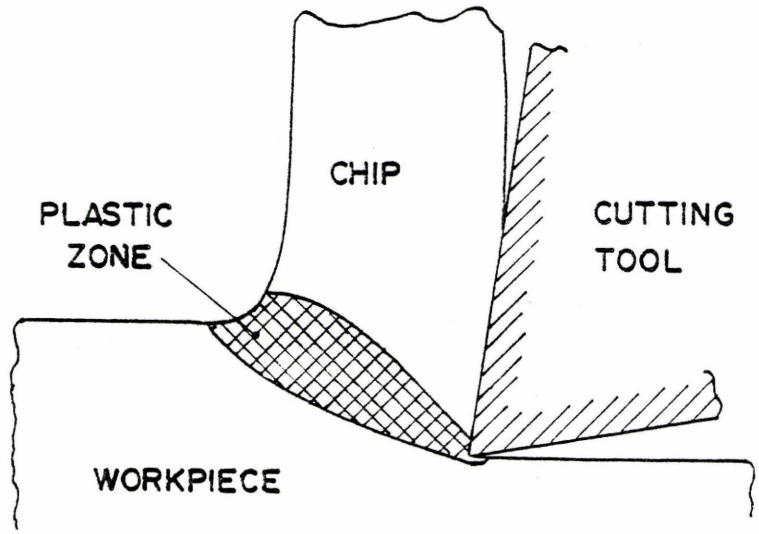

a) THICK SHEAR ZONE MODEL

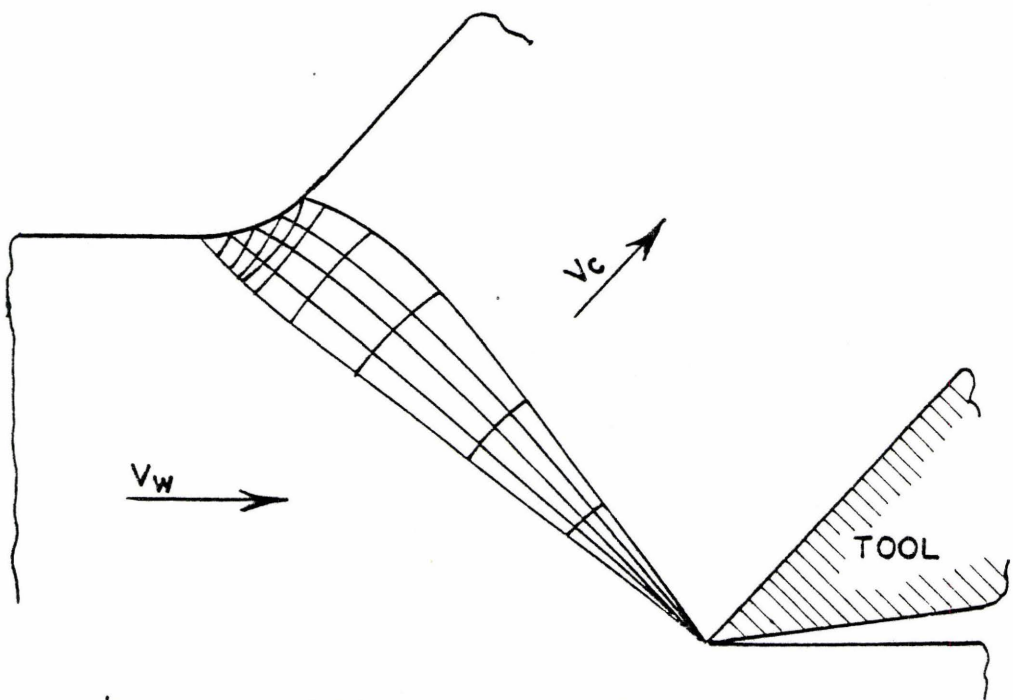

b) PROPOSED SLIP LINE FIELD

Figure 4.21

Thick shear zone model and slip-line field proposed by Palmer and Oxley [147]

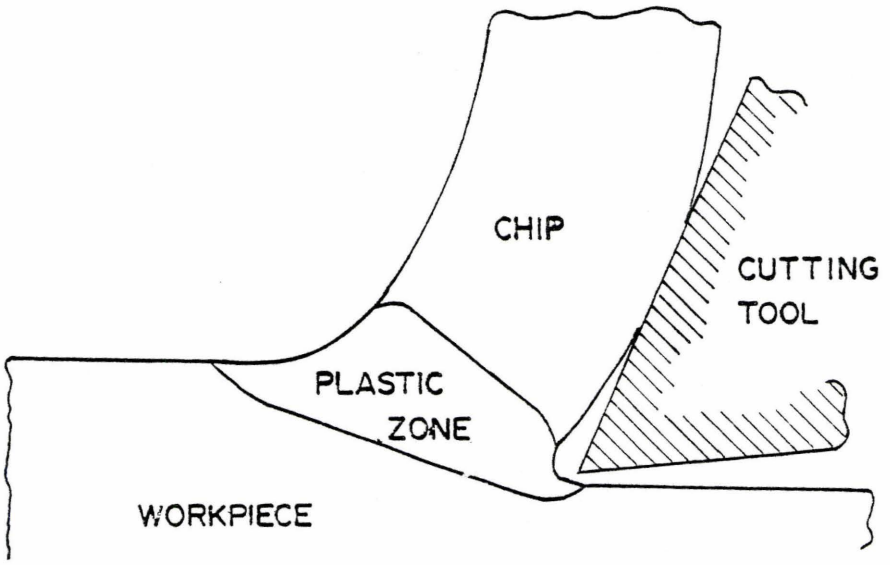

a) PROPOSED CUTTING MECHANISM

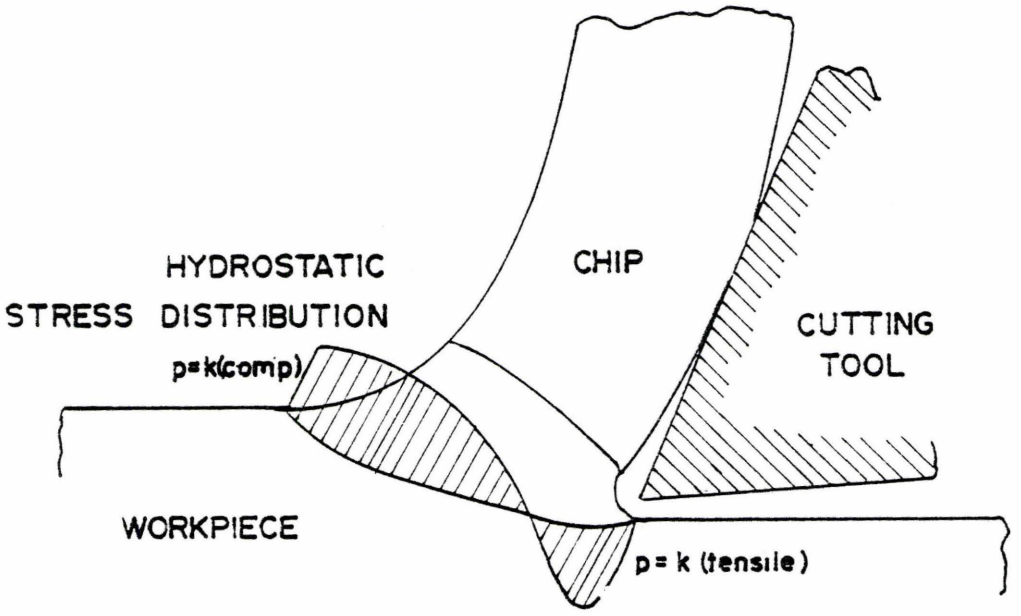

b) STRESS DISTRIBUTION ACROSS SHEAR ZONE

Figure 4.22

Schematic figure of cutting mechanism proposed by Palmer and Oxley [147] to explain tensile hydrostatic stress distribution at cutting edge

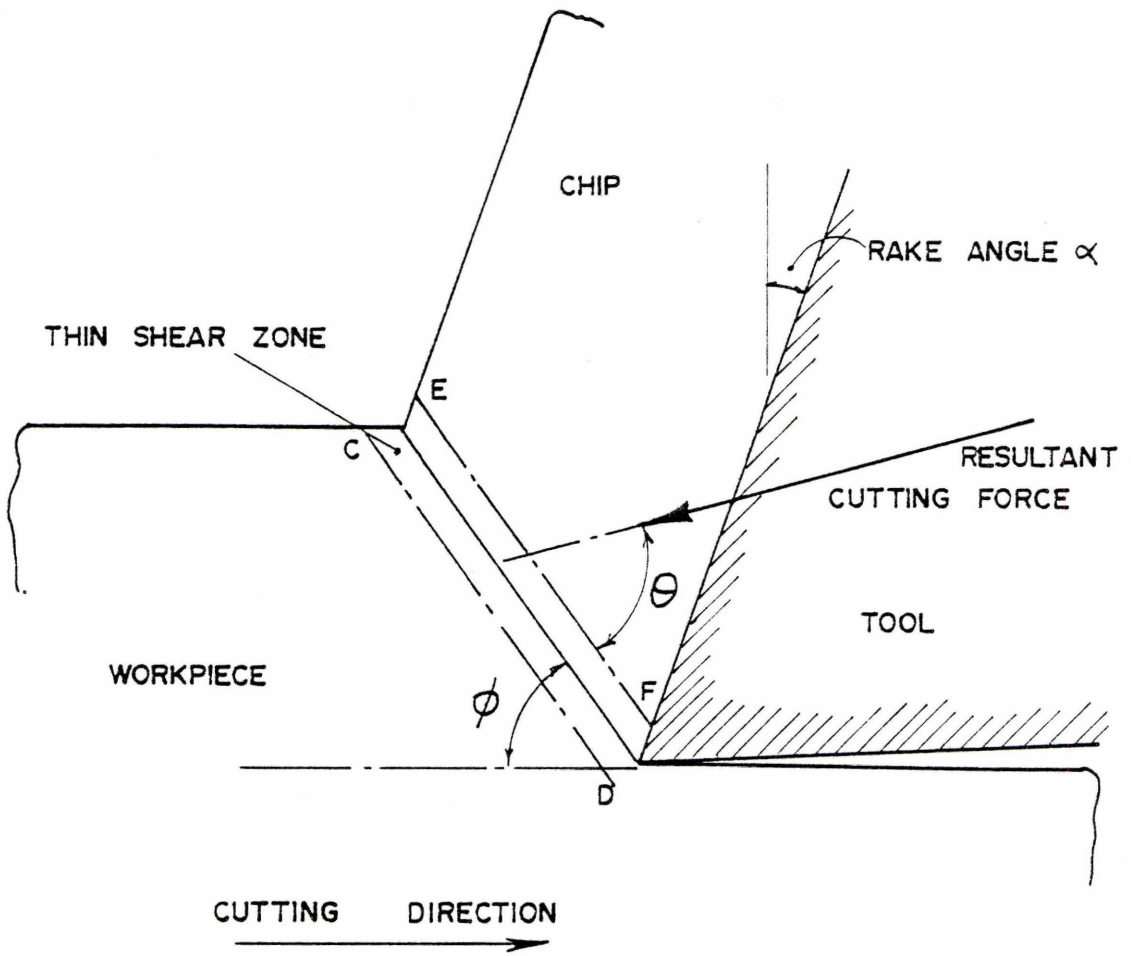

Figure 4.23

Thin shear zone model proposed by Oxley [148] for orthogonal machining

In 1963 Oxley [148] proposed a thin shear zone model as shown in Figure 4.23 where he assumed that CD and EF were planes of maximum shear strain rate and that CDEF could be regarded as a slip-line field. The modified Henky equations developed by Christophersen et al. [149] were used to develop an expression for θ, the angle between the cutting force and the shear plane, indicated in Figure 4.23. A second relationship for θ was obtained from the geometry of the shear zone and the two equations solved to give ϕ, the shear angle, for a given rake angle and friction condition.

Oxley and Hatton [150] utilized the thin shear zone model but based the assumed stress distribution between the tool and the chip on experimentally observed distributions. The theoretical values for the shear zone inclination were shown to correlate well with experimental results.

Having developed a theory in which the plastic shear zone had a finite width the analysis of the effect of strain rate [151, 152, 153], strain hardening [148, 154] and temperature [155] could be accommodated. Some investigators [151, 153] indicated that there appeared to be a ratio between the shear zone thickness and the shear zone length and that this might a constant for a particular material; values ranged from

$$4 < 1/b < 15 \qquad (4.29)$$

If the shear zone thickness is known, the strain rate within the plastic zone can be evaluated and compared with experimentally determined values.

4.6.1 Determination of Shear Zone Size

The first experimental investigation to examine the thickness of the shear zone was undertaken by Kececioglu [156] in 1956 and was concerned with determining the strain rate in metal cutting processes. Various estimates of the strain rate have been made; Drucker [157] calculated $\dot{\gamma}$ = 40000 per second while Choa and Biscare's [158] estimation was 10^3 to 10^6 per second. Shaw [159] stated that the strain rate could be as high as 10^6 per second which is very high when compared with the strain rate in a tensile tests which is typically of the order of 10^{-3} per second.

Kececioglu's experimental technique was to utilize a "quick stop" device to freeze the cutting action. The shear zone was recognized by the deformation of the grain structure when examined microscopically. The lower boundary between the work material and the shear zone was clearly defined. The selection of an upper boundary between the shear zone and the chip, however, was open to speculation. The results of this work indicated that the strain rate in the cutting process is of the order of 10^4 per second and that the shear zone thickness varied between

$0.0007 < b < 0.007$ ins $\quad (0.018 < b < 0.18$ mm)

In 1966 Clack and Brewer [160] presented a new technique for measuring the shear zone thickness and compared their results with those of Kececioglu. A "quick stop" device was again used to freeze the cutting process. Microhardness explorations were conducted on grids of varying sizes, the smallest being 0.002 inch (0.05 mm) square. A number

of methods of analysing the data were attempted and it was found that drawing a map of the shear zone area and joining points of equal hardness gave the most critical assessment of the area. Little else has been published concerning the direct determination of the shear zone thickness although a few techniques and results have been published in papers dealing with the mechanics of metal cutting.

Goriani and Kobayashi [161] in an analysis of the cutting of steel determined experimentally the distribution of strain and strain rate through the deformation zone. They indicated that the effective strain rate varies from zero to a maximum of about 900 per second and that the thickness of the deformation zone is approximately uniform at 0.009 inches (0.23 mm).

Roth and Oxley [162] have indicated a slip-line field which was determined from an experimentally observed flow field. This analysis considers the force between the chip and the tool which, in the simplified analyses mentioned thus far, has been omitted. A mean shear zone thickness of 0.007 inches (0.18 mm) is predicted for this field.

Stevenson and Oxley [153] investigated the influence of speed on the strain rate and the plastic zone size. Experimental results were reported over a wide range of cutting speeds, 17 → 817 ft/min. (86 → 4150 mm/sec), and depths of cut, 0.005 → 0.0108 inches (0.13 → 0.27 mm) on a low carbon steel. The results indicate that the shear zone size does not change substantially with cutting speed but is signficantly affected by the depth of cut as shown in Figure 4.24. The variation of shear zone size with depth of cut had been noted previously in the

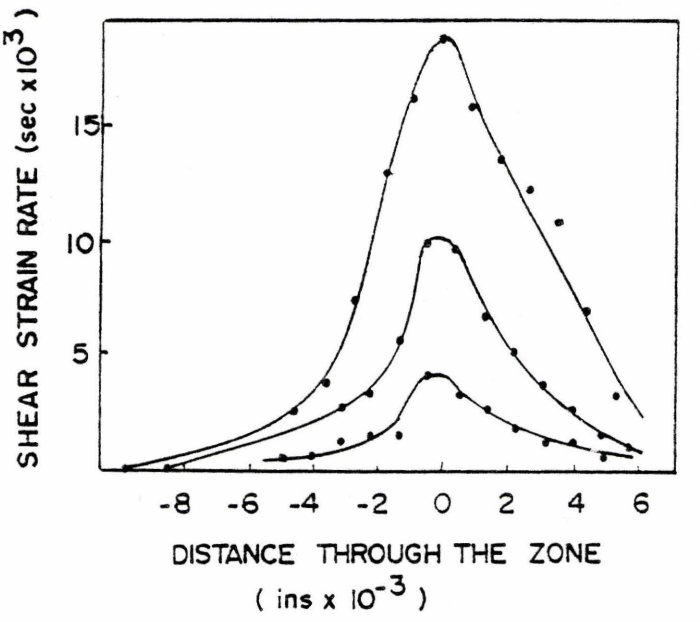

a) INFLUENCE OF CUTTING SPEED

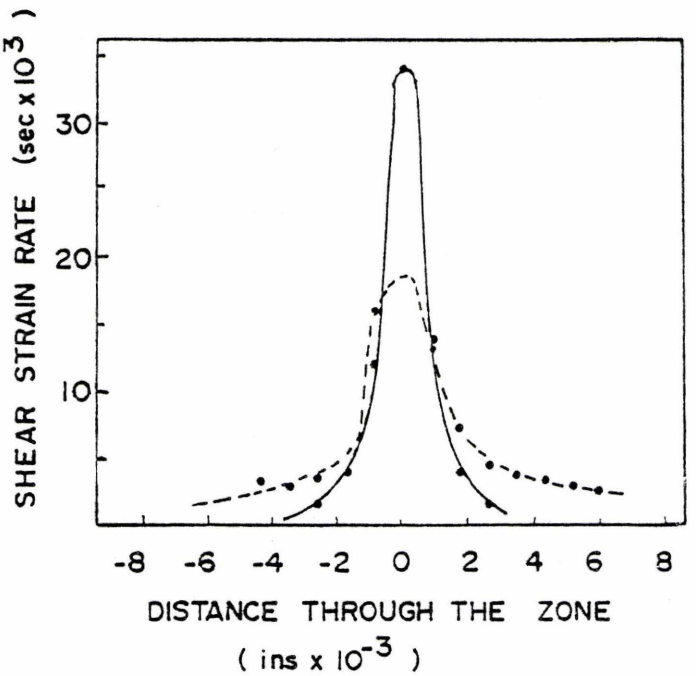

b) INFLUENCE OF DEPTH OF CUT

Figure 4.24

Strain rate distribution within the shear zone during orthogonal machining; from ref. [152]

discussion of a paper by Fenton and Oxley [155]. Knight observed that with a vibrating tool the width of the shear zone increases with increasing depth of cut.

4.6.2 Summary of Metal Cutting Shear Zone Size Determination

It has not been the purpose of the foregoing paragraphs to give a comprehensive review on the literature on the mechanics of metal cutting. A complete review is given in the standard texts such as Armarego and Brown [163]. The mechanics of machining are extremely complex and Hill [164] has suggested that any analysis should not try to define a unique solution but should attempt to locate the possible bounds within which the shear angle must lie. Unfortunately however, the limits established by Hill are too large to be of practical use.

The work presented in the literature on the determination of the shear zone size has been reviewed and it is evident that in the machining process a thin shear zone exists. This shear zone is of the order of 0.005 to 0.010 inches (0.13 to 0.26 mm) wide depending on the depth of cut. It has been suggested [150, 152] that the shear zone thickness and the shear zone length are dependent variables and that the shear zone thickness to length ratio lies in the range

$$4 < l/b < 15$$

4.6.3 Application of the Concept of a Zone Thickness Ratio to the Upper Bound Solution for Rate Sensitive Materials

In the analysis presented in section 4.3 the concept of a thin shear zone of constant shear strain rate was introduced; the width of this shear zone was not discussed. It would, however, be appropriate to assume a shear zone thickness ratio similar to that wich has been shown to exist for the machining of metals. In later chapters, where numerical results are generated for particular materials a thickness ratio of 10 will be assumed initially. The effect of variations in this parameter will be examined.

4.7 Summary

In this chapter the upper bound technique has been reviewed and the way in which strain hardening and strain rate sensitivity have been accommodated within the theory for rigid perfectly plastic materials indicated. Three tangential velocity fields, for the side extrusion process, have been discussed in detail and compared with the slip line field solution assuming a rigid plastic material. One of these was selected for further analysis.

An upper bound solution has been presented for the bulk deformation of rate sensitive materials and the analysis indicates that the velocity field geometry and extrusion pressure are functions of the strain rate sensitivity. The concept of a thin shear zone was introduced in the analysis and it was shown that this concept is not a new one to researchers in the field of metal cutting. The effect of

process variables in the machining process has indicated that a constant shear zone thickness to length ratio is appropriate. Details of the experimental work reported in the literature on the determination of the shear zone size has been reviewed.

CHAPTER 5

MATERIAL PARAMETIZATION AND SIDE EXTRUSION EXPERIMENTS

5.1 Introduction

The side extrusion process has been indicated previously and a review of the work published to date has been presented in Chapter 3. This chapter describes details of experimental work undertaken by the author. The chapter is divided into two parts: the first describes the material selection and parametization while the second part indicates details of experimental work on the side extrusion process.

5.2 Determination of Material Properties

The materials selected were commercially pure lead and the tin-lead eutectic (Pb 37 Sn 63). These materials were chosen because

a) they are essentially non-work hardening

b) have significantly different strain-rate sensitivities

c) exhibit strain-rate sensitive properties at room temperature.

The mechanical behaviour of these alloys can be described by the constitutive equation

$$\sigma = \sigma_o \dot{\varepsilon}^m \qquad (5.1)$$

where m the strain rate sensitivity and σ_o, the flow stress constant,

must be determined from experimental observation. Compression and tension tests are commonly used to determine the values of these constants for a particular alloy [165-168] and processing history. However conflicting information is found in the literature concerning the measurement of the strain rate sensitivity, m, which is normally evaluated by one of two methods. The first procedure involves the determination of stress, strain-rate data at a particular strain from a number of tests at different crosshead speeds. The curve which best fits this data is then used to define the strain rate sensitivity and flow stress constant.

The second procedure was proposed by Backofen [165] and is commonly referred to as the "velocity step change method". In this technique a number of step changes in the crosshead velocity are made during a single test. Figure 5.1 is a schematic diagram of the load time record covering a change of velocity at time t from v to v_1. The lower curve at speed v can be extrapolated to B to establish a common strain for both speeds. If the assumption is made that the strain rate sensitivity is independent of the straining history then

$$m = \frac{\ln (p_A/p_B)}{\ln (v/v_1)} \tag{5.2}$$

The variation of m with strain rate determined by the two methods is compared in Figure 5.2 and in general the results do not agree. The inconsistency in these curves is significant and has been attributed to uncertainties in the true stress and strain rate, as a result of plastic instability occurring during the change of velocity [166, 167] and to

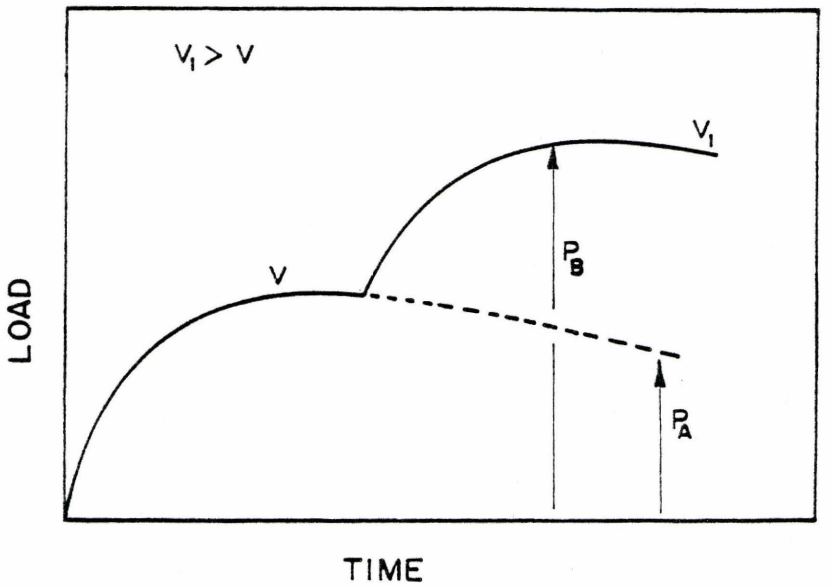

Figure 5.1

Schematic diagram of load time record for velocity step change test

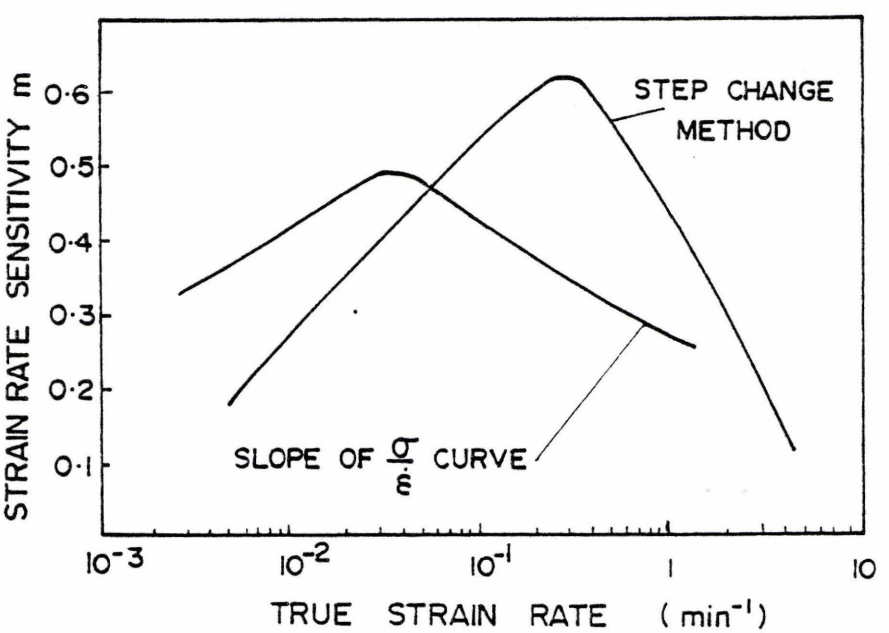

Figure 5.2

Variation of strain rate sensitivity determined by two different methods for an Aluminium Bronze, from ref. [166]

grain growth during the test [168]. The Backofen step change method appears to be the more popular technique because of its simplicity and the number of data points which can be generated from a single test specimen.

In the work reported here constant crosshead speed compression tests were used throughout. However, instead of plotting a single point associated with a particular strain the entire strain rate history of each test is plotted. This results in a number of curves, each representing a single test and covering a small strain rate regime on the plot of stress and strain rate. The envelope of these data curves is used to define the material parameters. This method of presenting data has recently been used by Schelosky [169] and provides the most realistic representation of material behaviour in a process in which sudden changes of strain rate do not occur.

5.2.1 Material Preparation

a) Lead

Commercially pure lead was cast into blocks 3 1/2*3/4*24 inches (88.9*19*610 mm) and side extrusion billets and compression specimen were machined from this cast material. Two series of compression tests were performed with different size specimen; the dimensions of the specimen are shown in Figure 5.3.

b) Tin-lead eutectic

The tin-lead eutectic was chosen for these experiments because it could be processed to provide a fine grained alloy which has a high rate

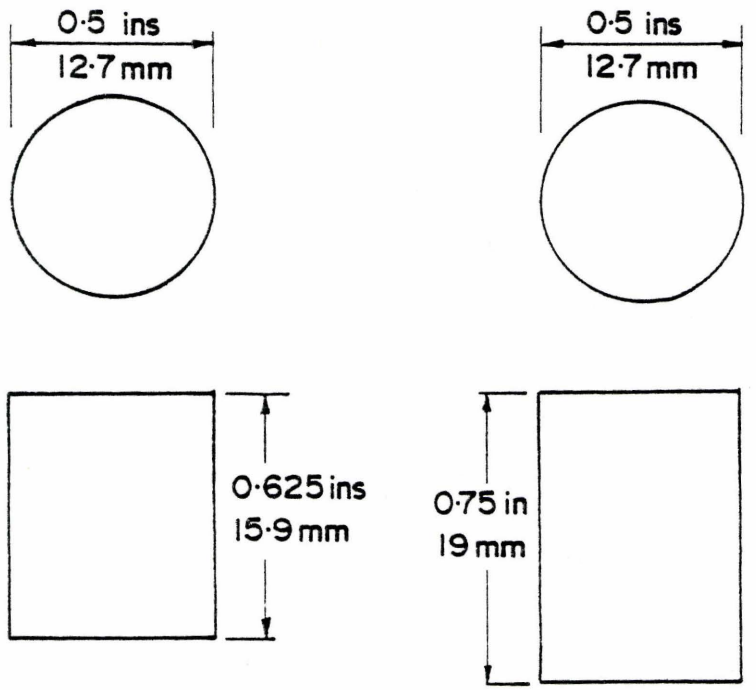

Figure 5.3

Dimensions of lead specimen used in compression tests

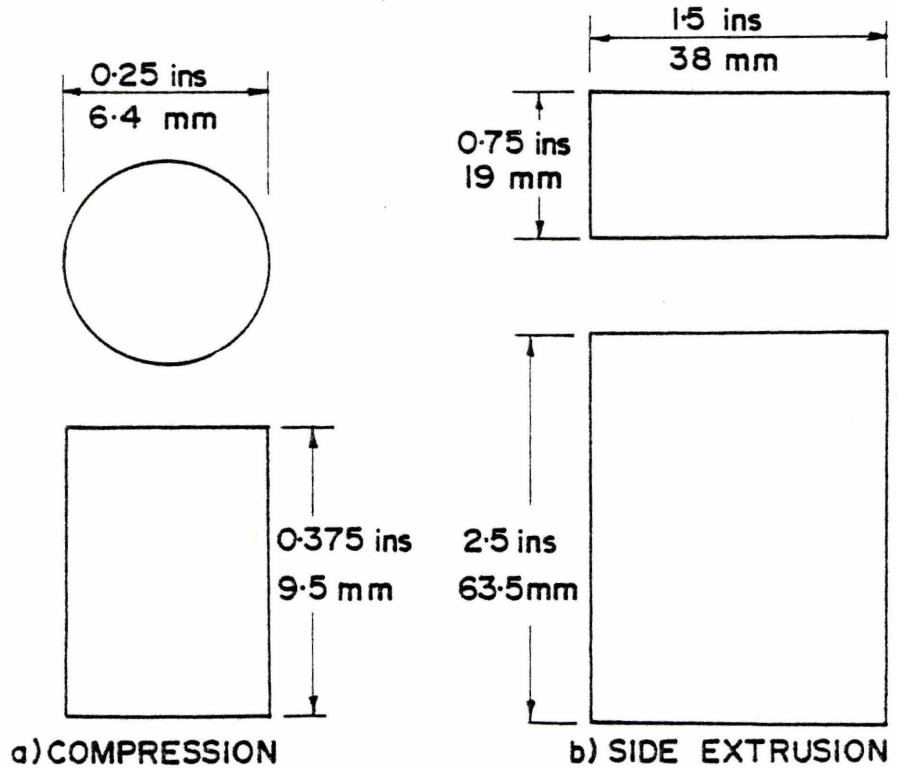

Figure 5.4

Dimension of compression specimen for the tin lead eutectic and the side extrusion billet

sensitivity. The alloy was received in the form of 1 lb. cast bars and was remelted and chill cast into billets 4.625*2.875*5 inches (117.5*73*127mm). These blocks were upset from 4.625 inches (117.5 mm) to a height of 1.25 inches (31.8 mm). The barrelled portions of the block were removed to produce a uniform 1.25 inch (31.8 mm) high billet which was subsequently reduced by rolling to a thickness of between 0.370 and 0.375 inches (9.4 and 9.5 mm). Side extrusion and compression specimen were machined from this sheet to the dimensions indicated in Figure 5.4. The large upsetting and rolling reduction were performed to refine the microstructure of the cast material. It has been shown [170] that for the tin lead eutectic, mechanical processing in which the reduction is greater than 90% will produce the microstructure necessary for super-plastic deformation. The microstructure of the as-cast and mechanically worked material is shown in Figure 5.5. It will be observed that the structure of the cast material is very fine, Figure 5.5a. This has been reported by Avery [170] who found that the grain structure had to be approximately equiaxed for superplastic flow; that is, a fine grain structure is not sufficient for superplastic behaviour. The structure of the cast material, perpendicular to that indicated in Figure 5.5a, is shown in Figure 5.5b and it will be seen that the structure is not homogeneous. The microstructure of the rolled material is shown in Figures 5.5c and d, and the typical fine-grained structure is evident. No attempts were made to measure the grain size in this study since the micrographs were taken only to confirm the existence of the anticipated structure. The compression specimen and side extrusion

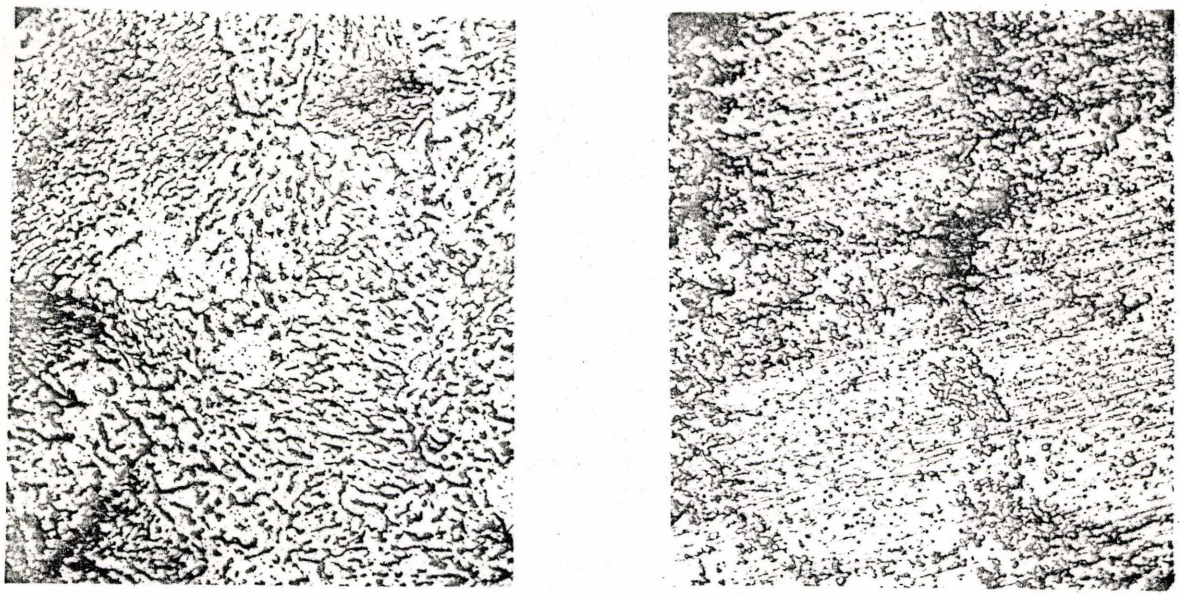

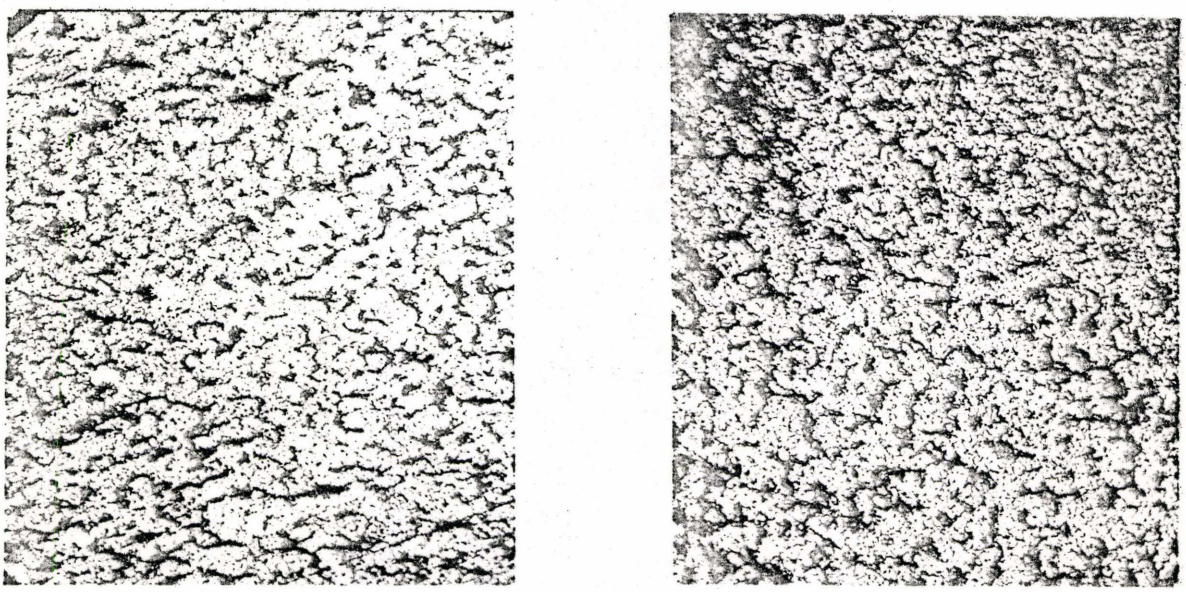

Figure 5.5

Microstructure of the tin lead a) and b) as cast
c) and d) after rolling

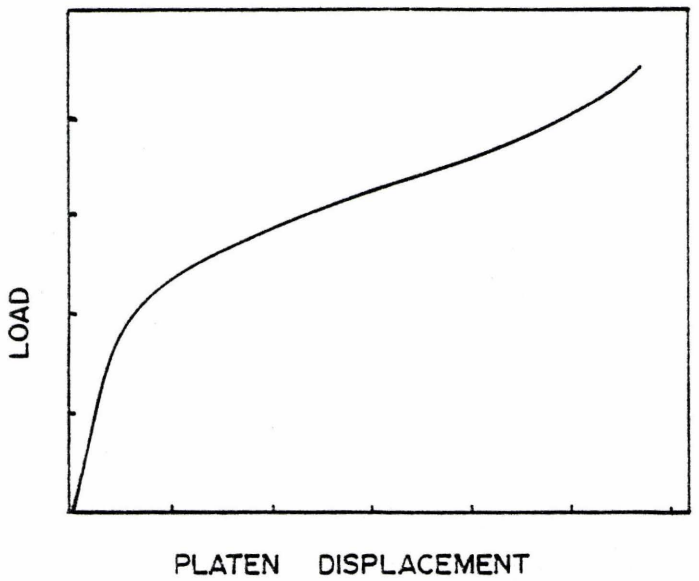

Figure 5.6

Typical load displacement curve for compression tests

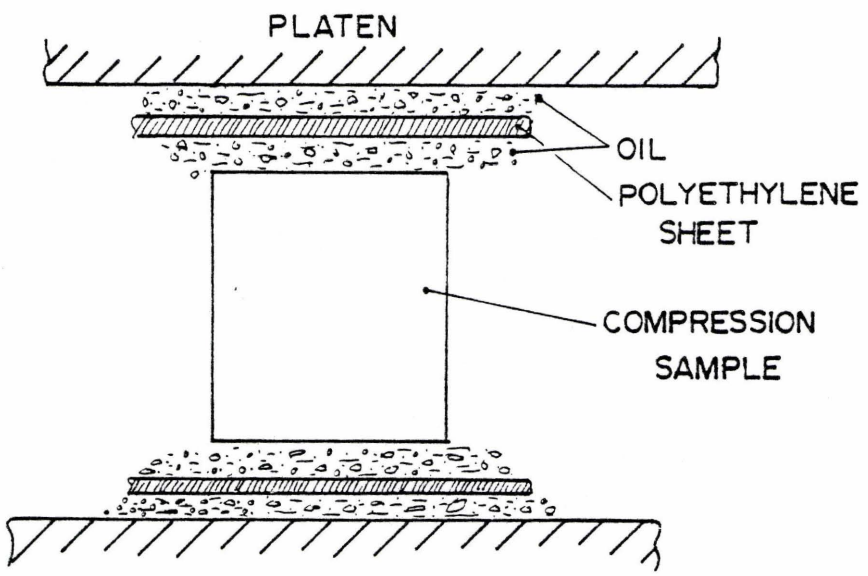

Figure 5.7

Schematic diagram of lubrication of compression specimen

billets were stored in a freezer until needed to prevent grain growth.

5.2.2 Test Procedure and Results

a) Lead

Compression tests were performed in a standard 10,000 lb. Instron tesing machine set up for compression. Constant crosshead velocity tests were performed in the range

$$0.02 < V_c < 5.0 \text{ ins/min.}$$

$$0.0085 < V_c < 2.12 \text{ mm/sec.}$$

and the load, platen displacement recorded. Figure 5.6 is a typical load displacement curve obtained from a test.

Lubrication was effected with a polyethylene film and a light machine oil as shown in Figure 5.7. Comparison tets were made between tests which were interrupted and relubricated and a single continuous test; the load displacement curves were identical.

The true stress, natural strain and instantaneous strain rate were evaluated for each test, and Figure 5.8 indicates the true stress natural strain characteristics for a number of tests. It is clear that the material initially hardens but can be considered to have a constant yield stress for strains greater than 1. These curves are in agreement with data available in the literature [101].

The flow stress strain rate path for each test is indicated in Figure 5.9. The envelope of the curves is drawn to obtain the parameters in the constitutive equation, Eqn. (5.1) and are presented in Table 5.1.

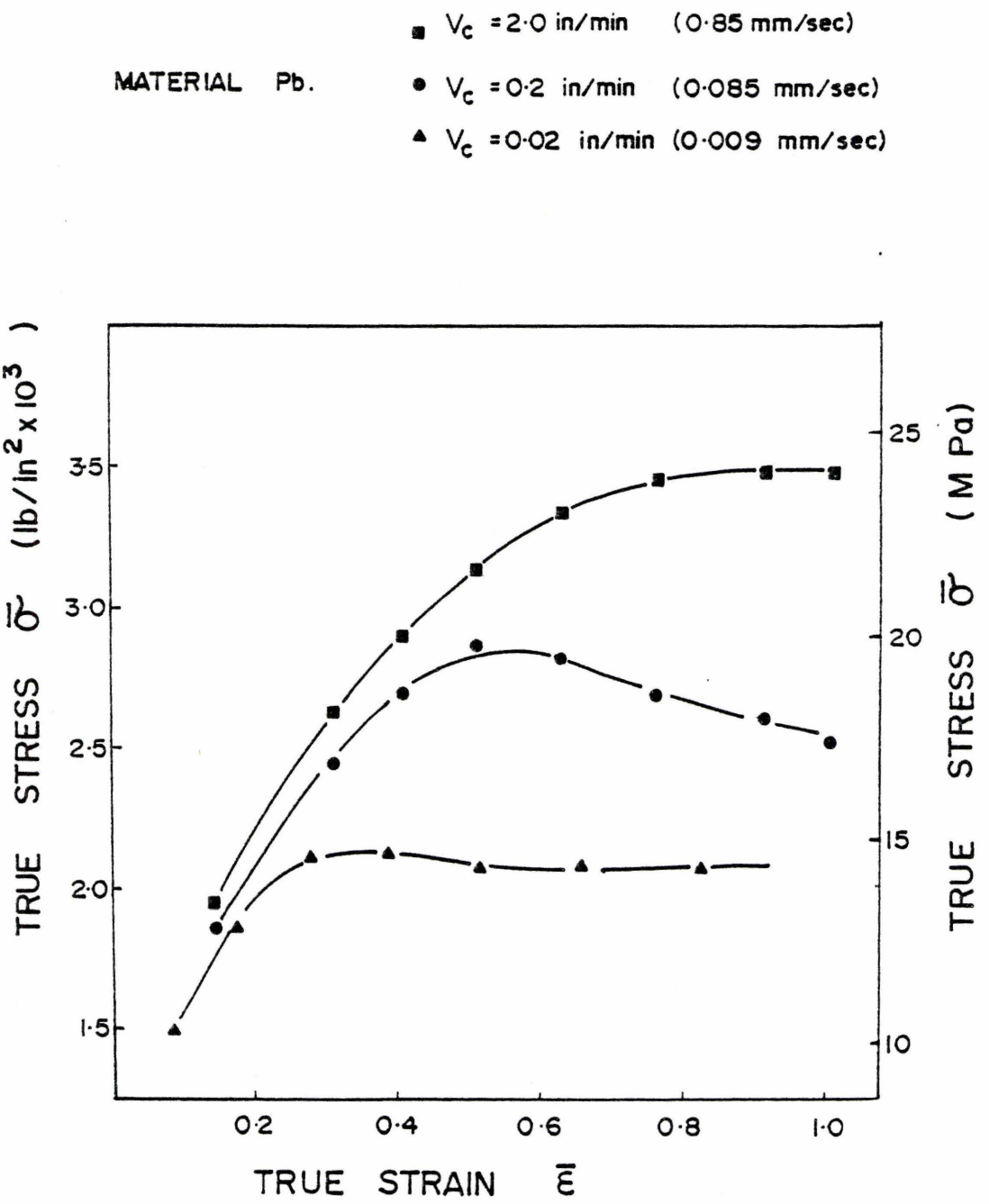

Figure 5.8

True stress natural strain characteristics for pure lead at different crosshead velocities

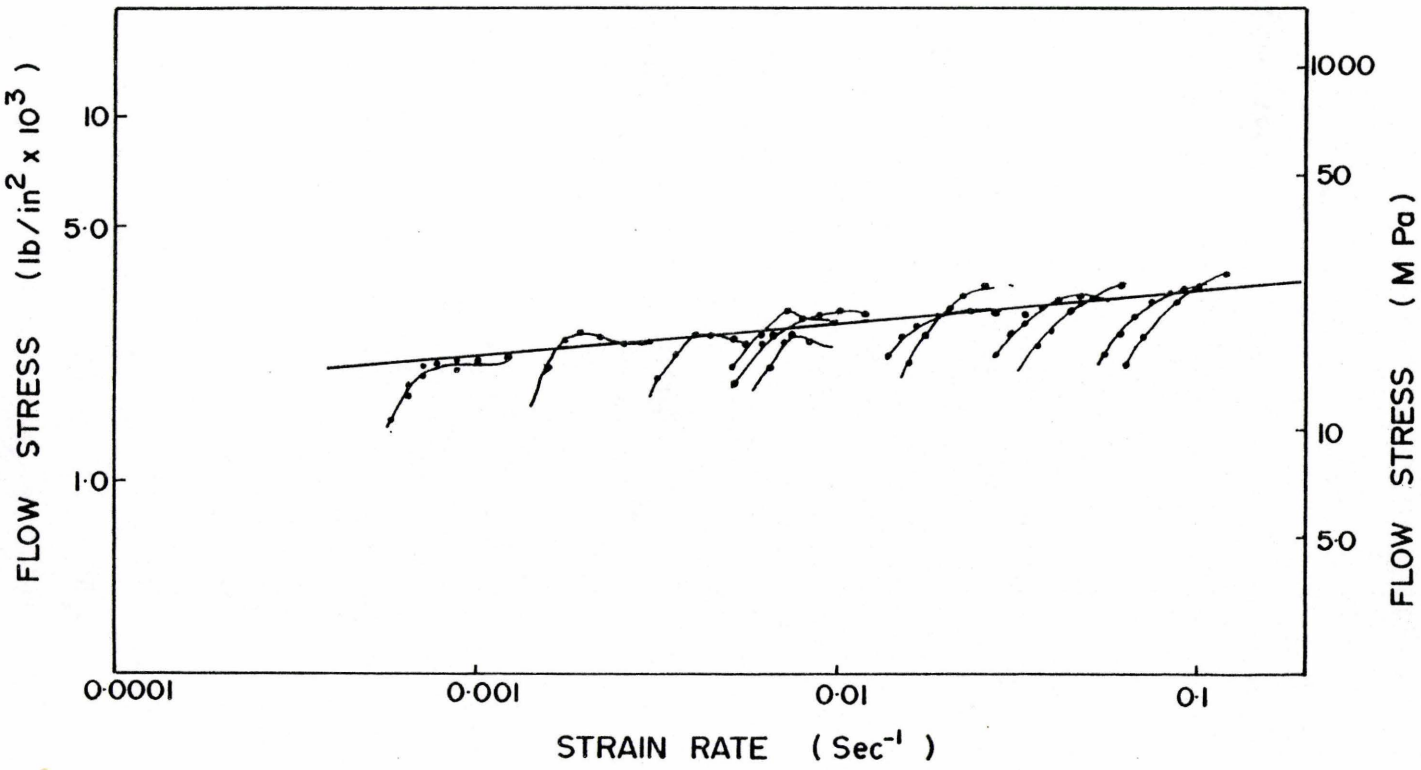

Figure 5.9

True stress, strain rate characteristics for pure lead at 20°C.

b) Tin-lead eutectic

Compression and tensile tests were conducted, at room temperature, in a standard 10,000 lb. Instron testing machine. Constant crosshead velocity tests were performed in the range

$$0.002 < V_c < 2.0 \text{ ins/min.}$$

$$0.0085 < V_c < 8.5 \text{ mm/sec.}$$

Lubrication in the compression tests was with teflon tape and a light machine oil as indicated previously for the tests on lead. The true stress, natural strain characteristics are shown in Figure 5.10 and it is evident that the material does not work harden and, at a given constant crosshead velocity, has a constant flow stress.

The flow stress strain rate path for each test is indicated in Figure 5.11. The material parameters determined from the envelope of these curves are given in Table 5.1.

Material	Constant σ_o $lb/in^2\ sec^m$ ($MPa\ sec^m$)	strain rate sensitivity m	$\dot{\bar{\varepsilon}}_{max}$ sec^{-1}	$\bar{\sigma}_{max}$ lb/in^2 (MPa)
Pure lead	4300 (29.6)	0.094	0.5	6500 (44.8)
Tin lead eutectic	38500 (265)	0.4	0.012	7400 (51.0)

TABLE 5.1

Material constants for pure lead and tin lead eutectic determined from compression tests

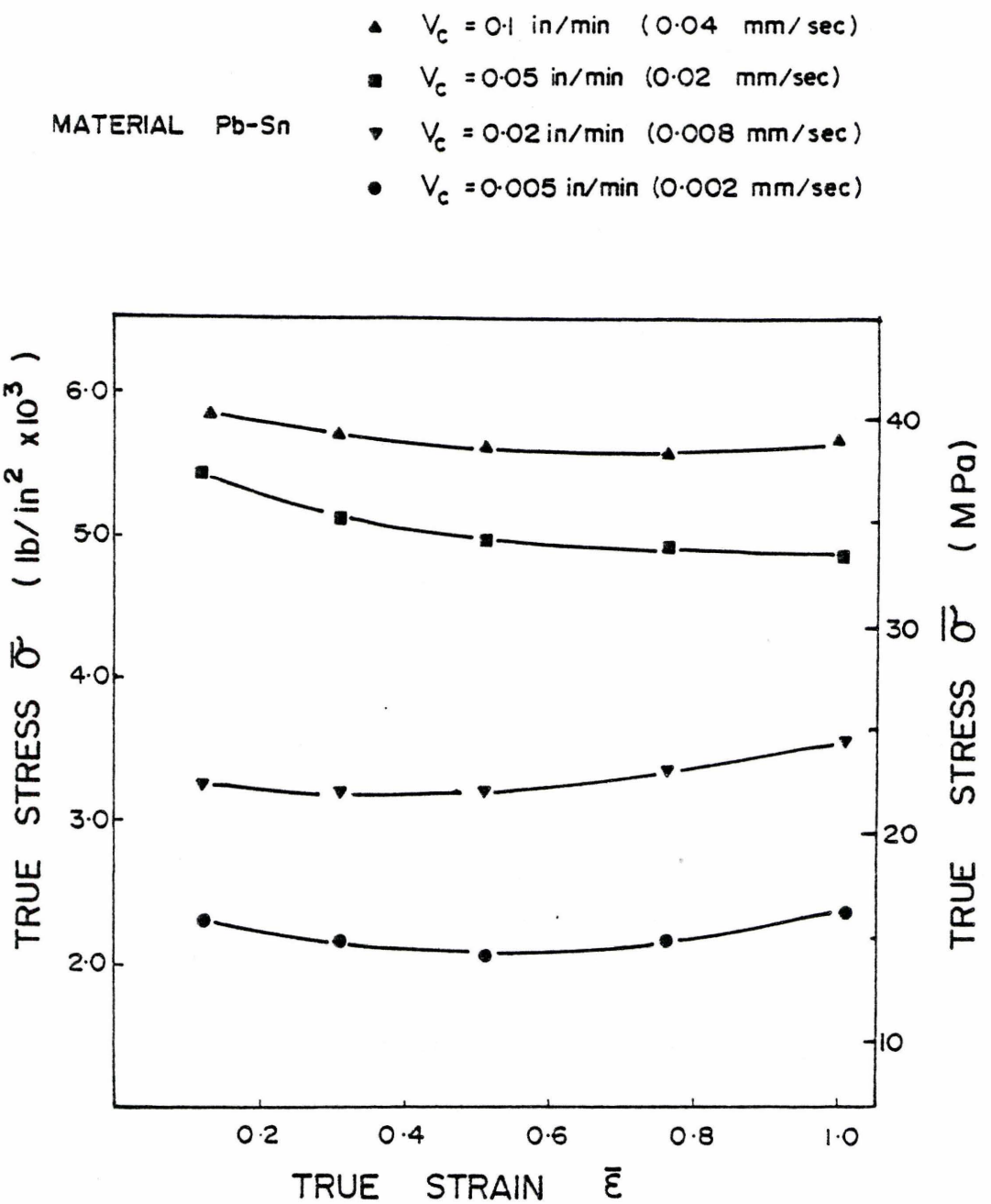

Figure 5.10

True stress natural strain curves for compression of tin lead at different crosshead velocities

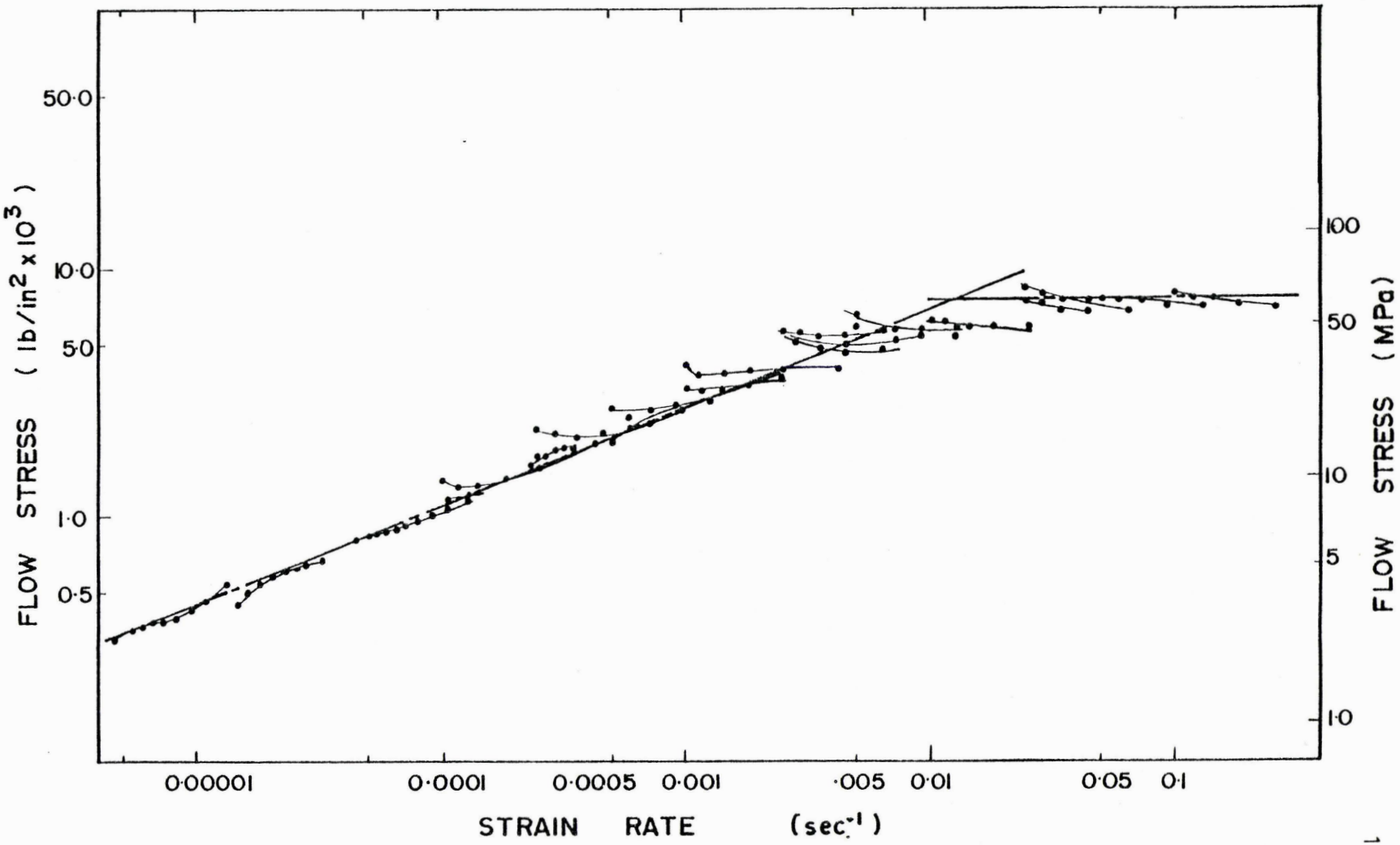

Figure 5.11

True stress strain rate characteristics for tin lead eutectic at 20°C

5.2.3 Summary of Material Characterization

Commercially pure lead and eutectic tin lead have been tested and their material properties evaluated. True stress, natural strain curves presented for both materials indicate that they can be considered to be non-hardening materials. The stress, strain rate curves presented indicate that the tin-lead eutectic, after processing, is superplastic having a strain-rate sensitivity of 0.4. The pure lead, however, can be considered to be rate insensitive having a strain rate sensitivity of the order of 0.1. The stress strain rate curve is sigmoidal in shape and it is common to examine only the linear portion of superplastic flow. It is important, however, to identify the strain-rate regime during which material properties can characterized by Eqn. (5.1). Outside this regime the material is assumed to have a constant flow stress, independent of strain rate. The material parameters, defined in Figure 5.12 are presented in Table 5.1.

5.3 Side Extrusion Experiments

5.3.1 Equipment

A plane strain side extrusion sub press was designed by the author and constructed at McMaster for use in the McMaster Mand hydraulic press. This press is a servo controlled hydraulic testing machine and has the dual capability of controlling either the platen displacement or the applied load. Figure 5.13 is a photograph of the press. The Mand control unit can be seen to the right of the press while a small hydraulic power pack is at the left. The small pump

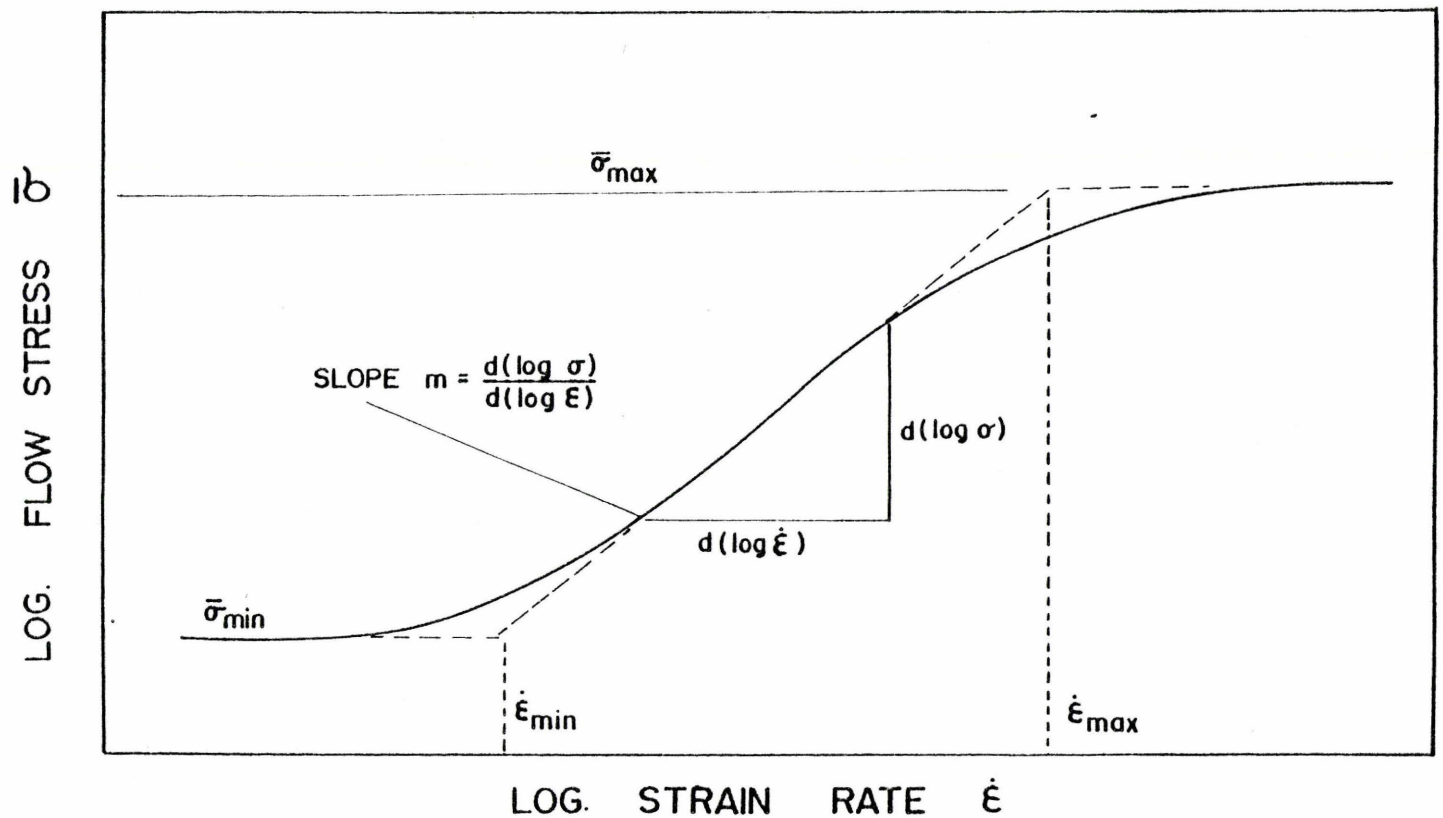

Figure 5.12

Schematic of the true stress strain rate behaviour indicating variables

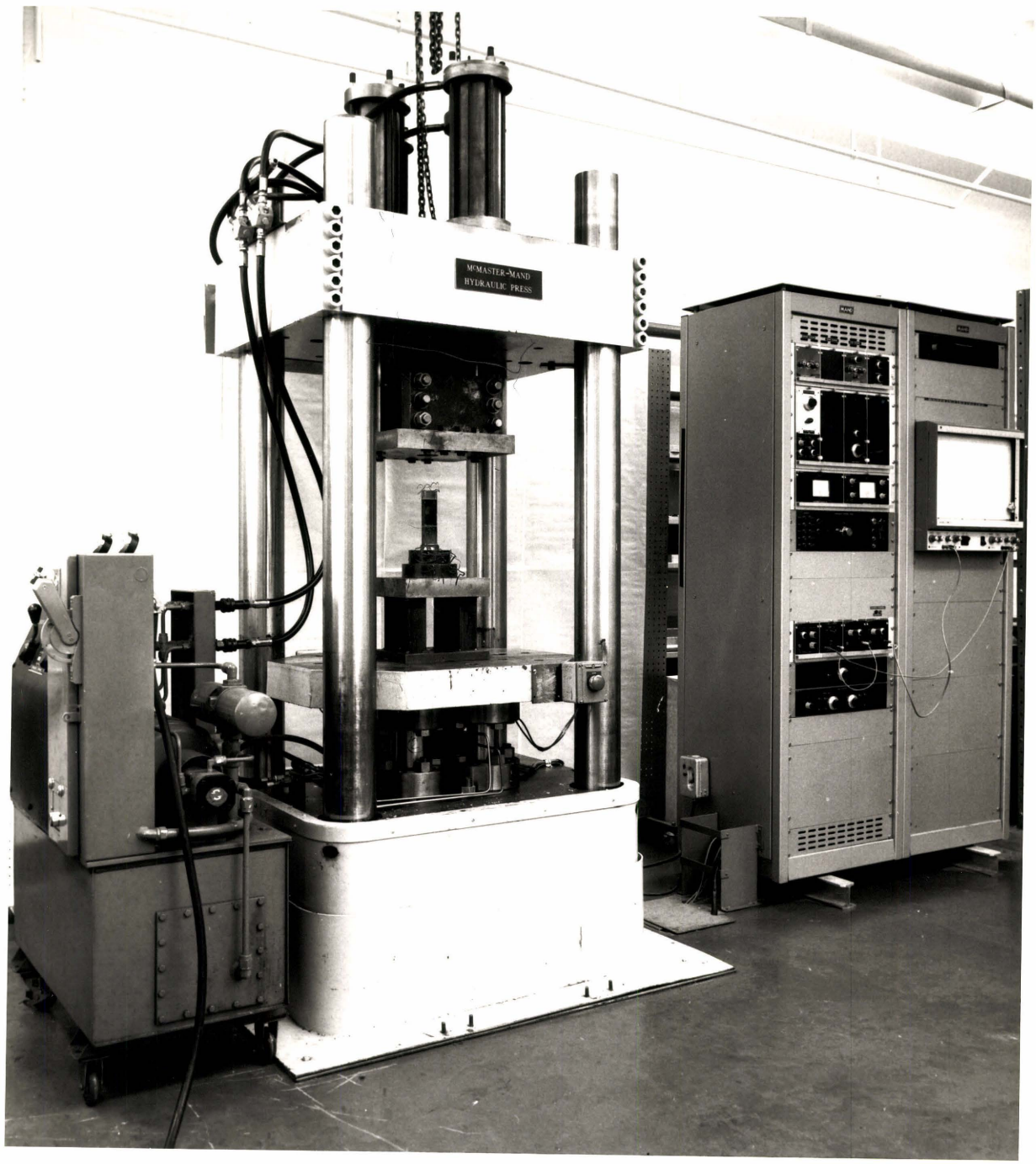

Figure 5.13

Photograph of the McMaster Mand press and ancillary equipment.

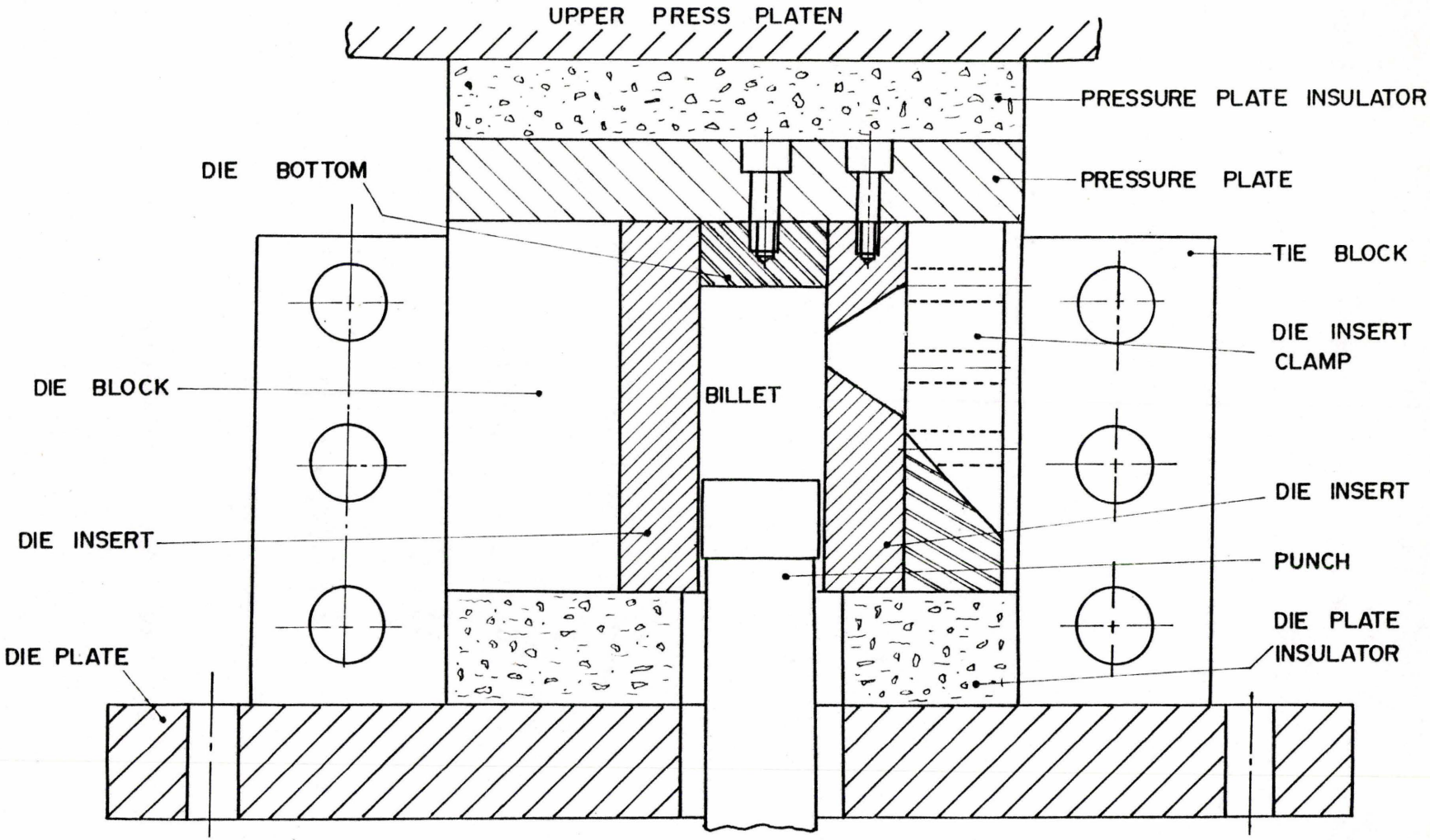

Figure 5.14

Schematic of the side extrusion sub press.

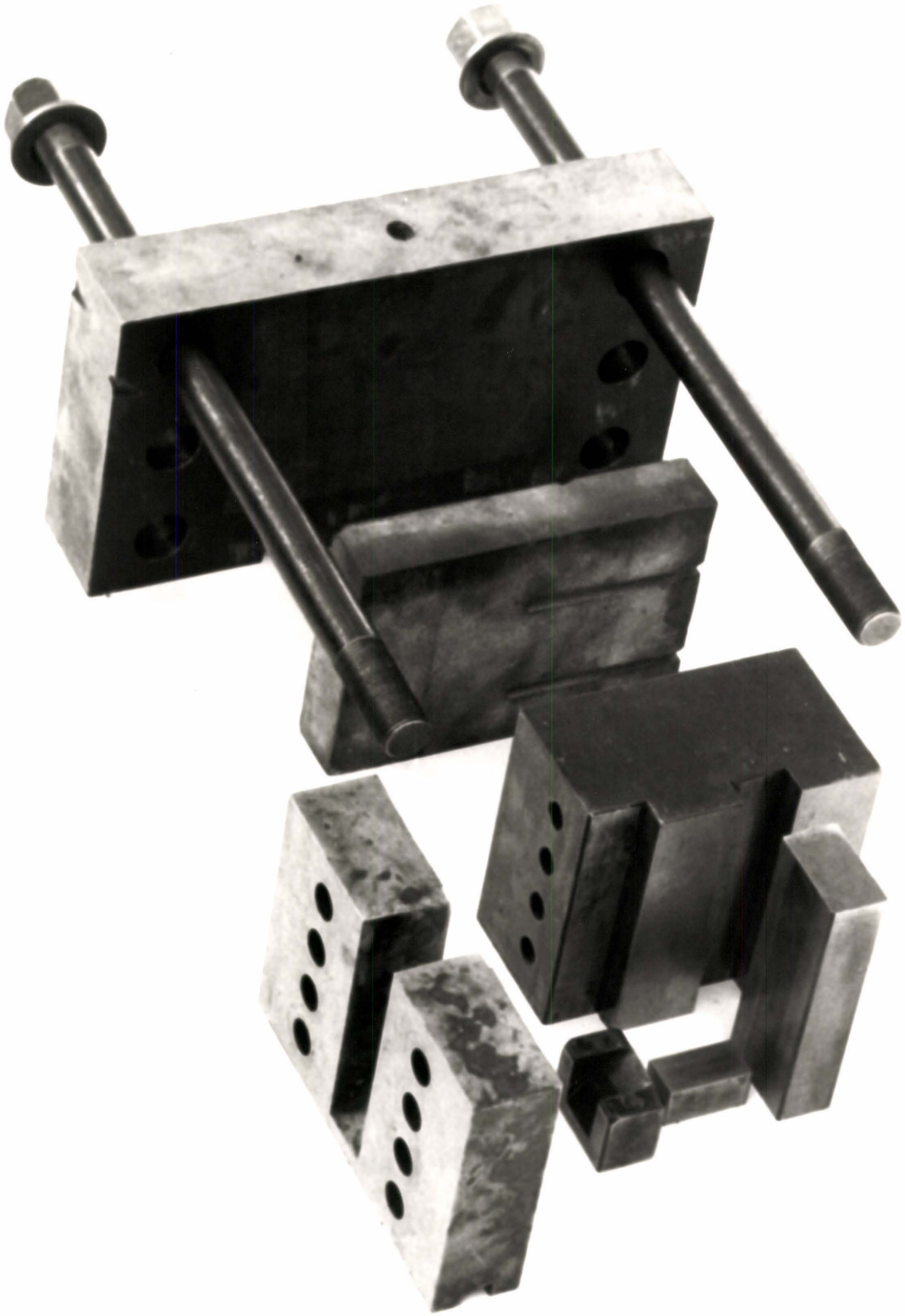

Figure 5.15(a)

Exploded photograph of the side extrusion sub press.

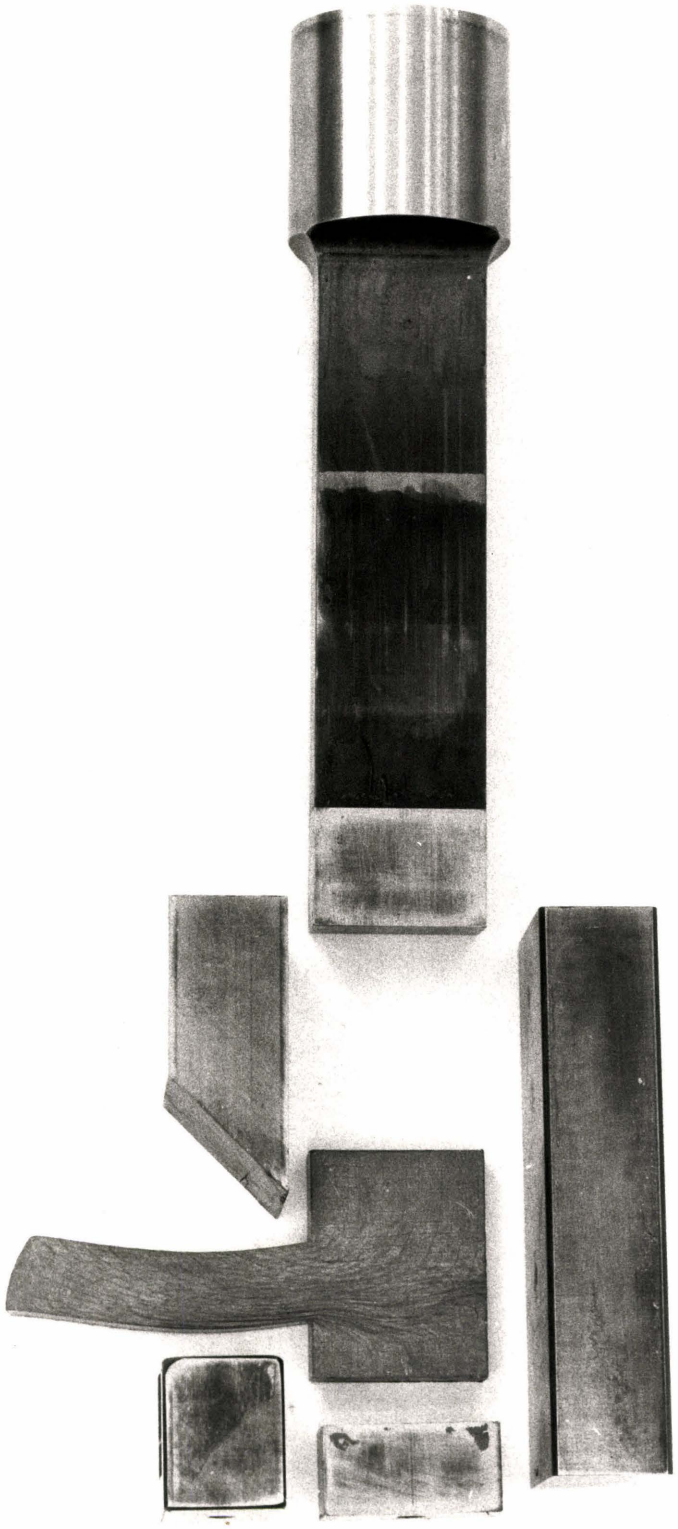

Figure 5.15(b)

Exploded photograph of the die geometry.

operates the auxilary hydraulic cylinders on the upper platen which are used, in this study, to separate the die so that the extruded product can be removed.

The side extrusion sub press is shown schematically in Figure 5.14. The composite die construction allows the extrusion ratio and die geometry to be changed with ease. Figure 5.15(a) is an exploded photograph of some of the major parts of the sub-press; only one half is shown for clarity. Figure 5.15(b) is an exploded photograph of the die inserts and punch and illustrates the basic die geometry.

5.3.2 Experimental Procedure

The die geometry indicated in Figure 5.16(a) was used for the majority of the tests at different ram speeds and extrusion ratios. A number of experiments, with the tin lead, were also performed using the die geometry shown in Figure 5.16(b). These latter experiments were performed to examine the effect of die geometry on the extrusion pressure.

Constant ram velocity experiments were performed over three decades of speed in the range

$$0.012 < V_{in} < 1.2 \text{ ins/min.}$$

$$0.0051 < V_{in} < 0.51 \text{ mm/sec.}$$

with extrusion ratios between,

$$2 < ER < 12$$

All the tests were performed at a room temperature of $70^{\circ}F$ ($21^{\circ}C$). This represents the hot working of these alloys since room temperature is

above half the absolute melting point. The homologous temperature is:

For the tin lead $T/T_m = 0.64$

For the pure lead $T/T_m = 0.49$

The load/platen displacement was recorded for each test and a typical diagram is shown in Figure 5.17. The form of this autographic diagram did not change significantly with the material being tested. At the higher ram velocities the steady state portion was attained sooner without the initial peak shown in Figure 5.17. It will be observed that the load rises steadily as the billet fills the chamber and that, as extrusion begins, the load falls slightly. A steady state phase exists during which the product is extruded as the ram moves into the die. In some cases there was a steady fall in the extrusion pressure indicating a small additional work component due to friction. As the ram approaches the die orifice and begins to interfere with the deformation zone there is a drop in the extrusion pressure to a minimum followed by a sharp rise as the effective extrusion ratio increases. Only a few experiments were continued to this point. The majority were interrupted during the steady state extrusion period.

In all the experiments split billets were made up of two halves machined to the dimensions shown in Figure 5.4. On one of the central faces a grid of 0.1 inch (2.54 mm) squares was scribed to obtain grid distortion patterns and to observe material flow. No quantitative grid strain analysis was attempted.

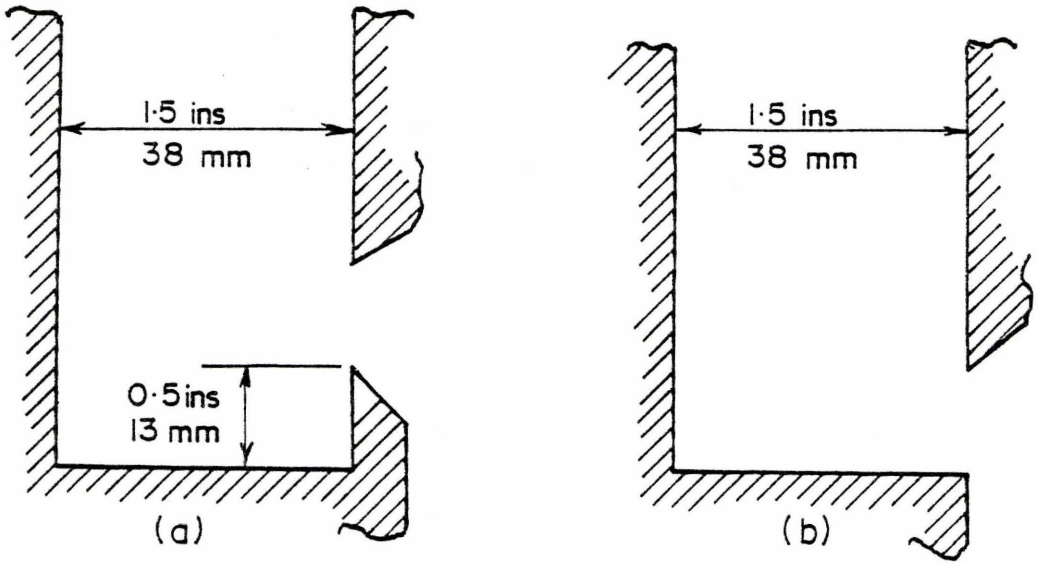

Figure 5.16

Schematic diagram of side extrusion geometries investigated; a) Primary die, b) Secondary die

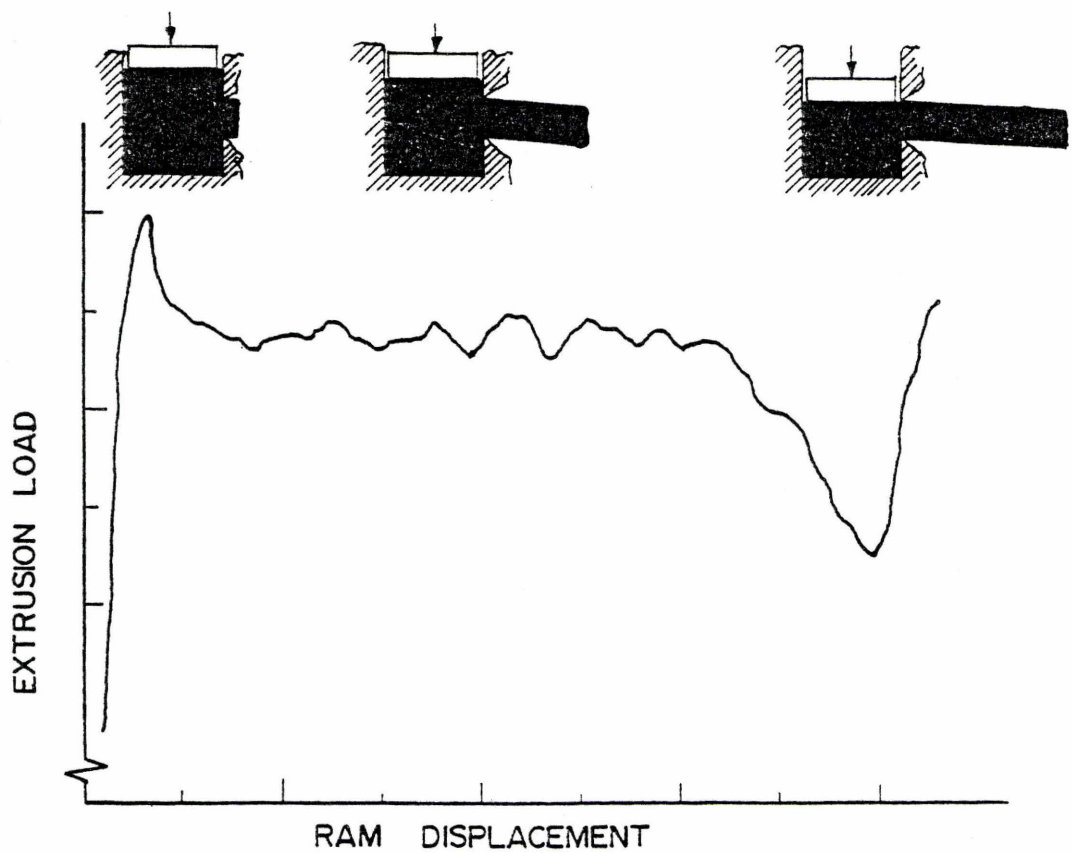

Figure 5.17

Typical laod displacement diagram for the side extrusion test

5.3.3 Lubrication

The die assembly was dismantled and cleaned prior to each set of experiments at a different extrusion ratio. During the tests the die was cleaned and re-lubricated for each test. The billet and die were both lubricated with a standard oil, SAE 80, at the start of each test and care was taken to ensure that adequate lubrication was available to reduce friction. Two comparative tests were conducted to see if the lubrication was effective. In the first the billet was lubricated and the test conducted while the second test was interrupted a number of times, the billet removed, lubricated again and the test continued. The load displacement curves for these two tests were identical.

5.4 Experimental Side Extrusion Results

In the following paragraphs the qualitative and quantitative results of the side extrusion tests are presented. No comparison is made between theoretical predictions and experimental results since this will be the subject of Chapter 6. The variation of the extrusion pressure for the different materials and die configurations will be given. This will be followed by a qualitative assessment of the effect of various parameters on the exit geometry. Finally a few paragraphs will be devoted to an examination of the distorted grid patterns and a qualitative assessment of the effect of various parameters on the deformation zone geometry.

5.4.1 Extrusion Pressure Variation

The extrusion pressure is defined as the steady state extrusion load divided by the ram cross-sectional area. Although the load drops significantly at the end of the ram stroke as the ram moves beyond the die aperture this cannot be used to define the minimum load since the deformation is transient and not one of steady state.

The variation of the extrusion pressure with fractional reduction, at different ram velocities, is shown in Figures 5.18 and 5.19 for the pure lead and tin lead respectively. The effect of ram velocity on the extrusion pressure is clearly demonstrated in each of these figures. Figure 5.18, for the lead, shows that the extrusion pressure is not very sensitive to the ram velocity. The effect of velocity on the extrusion pressure for a rate sensitive material, however, is clearly shown in Figure 5.19 for the tin lead.

The variation of extrusion pressure for different ram velocities is presented in Figure 5.20 for the extrusion of the tin lead in the second die geometry indicated previously in Figure 5.16(b). No tests with the pure lead were conducted using this die geometry.

5.4.2 Exit Geometry

For the experiments reported here material was not extruded in a straight line as expected. In all the tests there was a radius of curvature associated with the particular extrusion ratio and velocity. This curvature of the product led to some problems at the higher extrusion ratios since the extrudate tended to hit the die block. To

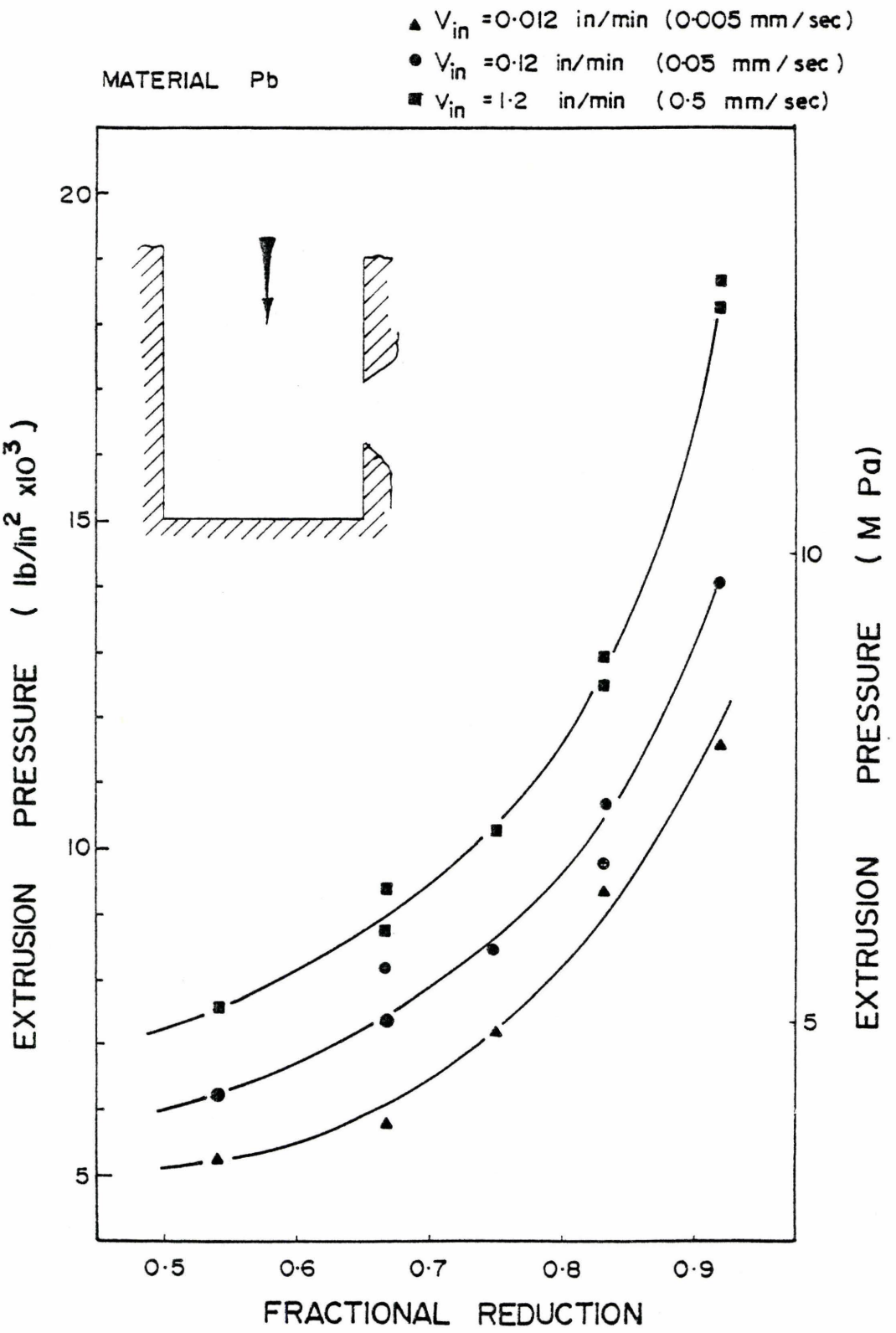

Figure 5.18

Variation of extrusion pressure with fractional reduction at different constant ram velocities; Pure lead

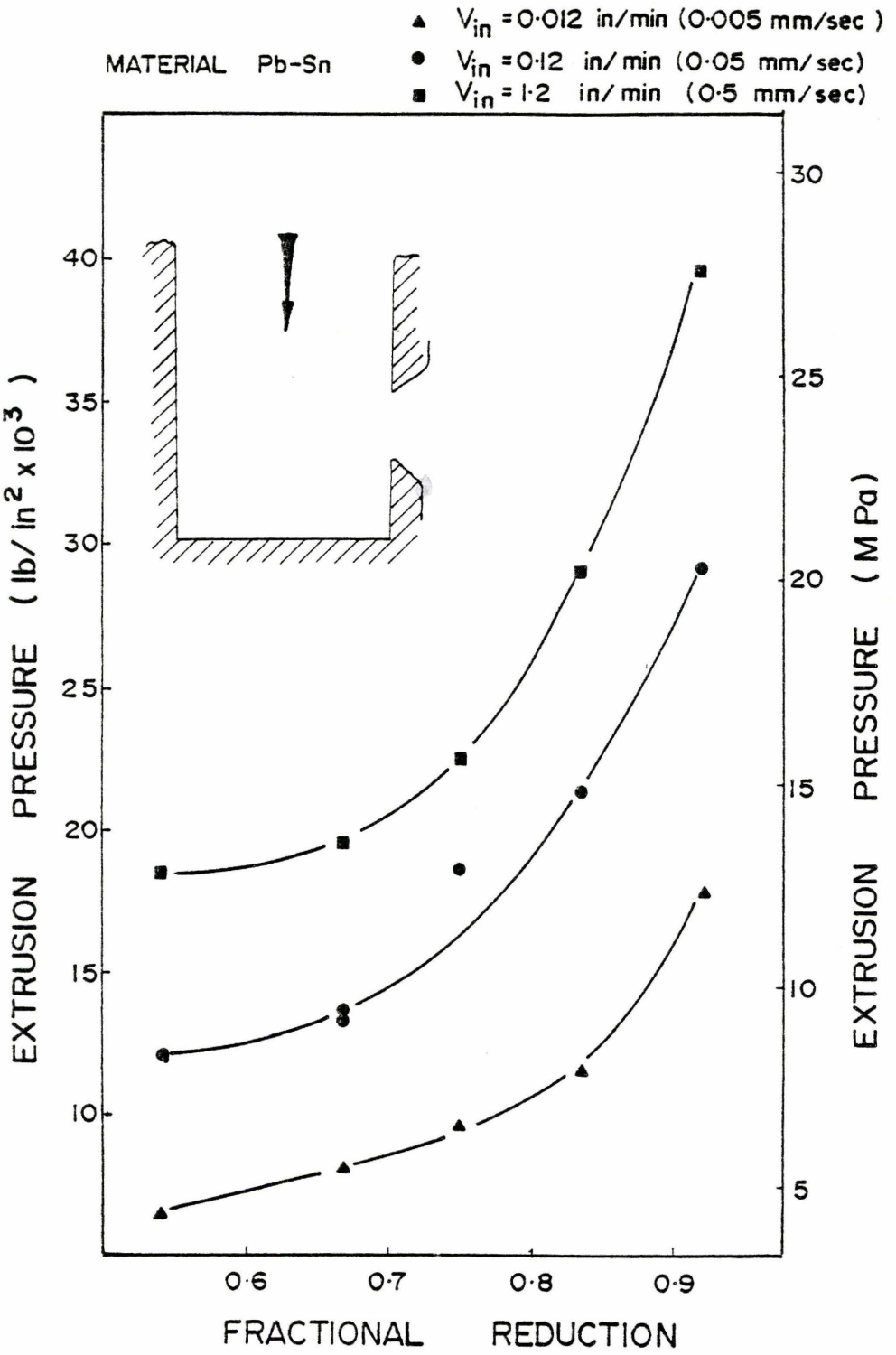

Figure 5.19

Variation of extrusion pressure with fractional reduction at different constant ram velocities; Tin-lead eutectic

overcome this problem the process was interrupted when necessary, the billet ejected, and the extruded product sawn off. The billet was relubricated and replaced in the die and the experiment continued. Figure 5.21 is a photograph of an assembled test piece which was removed and returned to the die. It is clear that had this precaution not been taken then the collision of the die block and extruded product would have interfered with the exit geometry. In the experimental work reported in the literature on the side extrusion process [9] there is no mention or comment of the rotation of the extrudate. In the work reported here the extruded product of every test was, to some extent, curved.

The most striking visual observation of the current investigation is a characteristic difference in the exit geometry associated with the curvature of the product for the two materials tested. That is, for lead the extrudate tended to rotate towards the ram while, for the tin lead, the product tended to rotate away from the ram movement. Figure 5.22 is a photograph of a lead and tin lead specimen extruded under nearly identical conditions. The rotation of the extrudate of the two materials is shown schematically in Figure 5.23. In the following paragraphs the exit geometry of the two materials is compared with respect to the effects of velocity, extrusion ratio and material strain rate sensitivity.

a) Effect of Velocity

The effect of velocity on the exit geometry for two extrusion ratios is shown in Figures 5.24 and 5.25 for the pure lead and the tin

Figure 5.21

Photograph of speciman which was removed from die to saw off extruded portion

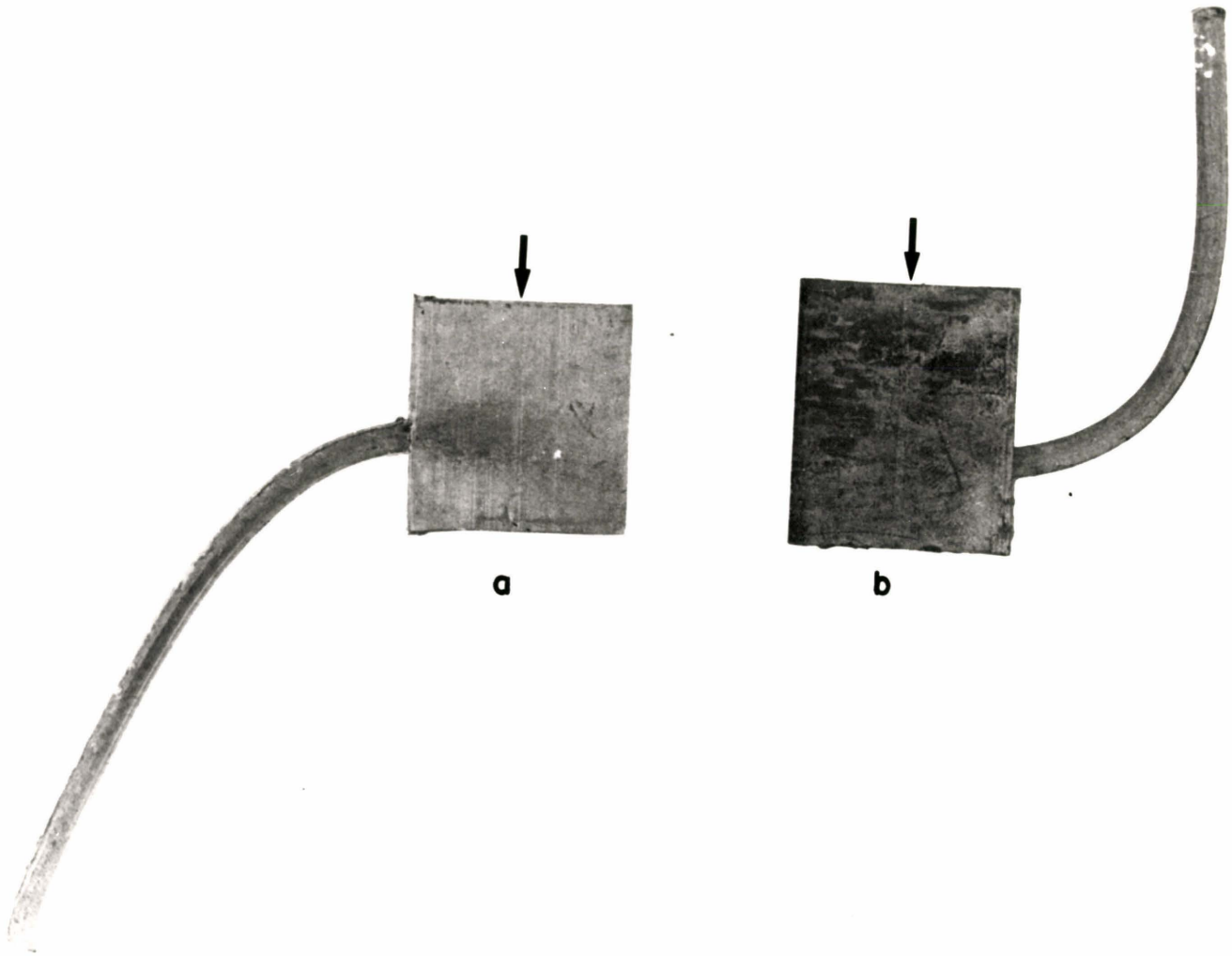

Figure 5.22

Photograph of characteristic curvature of the extrudate for the a) tin lead and b) the pure lead, extruded under identical conditions

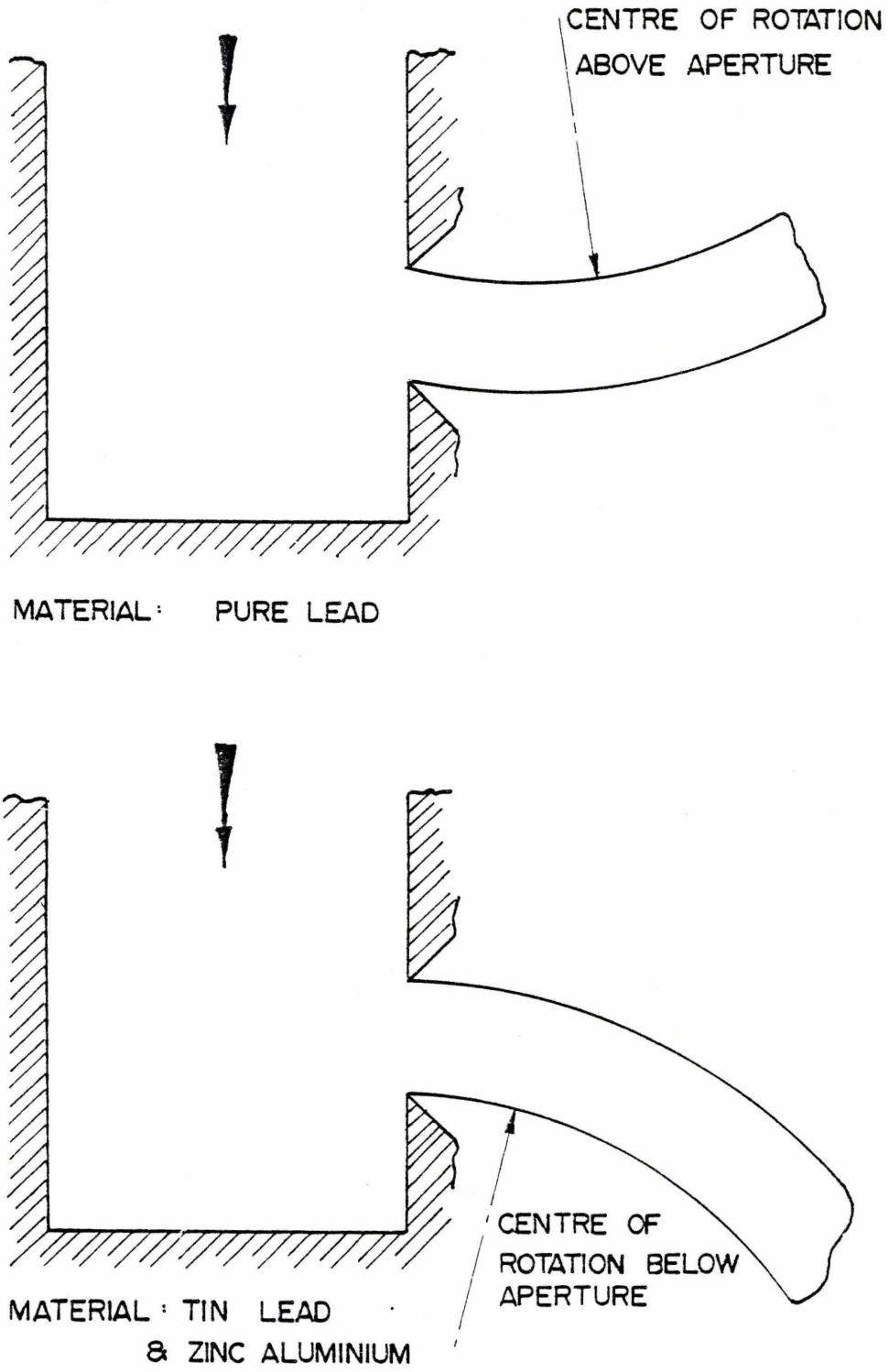

Figure 5.23

Schematic of the rotation of the extruded product for the two materials

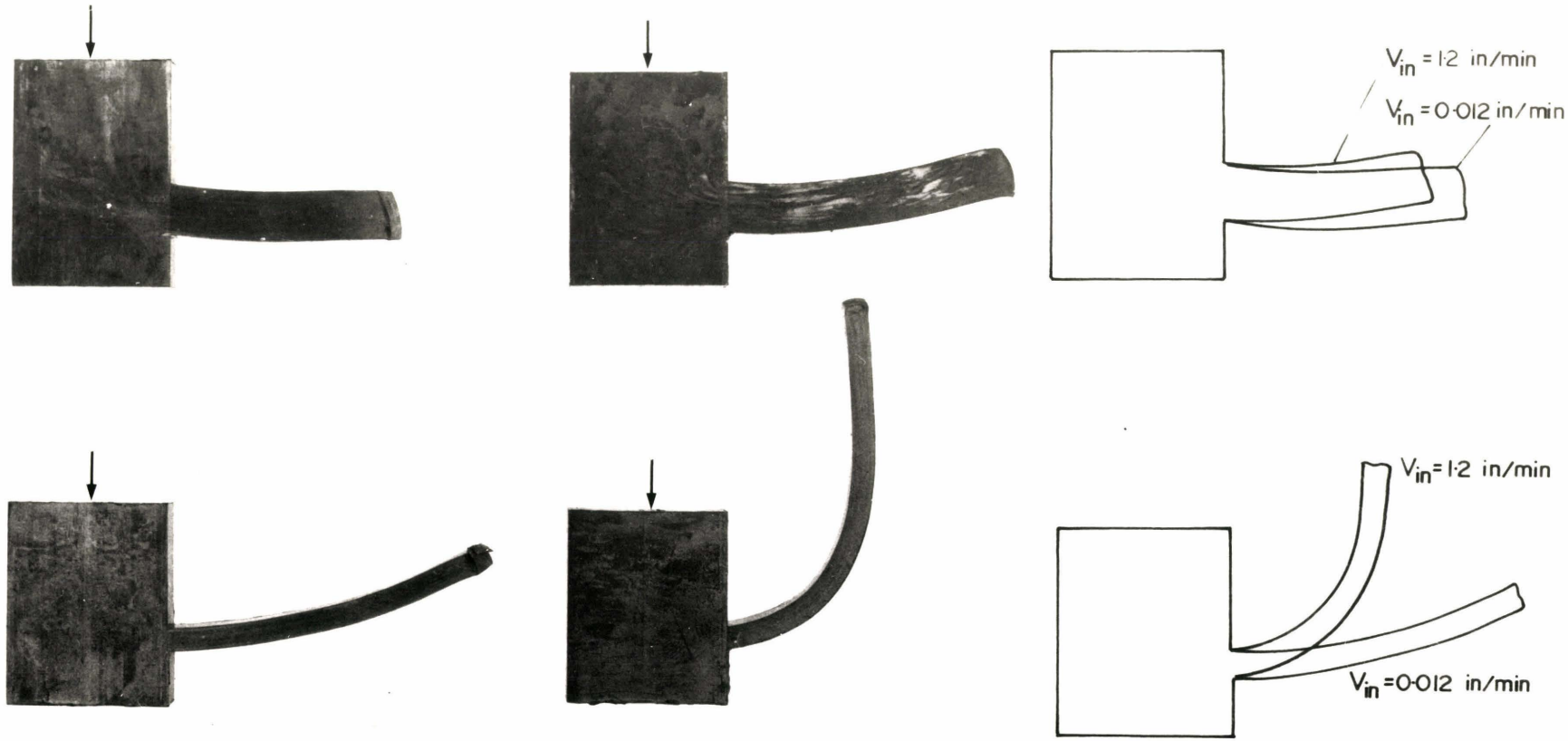

Figure 5.24

Photograph indicating effect of velocity at two extrusion ratios on the exit geometry for the pure lead

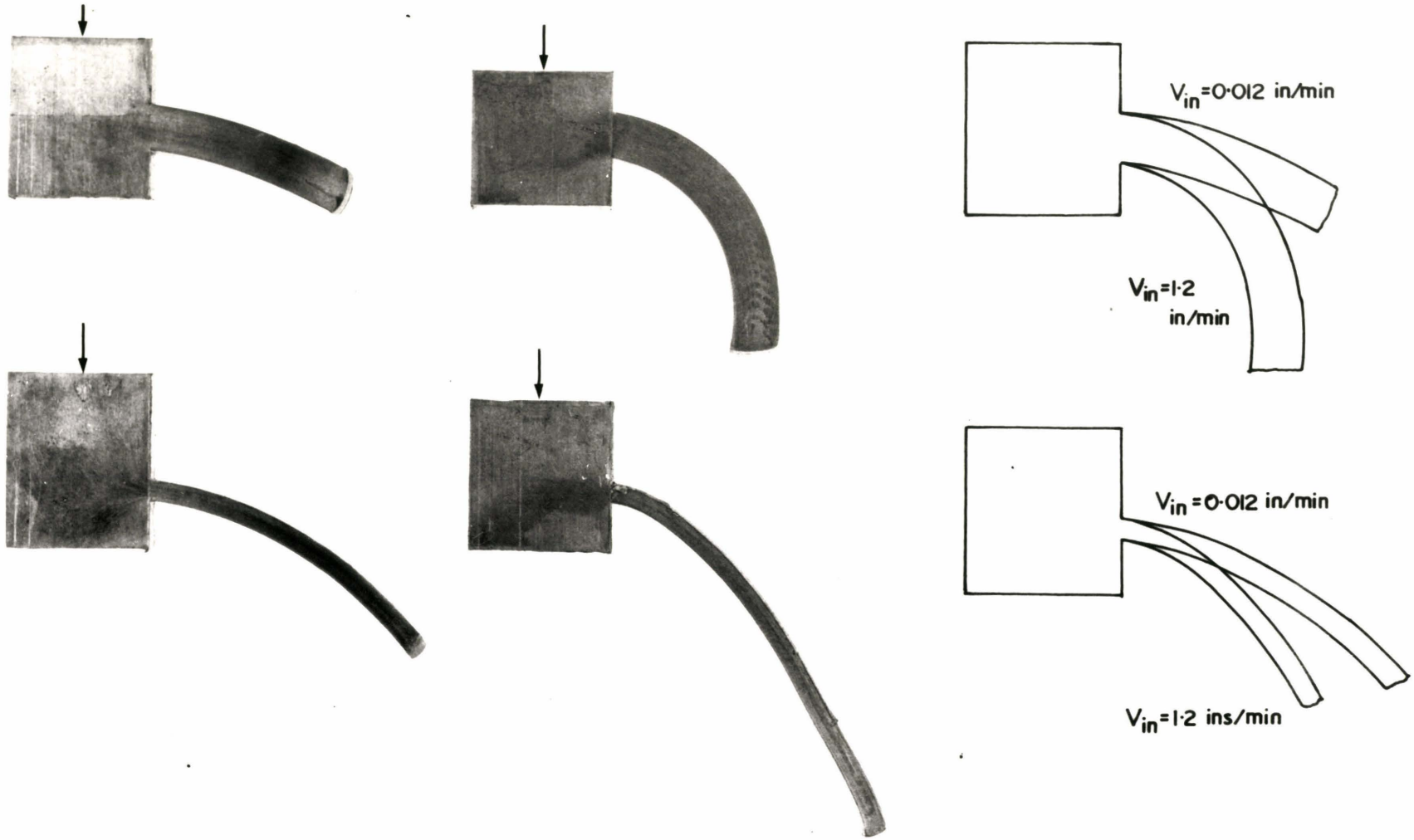

Figure 5.25

Photograph indicating effect of velocity at two extrusion ratios on the exit geometry for the tin lead eutectic

lead respectively. Identical trends are indicated for both materials; that is that the radius of curvature of the extruded product tends to reduce as the velocity increases. However, the centre of rotation for the lead is above the die aperture while, for the tin lead, the centre of rotation is below. The variation of the exit geometry, in the second die configuration, for the tin lead is shown in Figure 5.26. At the smaller fractional reduction increasing the velocity appears to reduce the exit angle but the profile of the extrudates are similar. At the higher extrusion ratio increasing the ram velocity tends to increase the radius of curvature of the product as shown.

b) Effect of Extrusion Ratio

Figures 5.27 and 5.28 illustrate the variation of the exit geometry with fractional reduction for the pure lead and tin lead respectively. Increasing the extrusion ratio can be seen to have the same effect as increasing the velocity. One might postulate that the decreasing radius of curvature is an effect due to increasing strain rate since, at the same ram velocity but a higher extrusion ratio, the strain rate for the process must be higher.

The effect of extrusion ratio in the side extrusion without a bottom, for the tin lead, is shown in Figure 5.29 for two velocities. Identical trends are observed for both velocities where the radius of curvature is decreased with increasing extrusion ratio.

c) Effect of Strain Rate Sensitivity

Two materials have been tested in depth and it is clear from these tests that the strain rate sensitivity has a marked effect on the

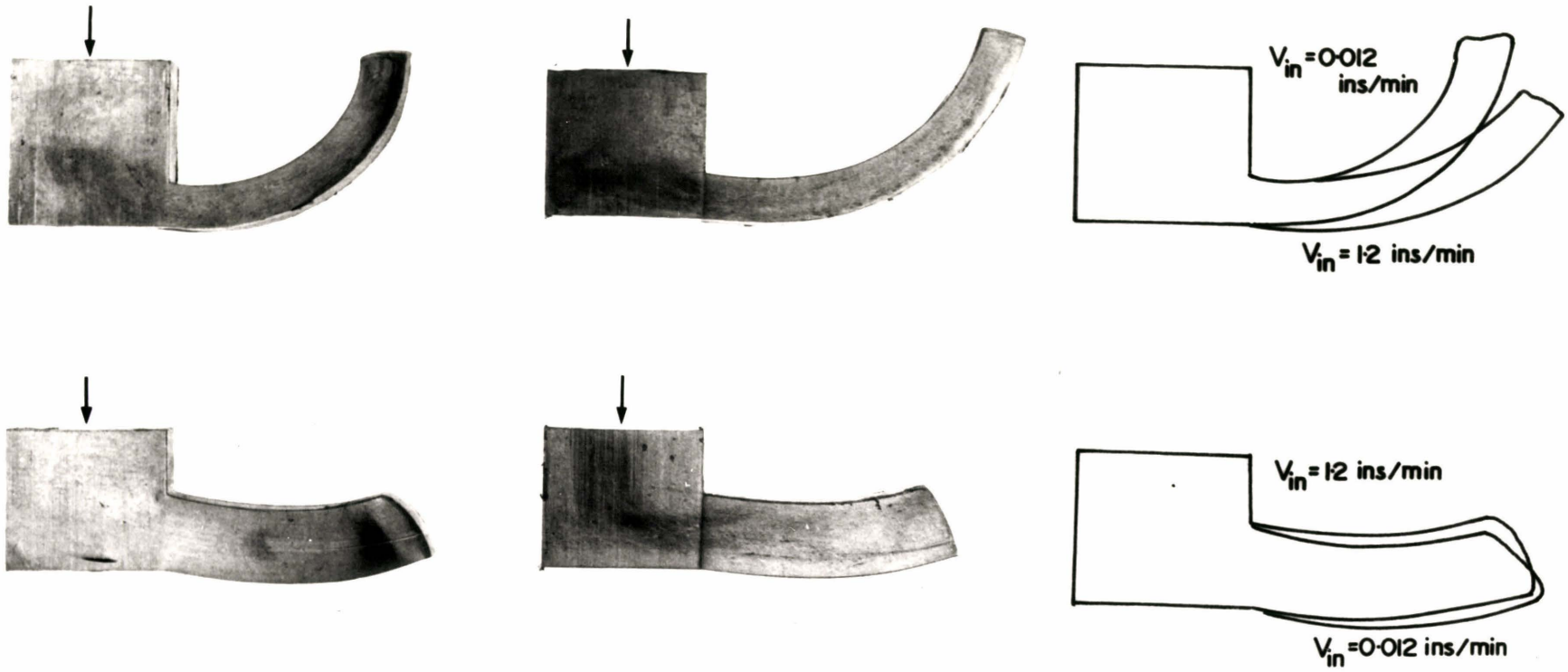

Figure 5.26

Photograph indicating effect of velocity on the exit geometry at two extrusion ratios for the tin lead eutectic in the secondary die

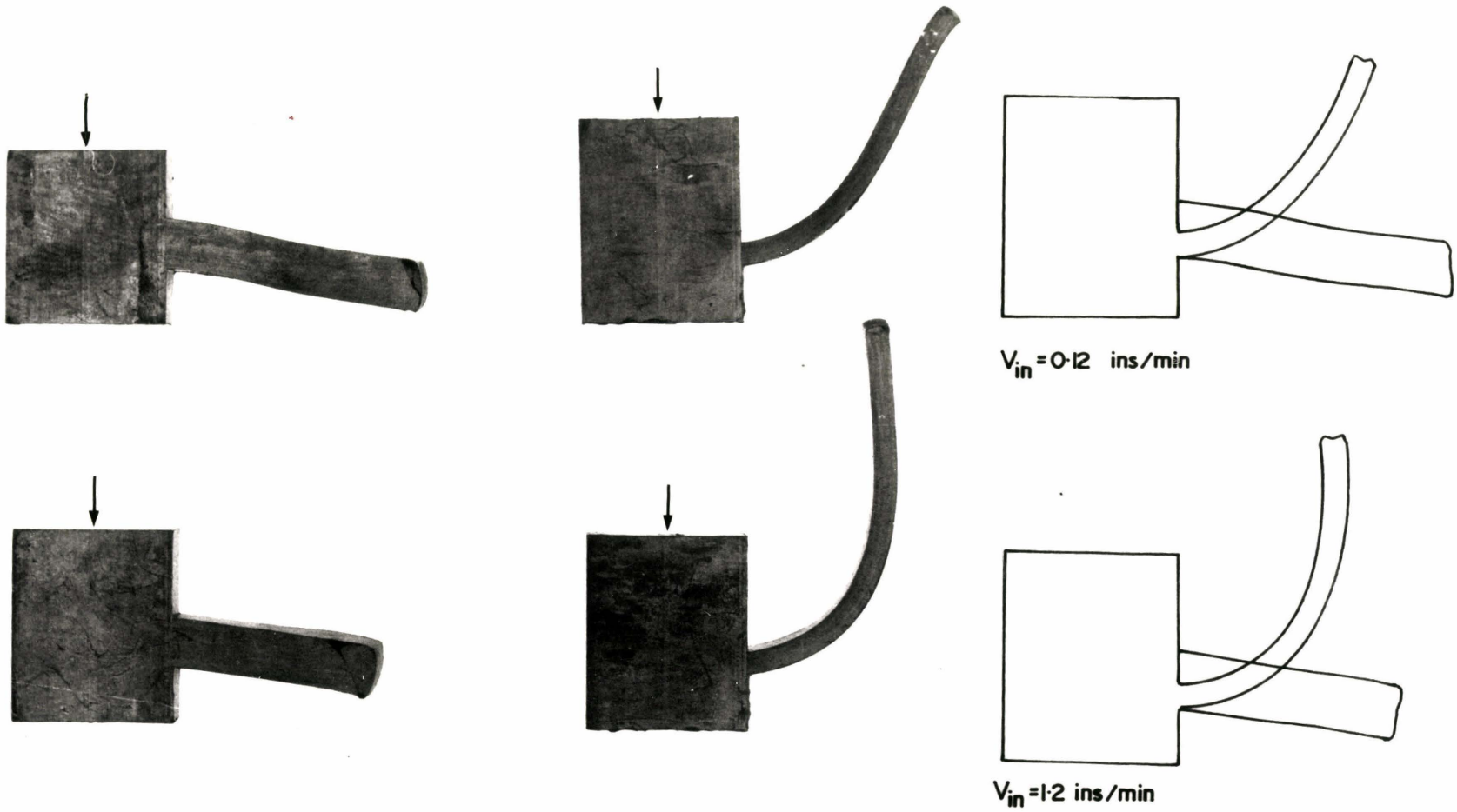

Figure 5.27

Photograph indicating effect of extrusion ratio at two velocities on the exit geometry for the pure lead

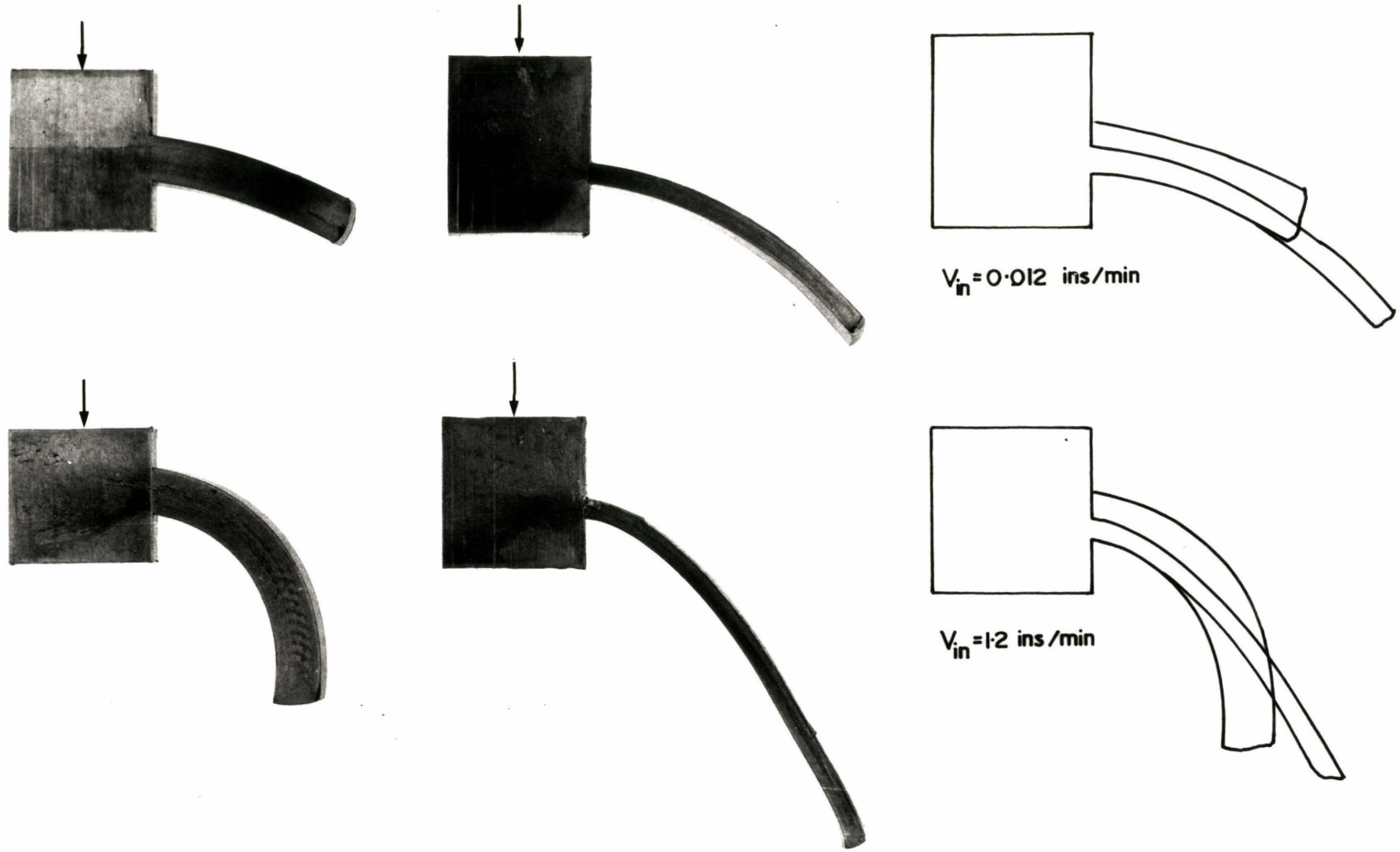

Figure 5.28

Photograph indicating effect of extrusion ratio at two velocities on the exit geometry for the tin lead eutectic

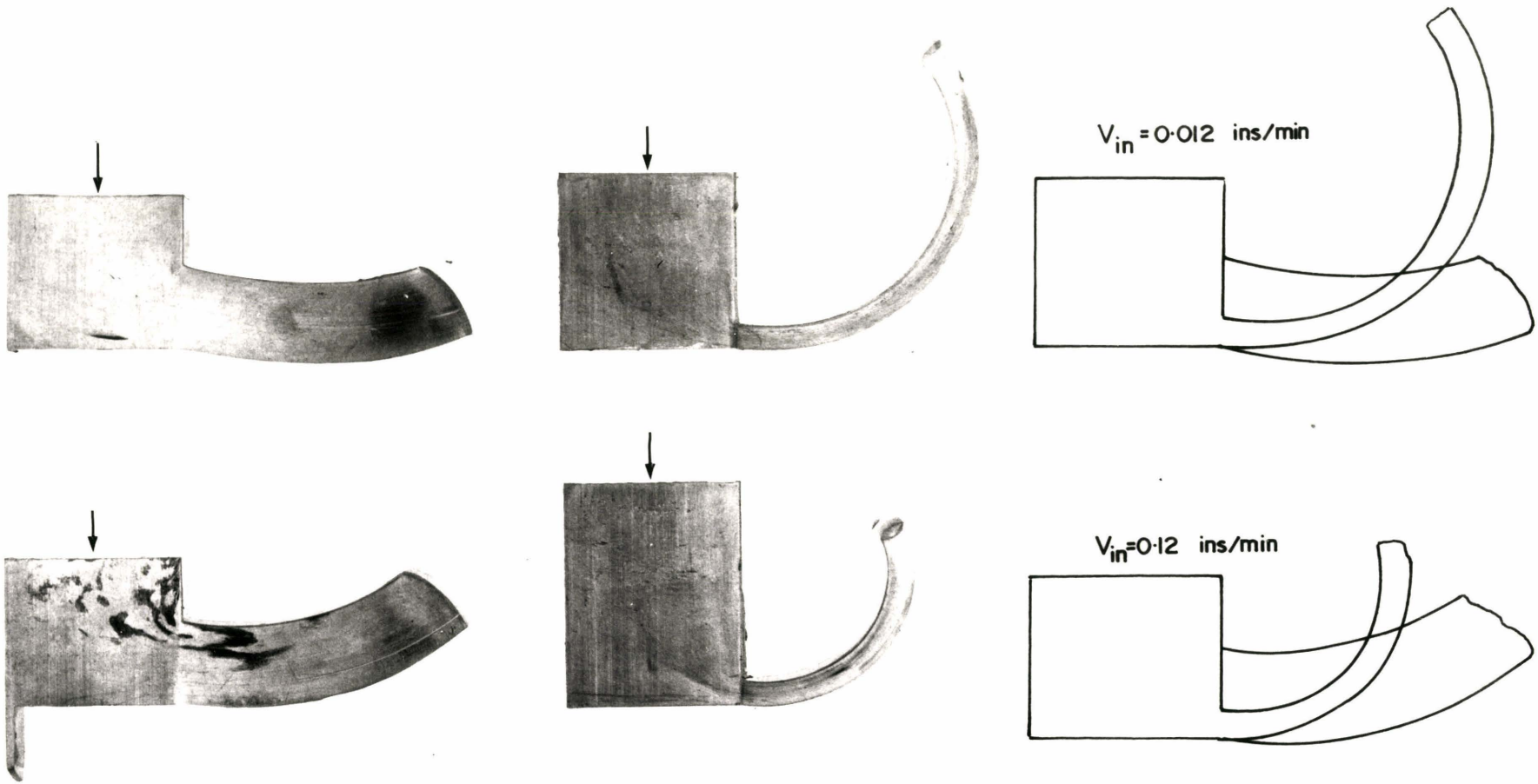

Figure 5.29

Photograph indicating effect of extrusion ratio at two velocities on the exit geometry for the tin lead eutectic in the secondary die

exit geometry and consequently on the deformation zone geometry. Figure 5.30 compares the exit geometry at two extrusion ratios but the same ram velocity, for the two materials tested. It is clear from Figures 5.30 and 5.22 that the exit geometry is a function of strain rate sensitivity. It is not possible at this stage to deduce, from the experiments, the nature of the relationship between the strain-rate sensitivity and the deformation zone geometry.

A few experiments have been performed with the zinc-aluminium eutectic which is superplastic, after suitable heat treatment, at 482^{o}F (250^{o}C). Figure 5.31 compares the exit geometry of the zinc aluminium, tin lead and pure lead and it will be observed that the zinc aluminium behaves in a similar manner to the tin lead. This test program was not pursued because of the extreme experimental difficulties with heating the dies to the appropriate forming temperature. The material properties for the zinc aluminium were determined in detail and indicated that the strain rate sensitivity was 0.42. The trends in the exit geometry for the zinc aluminium alloy are identical to those for the tin lead indicating that the exit geometry is similar for materials with similar strain rate sensitivities.

d) Exit Angle

The exit angle of the extrudate was measured on each specimen by drawing a tangent to the curve of the product at the aperture. The results for the different die geometries and materials are presented in Figures 5.32, 5.33 and 5.34.

Figure 5.32 for the pure lead indicates that the die angle

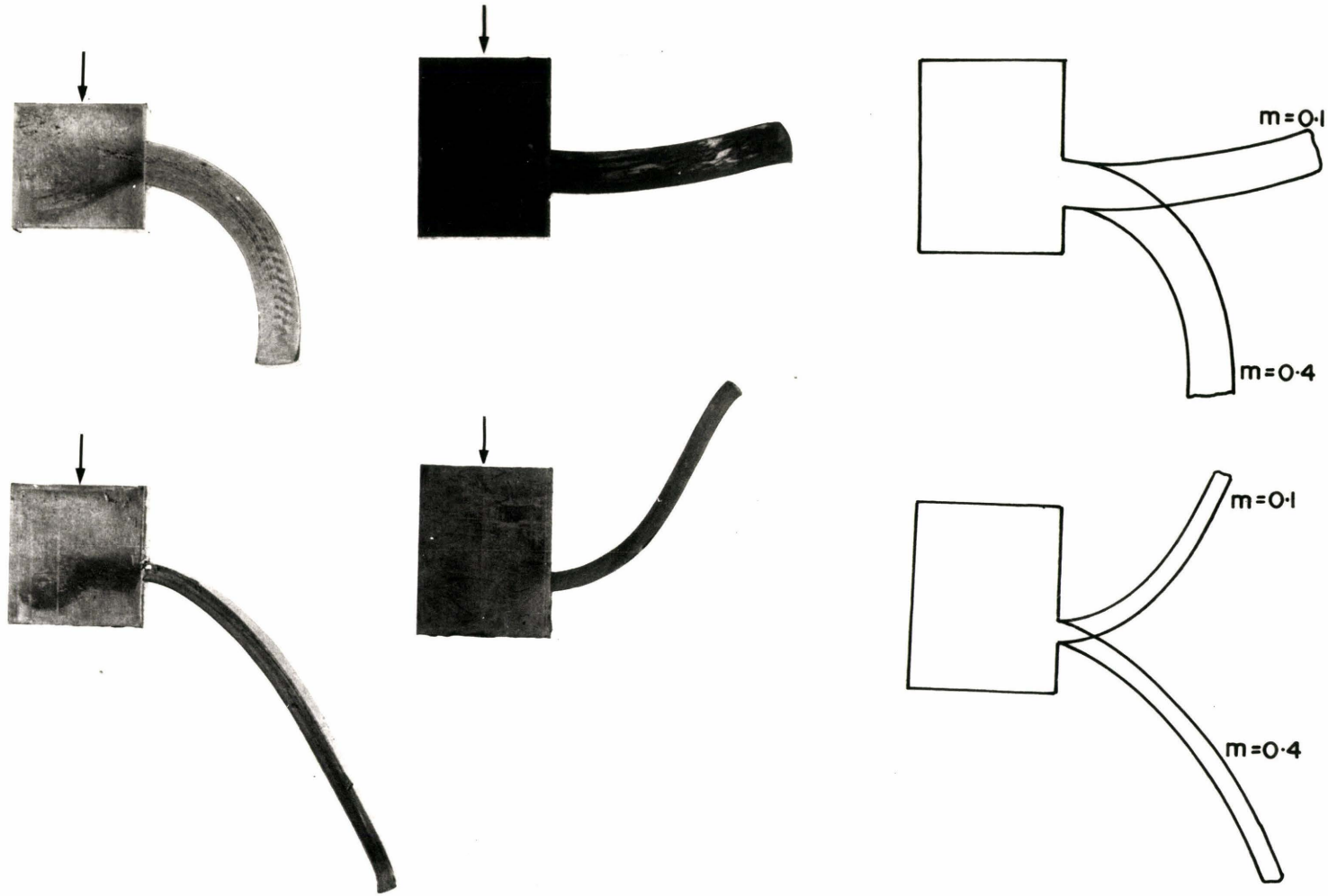

Figure 5.30

Photograph indicating effect of strain rate sensitivity on the exit geometry at two different extrusion ratios

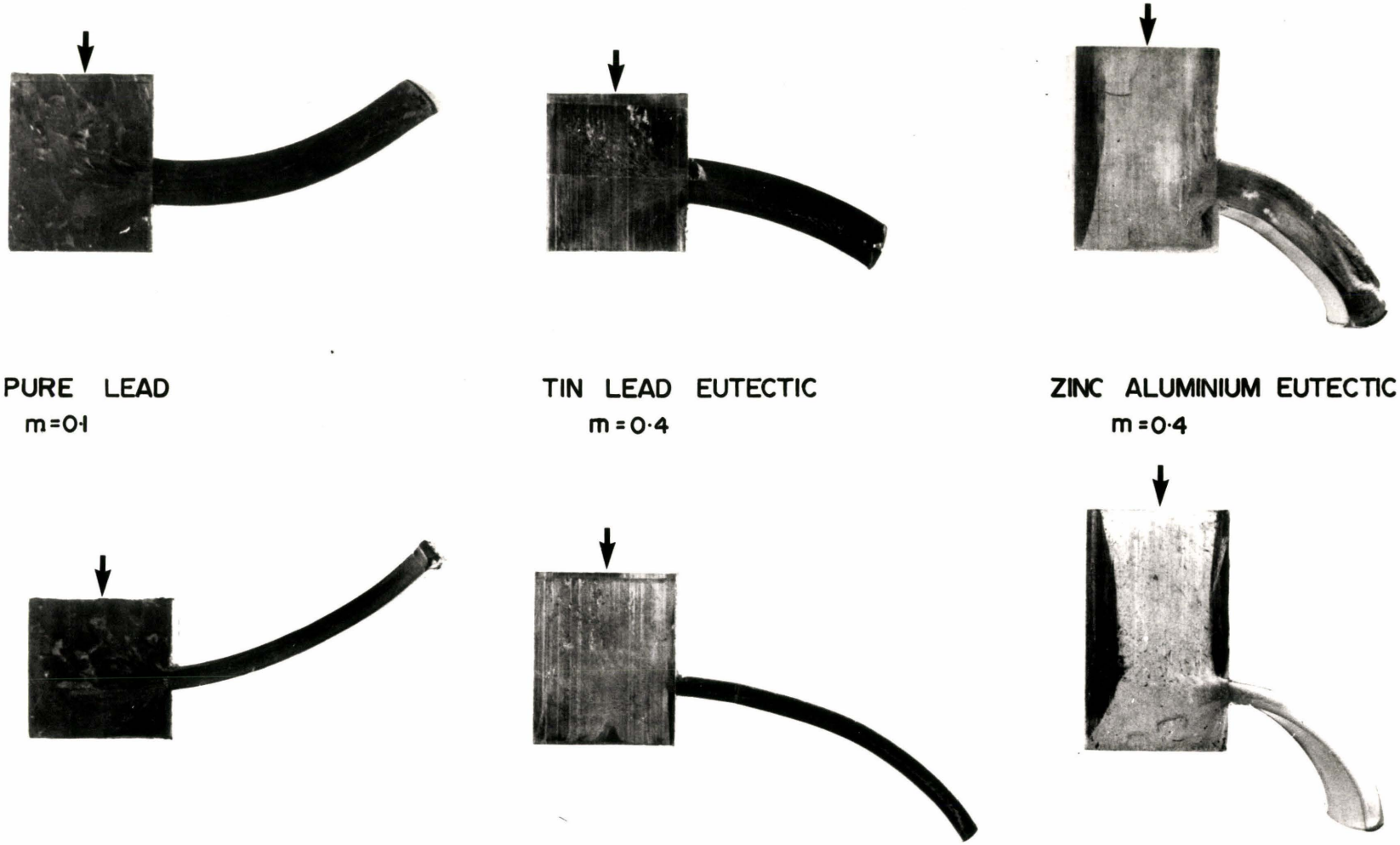

Figure 5.31

Photograph indicating exit geometry for pure lead, tin lead, eutectic and zinc aluminium eutectic

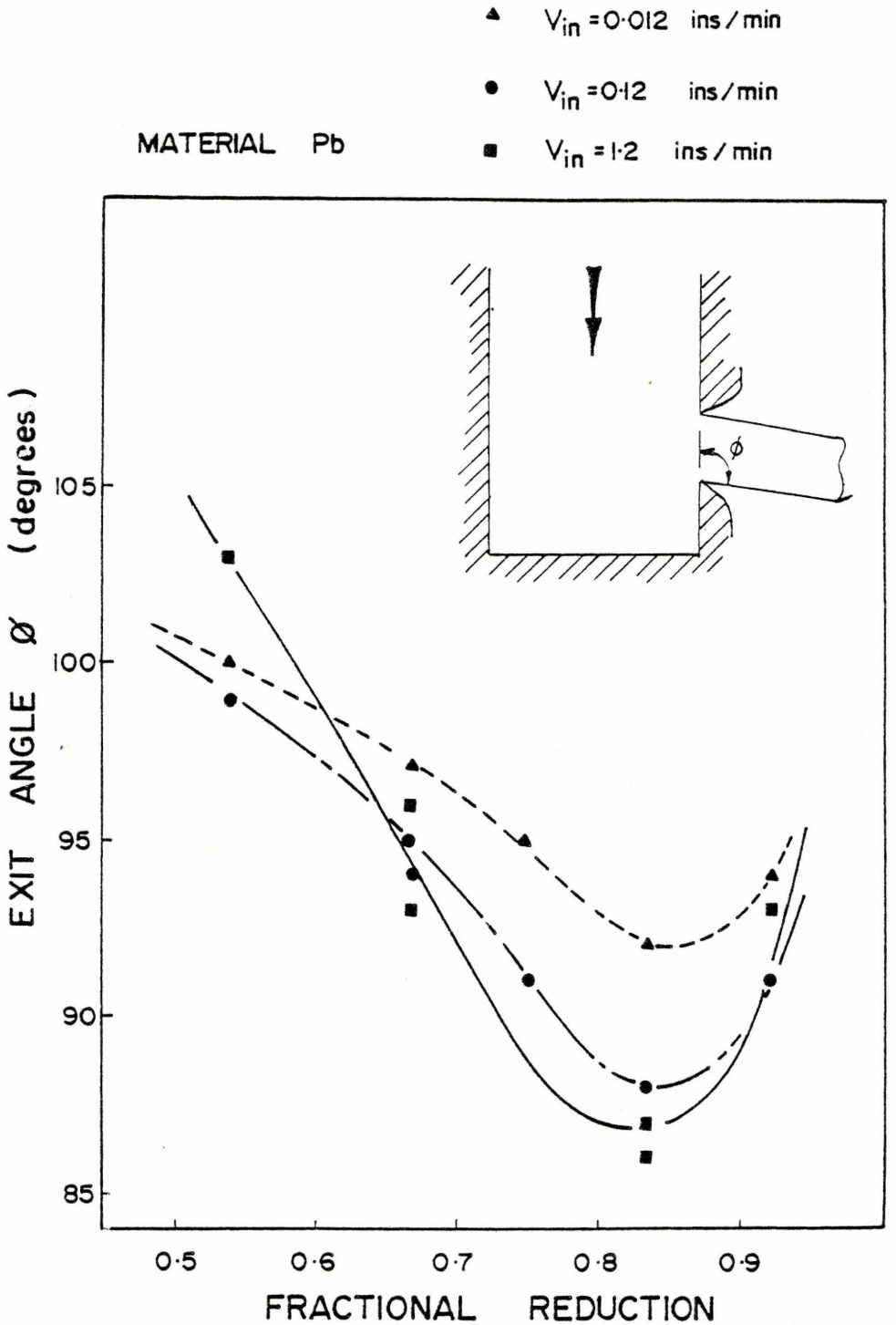

Figure 5.32

Variation of exit angle with fractional reduction at different ram velocities; pure lead

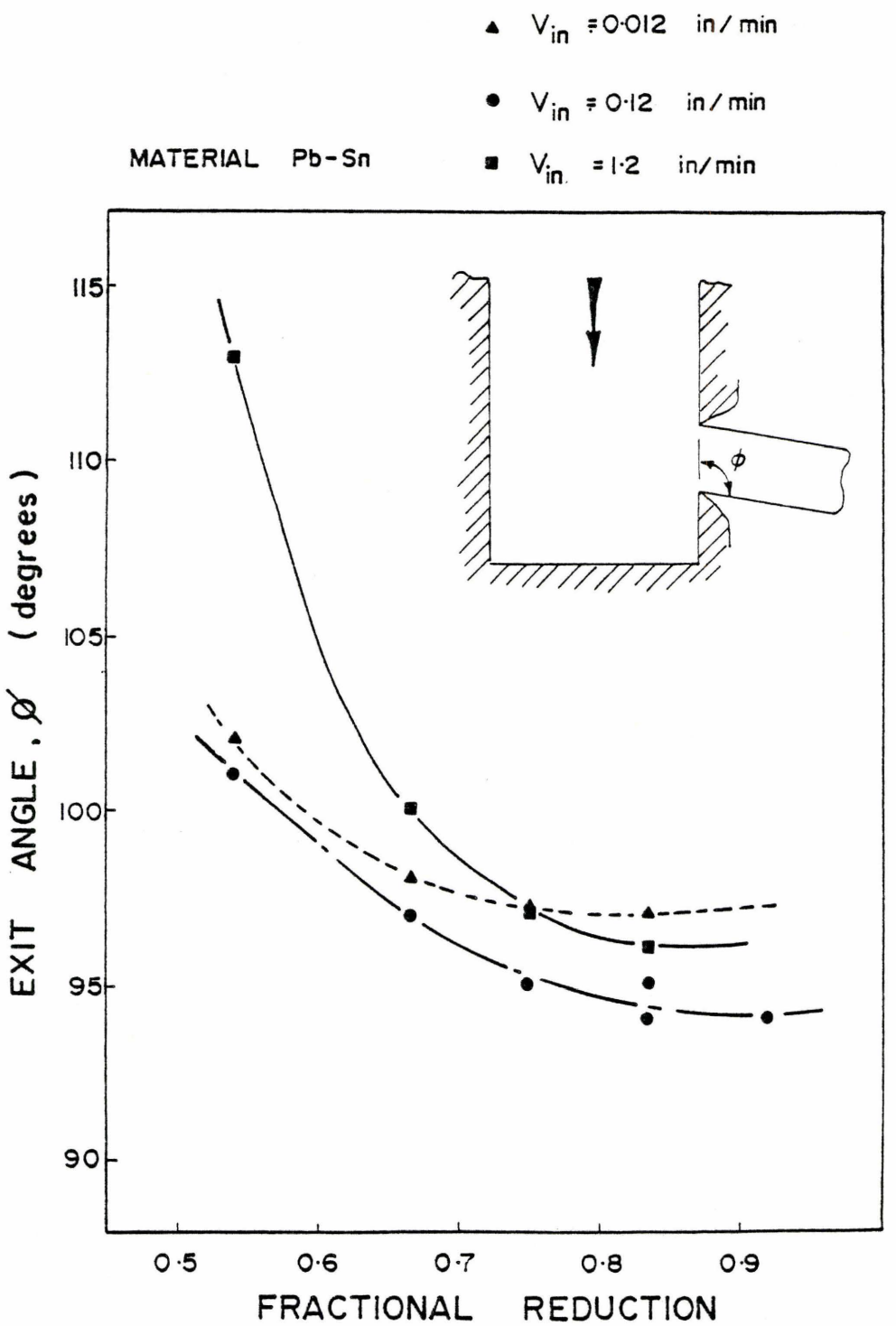

Figure 5.33

Variation of exit angle with fractional reduction at different ram velocities; tin lead eutectic

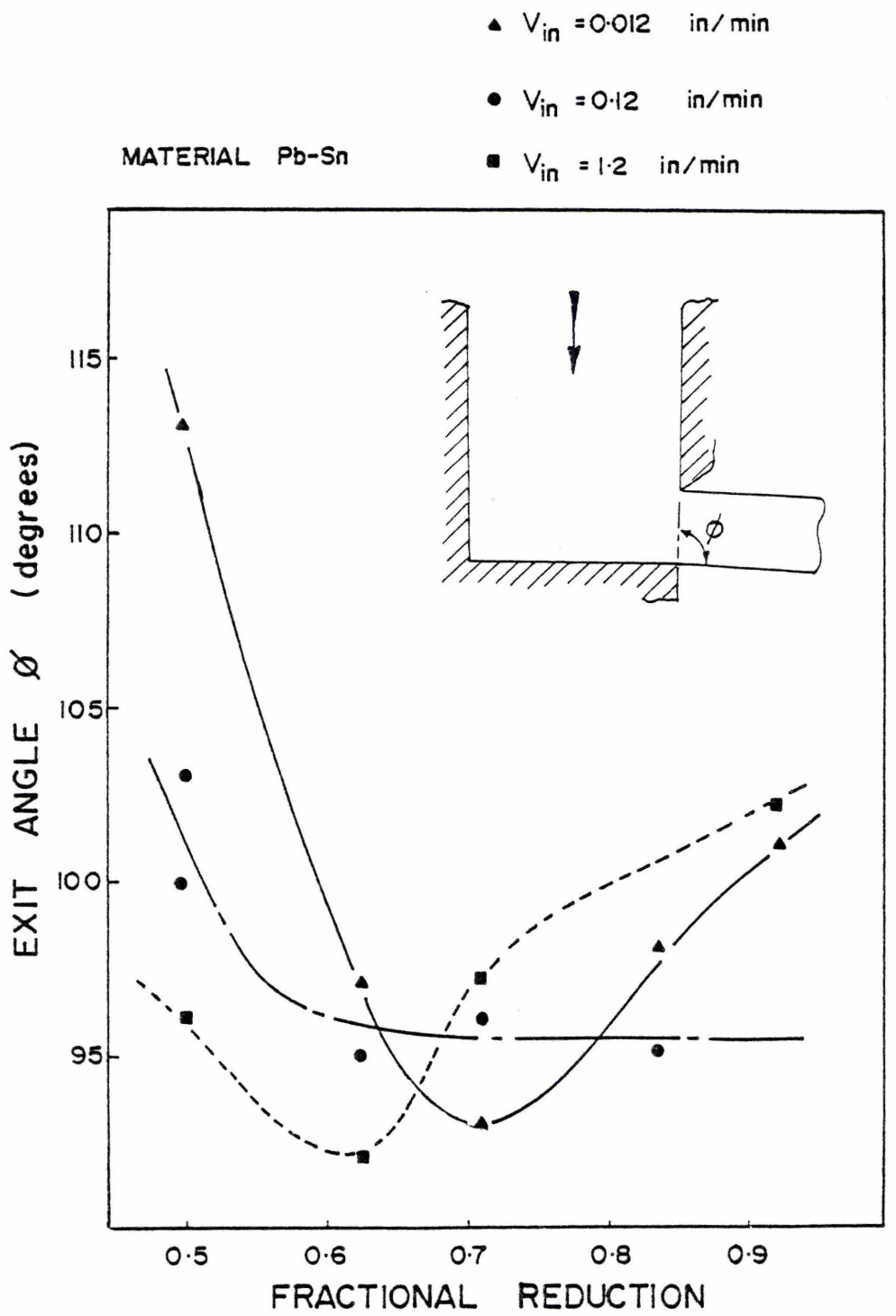

Figure 5.34

Variation of exit angle with fractional reduction of different ram velocities; tin lead eutectic in secondary die

decreases steadily with increasing fractional reduction to a minimum and then increases as the reduction increases. This minimum in the exit angle, at an extrusion ratio of approximately 6, is probably associated with a change in the type of deformation field geometry. Figure 5.33 for the tin lead, however, does not show any minimum but rather a trend towards a constant exit angle as the fractional reduction increases. The constant exit angle, however, does not appear to be a function of the ram velocity.

The variation of the exit angle with fractional reduction for the tin lead in the second die configuration is presented in Figure 5.34. A minimum value of the exit angle is again apparent but the results do not show the same trend for all ram velocities.

In all the above cases the exit angle is not a simple function of the extrusion ratio or the ram velocity. A minimum is apparent for the case of sideways extrusion of lead and it is probable that this is associated with a change in the mode of deformation as the extrusion ratio increases.

e) Radius of Curvature

The radius of curvature of the extruded product can be measured to a reasonable degree of accuracy (± 5%) using simple geometric relationships. If we assume that three points x_1, x_2 and x_3 lie on the arc of a circle, Figure 5.35, and that the linear distance between successive points is constant and equal to dx then the radius of curvature at the central point x_2 can be approximated by

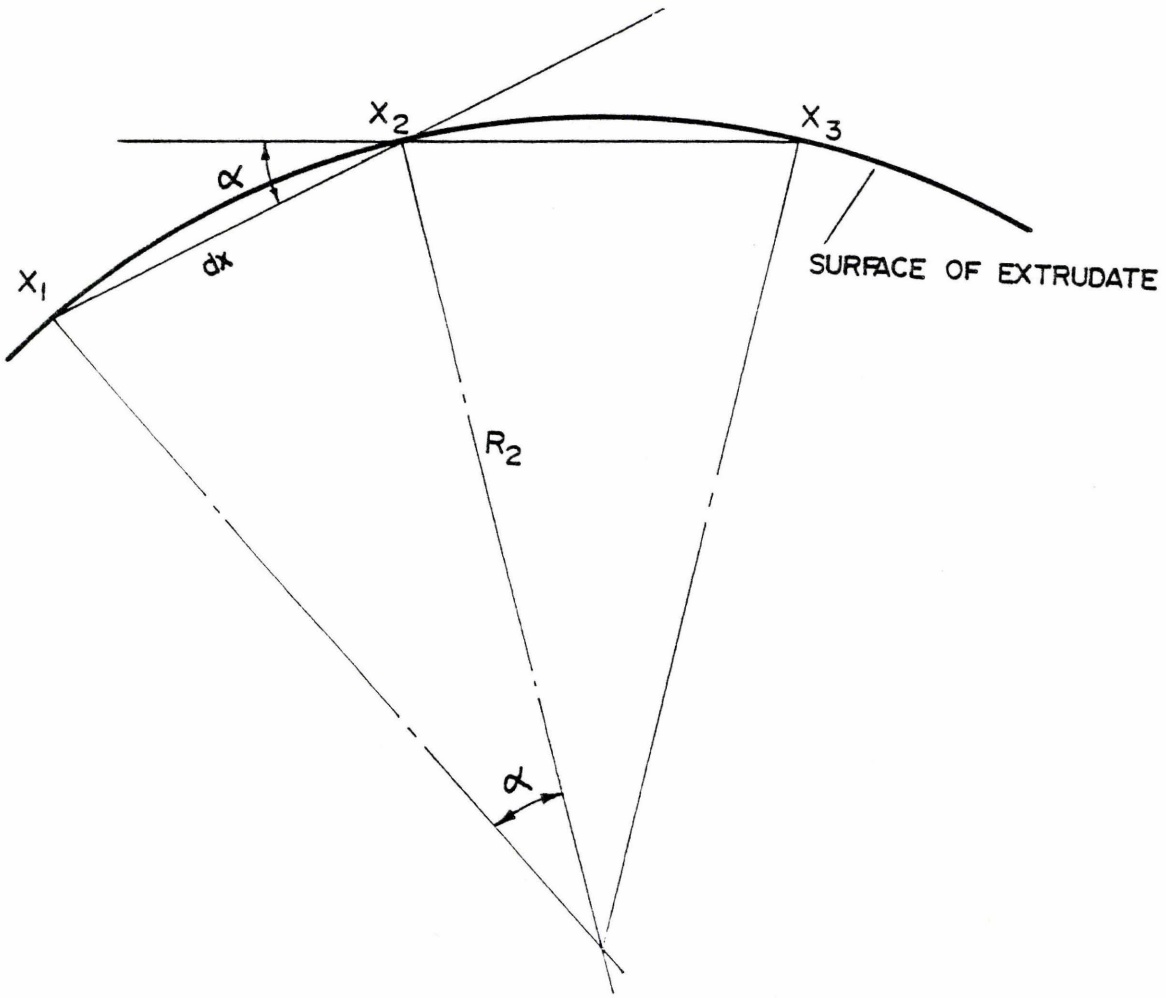

Figure 5.35

Schematic indicating the geometry used for the approximate measurement of the radius of curvature of the product

$$R_{x_2} = \frac{dx}{2} \cdot \frac{1}{\sin(\alpha/2)} \qquad (5.3)$$

where α is the angle between the lines joining x_1 to x_2 and x_2 to x_3.

The radius of curvature of the extrudate was measured in a majority of the tests by taking a slide of the test specimen and projecting the image to twice the real dimensions. The distance dx in Eqn. (5.3) was made equal to 0.5 inches (12.7 mm) which is equivalent to 0.25 inch (6.4 mm) intervals on the real specimen. The radius at each point was determined but because of the approximate method of measurement large differences between successive values were apparent. Since the radius of curvature is derived from information for three points a mean radius of curvature at each station was determined with respect to those on either side. A weighted numerical averaging formula of the type

$$\bar{R}_i = \frac{1}{4}(R_{i-1} + 2R_i + R_{i+1}) \qquad (5.4)$$

was used.

The results of these measurements are presented below. In general the radius of curvature of the product was not constant but certain trends can be observed; they are that:-

1) as the process proceeds the radius of curvature decreases for the tin lead in the major die configuration
2) as the process proceeds the radius of curvature increases for the pure lead in the major die configuratoin.
3) in general there is no simple experimental relationship for the radius of curvature of the product at any instant.

The variation of the curvature of the extrudate with distance from the die aperture is presented in Figures 5.36 and 5.37 for fractional reductions of 0.667 and 0.75 respectively. Both figures indicate the variation of the curvature for the pure lead and the tin lead.

The effect of the fractional reduction on the curvature of the extrudate is presented in Figures 5.38 and 5.39 for ram velocities of 0.012 ins/min (0.005 mm/sec) and 1.2 ins/min (0.5 mm/sec) respectively.

The variation of the curvature of the extrudate with velocity and fractional reduction for the tin lead in the secondary die is shown in Figures 5.40 and 5.41 respectively.

5.4.3 Observations of the Deformed Grid Patterns

In the preceeding paragraphs observations of the exit geometry have been described in a qualitative manner and results presented of an examination of the curvature of the extrudate. No definite conclusions were drawn concerning the results of the tests, however it was clear that the geometry of the deformation zone was a function of the material strain rate sensitivity. The effects of ram velocity and extrusion ratio on the resultant extrusion were described and these changes must be accomodated by changes in the deformation zone geometry. Each test specimen was made up of a split billet and on one of the central faces a 0.1 inch (2.54 mm) square grid was scribed using a vernier height gauge. The purpose of the grids was to allow a qualitative assessment of the distorted grid patterns after the experiments had been completed. No grid strain analysis was attempted to define the local strain-rate or

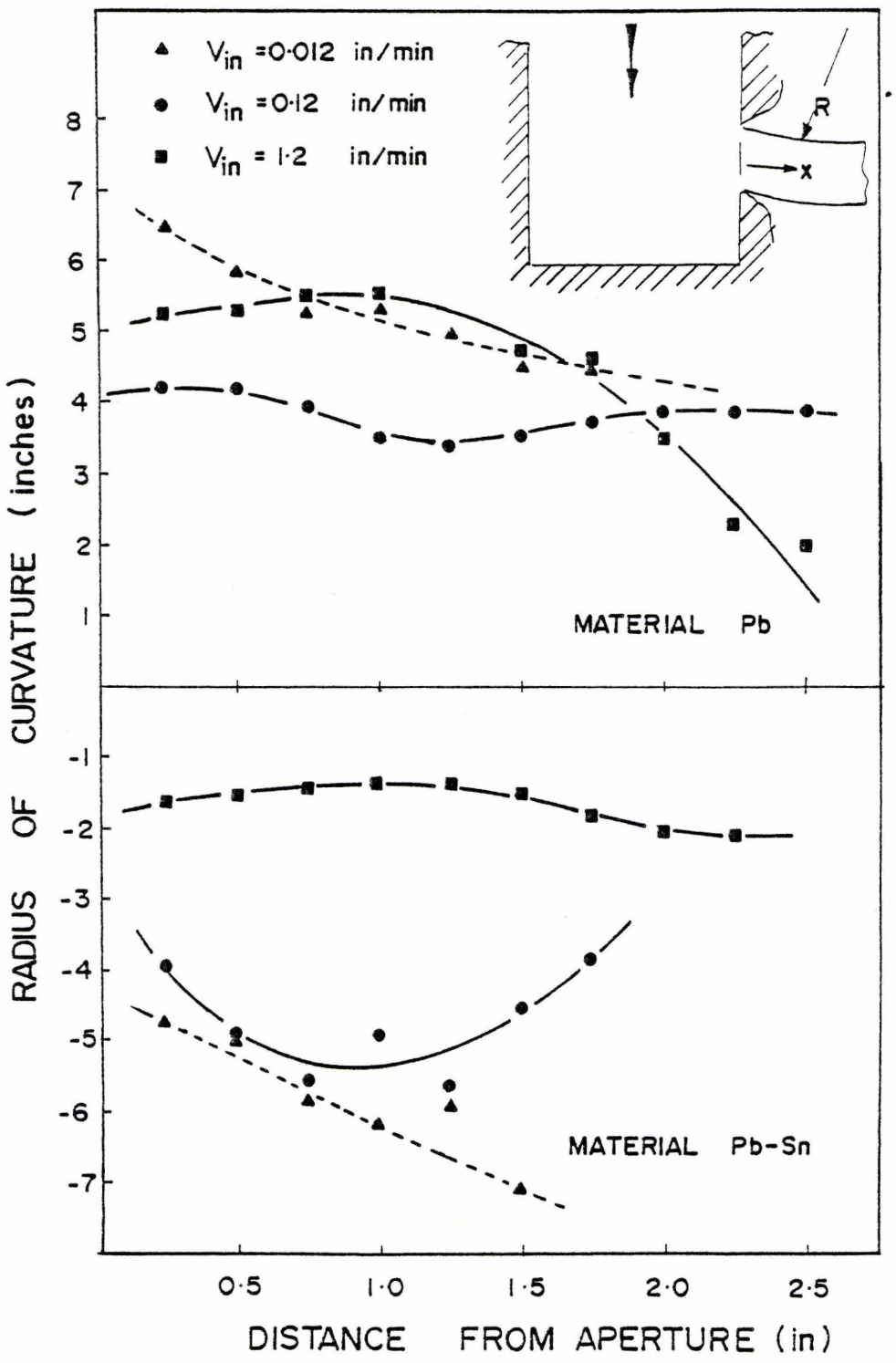

Figure 5.36

Variation of radius of curvature of the product with distance from the die aperture, at different velocities, for the two materials tested; fractional reduction 0.667

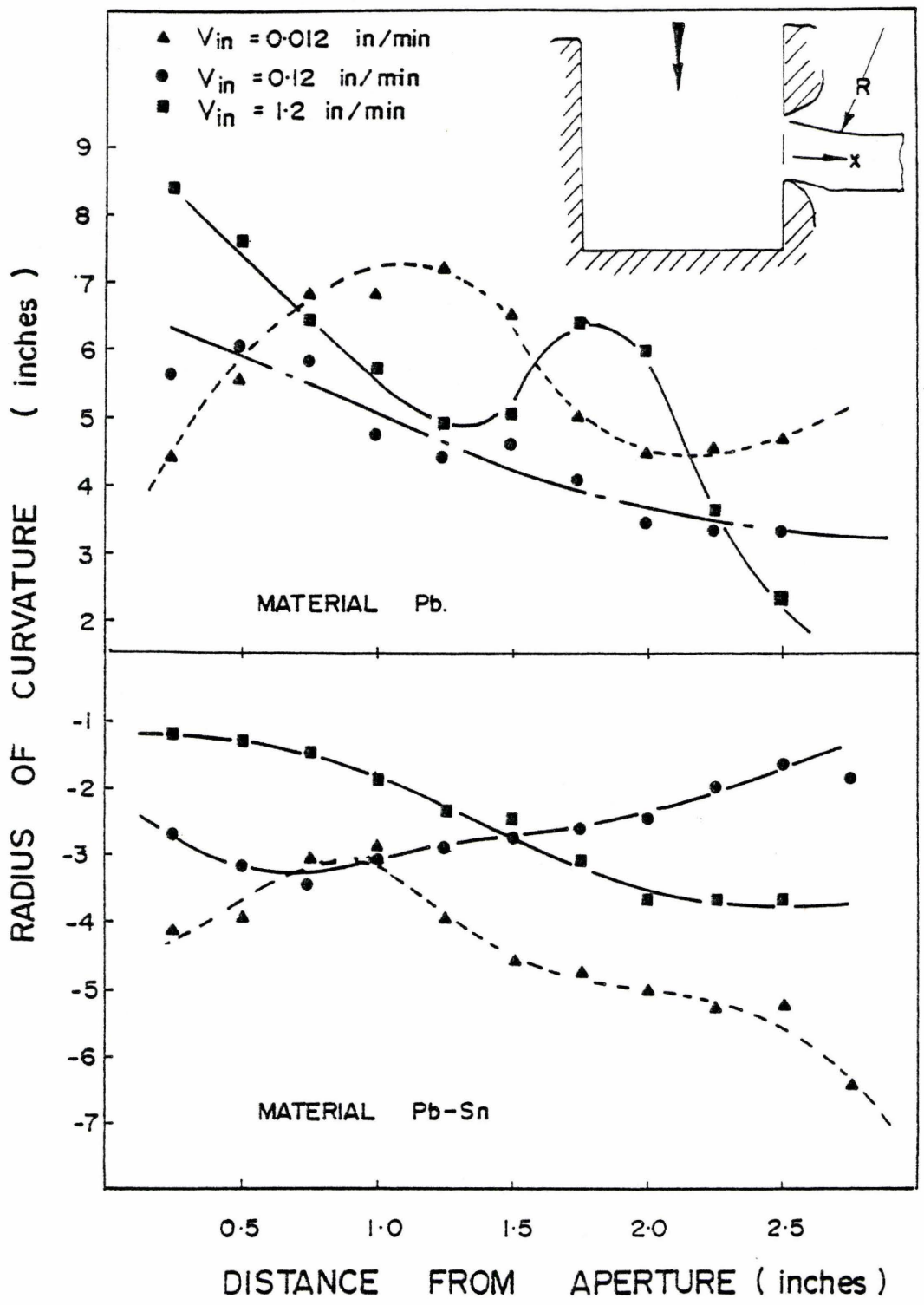

Figure 5.37

Variation of radius of curvature of the product with distance from the die aperture, at different velocities, for the two materials tested; fractional reduction 0.75

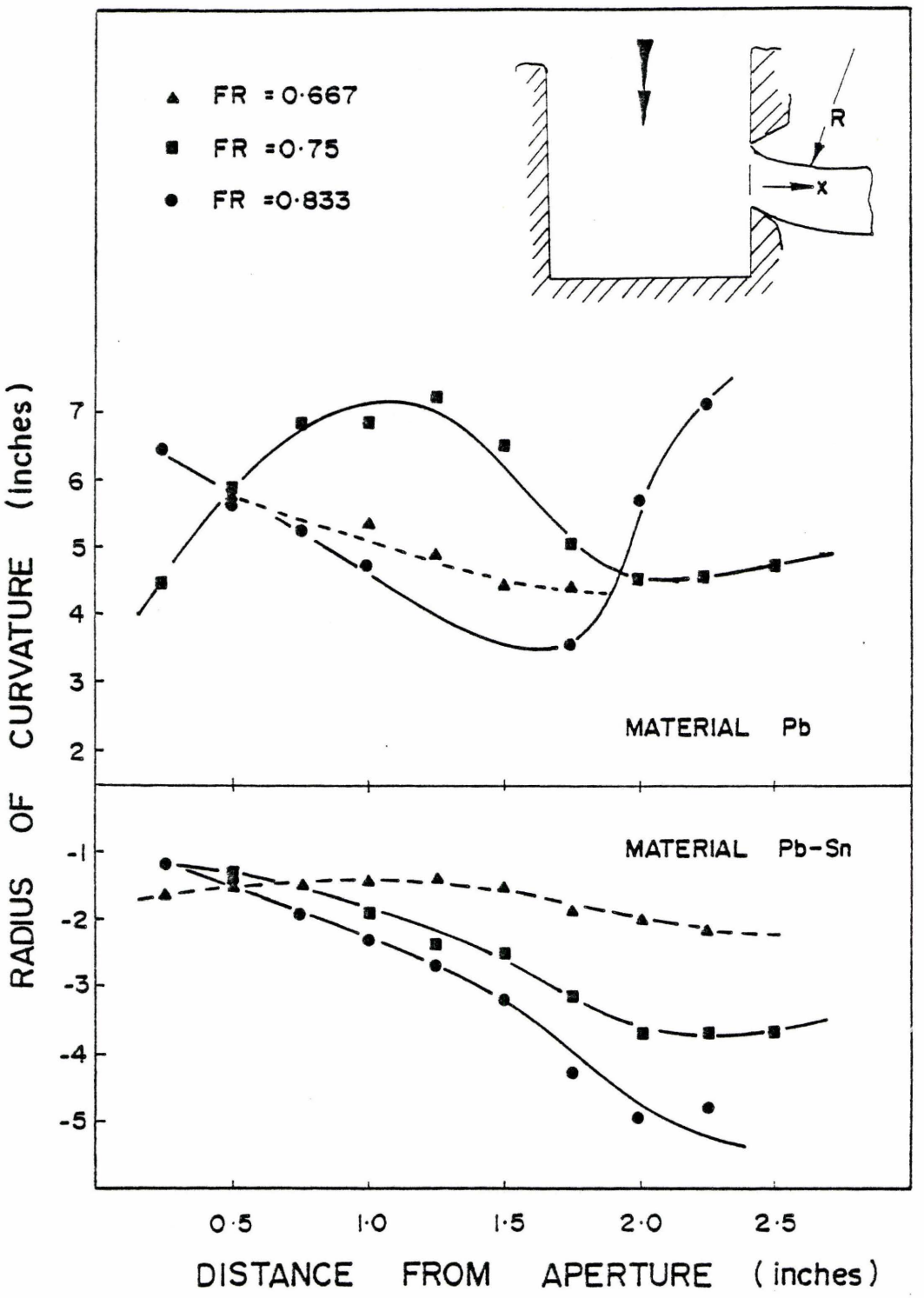

Figure 5.38

Variation of radius of curvature of the product with distance from the die aperture, at different fractional reductions, for the two materials tested; velocity 0.012 ins/min (0.0051 mm/sec)

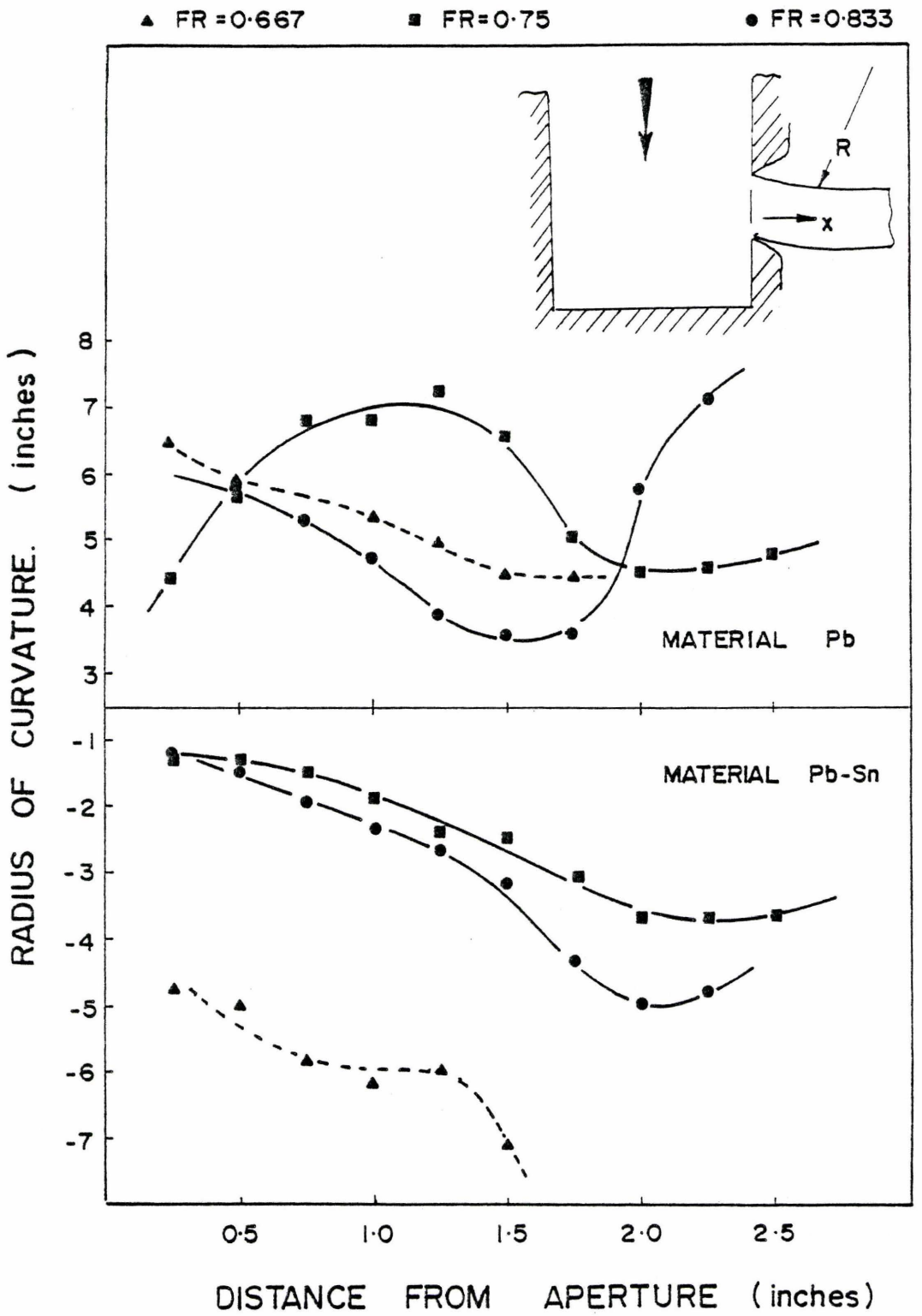

Figure 5.39

Variation of radius of curvature of the product with distance from the die aperture, at different fractional reductions, for the two materials tested; velocity 1.2 ins/min (0.51 mm/sec)

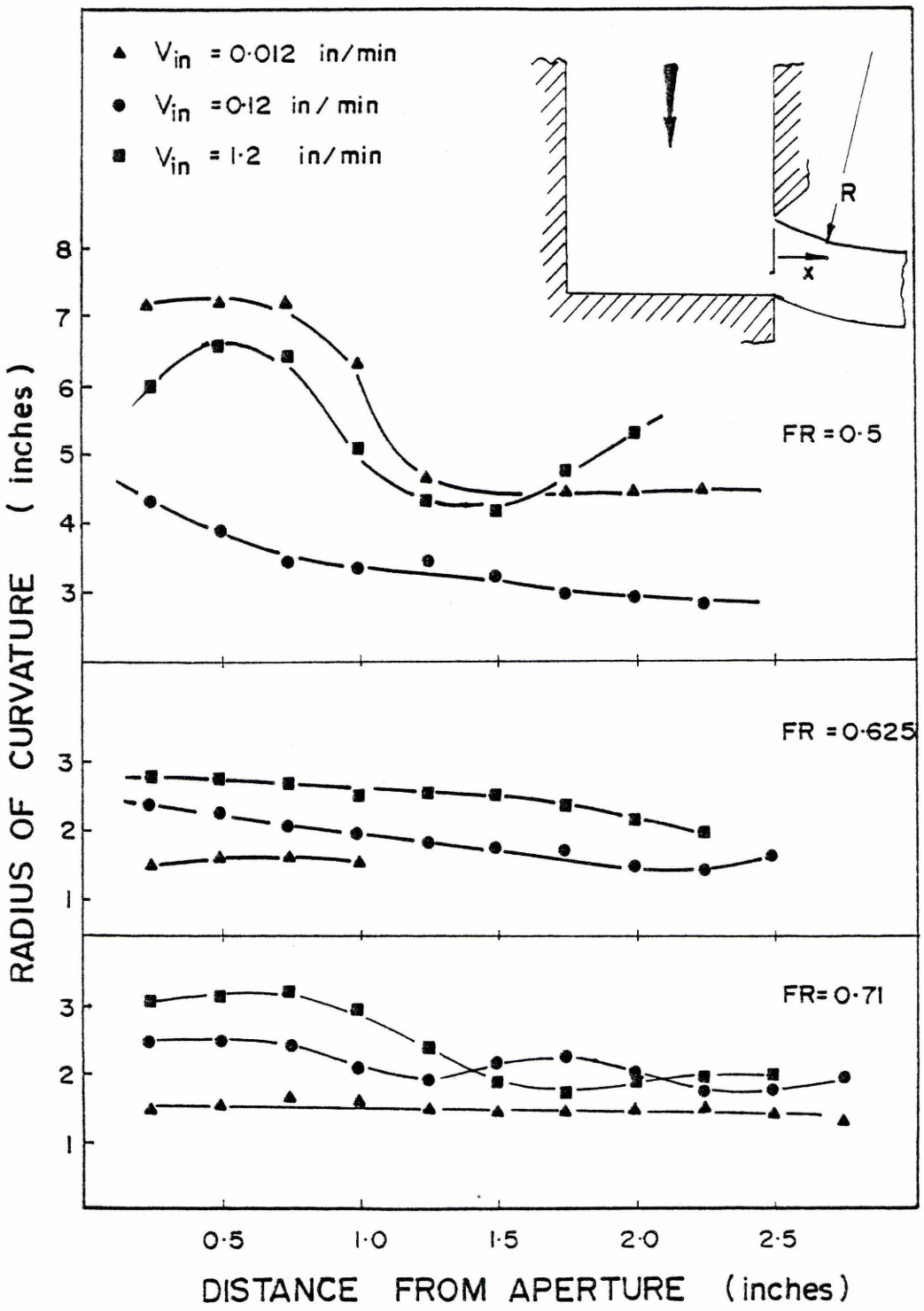

Figure 5.40

Variation of radius of curvature of the product with distance from the die aperture, at different velocities; tin lead in secondary die

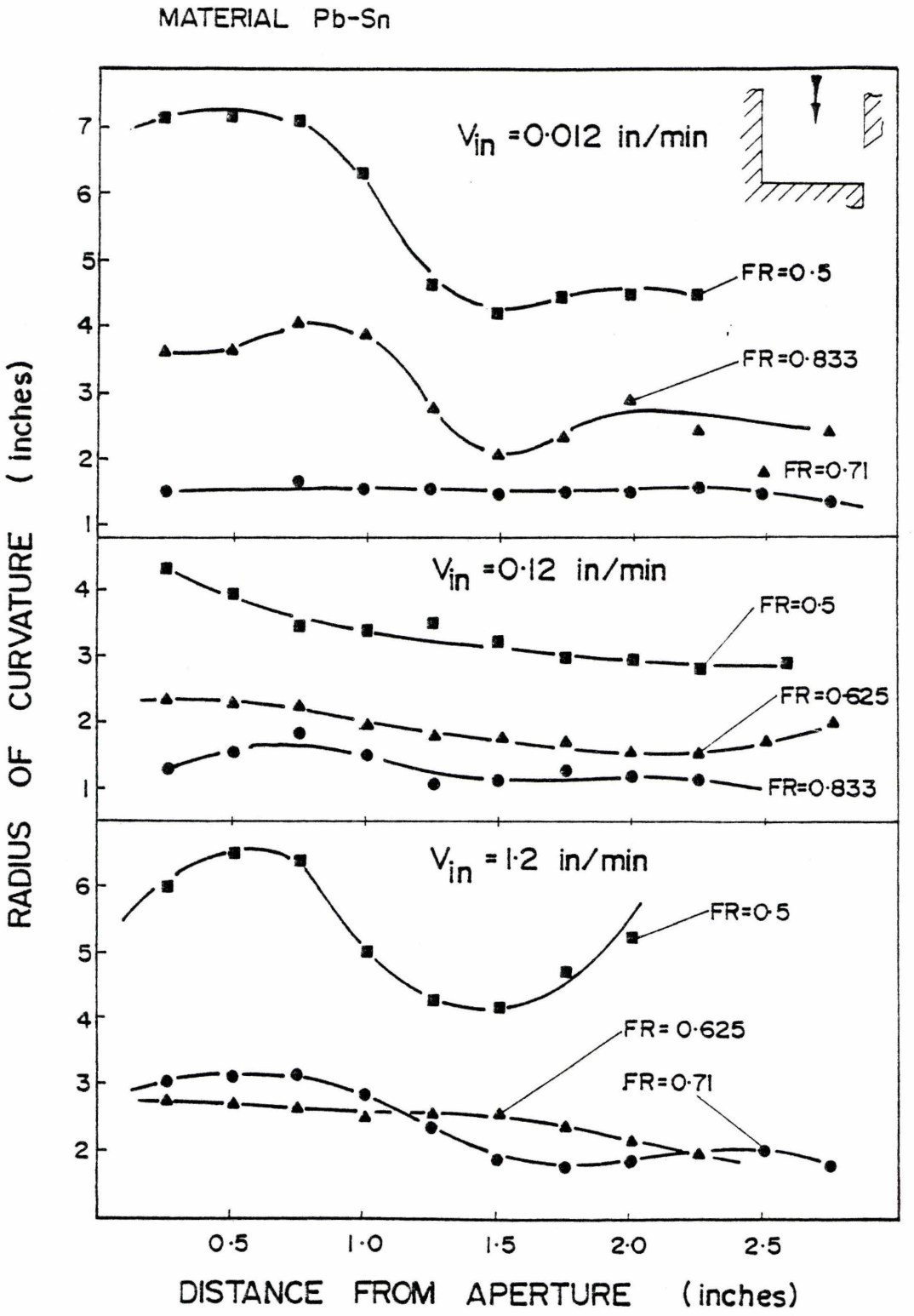

Figure 5.41

Variation of radius of curvature of the product with distance from the die aperture, at different fraction reductions; tin lead in secondary die

the plastic zone geometry. In the paragraphs below qualitative observations of the deformed grid patterns will be presented.

Figures 5.42 and 5.43 which are photographs of typical lead specimen at different extrusion ratios showing the distorted grids have a drawing of the slip line field superimposed on the photograph. A dead metal zone is clearly visible in both figures and, to a first approximation confirms the shape of the slip line field.

The distorted grid patterns for tin lead specimen extruded under similar conditions to those for the lead are shown in Figures 5.44 and 5.45. The slip line field for the rigid, perfectly plastic model is again superimposed on the photograph but it is clear that a dead metal zone is not as sharply defined as previously. The deformation is distributed more uniformally throughout the bulk of the material and the slip line field is not a good approximation.

With the lead samples the lower boundary of the deformation zone was clearly visible, however for the tin lead it is apparent that the deformation zone is much larger and that the die bottom may not be sufficiently far away from the aperture. The upper boundary of the deformation zone can be determined by careful examination and the following conclusions for the side extrusion of a rate sensitive material can be made.

1) That the deformation zone is larger than that predicted by the slip line field
2) In the current die geometry the base may not be sufficiently far away from the die aperture so as to not interfere with the

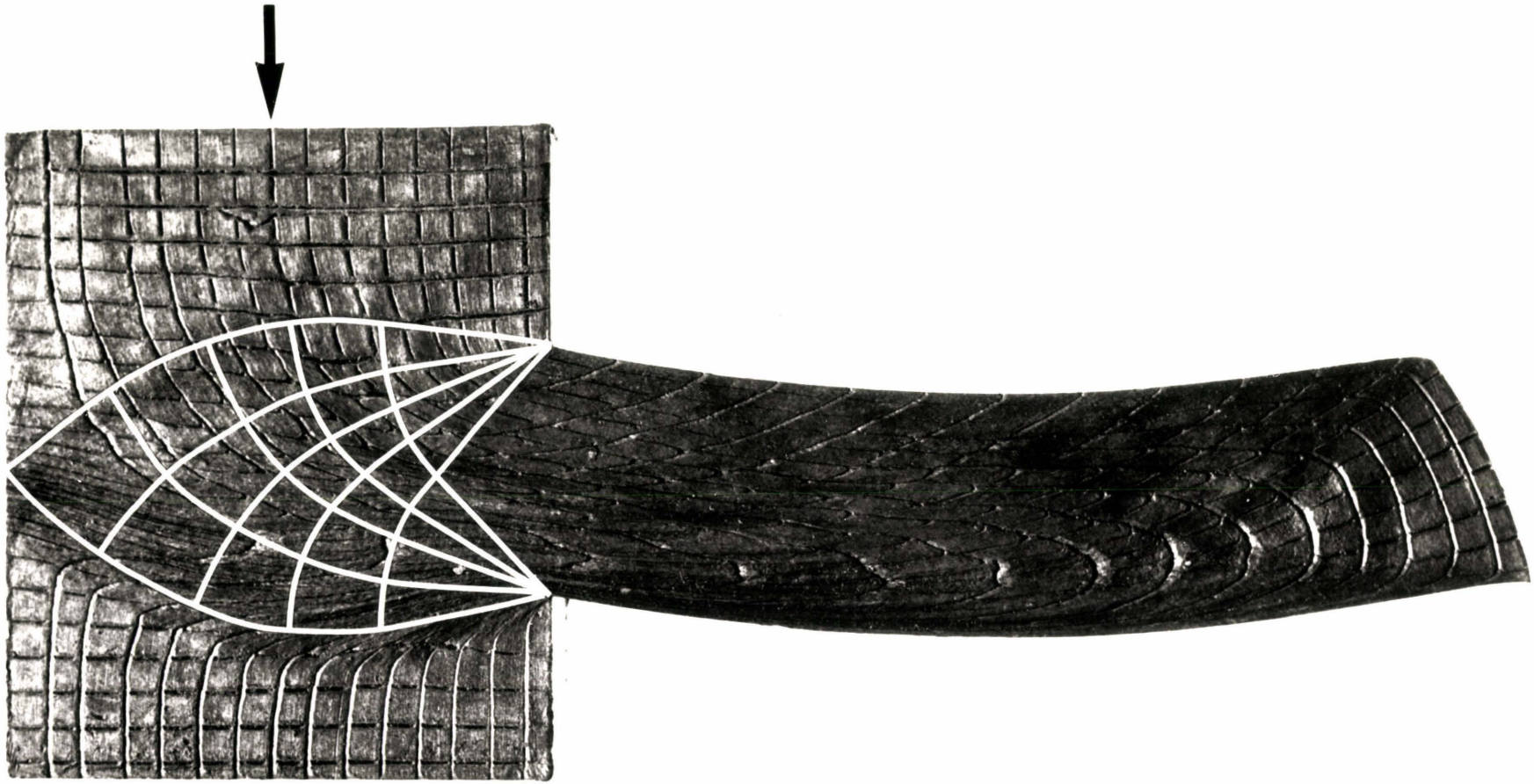

Figure 5.42

Photograph of distorted grid pattern; lead; V_{in} = 0.012 in/mm
Fractional reduction = 0.54

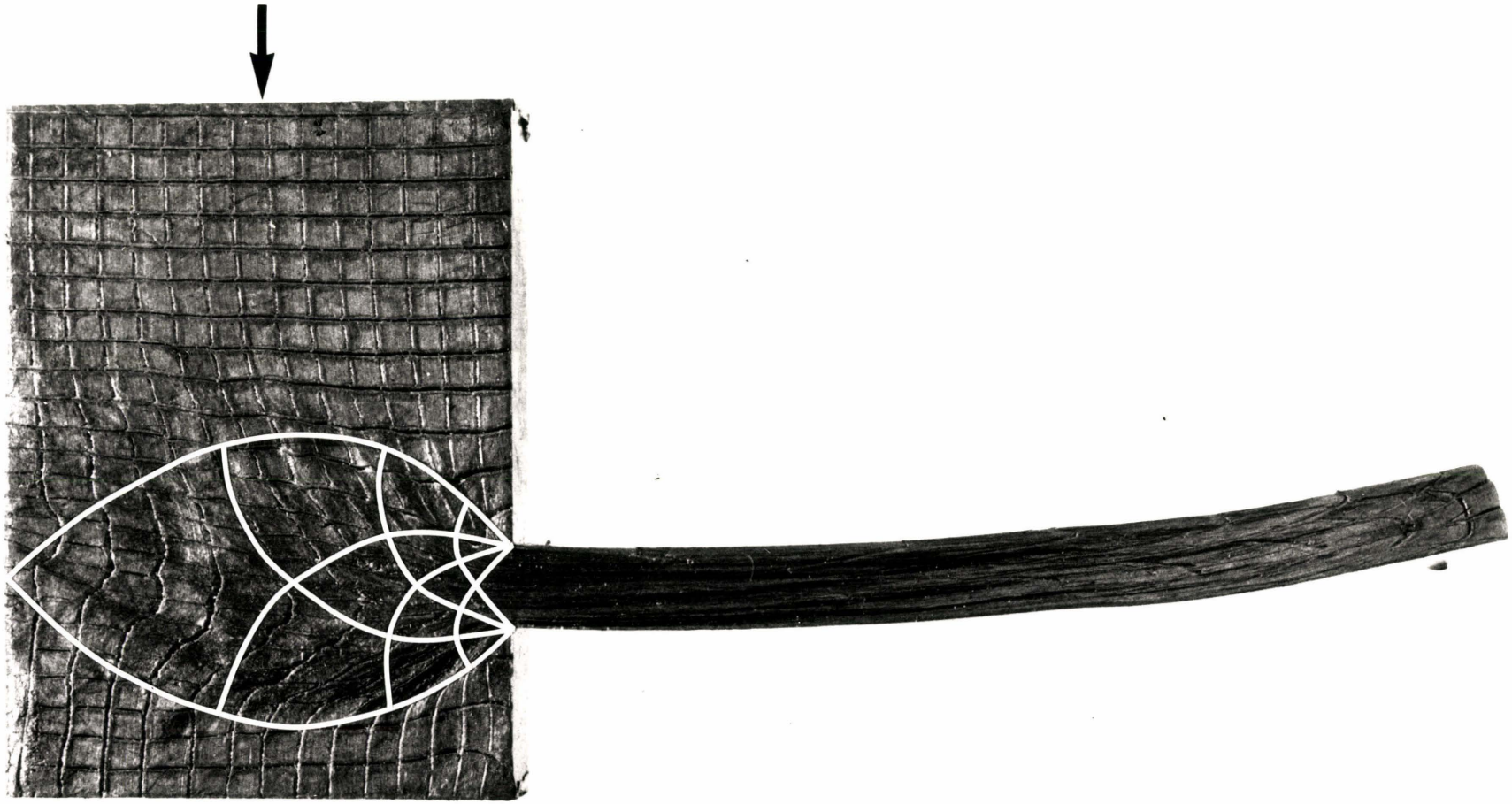

Figure 5.43

Photograph of distorted grid pattern; lead, V_{in} = 0.012 in/min
Fractional reduction = 0.833

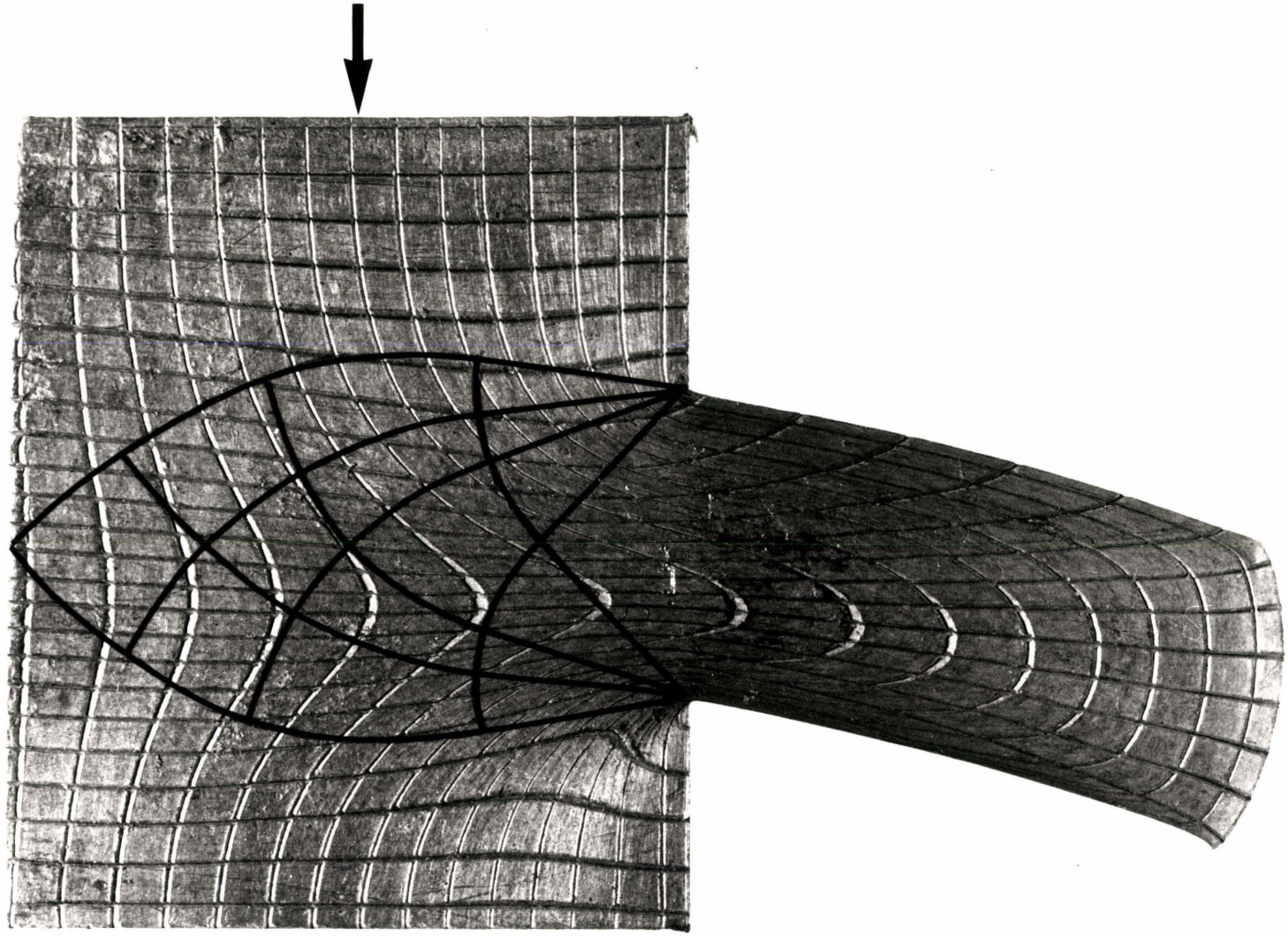

Figure 5.44

Photograph of distorted grid pattern; tin lead eutectic,
V_{in} = 0.012 ins/min, Fractional reduction = 0.54

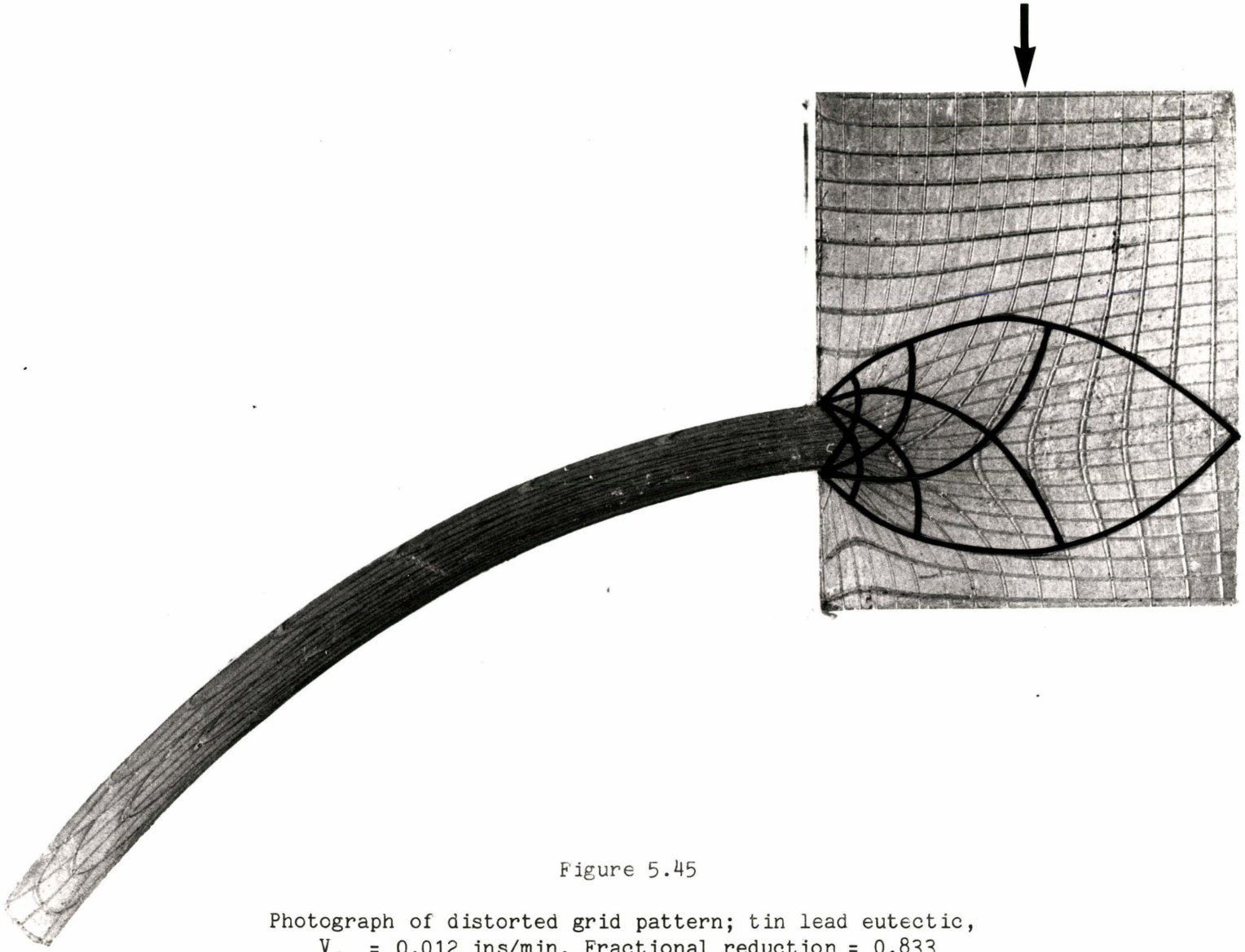

Figure 5.45

Photograph of distorted grid pattern; tin lead eutectic,
V_{in} = 0.012 ins/min, Fractional reduction = 0.833

deformation zone.

3) That the shape of the deformation zone is a function of the ram velocity and extrusion ratio.

4) That as the ram velocity increases the upper deformation zone boundary moves towards the base of the die.

5) As the extrusion ratio increases the deformation zone increases.

The deformed grid patterns for the tin lead in the second die configuration are shown in Figures 5.46 and 5.47; the slip line field is also shown superimposed on the photographs. The actual deformation zone is larger than that given by the slip line field.

5.5 Conclusions and Summary of Experimental Work

The major aspects of the experimental work undertaken during the course of the present study have been outlined and the results presented. Two materials have been examined in depth and their material properties characterized by the usual form of equations. Experiments were described for the side extrusion of pure lead and tin lead eutectic and it is evident that the variation of the extrusion pressure with ram speed is larger the higher the strain rate sensitivity.

The exit geometry of the extruded specimen is a function of the material and a characteristic difference between the two materials was recongized which has not been previously reported. Tests on another rate sensitive material gave results similar to those for the tin lead which leads one to conclude that the exit geometry is a function of the material properties, in this case the strain rate sensitivity.

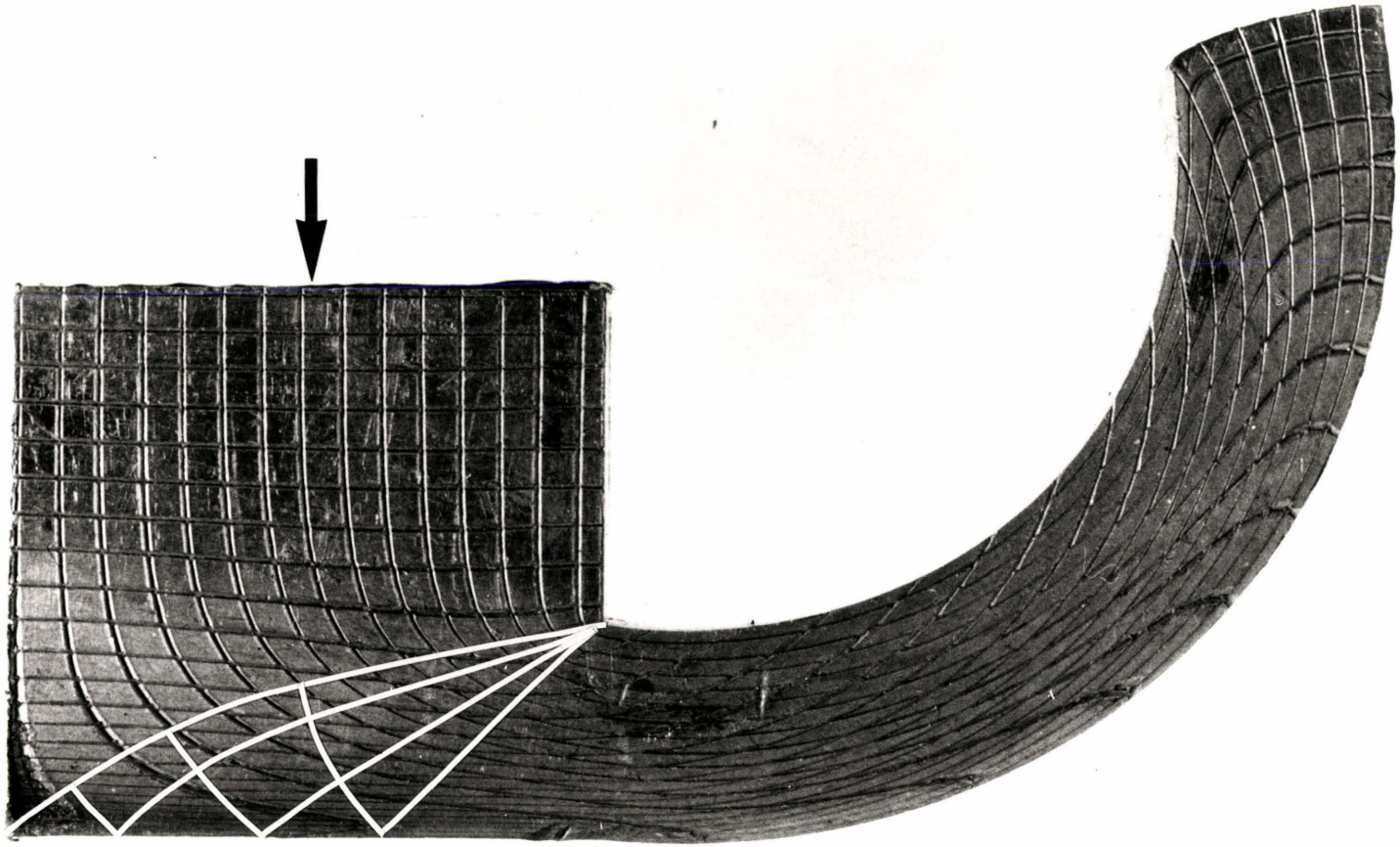

Figure 5.46

Photograph of distorted grid pattern; tin lead eutectic, secondary die, V_{in} = 0.12 ins/min, Fractional reduction = 0.625

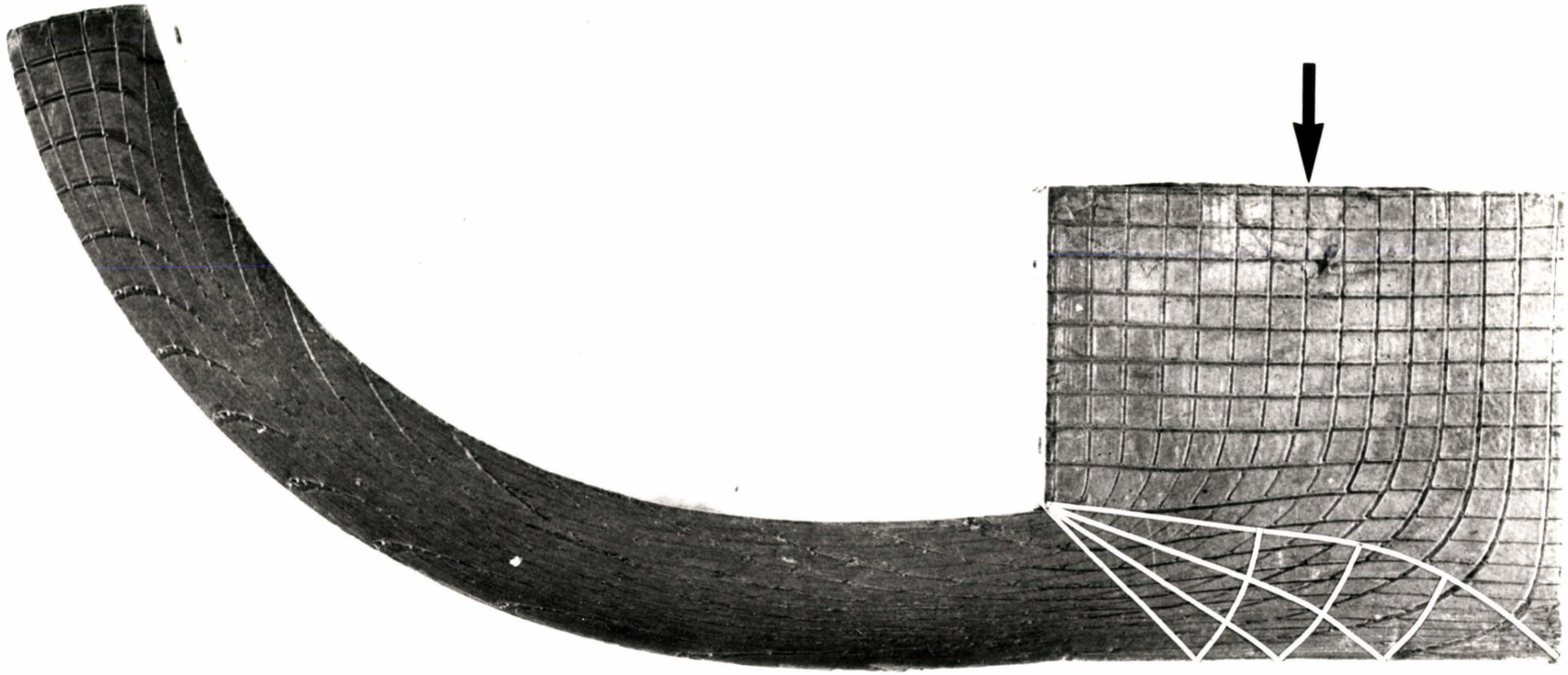

Figure 5.47

Photograph of distorted grid pattern; tin lead eutectic, secondary die, V_{in} = 1.2 ins/min, Fractional reduction = 0.71

The rotation of the extruded product, unreported in previous work, was recognized and measured; however the results do not lead to any generalized conclusions. The variation of the exit angle with fractional reduction was examined and a minimum was observed for the pure lead at an extrusion ratio of approximateley 6. This minimum was not observed under similar conditions for the tin lead. The minimum in the exit angle, it was postulated, could indicate a change in the deformation mode as the extrusion ratio increases.

A visual examination of the distorted grid patterns showed that the slip line and tangential discontinuity velocity fields proposed were suitable for the analysis of the side extrusion of lead. The deformation zone for the tin lead, however, was larger than that given by the slip line field.

CHAPTER 6

COMPARISON AND DISCUSSION OF THEORETICAL AND EXPERIMENTAL RESULTS

6.1 Introduction

In the preceeding chapters a theoretical solution for the bulk forming of rate sensitive materials was presented. Details of experimental work on two materials with different rate sensitivities indicated that there is a significant difference in the exit geometry of the extruded product and that this is a function of the strain rate sensitivity. The theoretical solution presented predicted that material should be extruded straight at some angle dependent on the extrusion die geometry; recall eqn. (3.1)

$$\theta = \tan^{-1} \frac{2D}{d} \tag{6.1}$$

where D is the die width

and d the aperture.

The experimental results, however, indicated that the extruded product rotates as it leaves the die. The difference between the theoretical and experimental observations are discussed in this chapter.

The concept of a thin shear zone was introduced in the analysis in Chapter 4 and a dimensionless parameter identified. The application of the model to determine the extrusion pressure for a rate sensitive

material was discussed and it was shown that a solution must be generated for each material. The sideways extrusion pressure is evaluated in this chapter for the two materials used in the experimental program and compared with the results given in Chapter 5. The exit geometry is discussed with reference to the curling of the extrudate and some new fields proposed which give solutions where the material leaves the die at a constant radius of curvature.

The shape of the discontinuity between a uniform transitional velocity field and a rotational field of constant angular velocity is discussed. A number of new velocity fields are then presented for a variety of metalworking process. These fields constitute a new type of 'mixed' field. Solutions to date have involved discontinuities which are either circular or straight. The solutions presented here involve velocity fields which are a combination of curved and straight tangential velocity discontinuities.

6.2 Determination of Extrusion Pressure

In Chapter 4 it was shown that an upper bound to the work rate for a material which is strain rate sensitive is given by:

$$\dot{W} = k' \sum v_i^* \left(\frac{s_i}{b_i^m}\right)^{m+1} \tag{6.2}$$

where b_i is the width of the shear zone.

The shear zone size in metal cutting was discussed and it was indicated that it is appropriate to assume that the shear zone thickness to length ratio is a constant and that a suitable value is 10. That is:

$$b_i = \frac{s_i}{10} \tag{6.3}$$

Computer programs were written to solve the side-extrusion problem using the second tangential velocity discontinuity model developed in Chapter 4. The work rate across each discontinuity was evaluated by considering the strain rate across each shear zone. If the strain rate was greater than $\dot{\varepsilon}_{max}$, as defined in Figure 5.12, the work rate for that shear zone was evaluated as for a rigid plastic material, i.e.

$$\dot{W}_i = \frac{\bar{\sigma}_{max}}{\sqrt{3}} (v_i^* s_i) \tag{6.4}$$

where $\bar{\sigma}_{max}$ is defined in Figure 5.12.

If the strain rate was less than $\dot{\varepsilon}_{max}$ then the work rate for that shear zone was evaluated using the rate sensitive work rate analysis,

$$\dot{W}_i = k' \, v_i^{* \, m+1} \frac{s_i}{b_i^m} \tag{6.5}$$

The material properties, ram velocities and shear zone thickness ratio were entered as data in a computer program which optimized the solution by minimizing the work rate as indicated in Chapter 4. It is clear that as the ram velocity increases the strain rate across each of the shear zones increases and that, in the limit, the yield shear stress for each discontinuity will reach the saturation stress σ_{max}^*. The

---

* The term "saturation stress" is used in the sense of a maximum flow stress which is insensitive to strain rate.

solution then becomes as for a rigid perfectly plastic material with a constant yield shear stress.

The theoretical extrusion pressure generated using the computer optimization programs is compared with the experimental results in Figures 6.1 and 6.2. The value of the shear zone thickness ratio was 10 and the ram velocities are as indicated. In Figure 6.1, for the tin lead, the correlation is excellent at the slower ram speed of 0.012 ins/min (0.005 mm/sec). An examination of the theoretical solution generated for a ram velocity of 0.12 ins/min (0.05 mm/sec) indicated that the flow stress across each of the discontinuities was equal to the saturation stress. The strain rate across each discontinuity at the lower ram velocity, however, is only greater than $\dot{\varepsilon}_{max}$, the limiting strain rate, when the fractional reduction is greater than 0.9.

Figure 6.2 compares the theoretical and experimental values for the side extrusion of pure lead. The correlation is excellent for all ram velocities. An examination of the strain rate across each shear zone, at each ram velocity, indicated that none of the strain rates was greater than $\dot{\varepsilon}_{max}$; the solution is entirely due to the rate sensitivity of the material properties.

The side extrusion of the tin lead in the second die configuration is compared in Figure 6.3. The theoretical solutions generated for ram velocities of 0.12 and 1.2 ins/min (0.05 and 0.5 mm/sec) are identical for fractional reductions greater than 0.7. This is because the solution at a ram velocity of 1.2 ins/min ((0.5 mm/sec) is an upper bound solution for all fractional reductions since the

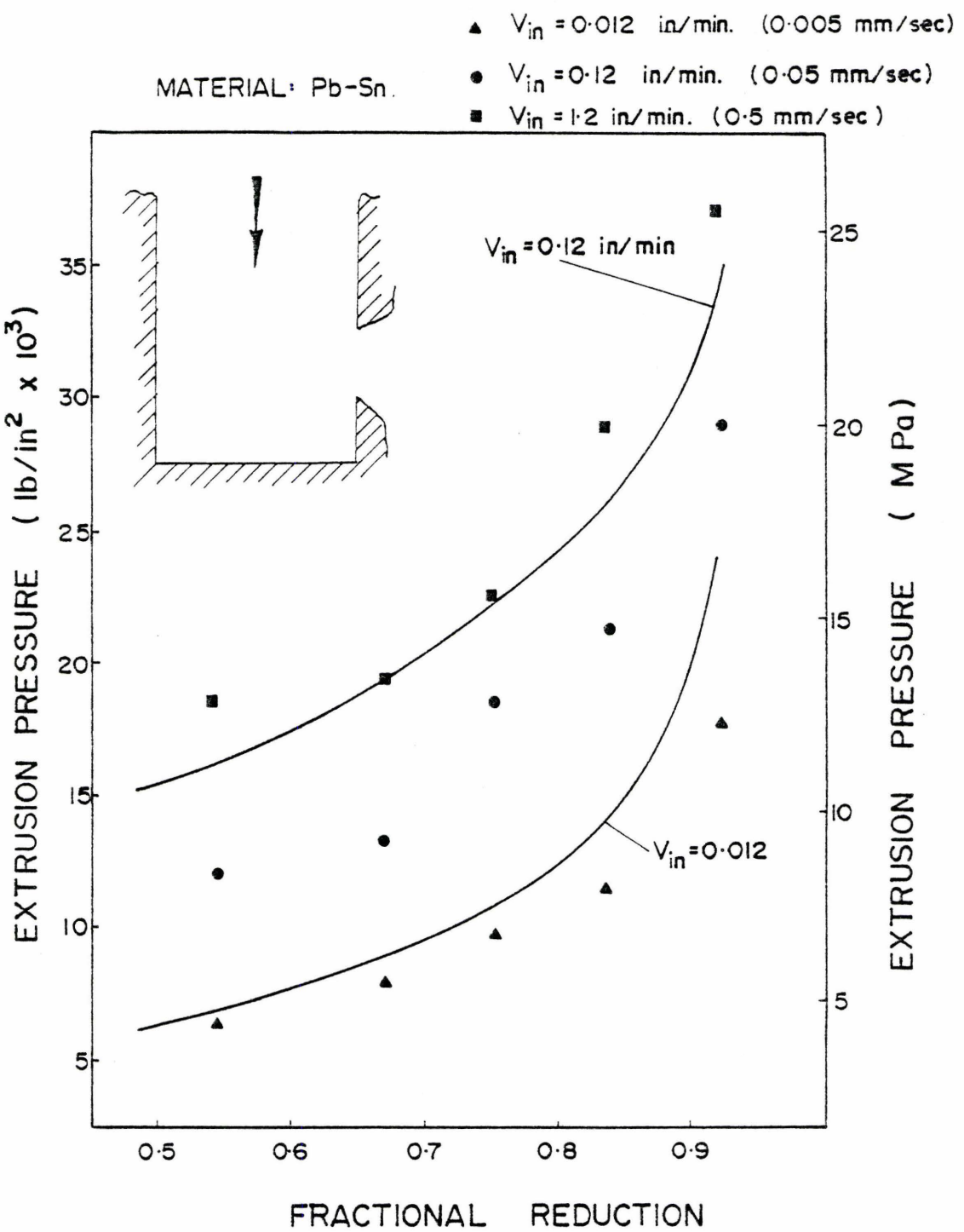

Figure 6.1

Comparison of theoretical and experimental extrusion pressures: tin lead, shear zone ratio 10

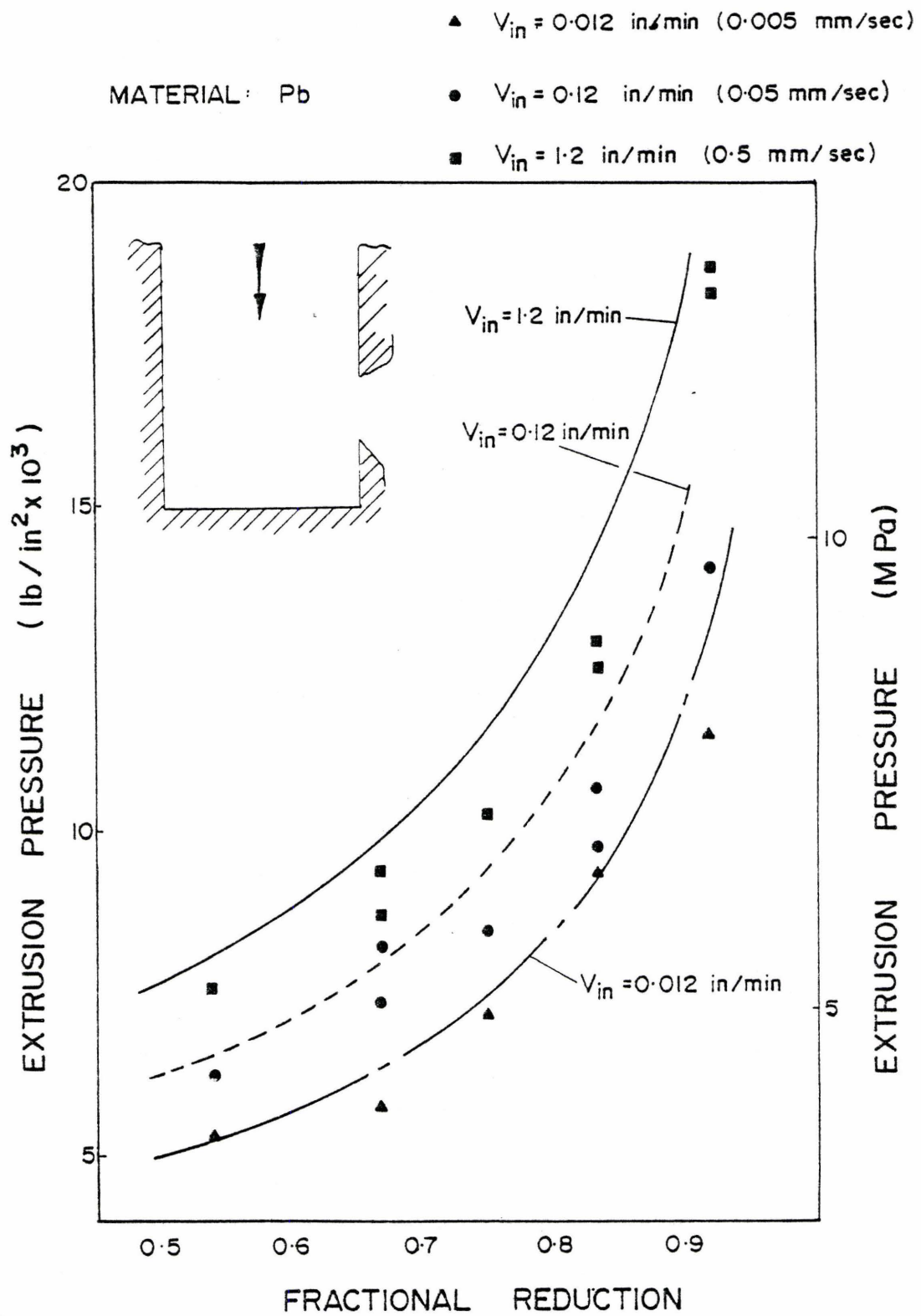

Figure 6.2

Comparison of theoretical and experimental extrusion pressures: Pure lead, shear zone ratio 10

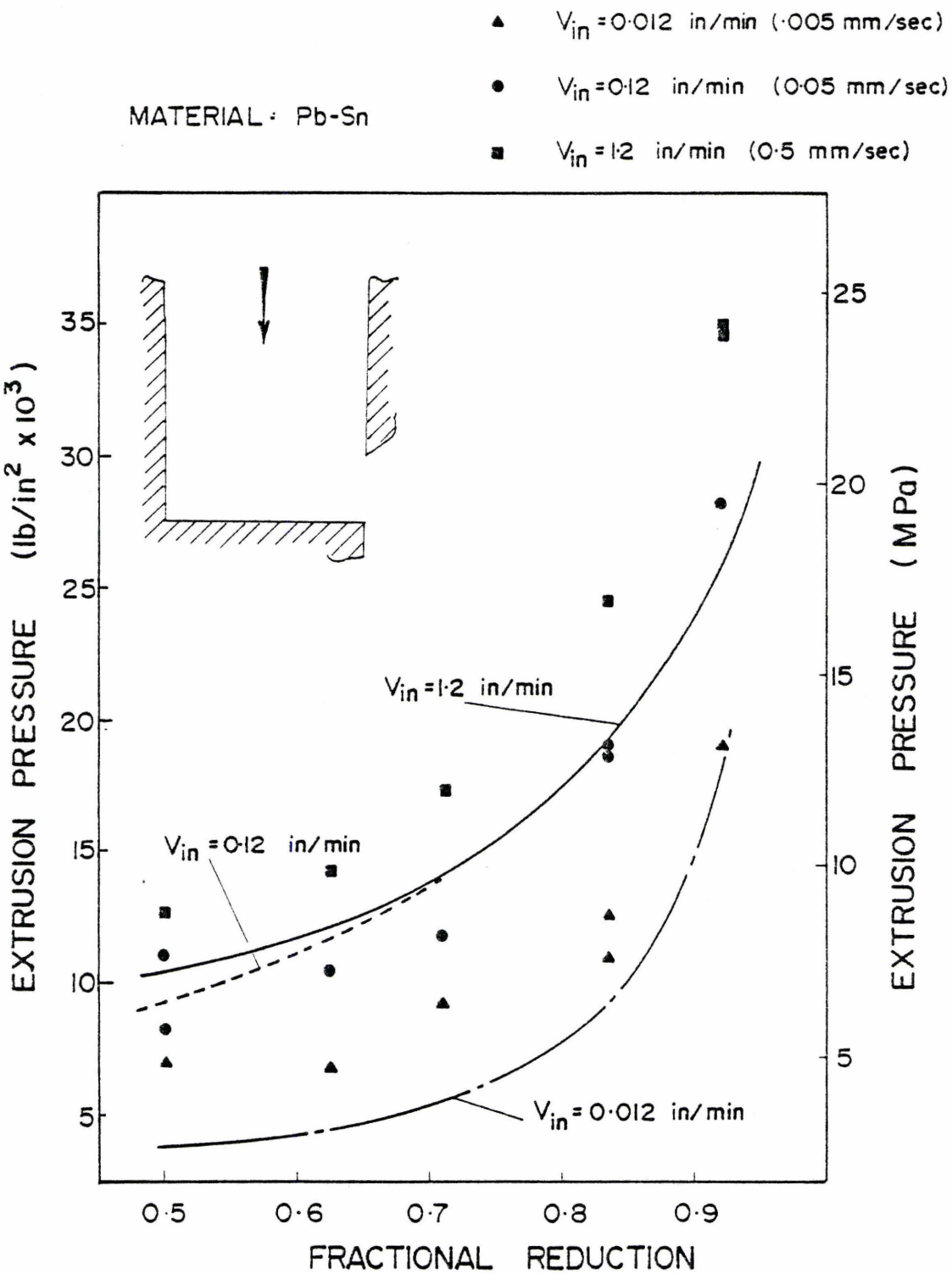

Figure 6.3

Comparison of theoretical and experimental extrusion pressures for second die configuration: tin lead, shear zone ratio 10

saturation stress $\bar{\sigma}_{max}$ has been reached in crossing every shear zone discontinuity. The solution for a ram velocity of 0.12 ins/min (0.05 mm/sec) begins, at low fractional reductions, with the flow stress associated with certain discontinuities being below the saturation stress. As the fractional reduction increases and the strain rate approaches $\dot{\varepsilon}_{max}$ then the flow stress approaches the saturation level and the solution converges to the upper bound. For a ram velocity of 0.012 in/min (0.005 mm/sec) the solution generated indicates that the strain rates across the shear zones are well below $\dot{\varepsilon}_{max}$, even at the higher fractional reductions. However, the theoretical solution underestimates the extrusion pressure by some 40% at the lower reductions.

In all the theoretical solutions generated the assumption has been made that the process is frictionless. Based on the results of comparative tests performed in the primary die geometry associated with Figure 6.1 and 6.2 this assumption is reasonable. For the second die geometry examined this assumption may not be completely valid. The material slides along the base of the container and, while there is probably adequate lubrication at the start of the experiment, it is doubtful that this is true throughout the experiment.

The optimum field geometries generated by the computer for the pure lead and tin lead eutectic is different than that for a rigid perfectly plastic material and is illustrated in Figure 6.4. Only one half of the field is shown but the variation with material properties is clearly shown.

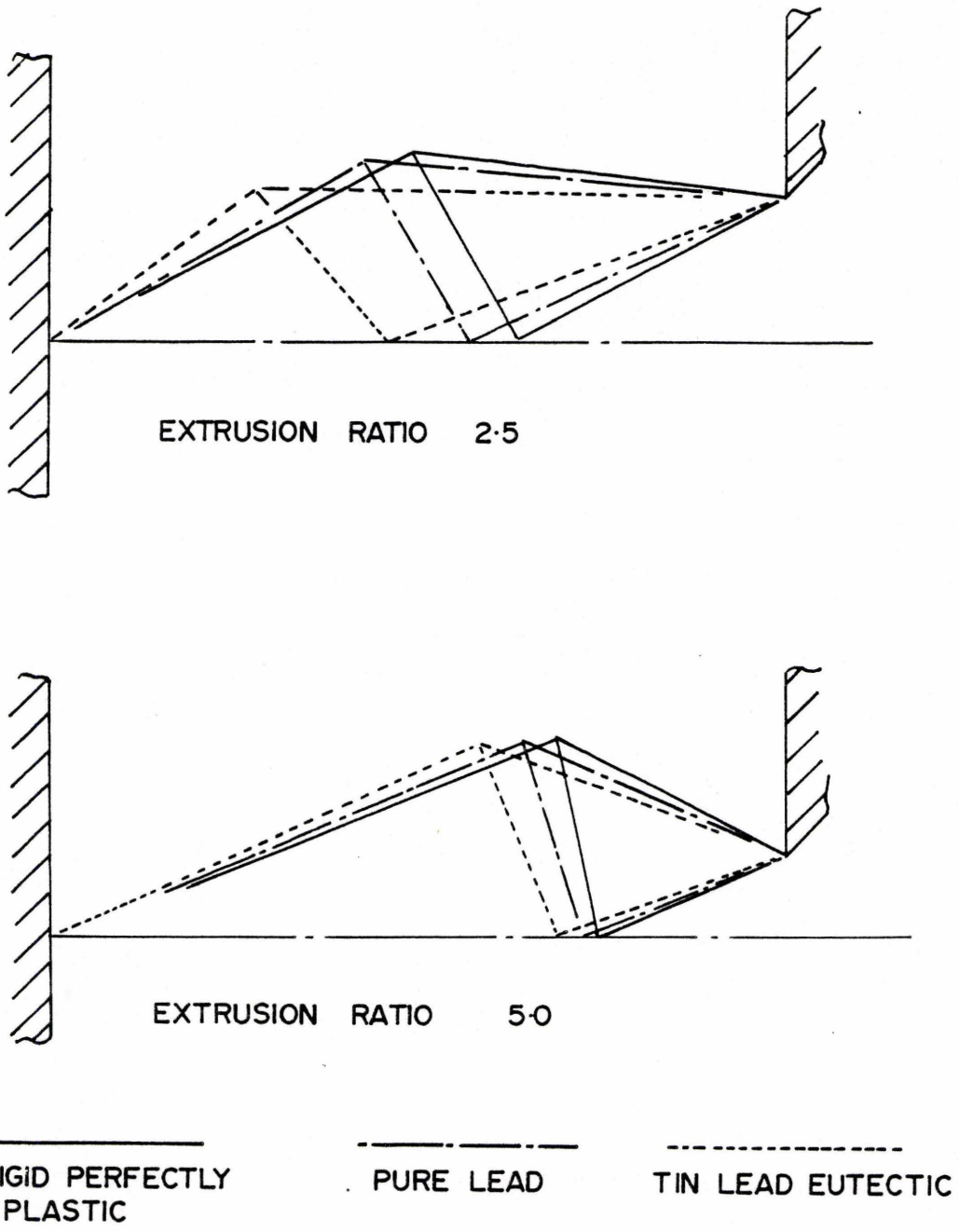

Figure 6.4

Comparision of optimum velocity fields generated by the program for pure lead, tin lead eutectic and a rigid perfectly plastic material.

6.2.1 Effect of Shear Zone Width to Length Ratio

The value of the shear zone ratio assumed in the computer programs was 10. This value was based on experimental observations of the shear zone associated with the mechanics of metal cutting. Clearly the smaller the ratio the larger the shear zone and, consequently, the lower the strain rate. The calculated extrusion pressure would also diminish as the width to length ratio increased. It is therefore necessary to assign an arbitrary value to the width to length ratio. Values for the ratio, as discussed in Chapter 4, have been shown to lie in the range of 5 → 15. Figure 6.5 illustrates the variation of the extrusion pressure when the shear zone ratio is changed. As expected, as the ratio increases the extrusion pressure increases. In the limit, for very large shear zone ratios, the solution would converge to that given by the upper bound method for rigid plastic materials.

6.2.2 Comparison with Previous Work

Experimental results have been presented by Duncan et al. [9] for the side extrusion of pure lead and tellurium lead. No details of the exit geometry were presented and it is believed that the current investigation is the first to report the curling of the extruded product. The variation of the extrusion pressure with ram speed and fractional reduction was presented and this data has been extracted from reference [9]. Figure 6.6 compares the extrusion pressures from the present test program with those reported by Duncan et al. It is clear that the extrusion pressure results for the current program do not

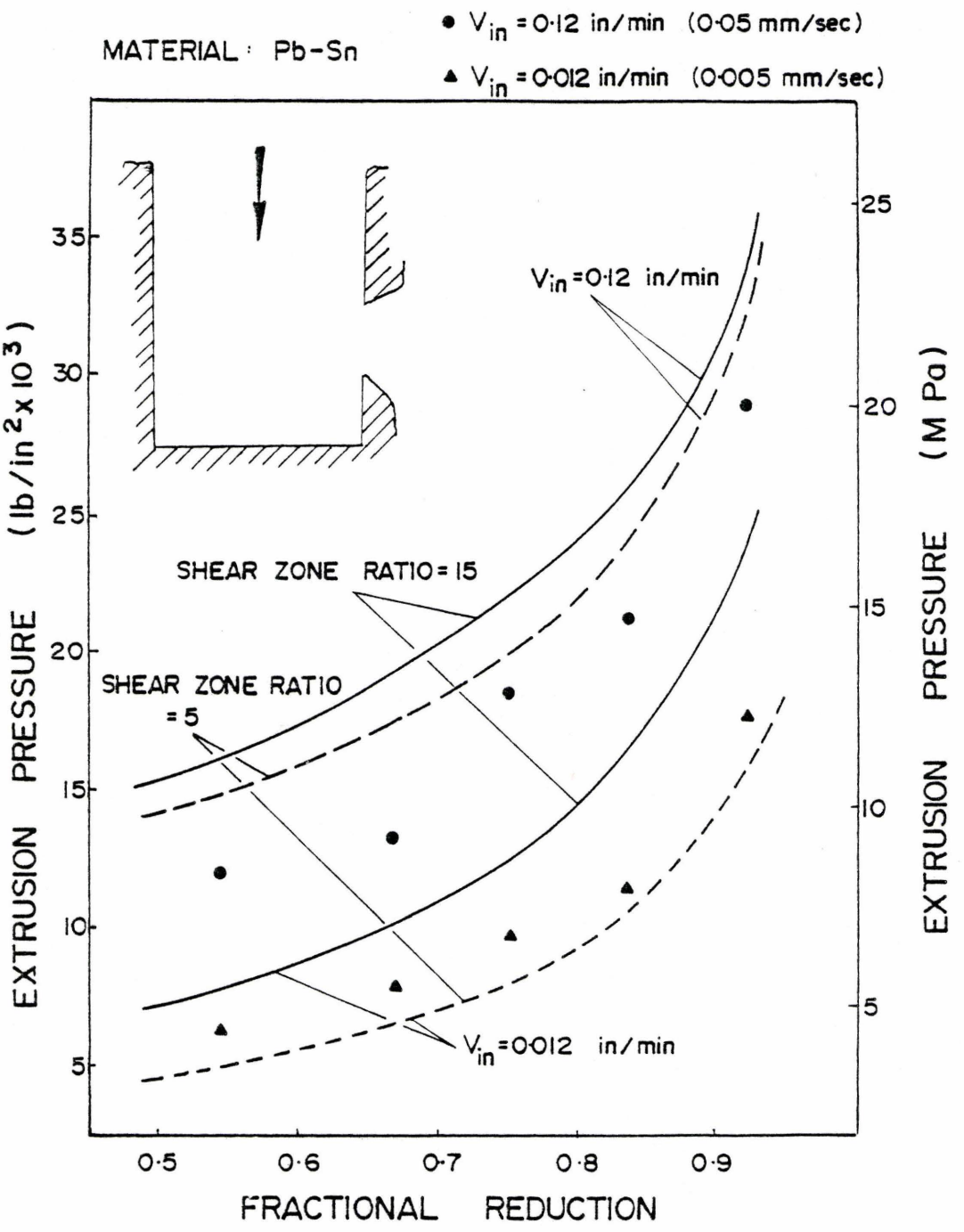

Figure 6.5

Variation of theoretical extrusion pressures with different shear zone ratios

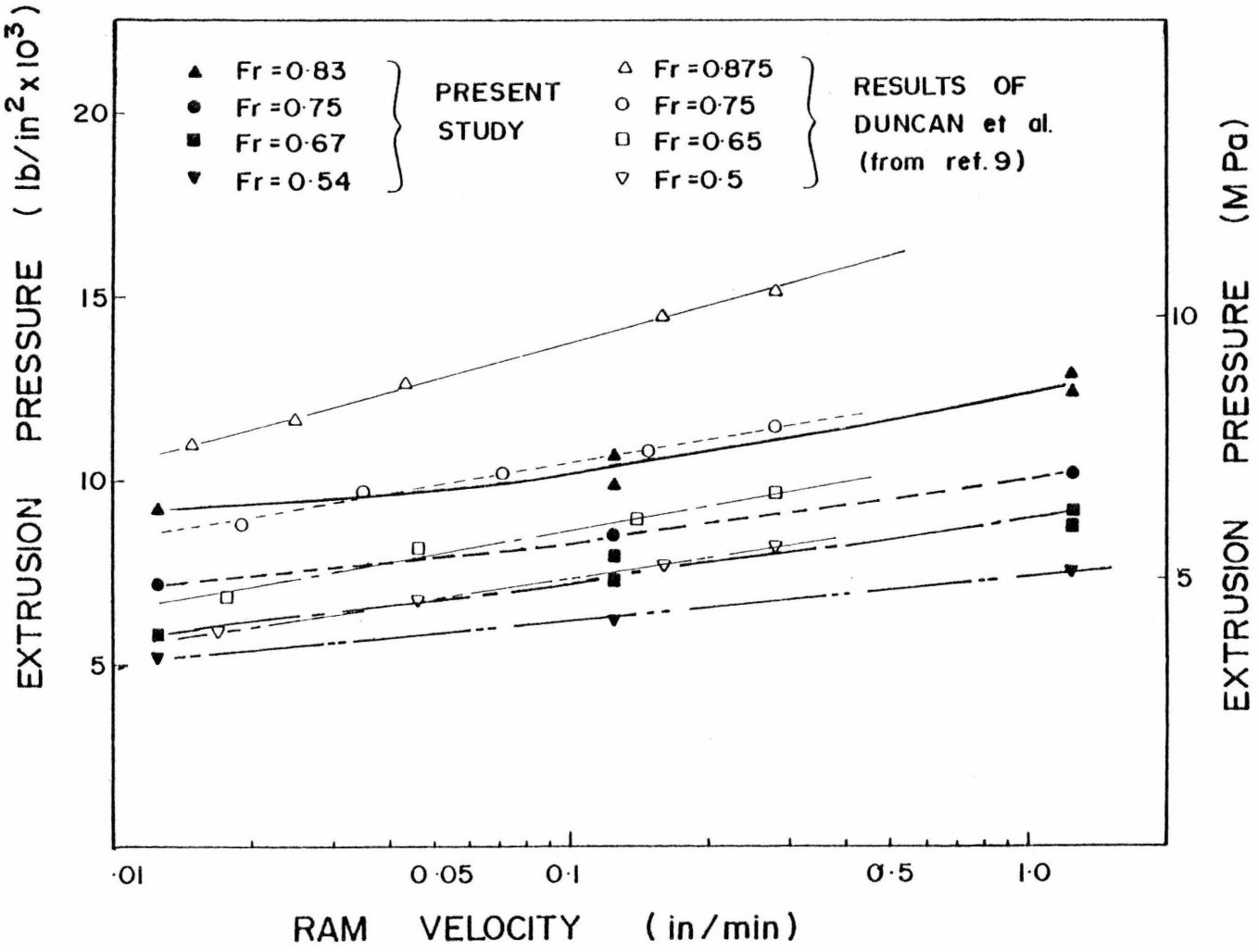

Figure 6.6

Comparison of extrusion pressure for the sideways extrusion of lead with results presented by Duncan [9]

correlate well with those of Duncan et al. which are, in all cases, higher.

An examination of the stress strain rate data for the pure lead used by Duncan indicates a flow stress similar to that for the material used in the present study. No details were given by Duncan of the die dimensions and it is difficult to postulate reasons for the poor correlation. A difference in friction conditions and die geometry could provide a possible explanation however further studies of the side extrusion process would be useful in clearly indicating the correct solution.

6.3 Exit Geoemtry: Further Considerations

The experiments performed by the author indicated that material leaves the die at a particular angle and radius of curvature. This is not predicted by any of the analyses available and has not been reported by earlier researchers. The theoretical solutions predict that the product will exit straight but inclined at some angle which is a function of the die geometry and the friction conditions.

It might be anticipated that the effects of the increasing billet temperature during the extrusion due to the plastic work may be responsible for the large difference between the experimental and theoretical results. The evaluation of the temperature distribution due to plastic work and the problems of conduction in a moving body are complex. However, certain simplifying assumptions can be made which allow the problem to be examined in an approximate fashion. The results

of computations of the maximum temperature rise and distribution during the extrusion are presented below and the literature of the effects of plastic work on the temperature distribution discussed.

Johnson [171→173] has presented a number of papers on the application of the upper bound technique with curved discontinuities. The analysis of extrusion through circular dies [173] was considered and using circular arcs, along which a constant magnitude velocity discontinuity occurs, an upper bound solution obtained. Johnson examined the case of unsymmetric end extrusion with circular dies and showed that rotation of the product is predicted. In the analyses presented below the velocity field proposed in Chapter 4 is examined and alternative fields studied which predict the rotation of the extruded product. The solution for rigid perfectly plastic materials is examined and the extrusion parameter ($\bar{p}/2k$) used for comparative purposes.

6.3.1 Effect of Temperature

The ram velocities for the experiments described in Chapter 4 were chosen for the following reasons:

a) The hydraulic press used in the experiments was capable of handling all velocities with ease.

b) The strain rate for the process would be in the strain rate regime where the material properties are rate sensitive.

c) That the process would be slow enough to be considered to be isothermal.

All the tests were conducted at room temperature, $68^{\circ}F \pm 2^{\circ}F$ ($20^{\circ}C$). No

measurements were made of the temperature of the extrudate or the billet during the extrusion process. There was, however, no discernible increase in the temperature of the billet when it was removed from the die.

The rotation of the extrudate could be explained by either of the following mechanisms.

a) the temperature rise associated with plastic deformation produces a significant temperature distribution across the exit of the die and consequently a change of material properties. The change of material properties produces the curvature of the product.

b) that the extrudate bends under the action of its own weight as it leaves the die.

The increase in temperature during the plastic deformation of a metal has been the subject of a number of theoretical and experimental papers. Bishop [174] gave an approximate numerical solution, based on the slip line field, which gave the temperature distribution for a rigid perfectly plastic material. A simplified analysis was presented by Tanner and Johnson [175] to determine an upper bound to the temperature distribution in certain fast processes. Tanner indicated that the heat conduction back into the billet can be ignored if the ram velocity is of the order of inches per second. While these values are typical of industrial extrusion presses the ram velocity in the experiments performed during the course of the current investigation are well below this value. Heat conduction away from the deformation zone will

therefore be appreciable and the method of Tanner and Johnson will overestimate the temperature rise. In the following paragraphs the temperature distribution associated with the plastic work is evaluated and an upper bound to the temperature rise for the process computed.

A tangential velocity discontinuity field is assumed and the work rate, per unit volume, in crossing any discontinuity is given by

$$w = k\, v^{*} \frac{s}{s_n} \tag{6.6}$$

where k is the yield shear stress

v^{*} is the tangential velocity change

s the length of the discontinuity

and s_n the width of the discontinuity normal to the direction of the velocity on the upstream side.

It can be shown that

$$\frac{s}{s_n} = v_n \tag{6.7}$$

where v_n is the normal component of the velocity across the discontinuity. The work rate per unit volume in crossing any discontinuity is then given by:

$$\dot{W} = k \frac{v^{*}}{v_n} \tag{6.8}$$

Farren and Taylor [176] have indicated that 90% of the energy of plastic work is converted into heat energy and eqn. (6.8) can be rewritten as

$$E_H = 0.9k \frac{v^*}{v_n} \tag{6.9}$$

where E_H is the energy which is converted into heat energy.

The energy input to raise the temperature of unit volume of material is given by

$$Q = \rho\, c\, \Delta T \tag{6.10}$$

where ρ is the density

c is the specific heat

and ΔT is the temperature change.

Equating eqns. (6.9) and (6.10) and including the conversion of mechanical energy to heat energy we obtain

$$\Delta T = \frac{0.9\, k\, v^*}{J\, \rho c\, u_n} \tag{6.11}$$

or

$$\Delta T = A \frac{v^*}{v_n} \tag{6.12}$$

where A is a constant for different materials. For the lead and tin lead the values of A are 28.4 and 33.7 respectively where v^* and v_n are in inchs/unit time and ΔT is in ^{o}F.

Solutions have been determined using the optimum field geometry, given in Chapter 4, for velocity field model #2. The results are presented in Figures 6.7 and 6.8 for the side extrusion of tin lead and lead at two different extrusion ratios. Figure 6.9 presents the

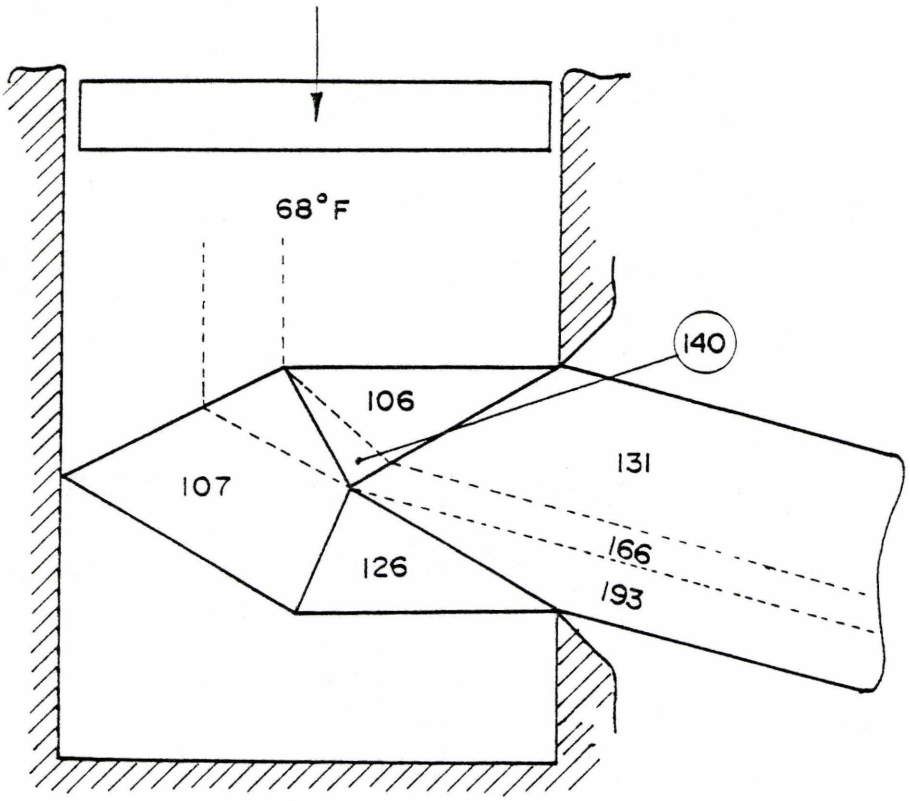

EXTRUSION RATIO = 2

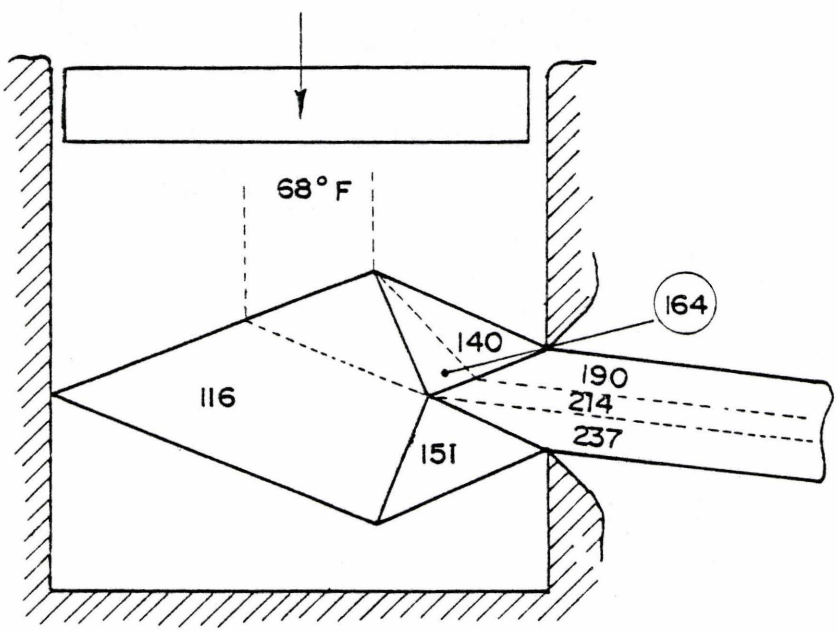

EXTRUSION RATIO = 5

Figure 6.7

Temperature distribution through the deformation zone for the fast extrusion of tin lead

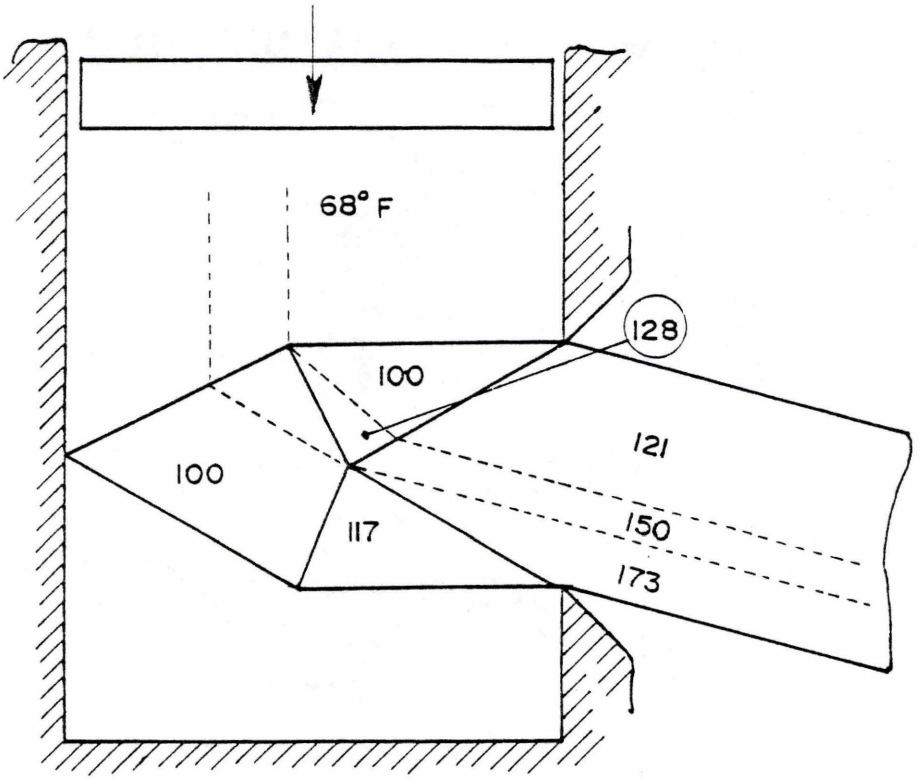

EXTRUSION RATIO = 2

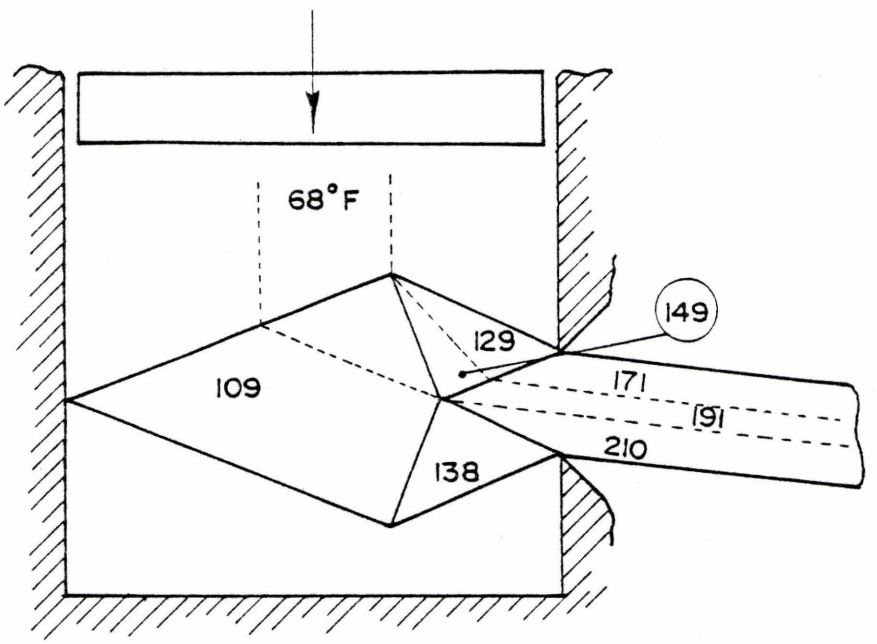

EXTRUSION RATIO = 5

Figure 6.8

Temperature distribution through the deformation zone for tne fast extrusion of pure lead

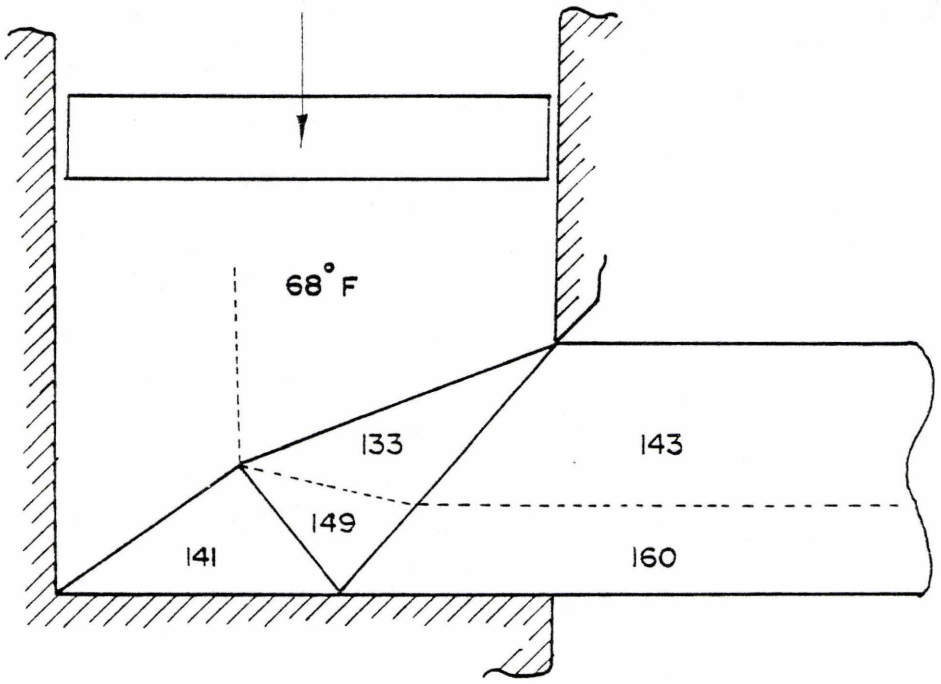

EXTRUSION RATIO - 2

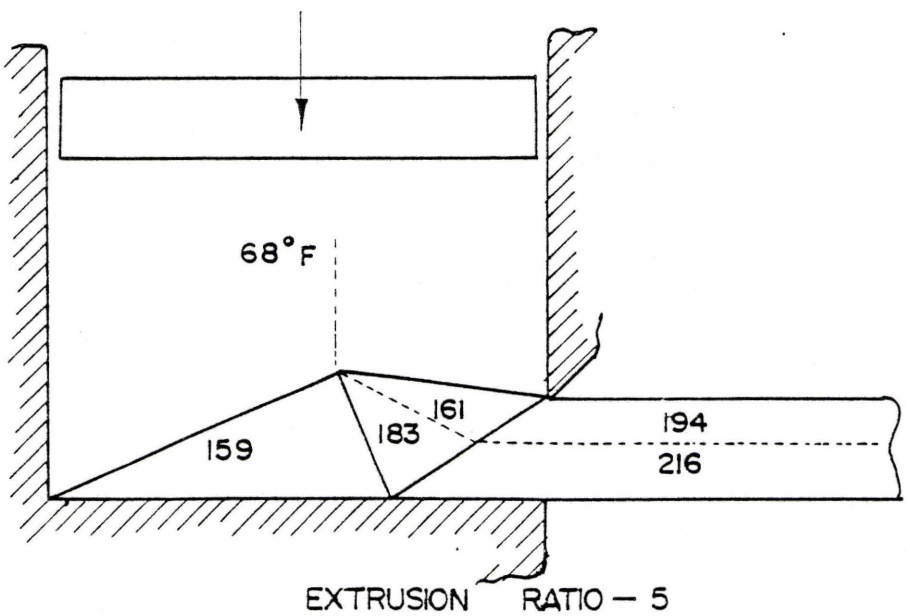

EXTRUSION RATIO — 5

Figure 6.9

Temperature distribution through the deformation zone for the fast extrusion of tin lead in the second die configuration

temperature distribution for the extrusion of tin lead with the second die geometry.

The temperature rise is significant and the effect on the material properties would be important if experiments were conducted at ram speeds greater than 1 inch/sec (25.4 mm/sec). The temperature distribution across the exit of the die would indicate that the extruding material would bend towards the direction of the ram travel; that is, similar to the experimental results for lead. Experiments performed by Bailey and Singer [101] to determine the stress strain rate properties of lead and aluminium at various temperatures indicate that the flow stress is reduced by approximately 50% if the specimen temperature varies from $72^{o}F$ ($22^{o}C$) to $230^{o}F$ ($110^{o}C$).

An upper bound to the temperature distribution has been evaluated for completeness to indicate the nature of the distribution across the product as the process continues. Experimentally the ram velocities used during the current investigation were in the range

$$0.0002 < V < 0.02 \text{ ins/sec}$$

$$0.05 < V < 5.0 \text{ mm/sec}$$

and this is far below the value of 1 inch/sec (25.4 mm/sec) necessary for the back conduction into the billet to be ignored.

The temperature rise during extrusion has been investigated experimentally by a number of researchers. Pugh and Watkins [47] examined the temperature just ahead of the punch for the extrusion of aluminium and showed that, for an extrusion ratio of 7 and a ram speed of 0.4 inch/min (0.17 mm/sec), the temperature rise was approximately

27°F (15°C) during the course of the extrusion. Singer and Coakham [177] examined the rise of the emergent temperature for the extrusion of aluminium, tin and lead. The results for lead at an extrusion ratio of 16 and a ram speed of 1 inch/min (0.42 mm/sec) indicated that the temperature increased to a steady state working temperature. The steady process temperature was approximately 90°F (32.2°C), a rise of 18°F (10°C) from the initial billet temperature.

6.3.2 Summary

The effect of plastic deformation on the increase of the temperature of the billet has been examined briefly. It is clear that for high ram velocities the variation of the material properties with temperature is important and must be considered in the analysis. Figures were presented, based on an upper bound solution due to Tanner and Johnson which indicated the temperature distribution through the velocity field and in the extruded product if heat conduction were ignored. This situation must represent an upper bound to the temperature distribution attainable.

The ram speeds used in the present investigation are far below those necessary for the heat conduction problem to be ignored. Heat generated due to the plastic work will be conducted away from the deformation zone and absorbed by the surrounding die. The rise in temperature of the billet was not detectable. An examination of the experimental evidence reported in the literature indicated that, for speeds above the maximum speed used in the present study, the rise in

temperature of the billet was approximately 27°F (15°C). Consequently the assumption that the tests can be considered to be isothermal would appear to be reasonable.

6.3.3 Rotation of the Product

In the following sections a number of velocity fields will be examined in an attempt to describe the rotation of the product observed experimentally. The simple fields presented are examined only as examples which predict the rotation of the product. They are not considered to be representative of the actual deformation mode.

6.3.4 Simple Two Line Discontinuity Velocity Field

The simplest discontinuity model which one could imagine for the side-extrusion process is shown in Figure 6.10. We do not assume that the field is symmetrical but is defined by the angle ϕ which will give the minimum work rate. The solution for the minimum work can be determined explicitly from the geometry of the physical plane diagram and hodograph; the derivation is presented in Appendix 5. The exit angle is given by

$$\phi = \tan^{-1} \left\{ \frac{2D}{d} \right\} \qquad (6.3)$$

The variation of the exit angle and the extrusion parameter, $\bar{p}/2k$, with fractional reduction is given in Table 6.1.

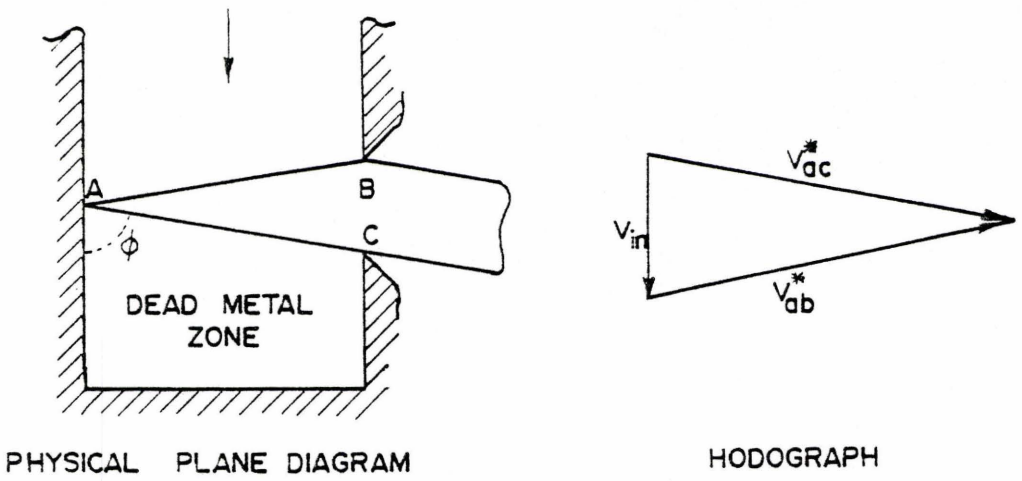

Figure 6.10

Simple two line discontinuity model -
straight discontinuities

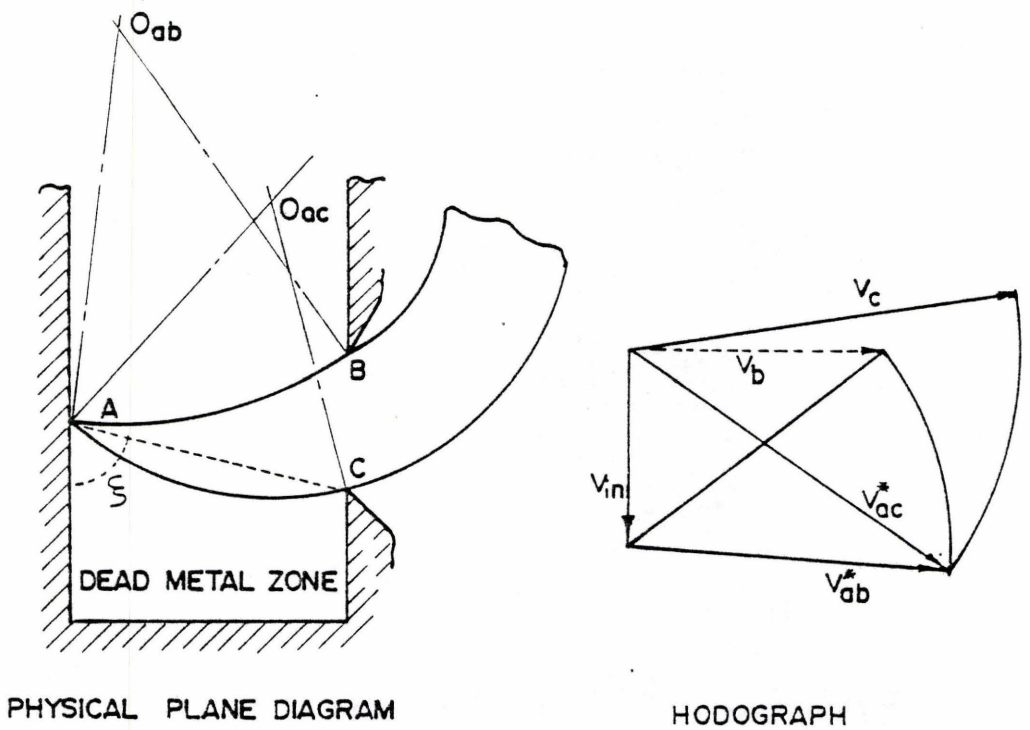

Figure 6.11

Simple two line discontinuity model -
curved discontinuities

Fractional reduction	0.5	0.75	0.833	0.875	0.9	0.95
Exit angle, deg.	104	97.1	94.8	93.6	92.9	91.4
Extrusion parameter ($\bar{p}/2k$)	2.13	4.07	6.04	8.03	10.3	20.01

Table 6.1

Variation of exit angle and extrusion parameter with fractional reduction for simple two line discontinuity model

6.3.5 Simple Two Line Model: Curved Discontinuities

Consider that the discontinuities AB and AC are circular arcs as shown in Figure 6.11, and that the product rotates with the same radius of curvature as the discontinuity AC. The point of intersection of the discontinuity AC with the wall is defined by the angle ξ. The geometry of the field for a given extrusion ratio is a function of two variables, the angle ξ and the radius of curvature of the discontinuity AC. The algebraic expressions for the arc lengths and the velocity discontinuities are given in Appendix 6. The solution for the exit angle and extrusion parameter obtained by minimizing the work equation by trial and error is given in Table 6.2.

Fractional Reduction	0.5	0.67	0.75	0.833	0.92	0.95
Exit angle deg.	102.9	99.6	96.9	94.7	92.1	91.4
Radius of curvature of product	7.5	10.0	14.0	18.5	47.5	67.0
Extrusion parameter ($\bar{p}/2k$)	2.14	3.0	4.07	6.05	12.02	20.01

Table 6.2

Variation of exit angle, extrusion parameter and exit radius of curvature with fractional reduction for simple velocity field with two curved discontinuities.

Comparative figures have been drawn for the two models indicated and are shown in Figure 6.12 for the exit angle and Figure 6.13 for the extrusion parameter. The solution for the extrusion pressure for the curved discontinuities is identical to that for the straight discontinuities. However it is larger than that given by the models presented in Chapter 4.

The purpose of this examination has been to illustrate that straight discontinuities can be replaced by ones which are circular and constitute discontinuities of constant velocity change without changing the solution for the work rate.

6.4 The Shape of Velocity Discontinuities to give a Uniform Flow Field an Angular Rotation

In the preceeding sections a circular arc of discontinuity was assumed and this has been "tacitly assumed" previously by Johnson [173]. In the analysis presented below we examine a uniform flow field as shown in Figure 6.14. Material to the right of AB is moving with velocity V while that to the left of AB is rotating about an instantaneous centre I_c with an angular rotation of ω. The detailed geometries of the physical plane diagram and hodograph are shown in Figure 6.15. The co-ordinate system is centred at A on the discontinuity ABC... The centre of rotation I_c has co-ordinates $(X_c;Y_c)$. We consider a small element at radius R_x. The flow rate across BC is constant and is given by

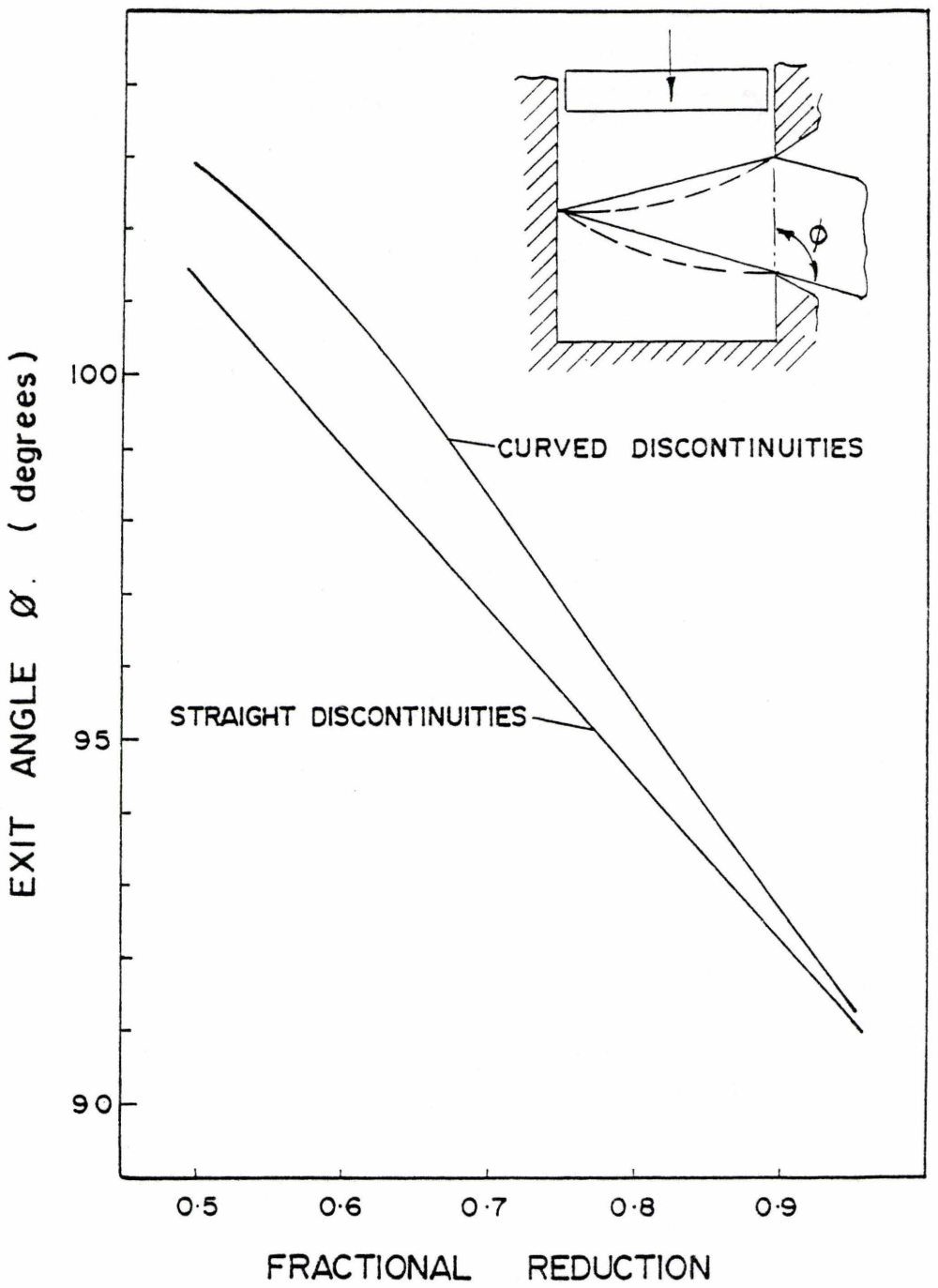

Figure 6.12

Variation of predicted exit angle for the two models suggested

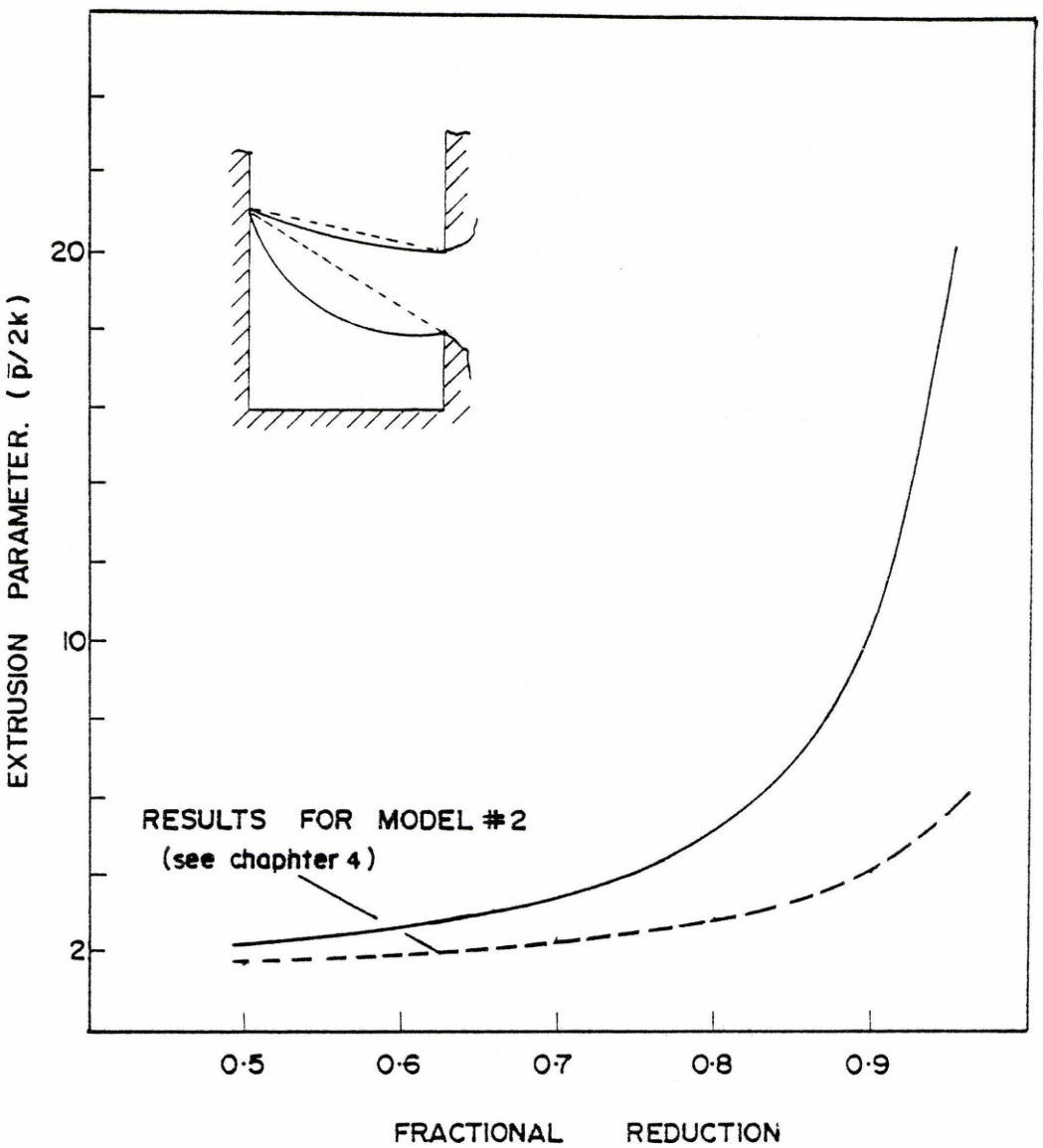

Figure 6.13

Comparison of the extrusion parameter with fractional reduction predicted by the two models

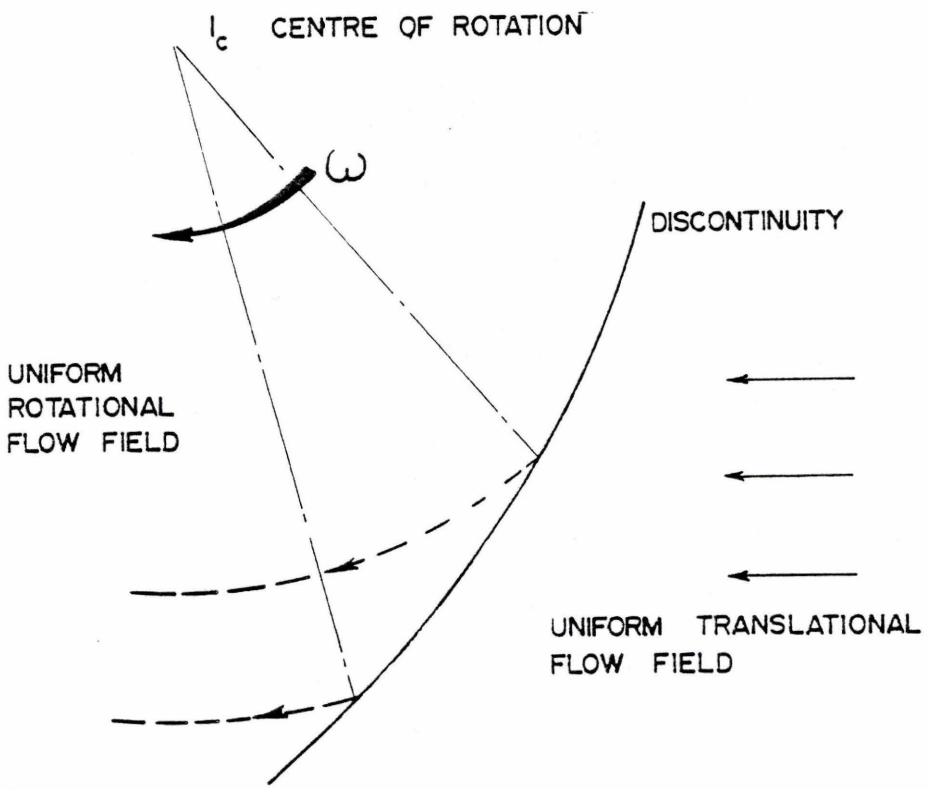

Figure 6.14

Schematic of a uniform translational flow field crossing a discontinuity AB into a uniform rotational flow field

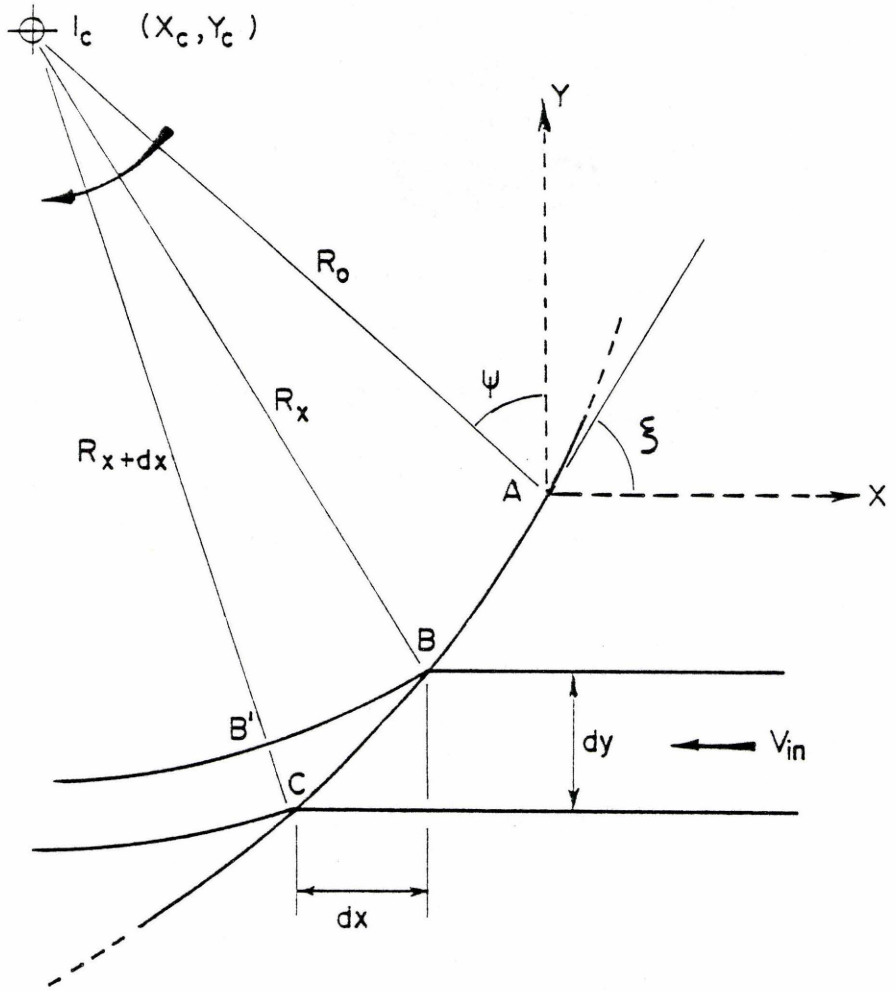

PHYSICAL PLANE DIAGRAM

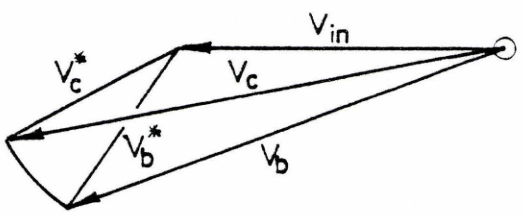

HODOGRAPH

Figure 6.15

Detailed geometry of physical plane diagram for transition from uniform translational flow field to a uniform rotational flow field

$$\dot{Q}_{BC} = V_{in}\, dy \tag{6.13}$$

At B'C the flow rate is given by

$$\dot{Q}_{B'C} = \frac{\omega}{2} [R^2_{x+dx} - R^2_x] \tag{6.14}$$

Equating 6.13 and 6.14 we obtain

$$V_{in}\, dy = \frac{\omega}{2} [R^2_{x+dx} - R^2_x] \tag{6.15}$$

The radius at C is given by:

$$R^2_{x+dx} = (X_c - X - dx)^2 + (Y_c + Y + dy)^2 \tag{6.16}$$

The radius at B is given by:

$$R^2_x = (X_c - X)^2 + (Y_c - Y)^2 \tag{6.17}$$

Substituting Eqns. (6.17) and (6.16) into (6.15) and simplifying gives:

$$\frac{2V_{in}dy}{\omega} = 2Y_c dy + 2Ydy + 2Xdx - 2X_c dx \tag{6.18}$$

Integrating Eqn. (6.18) we obtain

$$\frac{2V_{in}}{\omega} Y = 2Y_c Y + Y^2 + X^2 - 2X_c X + A \tag{6.19}$$

but at X=0 Y=0 therefore A=0

Rewriting Eqn. (6.19)

$$X^2 + Y^2 + 2Y\, Y_c - \{\frac{V_{in}}{\omega}\} - 2X_c X = 0 \tag{6.20}$$

Equation (6.20) is the equation of the discontinuity ABC... Manipulation of Eqn. (6.20) gives

$$[Y - \{\frac{V_{in}}{\omega} - Y_c\}]^2 + (X - X_c)^2 = \{\frac{V_{in}}{\omega} - Y_c\}^2 + X_c^2 \qquad (6.21)$$

which is the equation of a circle; recall that

$$(X - X_o)^2 + (Y - Y_o)^2 = R^2$$

where the centre is at X_oY_o and the radius is R.

Therefore, the discontinuity is a circular arc of radius

$$R = [\{\frac{V_{in}}{\omega} - Y_c\}^2 + X_c^2]^{1/2} \qquad (6.22)$$

and the centre of this arc is at

$$X = X_c \quad \text{and} \quad Y = \frac{V_{in}}{\omega} - Y_c \qquad (6.23)$$

Rewriting Eqn. (6.22) with the original variables defined in Figure 6.15

$$R = [\{\frac{V_{in}}{\omega} - R_o \, Cos\psi\}^2 + (R_o \, Sin\psi)^2]^{1/2} \qquad (6.24)$$

The center is inclined at an angle θ where

$$\tan\theta = \frac{R_o \, Sin\psi}{(V_{in}/\omega) - R_o \, Cos\psi} \qquad (6.25)$$

but $\theta = \xi$

therefore

$$\frac{V_{in}}{\omega} = R_o \, Cos\psi + \frac{R_o \, Sin\psi}{Tan\xi} \qquad (6.26)$$

Substituting Eqn. (6.26) into (6.24) gives the radius of the discontinuity as

$$R = R_o \, \mathrm{Sin}\psi \left[1 + \frac{1}{\mathrm{Tan}\xi}\right]^{1/2} \qquad (6.27)$$

6.4.1 Summary

We have examined the case of a uniform translational flow field crossing some discontinuity into a uniform rotational flow field with a constant angular velocity. It has been shown that the shape of this discontinuity must be a circular arc and that, for a given initial geometry, the radius of curvature of the discontinuity is given by Eqn. (6.27).

6.5 Application of Circular Discontinuities to Upper Bound Solutions

The application of a 'mixed' solution of circular and straight discontinuities to the side extrusion process is indicated below. No values for the extrusion pressure or work rate have been generated; however it is anticipated that optimum solutions can be obtained which will not give pressures higher than an equivalent straight line model as shown in section 6.3. The drawing of the physical plane diagram and hodograph is not immediately clear and is explained in detail for a single case of side extrusion.

6.5.1 Method of Solution - Side Extrusion

The physical plane diagram and hodograph for side extrusion at an extrusion ratio of 2 are shown in Figure 6.16. The steps in obtaining

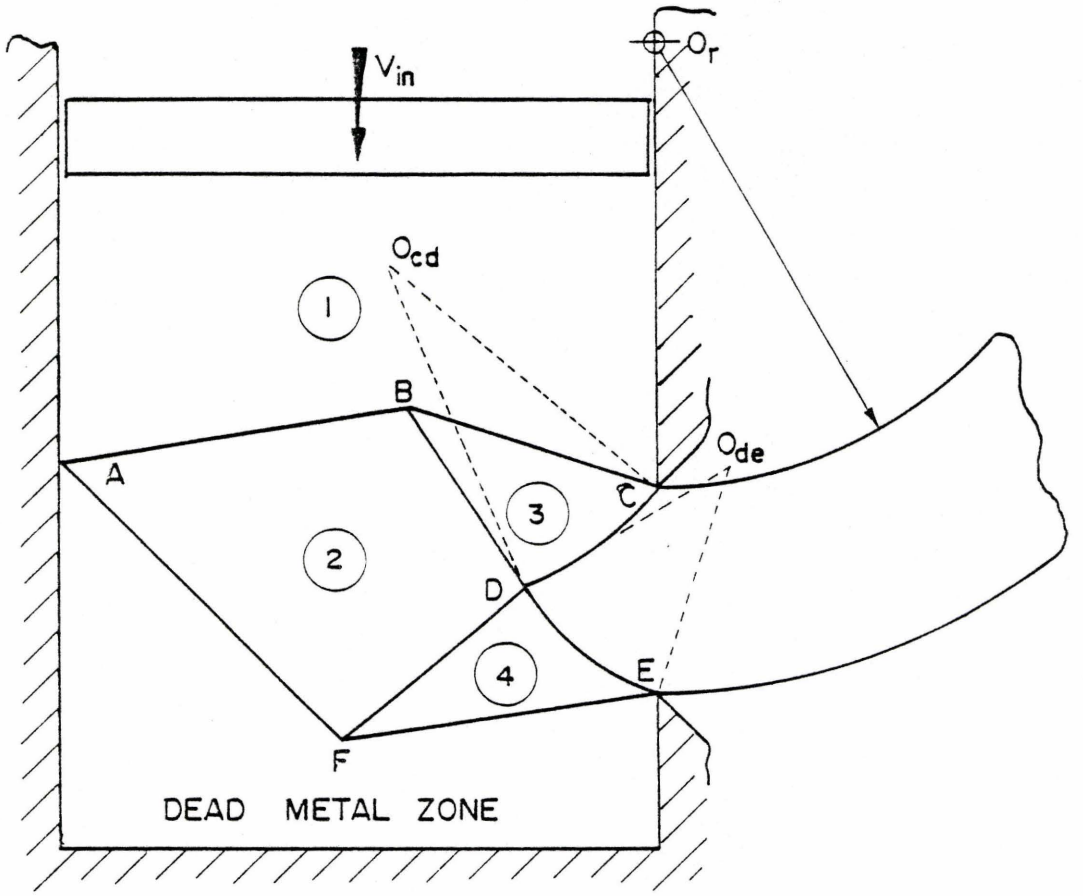

PHYSICAL PLANE DIAGRAM

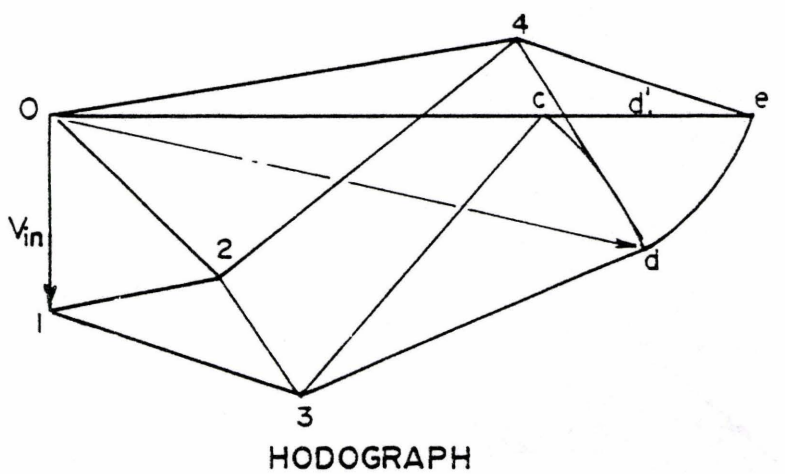

HODOGRAPH

Figure 6.16

Tangential velocity discontinuity field for side extrusion which predicts rotation of the product

this diagram are outlined below.

1) Draw physical diagram showing die geometry.

2) Choose the position of O_r the centre of curvature of the product in line with the aperture.

3) Choose the position of B and D in the physical plane.

4) Draw the ram velocity 01 in the hodograph and the exit velocity directions ocd'e perpendicular to OCD'E.

5) Draw Ocde in the hodograph similar to O_rCDE in the physical plane diagram.

6) Construct a line parallel to BC in the hodograph through 1.

7) Construct bisector of cd in the hodograph to intersect line drawn in step 6 to obtain point 3. The lines c3 and d3 in the hodograph define the radius of curvature of the arc CD in the physical plane diagram since $DO_{cd}C$ and c3d are similar.

8) Choose point F.

9) Construct line perpendicular to EF which passes through the centre of rotation O_r.

10) Construct the perpendicular bisector of DE. The intercept of this line with that drawn in step 9 determines the centre O_{de} of the arc DE.

11) Point 4 in the hodograph can now be determined by constructing triangle e4d similar to triangle $EO_{ed}D$.

12) Lines 42 and 32 are constructed in the hodograph parallel to DF and BD respectively to determine point 2.

13) The position of A in the physical plane diagram is now

defined by constructing AB and AF parallel to 12 and 02 respectively.

The construction steps above will give a valid velocity field based on the arbitrary choice of points B D and F and the centre of rotation O_r.

In the paragraphs above the method of solution for the sidways extrusion has been discussed. The new type of mixed field comprised of straight and circular discontinuities predicts the rotation of the product. In the following sections a number of velocity fields for common metalworking process will be presented. No evaluation of the extrusion pressure or optimization of these fields will be given.

6.5.2 Side Extrusion - Downward Rotation of the Product

The downward rotation of the extrudate in the side extrusion process is predicted by the velocity field shown in Figure 6.17. The centre of rotation is below, but in line with, the aperture CE. The points BDF and the centre of curvature O_r are assumed and the point A determined by constructing the hodograph and physical plane diagram simultaneously as indicated previously.

6.5.3 Side Extrusion - Centre of Rotation Not in Line with Aperture

The case of side extrusion with the upward rotation of the product when the centre of rotation is not in line with the aperture is shown in Figure 6.18. The centre of rotation O_r and the points BD and F are assumed and the hodograph and physical plane diagrams completed to give the position of A. A similar field can also be generated for the

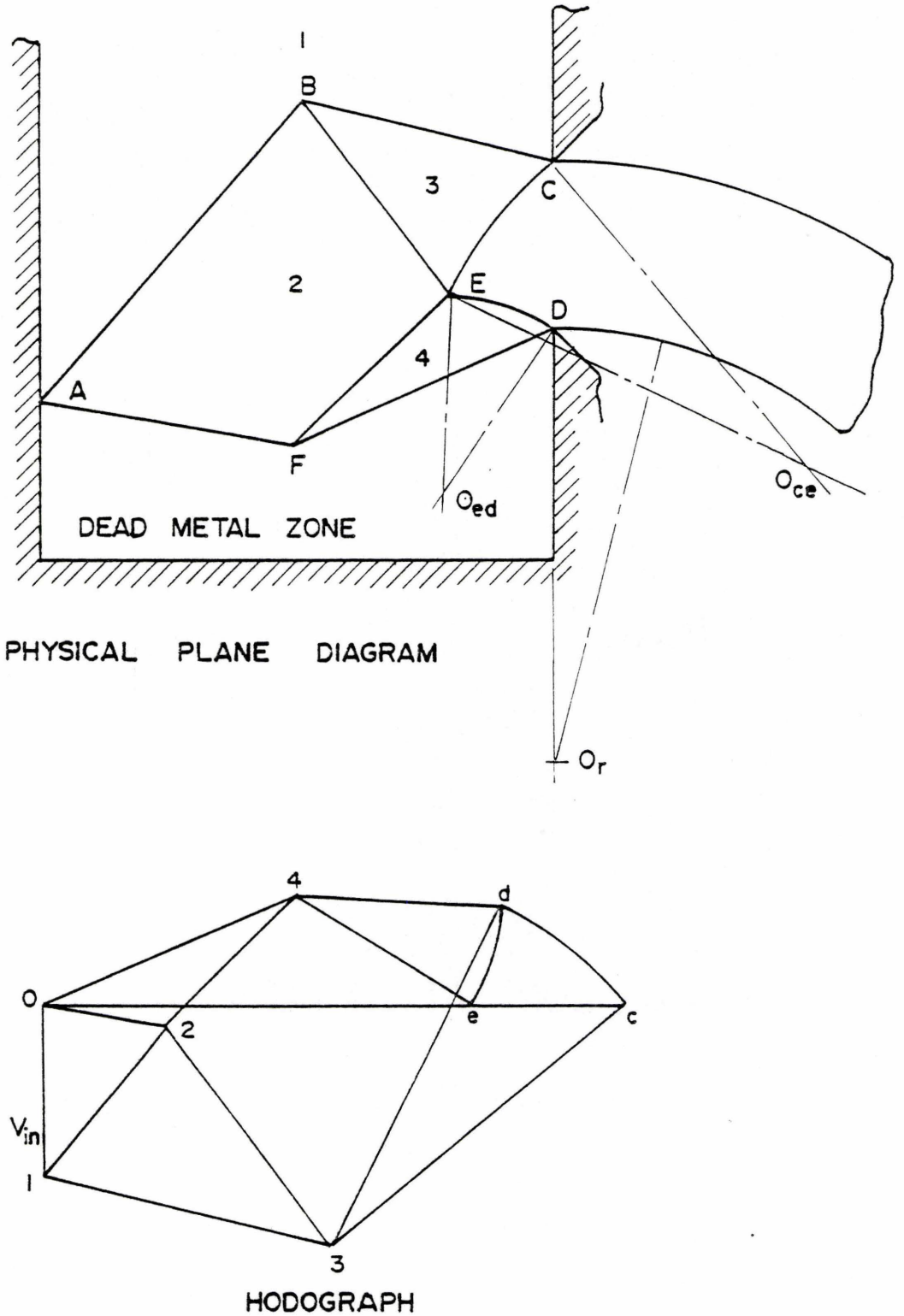

Figure 6.17

Velocity field for sideways extrusion - downward rotation of the product

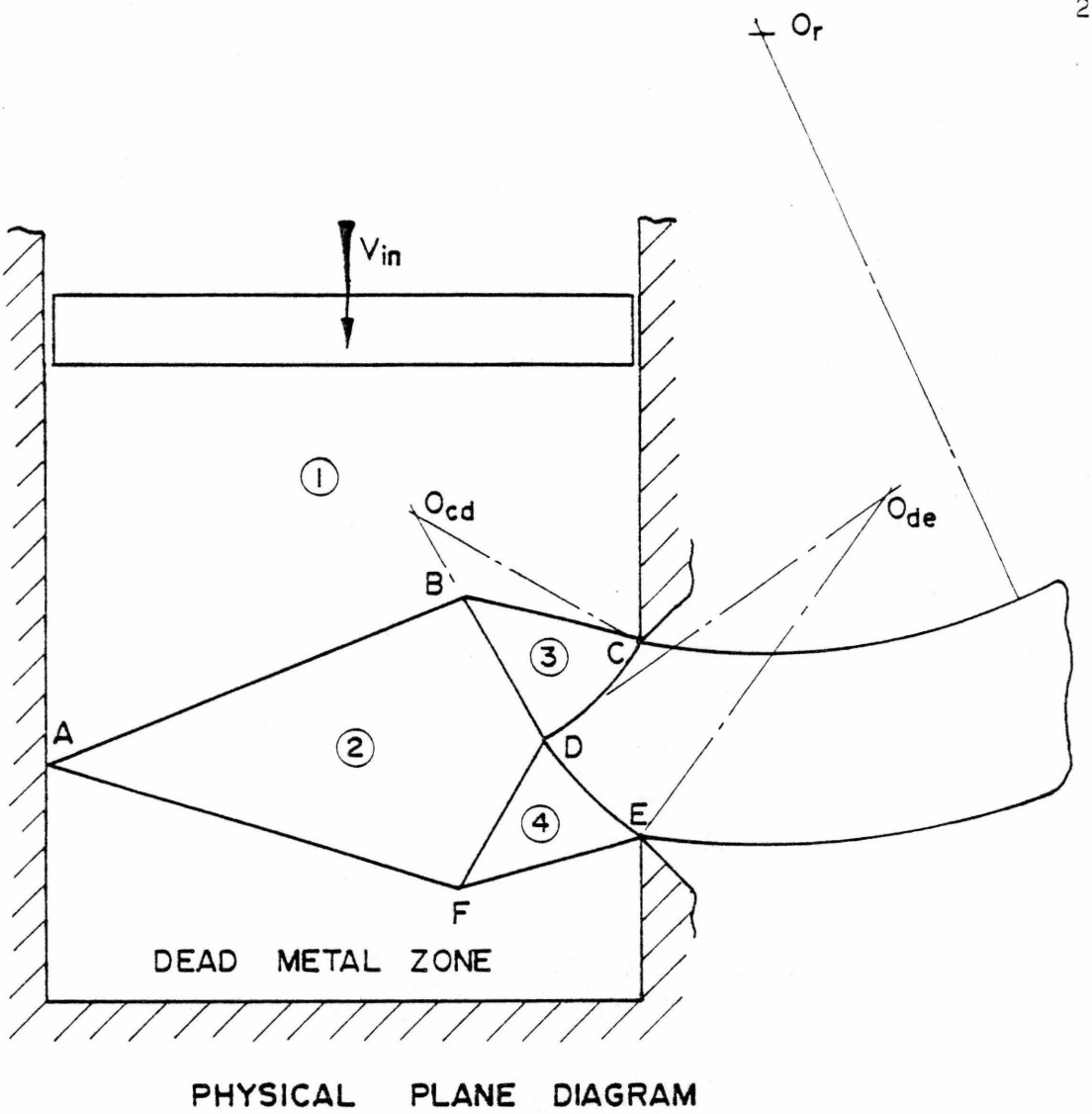

PHYSICAL PLANE DIAGRAM

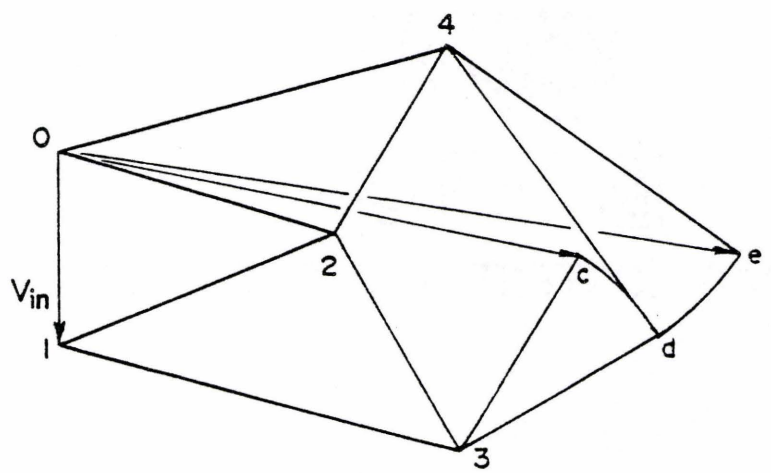

HODOGRAPH

Figure 6.18

Velocity field for sideways extrusion - centre of rotation not in line with aperture

downward rotation of the product.

6.5.4 Side Extrusion - Bottom of Die in Line with Aperture

The sideways extrusion case when the bottom of the die is at the aperture is a special case of the velocity field indicated previously. The discontinuity EF, Figure 6.19, is assumed to lie along the bottom of the die and a dead metal zone exists in the back corner as shown. The points BDF and the centre of curvature O_r, are assumed and the hodograph and physical plane diagram completed. The point A is defined in the hodograph and can be translated from the hodograph to the physical plane diagram.

6.5.5 Symmetric End Extrusion

Velocity fields and hodographs for direct symmetric end extrusion are presented in Figures 6.20 and 6.21 for the upward rotation of the product. While it is not common to propose rotation of the product in the modeling of the symmetric case the rotation in the unsymmetric case has been considered, as shown in Figure 3.4. In actual extrusion it is well known that even with symmetric tooling the extruded bar does not necessarily emerge straight. In many cases equipment must be provided to straighten the bar after extrusion. It is possible therefore that a mode, such as in Figure 6.20 could exist in practice. A simple velocity field and hodograph which predicts rotation of the extrudate is shown in Figure 6.20. The point A is assumed and this defines the centre of rotation of the product O_r and the postion of C. The point E can be

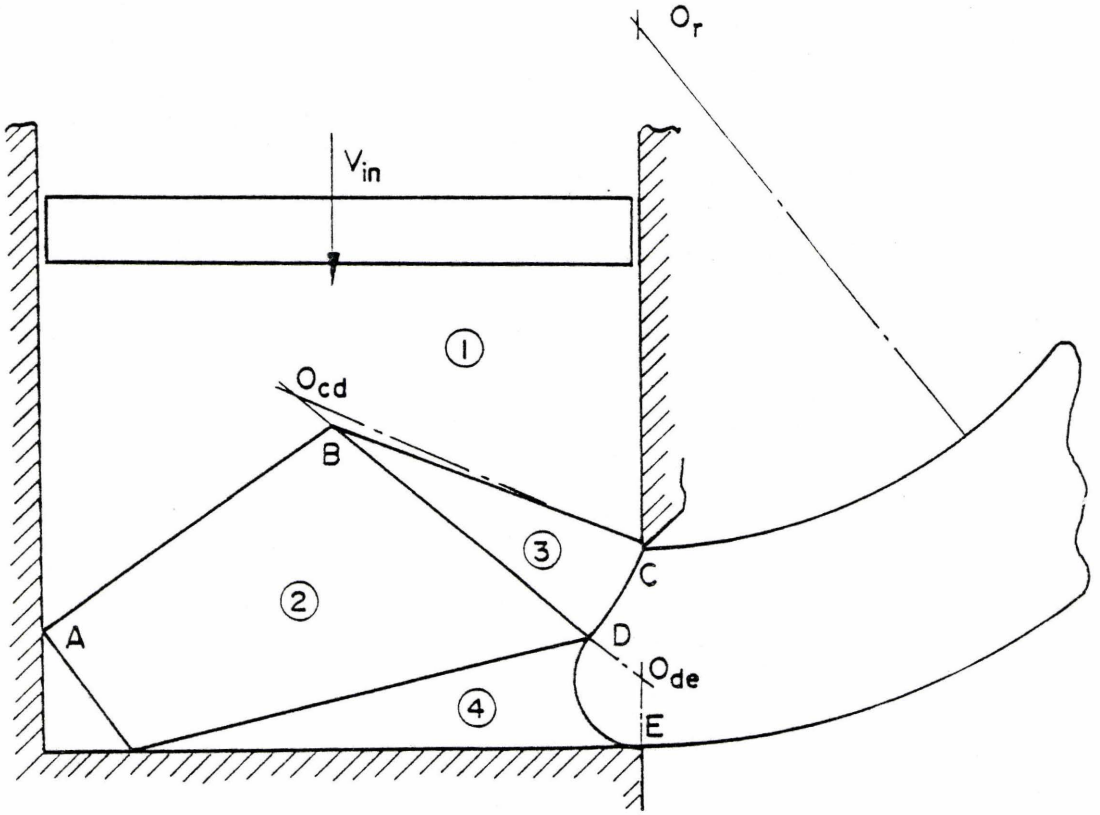

PHYSICAL PLANE DIAGRAM

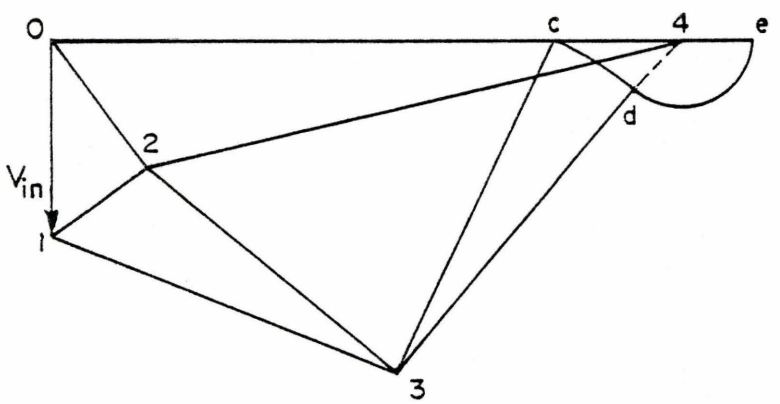

HODOGRAPH

Figure 6.19

Velocity field for sideways extrusion - bottom of die in line with aperture

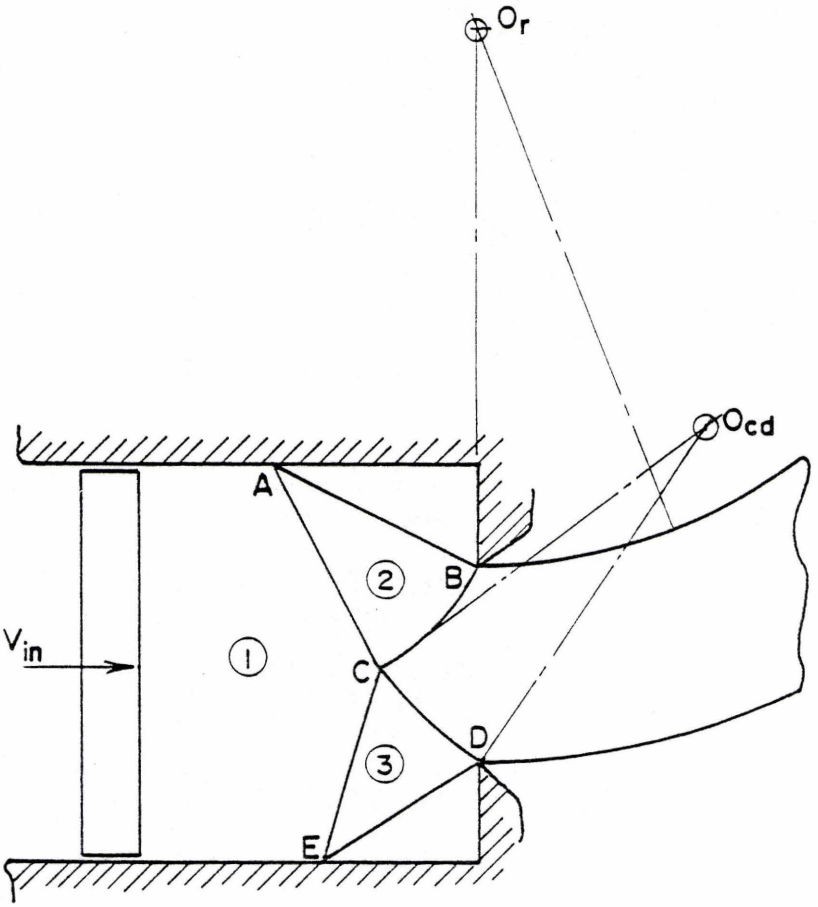

PHYSICAL PLANE DIAGRAM

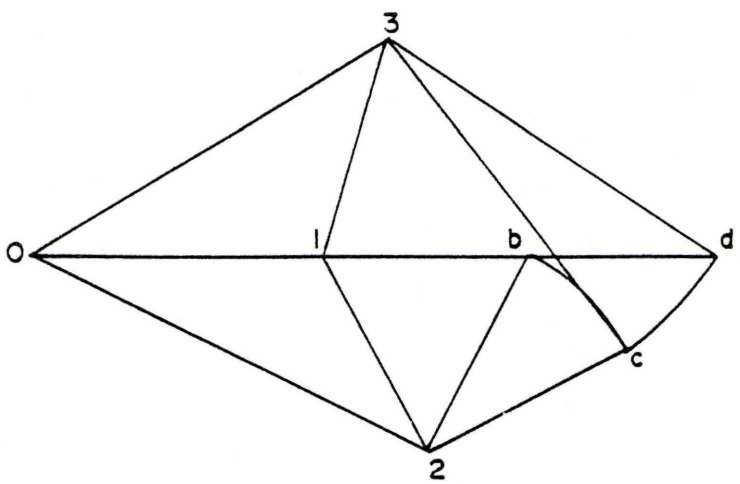

HODOGRAPH

Figure 6.20

Velocity field for direct end extrusion

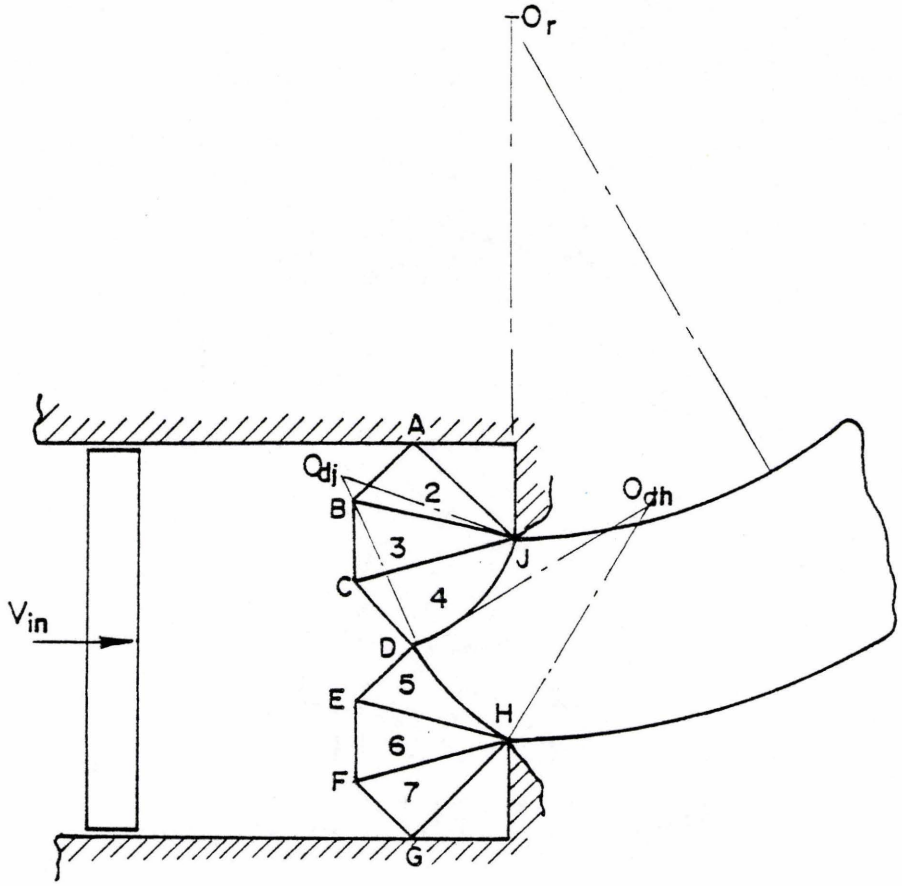

PHYSICAL PLANE DIAGRAM

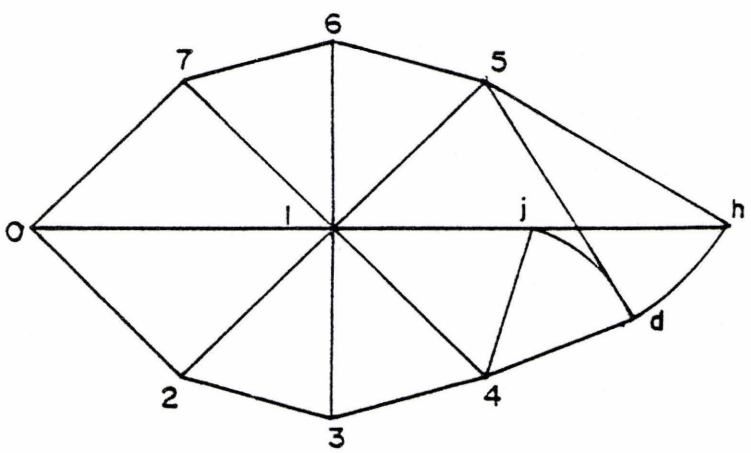

HODOGRAPH

Figure 6.21

Velocity field for direct end extrusion based on the slip line field

located at any position along the side of the extrusion container.

A more complex velocity field, based on the slip-line field, is shown in Figure 6.21.

6.5.6 Unsymmetrical End Extrusion - with Rotation

The case of unsymmetrical end extrusion has recently been examined by Chitkara et al. [132, 133] and results presented from experimental and theoretical studies. The slip-line fields suggested by Green were evaluated and predictions of the extrusion pressure were within 10%.

The upper bound technique which is simpler to apply than the slip-line field solution does not predict the rotation of the product. A new velocity field is presented in Figure 6.22 which predicts this rotation.

The position of centre of rotation of the product O_r is assumed and is in line with the aperture BD and is assumed. The position of A, the centre of arc BC is determined since angle O_rAB is 90°. C is found by constructing the hodograph where angle 12c must be 90° to maintain the similarity of the hodograph and physical plane diagrams. The point 3 along the bisector of cd in the hodograph can be chosen arbitrarily and defines the position of E and the radius of the arc BD in the physical plane diagram.

6.5.7 Indentation - Rotation of the Strip Ends

The slip line fields originally proposed for the side extrusion

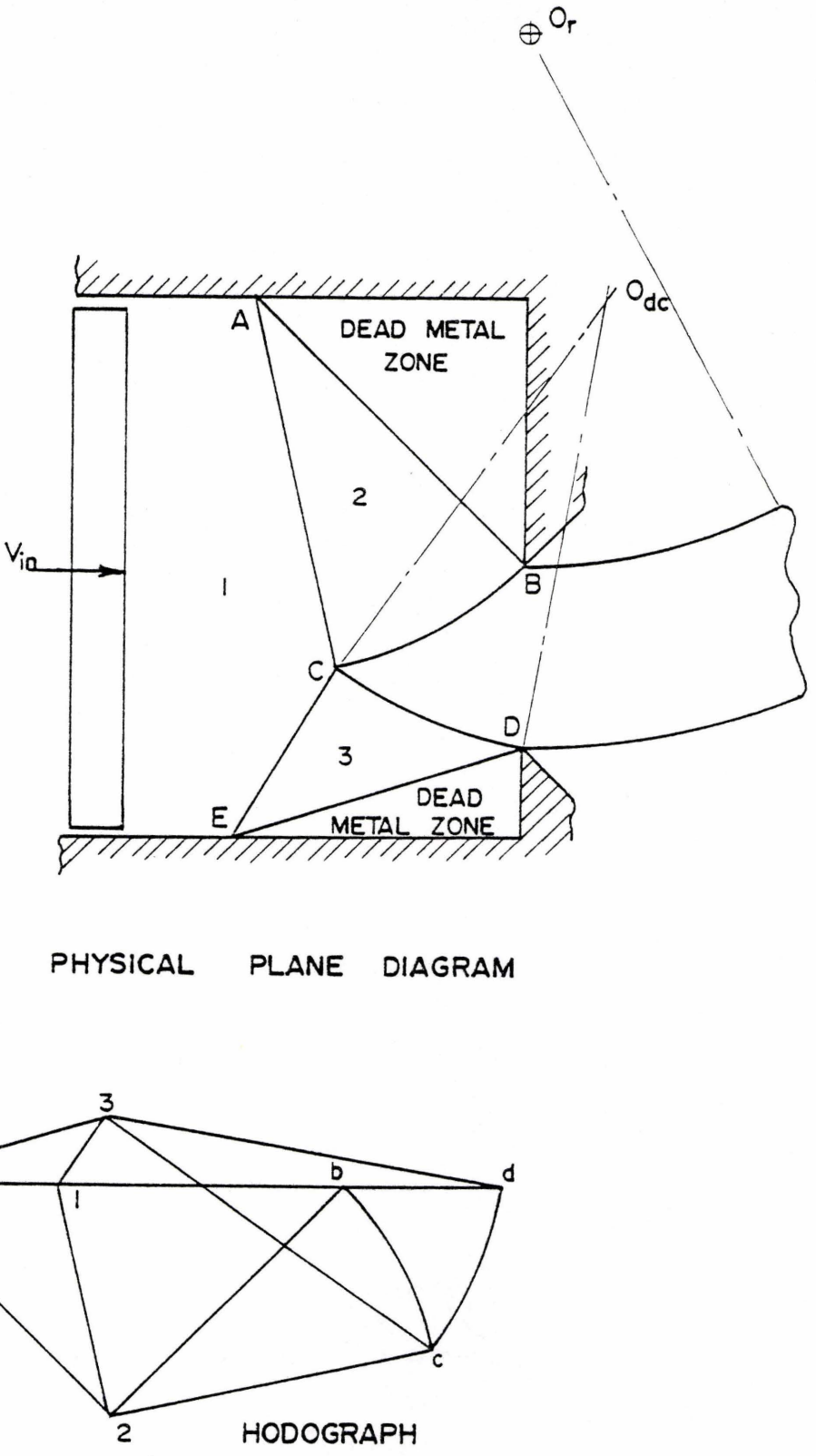

Figure 6.22

Velocity field for unsymmetric end extrusion

case were based on the solutions given by Hill [25] for indentation. The early fields assumed that the material moved perpendicular to the action of the indenter. Dugdale [178] has shown that the material in fact curves upward and does not remain in contact with the anvil. He proposed a velocity field which allowed for the curvature of the strip and indicated that the work rate was identical to that given assuming straight line motion of the ends of the strip.

An analysis of the plane strain indentation of a flat strip has been given by Dewhurst [179]. Slip line fields were presented which indicated that the strip would lift off the base. It was suggested that this rotation was a fundamental mode of deformation and was not a secondary effect due to unequal friction forces or the strain hardening of the material.

A simple tangential velocity discontinuity diagram is shown in Figure 6.23 based on the slip line field originally proposed by Hill [25]. This solution is an "intantaneous" field in that it describes the velocity only at the specific height to width ratio shown. As the indenter moves into the block a series of fields would have to be constructed to evaluate the curvature of the sheet and the variation of the indenter pressure. The centre of rotation of the extrudate O_r lies on the centre line of the punch and its position is initially assumed. The position of B is also assumed. The location of a, b and c in the hodograph and the bisectors of ab and bc can be determined. The position of 4 in the hodograph is defined by the bisector of bc since arc bc is centered at 4. The position of 2 in the hodograph is assumed

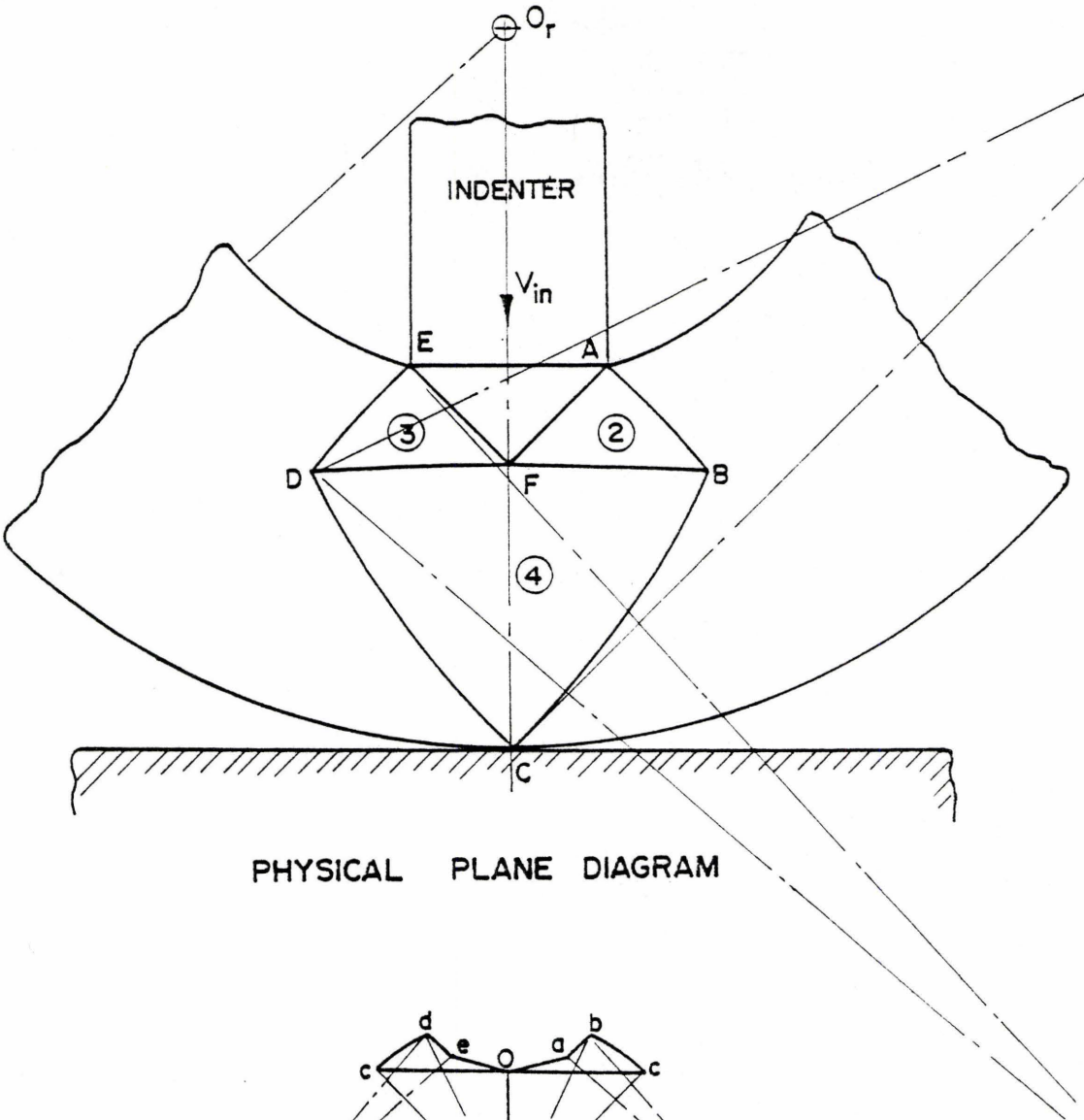

PHYSICAL PLANE DIAGRAM

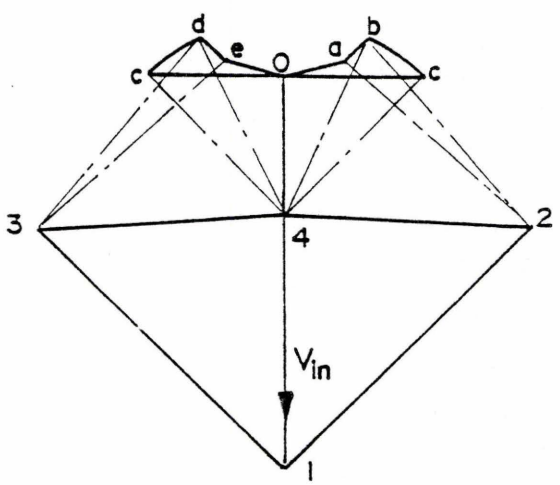

HODOGRAPH

Figure 6.23

Velocity field for indentation

and the centres of the arcs AB and BC, in the physical plane diagram, defined.

6.5.8 Restricted Edge Machining

Plane strain restricted edge machining is examined in Figure 6.24. A velocity field is proposed which predicts the rotation of the chip. The position of the centre of rotation of the chip O_r along the perpendicular, to AD and the angle α are assumed for a given chip thickness. a and b can be determined in the hodograph and by striking an arc centred at 2 through a and an arc centred at 1 through b the position of c is located. The radii of curvature of the arcs AB and BC in the physical plane diagram are defined within the hodograph since ca2 and ACO_{AC} and bc1 and BCO_{BC} are similar.

The rotation of the chip is clearly indicated.

6.5.9 Summary of Proposed Tangential Velocity Discontinuity Fields

Tangential velocity discontinuity diagrams have been presented for a variety of metalworking processes. The upper bound technique has found wide acceptance because of its simplicity but does not predict observed phenomena. The velocity fields developed in this chapter contain both and straight and circular discontinuities and represent a new type of mixed field. The diagrams have been developed with the purpose of predicting the observed phenomena of rotation. It will be appreciated that for the solution to be applicable the work rate must be smaller than, or at least equal to, that given by the straight line

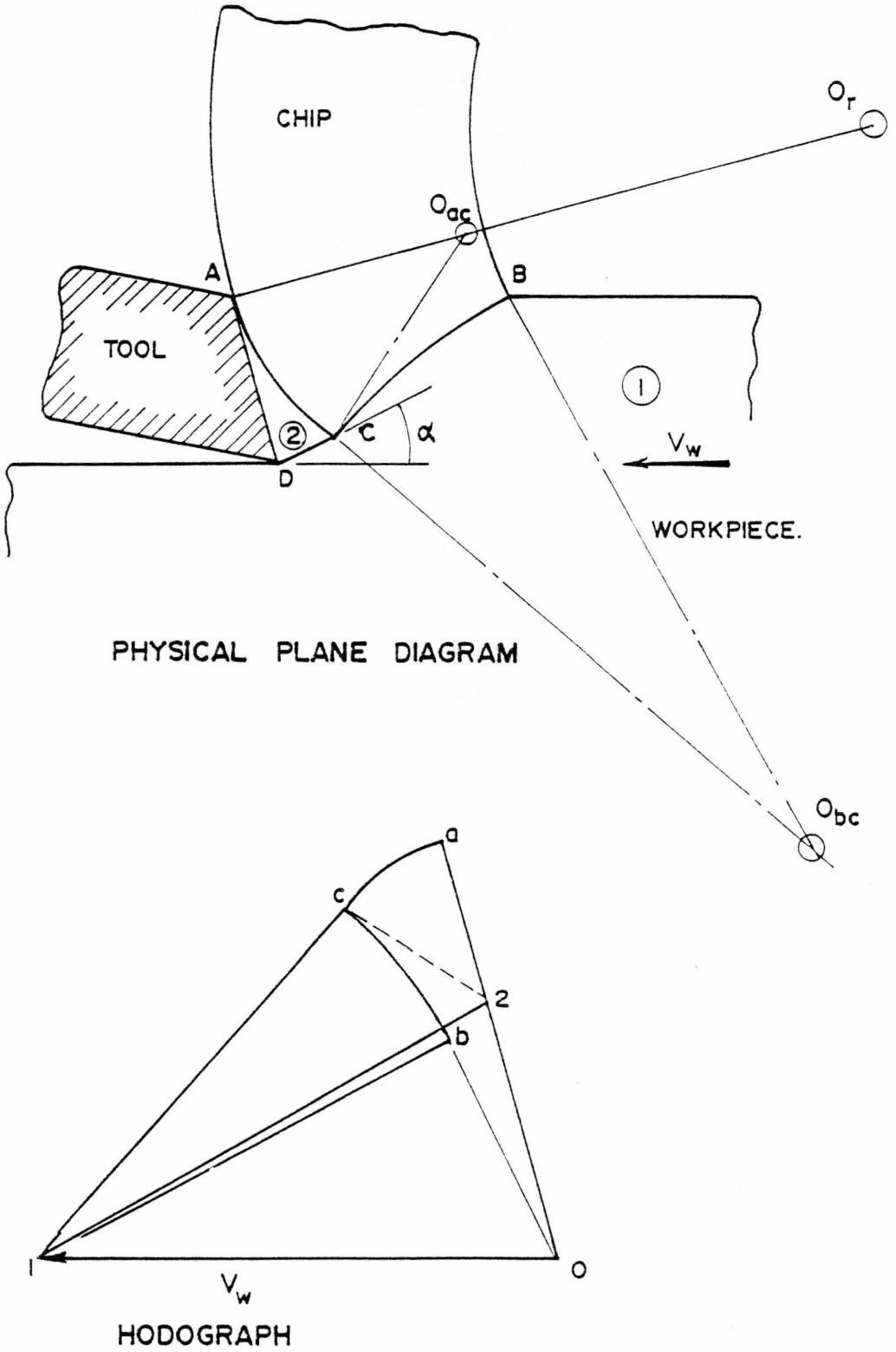

Figure 6.24

Velocity field and hodograph for restricted edge machining

discontinuity models.

No numerical solutions have been generated since the fields, as with any other upper bound solution, must be optimized to minimize the work rate.

6.6 Summary

The experimental values for the extrusion load have been compared with the theoretical values generated using the rate sensitive model developed in Chapter 4. The correlation was shown to be good and that the model predicted extrusion pressures which were a function of the ram velocity. It was shown that as the ram speed increases the flow stress across each discontinuity reaches a saturation level and that the solution is identical to that given for a rigid perfectly plastic material.

In an attempt to predict the curvature of the extruded product it was shown that the shape of the discontinuity between a uniform translational and a uniform rotational field is a circular arc. A simple two line velocity discontinuity model was examined and it was shown that the solutions for straight and curved discontinuities were identical. A new type of mixed tangential velocity discontinuity diagram was proposed which replaces some of the straight line discontinuities with circular ones across which the tangential velocity change is constant. A number of examples were presented which illustrated the velocity fields for a variety of plane strain metalworking processes. No attempt was made to minimize the work rate associated with each field.

CHAPTER 7

CONCLUSIONS AND SUGGESTIONS FOR FUTURE WORK

7.1 Conclusions

The aim of the current investigation was to examine the effects of velocity on the deformation zone geometry in the extrusion process. The general conclusions of this study are not restricted to the extrusion process but should be applicable to any bulk forming problem. The side extrusion process is not a significant industrial processing technique but was used as an example to indicate changes in the velocity field which would not be apparent in normal extrusion processes.

In the initial chapters of the thesis the reader was introduced to extrusion and the salient features of the process were discussed. A review of the literature related to the current investigation was presented and included a review of the work published on the side extrusion process. The upper bound analytical technique was introduced in Chapter 4 and a new analysis presented which extended the method to include the effects of strain rate sensitivity. The application of the model to real materials was discussed and the form of the solution indicated.

The analysis introduced the concepts of a shear strain rate discontinuity and a zone of constant shear strain rate. An appropriate value for the thickness of the shear zone was discussed and it was

shown, by considering the shear process in metalcutting, that the thickness is a function of the shear zone length; a value for the shear zone length to width ratio of 10 was assumed.

A number of velocity fields were proposed for the side extrusion process and were compared using the upper bound technique for a rigid perfectly plastic material. Computerized optimization techniques were used for the first time to optimize the velocity fields by minimizing the extrusion pressure. A single model was selected for further study based on the results of the optimization. It was shown that a simple upper bound solution which had been optimized to give the minimum work rate predicted extrusion pressures which were within 10 → 15% of those predicted by the slip-line field solution.

Experiments were performed by the author on the side extrusion of pure lead and the tin lead eutectic which had been processed to make it superplastic. Results were presented of the variation of the extrusion pressure with ram speed and fractional reduction. Details of the exit geometry of the extruded specimen were also presented. The results of the experimental investigation can be summarized as follows:

a) Material exiting the die is not straight but curved. A characteristic difference in the curvature of a rate insensitive and viscous material was identified. That is the tin lead eutectic curled away from the direction of ram movement while the pure lead curled towards the direction of the ram movement.

b) The deformation zone for the tin lead eutectic was larger

than that for the pure lead.

c) A definite dead metal zone existed at the bottom of the die for the tests with the pure lead. This was not evident for the tests with the tin lead eutectic.

d) The deformation zone geometry for side extrusion is well predicted by the slip-line field for the pure lead. The assumed velocity field is, however, inappropriate for the tin lead eutectic.

As indicated above the extrudate was curled. This had not been predicted by any of the models suggested to date which indicate that material leaves the die straight but inclined at some angle. The observation of extrudate curling led to the development of some new tangential velocity discontinuity fields. These fields can be described as a mixed type and use a combination of straight and circular discontinuities. The transition from a uniform translational field to one of uniform rotation was examined and the shape of the discontinuity was shown to be a circular arc. Across this circular discontinuity the tangential velocity change is constant. The application of this type of field was illustrated in some examples of typical metalworking processes.

7.2 Suggestions For Future Work

This study has attempted to indicate the effect of velocity on the deformation zone geometry using a rate sensitive material. Gridded specimens were used but no quantitative strain analysis was attempted.

It is suggested that this might be a fruitful area of study since it would clearly define the deformation zone and differences, due to changing variables, will be more evident.

The use of the side extrusion process as an analytical tool is unique to the present study and it is suggested that this be continued and used to examine the effects of strain hardening, friction and the other variables associated with particular bulk forming processes. An examination of the velocity fields for materials which show a negative strain rate sensitivity or a negative strain hardening characteristic would be interesting. It will be recalled that the double maxima patterns for aluminium, Figure 2.5, were associated with the negative strain hardening characteristic.

A number of new tangential velocity discontinuity fields have been developed in the thesis which predict the rotation of the product. No analysis was made of the work rate associated with these fields. It would be worthwhile to examine these fields in depth by optimizing their geometry and comparing the values for the work rate with an appropraite straight line model. In this way it will be possible to determine whether, as suggested by Dewhurst, the curling of the strip or extrudate is a fundamental mode of deformation.

It was indicated in Chapter 2 that there exists a serious shortage in the literature of a detailed study of the extrusion of rate sensitive materials as a class of alloys. The present study has not attempted to fill this void and it would prove worthwhile if a program of this nature were undertaken. A number of theories have been

presented for the extrusion of rate sensitive materials which are applicable to conical dies and it would be useful, for comparative purposes, if extensive experimental results were available which detailed the effects of strain rate sensitivity, ram velocity, extrusion ratio and die geometry.

7.3 Closing Comments

The upper bound solution is, in the author's opinion, a useful technique for obtaining an approximate value for the load requirement for a given process. The technique is particularly suitable in the teaching of students since it gives a clear, if somewhat elementary, understanding of the basic mechanics of bulk forming problems. In situations where computing facilities are not readily available the upper bound technique provides useful answers to some real technological problems. The advent of the digital computer in the 1960's and the development of powerful numerical techniques has provided the solution to a number of problems. As the finite element method continues to be developed and engineers become more familiar with the handling of large computer programs the solution of real bulk forming problems will be successfully achieved. In any process involving large plastic deformation the stress and strain throughout the part may be very different. The strain history associated with different parts of a component and the temperature rise due to the plastic deformation can result in local changes in the mechanical behaviour. All these processes can be handled by a computer program which has access to a

detailed analysis of the material properties. When this has been accomplished a truly detailed study of the mechanics of metalworking processes will be developed. While analyses of this nature will enhance our understanding of the problem at a minute level the gains of such a detailed study may not warrant the necessary expenditure of time and effort. The simpler techniques which have been developed to date will always provide a useful basis for further studies. For this reason the extension of such analytical techniques to cover different material properties is valuable.

There is an apparent need for interactive systems which will permit the tool designer to propose changes in tool configurations and then observe the effects of these on forming parameters such as the load and deformation zone geometry. With the present generation of interactive computers the time and storage capacity required to complete a solution using the more exact techniques, such as the finite element method, is prohibitive. It is suggested then that the kind of method developed here, in which the computer is used in completing approximate solutions of the upper bound type, will be extremely valuable in developing the kinds of computer aided tooling design systems which are being sought in the industry.

REFERENCES

[1] Bridgeman, P.W.: Studies in large plastic flow and fracture. McGraw Hill, 1952.

[2] Pugh, H.D.: "The mechanical properties and deformation characteristics of metals and alloys under pressure", A.S.T.M. Int. Conf. on Mats., Philadephia, Feb. 1964.

[3] Pugh, H.D., and Low, A.H.: "The hydrostatic extrusion of difficult metals", J. Inst. Metals, vol. 93, pp. 201, 1964.

[4] Beresnes, B.I., Vereshchagin, L.F., Ryabinin, Yu.N., and Livshits, L.D.: "Some problems of large plastic deformation of metals at high pressures", Pergamon Press, 1963. Translated from Russian original published by U.S.S.R. Academy of Sciences, 1960.

[5] Green, D.: "An experimental high speed machine for the practical exploitation of hydrostatic extrusion", J. Inst. Metals, vol. 93, pp. 65, 1964.

[6] Alexander, J.M., Lengyel, B.: Hydrostatic extrusion. Mills and Boon; London, 1971.

[7] Green, A.P.: "On unsymmetrical extrusion in plane strain", J. Mechs. Phys. of Solids, vol. 3, pp. 189, 1955.

[8] Duncan, J.L., Johnson, W., and Ovreset, A.: "Effect of tool geometry on extrusion pressure in side extrusion", Annals of C.I.R.P., vol. XIV, pp. 89, 1966.

[9] Duncan, J.L., Johnson, W., and Ovreset, A.: "Some experiments and theory for plane strain side extrusions", Applied mechanics convention, Cambridge, England, 1966.

[10] Johnson, W.: "Partial sideways extrusion from a smooth container", J. Mech. Phys. Solids, vol. 5, pp. 193, 1957.

[11] Ragab, A.R., and Duncan, J.L.: "Rate-dependent transient extrusion", Int. J. Mech. Sci., vol. 17, pp. 125, 1975.

[12] Edgecombe, D.A.: "The extrusion of steel", Proc. Third Tech. Conf. - Bar and Allied Products, Interscience, 1961.

[13] Anon.: "Hot extrusion of steel shapes", Can. Machry. Metwkg., pp. 32, July 1975.

[14] Pearson, C.E., and Parkins, R.N.: The extrusion of metals. John Wiley and Sons, 1960.

[15] British Complete Specification No. 19356: "Improvements in the manufacture of metal tubes, tubular and hollow articles, plates, rods, bars, wires and the like, and in means and apparatus therefore", by. J. Robertson, 1893.

[16] Sejournet, J.: "The hot extrusion of steel", The Engineer, vol. 177, pp. 463, 1954.

[17] Green, D.: "Hydrospin - A new concept of extrusion", J. Inst. Metals, vol. 99, pp. 76, 1971.

[18] Green, D.: "Continuous extrusion forming of wire sections", J. Inst. Metals, vol. 100, pp. 295, 1972.

[19] Fuchs, F.J.: "High pressure continuous wire forming", pp. 145, Engineering Solids Under Pressure, H.Li.D. Pugh, ed., Inst. Mech. Engrs., London, 1971.

[20] Tirosh, J., and Grossman, G.: "Continuous extrusion by viscous drag". Trans. A.S.M.E., J. of Eng. Mats. and Tech., vol. 99, pp. 52, 1977.

[21] Samanta, S.K.: "Helical gear: A novel method of maufacturing it", Proc. Fourth North American Metalworking Research Conf., Ed. T. Allan, pp. 199, 1976.

[22] "Apparatus and method for cold extrusion of gears", Inventor: S.K. Samanta, Assignee, Ford Motor Co., Dearborn, MI Patent No. 3,910, 091, dated October 7, 1975.

[23] Johnson, W., and Kudo, H: The mechanics of metal extrusion. Manchester Univ. Press, 1962.

[24] Avitzur, B.: Metal forming - process and analysis. McGraw Hill, 1968.

[25] Hill, R.: The mathematical thoery of plasticity. Oxford Univ. Press, 1950.

[26] Thomsen, E.G., Yang, C.T., and Kobayashi, S.: Mechanics of plastic deformation in metal processing. MacMillan, 1965.

[27] Zholobov, V.V., and Zverev, G.I.: The extrusion of metals. Translated from Russian original 1959.

[28] Siebel, E., and Fangmeirer, E.: "Researches on power consumption in extrusion and punching of metal", Mitt. K.-W. Eisenforsch, vol. 13, pp. 29, 1931.

[29] Henky, H.: "Uber einige statisch estimmte falle des gleichgewichts in plastischen korpern", Zeits. ang. math. mech., vol. 3, pp. 214, 1923.

[30] Shield, R.T.: "On the plastic flow of metals under conditions of axial symmetry", Proc. R. Soc. A., vol. 233, pp. 267, 1955.

[31] Richmond, O. and Morrison, J.L.: "Streamlined wire drawing dies of minimum length", J. Mech. Phys. Solids, vol. 15, pp. 195, 1967.

[32] Thomsen, E.G.: "Comparison of slip-line solutions with experiment", Trans. A.S.M.E., J. .Appl. Mech., vol. 23, pp. 225, 1956.

[33] Thomsen, E.G.: "Plan strain and axially symmetric velocities and pressures in extrusions", Proc. Conf. Properties of Materials at High Rates of Strain, Inst. Mech. Engrs., London, 1957.

[34] Lee, E.H.: "The theoretical analysis of metal forming problems in plane strain", J.. Appl. Mech., vol. 19, pp. 97, 1952.

[35] Johnson, W., Sowerby, R., and Haddow, J.B.: "Plane strain slip line fields; Theory and bibliography", Edward Arnold Pub., 1970.

[36] Johnson, W.: "Experiments in plane-strain extrusion", J. Mech. Phys. Solids, vol. 4, pp. 269, 1956.

[37] Dodeja, L.C., and Johnson, W.: "On the multiple hole extrusion of sheets of equal thickness", J. Mech. Phys. Solids, vol. 5, pp. 267, 1957.

[38] Fenton, F.G., and Durai-Swamy, B.: "Plane strain plastic flow of strain-rate sensitive materials", Trans. A.S.M.E., J. of Eng. Mats. and Tech., pp. 238, July 1974.

[39] Yang, C.T., and Thomsen, E.G.: "Plastic flow in a lead extrusion", Trans. A.S.M.E., vol. 75, pp. 575, 1953.

[40] Firsch, J., and Thomsen, E.G.: "An experimental study of metal extrusion at various strain-rates", Trans. A.S.M.E., vol 74, pp. 599, 1954.

[41] Shabaik, A.H. and Thomsen, E.G.: "A theoretical method of the analysis of metal-working problems", Trans. A.S.M.E., vol. 90, pp. 343, 1968.

[42] Johnson, W.: "Estimation of upper bound loads for extrusion and coining operations", Proc. Inst. Mech. Engrs., vol. 173, pp. 61, 1959.

[43] Johnson, W., and Mellor, P.B.: Plasticity for mechanical engineers. Van Nostrand; London, 1970.

[44] Kudo, H.: "An upper bound approach to plain strain forging and extrusion I", Int. J. Mech. Sci., vol. 1, pp. 57, 1960.

[45] Kudo, H.: "An upper bound approach to plain strain forging and extension II", Int. J. Mech. Sci., vol. 1, pp. 229, 1960.

[46] Johnson, W.: "The pressure for cold extrusion of lubricated rod through square dies of moderate reduction at slow speeds", J. Inst. Metals, vol. 85, pp. 403, 1956.

[47] Pugh, H.D., and Watkins, M.T.: "Experimental investigation of the extursion of metals", Inst. Prod. Engrs. Conf., Brighton, England, Oct. 1960.

[48] Avitzur, B.: "Study of flow through conical converging dies", Proc. Symp. on Relation between Theory and Practice of Metal Forming, Cleveland, Ohio, Oct. 1970.

[49] Halling, J., and Mitchell, L.A.: "Use of upper bound solutions for predicting the pressure of the plane strain extrusion of materials", J. Mech. Eng. Sci., vol. 6, pp. 240, 1964.

[50] Farmer, L.E., and Pirog, B.Z.: "Estimation of maximum extrusion forces", Int. Conf. Prod. Technol., Melbourne, Australia, Aug. 1974.

[51] Medrano, R., Gillis, P., Hinesley, C., and Conrad, H.: "Application of visioplasticity techniques to axisymmetric extrusions", Proc. Symp. on Relation between Theory and Practice of Metal Forming, Cleveland, Ohio, Oct. 1970.

[52] Jovane, F., Shabaik, A.H., and Thomsen, E.G.: "Some extrusion studies of the eutectic alloy of Pb and Sn", Trans. A.S.M.E., vol. 91, pp. 680, 1969.

[53] Medrano, R., Gillis, P., Hinesley, C.P. and Conrad, H.: "Visioplasticity analysis of 2024 aluminium alloy extrusions", Int. J. Mech. Sci., vol. 15, pp. 955, 1973.

[54] Lambert, E.R., and Kobayashi, S.: "An approximate solution for the mechanics of axisymmetric extrusion", 9th Int. M.T.D.R. Conf., Manchester, England, Sept. 1968.

[55] Nagpal, V.: "General kinematically admisible velocity fields for some axiymmetric metal forming problems", Trans. ASME, J. of Eng. for Ind., Series B, vol. 96, pp. 1197, 1974.

[56] Campbell, J.D.: "Plastic instability in rate dependent materials", J. Mech. Phys. Solids, vol. 15, pp. 359, 1967.

[57] Hart, E.W.: "Theory of the tensile test", Acta. Met., vol. 15, pp. 351, 1967.

[58] Jain, K.K., Duncan, J.L. and Watson, T.W.: "Back extrusion and blow moulding of eutectoid Zn-Al alloys", Can. Metal. Quart., vol. 13, pp. 511, 1974.

[59] Al-Naib, T.Y.M., and Duncan, J.L.: "Superplastic metal forming", Int. J. Mech. Sci., vol. 12, pp. 463, 1970.

[60] Saller, R.A., and Duncan, J.L.: "Stamping experiments with superplastic alloys", J. Inst. Metals, vol. 99, pp. 173, 1971.

[61] Forster, J.A., Mogford, S.R., Grach, J., and Duncan, J.L.: Metalworking Research Report #20, Dept. of Mech. Eng., McMaster Univ., Hamilton, Ontario, 1973.

[62] Stewart, M.J.: "Superplastic forging of Zn-Al alloys", Can. Met. Quart., vol. 12, pp. 2, 1973.

[63] Shabaik, A.H., and Virani, A.M.: "The use of superplastic alloy of the eutectic lead-tin for the analysis of the hot extrusion process", Trans. A.S.M.E., vol. 94, pp. 1060, 1972.

[64] Wilcox, R.J., and Whitton, P.W.: "The cold extrusion of metals using lubrication at slow speeds", J. Inst. Metals, vol. 87, pp. 289, 1958.

[65] Chandra, T., and Jonas, J.J.: "The extrusion force and the mean strain rate during the extrusion of rate sensitive materials", Met. Trans., vol. 1, pp. 2079, 1970.

[66] Chandra, T., and Jonas, J.J.: "Experimental studies of the force to extrude a rate sensitive material", Met. Trans., vol. 2, pp. 877, 1972.

[67] Jonas, J.J., and Chandra, T.: "The extrusion of rate sensitive materials", A.I.M.E., Symp. on the Relation between Theory and Practice in Metal Forming, Cleveland, Ohio, Oct. 1970.

[68] Alto, A., and Giorleo, G.: "On the extrusion in superplastic conditions", Trans. ASME, J. of Eng. for Ind., Series B, vol. 97, pp. 1131, 1975.

[69] Cristescu, N.: "Plastic flow through conical converging dies using a viscoplastic constitutive equation", Int. J. Mech. Sci., vol. 17, pp. 425, 1975.

[70] Superplastic Zinc Alloys - publicity brochure Cominco Ltd., Sheridan Park Ontario, Canada.

[71] SPZ Mouldings in Focus - publicity brochure, ISC Alloys Ltd., Avonmouth, Bristol, England.

[72] Formetal - publicity borchure, Formet Technology Corp., Pittsburgh, U.S.A.

[73] Superplastic Zinc - Product News - The Engineer, pp. 43, Jan. 1978.

[74] New Superplastic alloy - Metal Bulletin, pp. 26, Jan. 10, 1974.

[75] Hartley, J.: "Stretching aluminium into strange shapes can lead to profits". The Engineer, pp. 22, July 14, 1977.

[76] Mortimer, J.: "Supral Panels for Lagondas", The Engineer, pp. 11, Oct. 20, 1977.

[77] Grimes, R., Stowell, M.J., and Watts, B.M.: "Superplastic Aluminium based alloys", Metals Tech. pp. 154, March 1976.

[78] Moles, M.D.C., Ph.D. Thesis, Cambridge University, Cambridge England, 19.

[79] Balliett, R.W., Forster, J.A., and Duncan, J.L.: "Precision forging of a high strength Zinc-Aluminium alloy", Superplastic Met. Trans., vol. 9A, pp. 1259, 1978.

[80] Stewart, M.J.: "Superplasticty in low alloy steels", Met. Trans. 7A, pp. 399, 1976.

[81] Fields, P.S., and Stewart, T.T.: "Strain effects in the superplastic deformation of 78 Zn-22Al.", Int. J. Mech. Sci., vol. 13, pp. 63, 1971.

[82] Duncan, J.L., Shapiro, E., Crane, J., and Taplin, D.M.R.: "Applications of superplastic metals", Proc. Symp. Appl. Solid Mechanics, Univ. of Waterloo, Canada, 1972.

[83] Moles, M.D.C., Private Communication, Jan. 1977. Research Manager, Accurate Stamp and Stencil, Hamilton, Ontario.

[84] Moles, M.D.C., Forster, J.A., and Duncan, J.L.: "Creep forging of an Aluminium-Bronze", Can. Met. Quart., vol. 15, no. 3, pp. 249, 1976.

[85] Cox, T.R., Private Communication, July 1978, President, Accurate Stamp and Stencil, Hamilton, Ontario.

[86] Hamilton, C.H., and Stacher, G.W.: "Superplastic forming of Ti-6A1-4V beam frames", Met. Prog., pp. 34, March 1976.

[87] Weisert, E.D. and Stacher, G.W., "Fabricating parts with SPF/DB Process", Metals Progress, pp. 33, March 1977.

[88] Corti, G.W., Gessigner, G.H., and Shabaik, A.H.: "Superplastic isothermal forging: a model metal flow study", J. Mech. Workg. Tech., vol. 1, pp. 35, 1977.

[89] Thomsen, T.H., Holt, D.L., and Backofen, W.A.: "Forming superplastic sheet metal in bulging dies", Metals. Eng. Quart., pp. 1, May 1970.

[90] Jain, K.K.: "Techniques for forming superplastic alloys", M.Eng. Thesis, Dept. of Mech. Eng., McMaster University, Hamilton, Ontario, Canada, 1972.

[91] Jain, K.K., Duncan, J.L., and Watson, T.W.: "Back extrusion and blow molding of eutectoid Zn-Al alloy", Can. Met. Quart., vol. 13, no. 3, pp. 511, 1974.

[92] Sellars, C.M., and Tegart, W.J.McG.:

[93] Feltham, P.: "Extrusion of metals", Metal Treatment and Drop Forging, pp. 440, Nov. 1956.

[94] Alexander, J.M.: "The application of experimental and theoretical results to the practice of hot extrusion", J. Inst. Metals, vol. 90, pp. 193, 1961.

[95] Hodierne, F.A.: "Discussion to Alexander", ref. 94, J. Inst. Metals, vol. 90, pp. 205, 1961.

[96] Blazynski, T.Z.: "Strain rates in wire drawing and tube making", The Engineer, pp. 627, April 1967.

[97] Atkins, A.G.: "Consequences of high strain rates in cold working", J. Inst. Metals, vol. 97, pp. 289, 1969.

[98] Fenton, F.G.: "Effects of ram speed and size on the required extrusion pressure", Proc. Third North American Metalworking Research Conf., M.C. Shaw, ed., Pub. by Carnegie Press, 1975.

[99] Fenton, F.G., and Durai Swamy, B.: "Extrusion pressure-effects of ram speed and size", Proc. Can. Cam. Conf., pp. 131, published in 1975.

[100] Swift, H.W.: "Plastic instability under plane stress", J. Mech. Phys. Solids, vol. 1, no. 1, 1952.

[101] Bailey, J.A., and Singer, A.R.E.: "Effects of strain rate and temperature on the resistance to deformation of aluminum, two aluminum alloys and lead", J. Inst. Metals, vol. 92, pp. 404, 1963.

[102] Alder, J.F., and Phillips, V.A.: "The effect of strain rate and temperature on the resistance of aluminium, copper and steel in compression", J. Inst. Metals, vol. 83, pp. 80, 1954.

[103] Tang, S.: "Steady extrusion of superplastic metallic alloys", Trans. A.S.M.E., J. of Basic Eng., vol. 93, pp. 659, 1971.

[104] Tang, S.: "Drawing and extrusion of superplsatic metals through cone-shaped dies", J. Franklin Inst., vol. 295, pp. 357, 1973.

[105] Wong, A.W., and Jonas, J.J.: "Aluminium extrusion as a thermally activated process", Trans. of the Met. Soc. of A.I.M.E., vol. 242, pp. 2271, 1968.

[106] Garofalo, F.: "An empirical relation defining the stress dependence of minimum creep rate in metals", Trans. Met. Soc. AIME, vol. 227, pp. 351, 1963.

[107] Farag, M.M., and Sellars, C.M.: "Flow stress in hot extrusion of commercial purity aluminium", J. Inst. Metals., vol. 101, pp. 137, 1973.

[108] Hinesley, C.P., and Conrad, H.: "Effects of temperature and ram speed on the flow pattern in axisymmetric extrusions of 2024 Al alloy", Mat. Sci. and Engrg., vol. 12, pp. 47, 1978.

[109] Sheppard, T., and Raybould, D.: "On load and temperature rise during the extrusion of superpure Al, Al-Zn, and Al-Zn-Mg alloys", J. Inst. Metals, vol. 101, pp. 33, 1973.

[110] Raybould, D., and Sheppard, T.: "Axisymmetric extrusion: the effect of temperature rise and strain rate on the activation enthalpy and material constants of some aluminium alloys and their relation to recrystallization, substructure, and subsequent mechanical properties", J. Inst. Metals, vol. 101, pp. 65, 1973.

[111] Tomita, Y., Sowerby, R. and Seguchi, Y.: "Note on an approximate deformation analysis of strain rate sensitive materials", Proc. 6th North American Metalworking Research Conf., University of Florida, p. 103, 1978.

[112] Tomita, Y., and Sowerby, R.: "An approximate analysis for studying the deformation mechanics of rate sensitive materials", Int. J. Mech. Sci., vol. 20, pp. 327, 1978.

[113] Hirst, S., and Ursell, D.H.: "Some limiting factors in extrusion", Metal Treatment and Drop Forging, pp. 409, Oct. 1958.

[114] Meadows, B.J., and Cutler, M.J.: "A theoretical derivation of stress/strain rate/temperature relationships in the extrusion of Al-Mg-Si type alloys", J. Inst. of Metals, vol. 97, pp. 321, 1969.

[115] Thomsen, E.G., and Lapsley, J.T.: "Experimental stress determination within a metal during plastic flow", Proc. Soc. Exp. Stress Analysis, vol. 11, pp. 59, 1954.

[116] Thomsen, E.G., and Frisch, J.: "Stresses and strains in cold extruding aluminium", Trans. A.S.M.E., vol. 75, pp. 1343, 1955.

[117] Shabaik, A.H., and Thomsen, E.G.: "Some additional studies of the mechanics of axisymmetric extrusions by the visioplasticity method", Annals of the C.I.R.P., vol. XVI, pp. 41, 1968.

[118] Altan, T., Kobayashi, S., DePierre, V., and Pierce, C.M.: "Plastic deformation of copper and steel in hot extrusion through conical dies", Trans. A.S.M.E., J. of Eng. for Ind., pp. 371, 1968.

[119] Singh, A., Dean, T.A., and Davies, R.: "The effects of temperature and speed on the warm extrusion of steel", Proc. 13th Int. Mach. Tool Des. Res. Conf., pp. 351, Ed. S.A. Tobais and F. Koenigsberger, Pub. by MacMillan, 1973.

[120] Farag, M.M., and Sellas, C.M.: "Analysis of double maximum flow patterns in axisymmetric extrsuion of H30 aluminium alloy", Metals Technology, vol. 2, pp. 220, 1975.

[121] Zimmerman, Z., and Avitzur, B.: "Metal flow through conical converging dies - A lower upper bound approach using generalized boundries of the plstic zone", Trans. A.S.M.E., J. of Eng. for Ind.

[122] Gurney, F.J., and DePierre, V.: "The influence of the interface condition on the platic deformation zone and the resultant product integrity in extrusion", Trans. A.S.M.E., J. Eng. for Ind.

[123] Alexander, J.M., and Whitlock, B.C.: "Extrusion of a bimetallic strip from separate containeres", Proc. Instn. Mech.. Engrs., vol. 180, Part 3I, pp. 250, 1966.

[124] Ross, E.W.: "On the plane plastic flow of an insert block", J. Appl. Mech., vol. 24, pp. 247, 1957.

[125] Johnson, W., Mellor, P.B., and Woo, D.M.: "Extrusion through single hole staggered and unequal multi-hole dies", J. Mech. Phys. of Sols., vol. 6, pp. 203, 1958.

[126] Private Communication. Prof. W. Johnson, University of Cambridge, Cambridge, England, June 1978.

[126a] Basu, S.K., M.Sc. Thesis, Faculty of Technology, Manchester University, England, 1963.

[127] Johnson, W., and Chitkara, N.R.: "Corrugated plate formed by side extrusion with two co-axial rams moving at different speeds", Int. J. Mech. Sci., vol. 15, pp. 199, 1973.

[128] Quenzi, P.J., Kauppila, R.W., and Weinmann, K.J.: "Analysis of lateral extrusion of 6061-0 alluminum by slip-line theory modified to include strain hardening", Trans. A.S.M.E., J. Eng. for Ind., pp. 971, Nov. 1972.

[129] Masura, G.P., Weinmann, K.J., and Kauppila, R.W.: "An investigation of defect formation in the cold lateral extrusion of 6061-0 aluminum", Proc. 3rd North American Metalworking Research Conf., M.C. Shaw, ed., Pub. Carnegie Press, pp. 191, 1975.

[130] Kobayashi, S., and Thomsen, E.G.: "Upper and lower-bound solutions to axisymmetric compression and extrusion problems", Int. J. Mech. Sci., vol. 7, pp. 127, 1965.

[131] Johnson, W., and Mamalis, A.G.: "Some force plane diagrams for plane strain slip line fields", Int. J. Mech. Sci., vol. 20, pp. 47, 1978.

[132] Das, N.S., Chitkara, N.R., and COllins, I.F.: "The computation of some slip line field solutions for asymmetric extrusion", Int. J. Num. Methods in Eng., vol. 11, pp. 1379, 1977.

[133] Chitkara, N.R., Das, N.S., and Johnson, W.: "A class of slip line field solutions for unsymmetrical extrusion and some experimental results", Proc. 17th Int. Machine Tool Design and Research Conf., Ed. S.A. Tobais, Pub. MacMillan Press, pp. 435, 1977.

[134] Dewhurst, P., and Collins, I.F.: "A matrix technique for constructing slip-line field solutions to a class of plane strain plasticity problems", Int. J. Num. Methods in Eng., vol. 7, pp. 357, 1973.

[135] Fenton, R..G.: "Radial flow velocity field for predicting upper bound solutions for plane strain extrusion", Trans. A.S.M.E., J. of Basic Eng., pp. 45, March 1968.

[136] Wilson, W.R.D.: "A simple upper bound method for axisymmetric metal forming problems", Int. J. Mech. Sci., vol. 19, pp. 103, 1977.

[137] Johnson, W., and Mamalis, A.G.: "Force polygons to determine upper bounds and force distribution in plane strain metal forming processes", Proc. 18th M.T.D.R. Conf., pp. 11, Pub. McMillan Press, Sept. 1977.

[138] Westwood, D., and Wallace, J.F.: "Upper bound values for the loads on a rigid plastic body in plane strain", J. Mech. Eng. Sci., vol. 2, No. 3, pp. 178, 1960.

[139] Green, J.W., and Wallace, J.F.: "Estimation of load and torque in the hot rolling process", J. Mech. Eng. Sci., vol. 4, no. 2, pp. 136, 1962.

[140] Green, J.W., Sparling, L.G.M., and Wallacee, J.F.: "Shear plane thoeries of hot and cold flat rolling", J. Mech. Eng. Sci., vol. 5, no. 3, pp. 219, 1964.

[141] Siddal, J.N.: Analytical decision making in engineering design, Published by Prentice Hall, New Jersey, 1972.

[142] Siddal, J.N.: "'OPTISEP' Designers optimization subroutines", Pub. by McMaster University, Hamilton, Canada, 1975.

[143] Ernst, H.: "Symposium on machining of metals, 1. Physics of metal cutting", Trans. Amer. Soc. Metals, 1938.

[144] Merchant, M.E.: "Mechanics of the metal cutting process", J. App. Phys., vol. 16, no. 5, pp. 267, 1945.

[145] Briks, A.: "Rezanie Metallor Stroganie", S.P.B., 1896.

[146] Finnie, I.: "Review of the metal cutting analyses of the past hundred years", Mech. Eng., vol. 78, pp. 715, 1956.

[147] Plamer, W.B., and Oxley, P.L.B.: "Mechanics of orthogonal machining", Proc. Instn. Mech. Engrs., vol. 173, no, 24, pp. 623, 1959.

[148] Oxley, P.L.B.: "Mechanics of metal cutting for a material of variable flow stress", Trans. A.S.M.E. J. Eng. for Ind., pp. 339, Nov. 1963.

[149] Christophersen, D.G., Oxley, P.L.B., and Palmer, W.B.: "Orthogonal cutting of a work hardening material", Engineering, pp. 113, July 1958.

[150] Oxley, P.L.B., and Halton, A.P.: "Shear angle solution based on experimental shear zone and tool chip interface stress distributions", Int. J. Mech. Sci., vol. 5, pp. 5, 1963.

[151] Oxley, P.L.B.: "Introducing strain rate dependent work material properties into the analysis of orthogonal cutting", Annals of the C.I.R.P., vol. XIII, pp. 127, 1966.

[152] Oxley, P.L.B.: "Rate of strain effect in mettal cutting", Trans. A.S.M.E., J. Eng. for Ind., pp. 335, 1963.

[153] Stevenson, M.G., and Oxley, P.L.B.: "An experimental investigation of the influence of speed and scale on the strain rate in a zone of intense plastic deformation", Proc. Instn. Mech. Engrs., vol. 1884, no. 31, pp. 561, 1969.

[154] Oxley, P.L.B., Humphreys, A.G., and Laxideh, A.: "The influence of rate of strain hardening in machining", Proc. Instn. Mech. Engrs., vol. 175, no. 18, pp. 881, 1961.

[155] Fenton, R.G., and Oxley, P.L.B.: "Mechanics of orthogonal machining: Allowing for the effects of strain rate and temperature on tool chip friction", Proc. Inst. Mech. Engrs., vol. 183, No. 22, pp. 417, 1968.

[156] Kececioglu, D.: "Shear strain rate in metal cutting and its effects on shear flow stress", Trans. A.S.M.E., pp. 158, 1958.

[157] Drucker, D.C.: "An analysis of the mechanics of metal cutting", J. Appl. Phys., vol. 20, pp. 1013, 1949.

[158] Choa, B.T., and Biscare, G.H.: "The effect of speed and feed on the mechanics of metal cutting", Proc. Instn. Mech. Engrs., vol. 165, pp. 1, 1951.

[159] Shaw, M.C.: Metal Cutting Principles, M.I.T. Publication, Cambridge, Mass., 1954.

[160] Clark, V.W., and Brewer, R.C.: "New technique for shear zone thickness determination in orthogonal metal cutting", Proc. Instn. Mech. Engrs., vol. 181, no. 25, pp. 667, 1966.

[161] Goriani, V.L., and Kobayashi, S.: "Strain and strain rate distributions in orthogonal metal cutting", Annals of C.I.R.P., vol. XV, pp. 425, 1967.

[162] Roth, R.N., and Oxley, P.L.B.: "Slip-line analysis for orthogonal machining based upon experimental flow fields", J. Mech. Eng. Sci., vol. 14, no. 2, pp. 85, 1972.

[163] Armarego, E.J.A., and Brown, R.H.: The machining of metals. Pub. by Prentice Hall Inc., New Jersey, 1969.

[164] Hill, R.: "The mechanics of machining: a new approach", J. Mech. Phys. of Solids, vol. 3, pp. 47, 1954.

[165] Backofen, W.A., Turner, I.R. and Aveny, D.H.: "Superplasticity in the Al-Zn alloy", Trans. A.S.M., vol. 57, pp. 980, 1964.

[166] Dunlop, G.L., and Taplin, D.M.R.: "The tensile properties of a superplastic Aluminum Bronze", J. of Mat. Sci., vol. 7, pp. 84, 1972.

[167] Ducheyne, P. and De Meester, P.: "Superplastic testing conditions and grain growth", J. of Mat. Sci., vol. 9, pp. 109, 1974.

[168] Nuttall, K.: Strain rate sensitivity in superplastic metals", Int. J. Mech. Sci., vol. 13, pp. 83, 1971.

[169] Schelosky, H.: "Beitrag zum verhalten superplastischer werkstaffe beim marsurumformen", Ph.D. Thesis, University of Stuttgart, Pub. by Verlag W. Girardet, Ersen, 1976.

[170] Avery, D.H., and Backofen, W.A.: "A Structural basis for superplasticity", Trans. ASM, vol. 58, pp. 551, 1965.

[171] Johnson, W.: "The plane strain extrusion of initially curved sheet", Int. J. Mech. Sci., vol. 8, pp. 163, 1966.

[172] Johnson, W.: "Some slip-line fields for swaging or expanding, indenting, extruding and machining for tools with curved dies", Int. J. Mech. Sci., vol. 4, pp. 323, 1962.

[173] Johnson, W., "Upper bound loads for extrusion through circular

dies", Appl. Sci. Rs., vol. 7A, pp. 437, 1957.

[174] Bishop, J.F.W.: "An approximate method for determining the temperatures reached in steady motion problems of plane plastic strain", Quart. J. Mech. and Appl. Math., vol. 9, part 2, pp. 236, 1956.

[175] Tanner, R.I. and Johnson, W.: "Temperature distributions in some fast metalworking operations", Int. J. Mech. Sci., vol. 1, pp. 28, 1960.

[176] Farren, W.S. and Taylor, G.I.: " " Proc. Roy. Soc., Series A, vol. 107, pp. 422, 1925.

[177] Singer, A.R.E. and Coakham, J.W.: "Temperature changes occurring during the extrusion of aluminium, Tin and lead", J. Inst. Metals, vol. 89, pp. 177, 1960.

[178] Dugdale, D.S.: "Indentation of strips with flat dies on a flat anvil", Int. J. Prod. Eng., vol. 3., pp. 141, 1964.

[179] Dewhurst, P.: "Plane strain identation on a smooth foundation: a range of solutions for rigid perfectly plastic strip", Int. J. Mech. Sci., vol. 16, pp. 923, 1974.

[180] Ragab, A.R. and Baudelet, B.: "Direct extrusion of rate sensitive materials through conical dies", Rev. Rhys. App., vol. 12, pp. 15, 1977.

[181] De Chiffre, L.: "Extrusion Cutting", Int. J. Mach. Tool Des. Res., vol. 16, pp. 137, 1976.

[182] Kudo, H., Kikuchi, Y., and Miyazaki, K.: "Study of cold pressure welding by divergent extrusion", Annals of the CIRP, vol. 27, pp. 165, 1978.

[183] Rowell, D.: "A new process for extruding large tubes", Wire Ind., vol. 43, pp. 903, 1976.

[184] Rowell, D.: "Large tube production by radial extrusion", Proc. 5 North Amer. Mtlwkg. Res. Conf., pp. 122, 1977.

[185] Rowell, D.: Private communication, Nov. 1978. Cable Consultants Corp., Larchmount, N.Y., U.S.A.

APPENDIX 1

Upper Bound Solution: Model #1

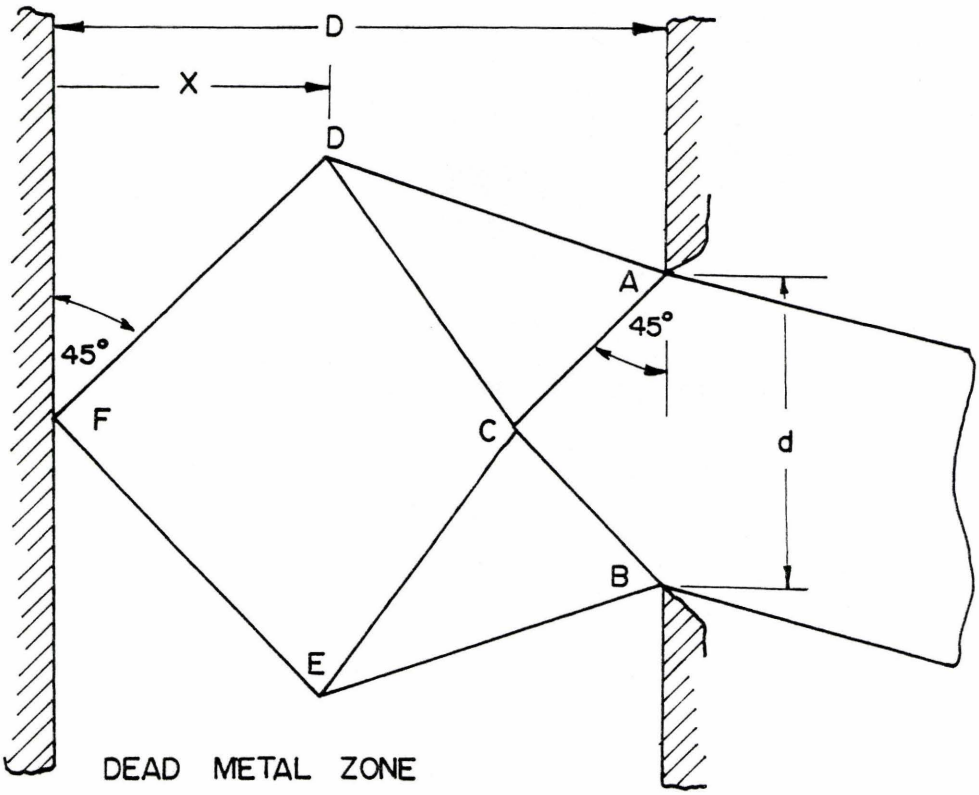

Figure A1.1

Physical Plane Diagram

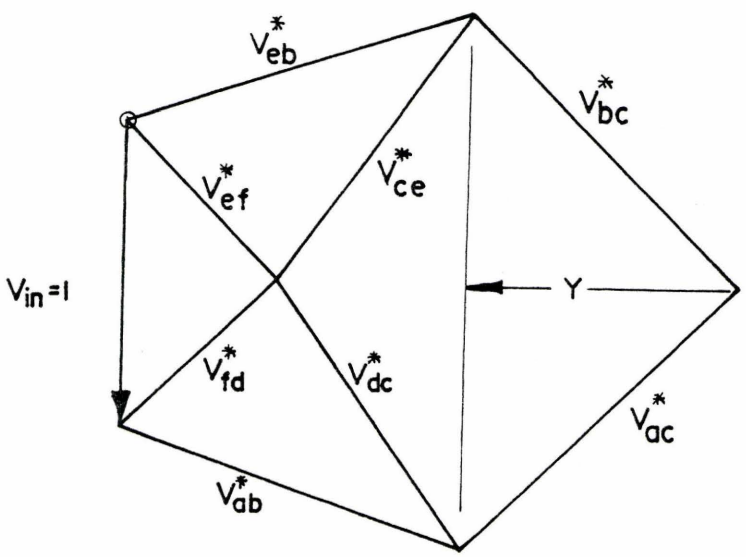

Figure A1.2

Hodograph

From Figure A1.1 the lengths of the discontinuities are given by

$$AC = BC = \frac{d\sqrt{2}}{2} \tag{A1.1}$$

$$EF = FD = x\sqrt{2} \tag{A1.2}$$

$$AE = BD = ((D-x)^2 + (x-d/2)^2)^{1/2} \tag{A1.3}$$

$$CE = CD = \{(D-x-d/2)^2 + x^2\}^{1/2} \tag{A1.4}$$

From figure A1.2 the lengths of the velocity vectors, assuming unit ram velocity, are given by,

$$v^*_{AC} = v^*_{BC} = y\sqrt{2} \tag{A1.5}$$

$$v^*_{EF} = v^*_{FD} = 0.5\sqrt{2} \tag{A1.6}$$

$$v^*_{AE} = v^*_{BD} = \{(D/d-y)^2 + (y-0.5)^2\}^{1/2} \tag{A1.7}$$

$$v^*_{CE} = v^*_{CD} = \{(D/d-y-0.5)^2 + y^2\}^{1/2} \tag{A1.8}$$

Relationship between x and y

From Figures A1.1 and A1.2 we obtain

$$\text{Tan } \alpha = \frac{D/d - y - 0.5}{y} = \frac{D - x - d/2}{x}$$

therefore

$$x\{D/d - 0.5\} = y\{D - d/2\}$$

therefore

$$y = x/d \tag{A1.9}$$

Substituting Eqn. (A1.9) into Eqns. (A1.5) → (A1.8) the equations for the velocity become:-

$$v^*_{AC} = v^*_{BC} = \frac{x}{d}\sqrt{2} \tag{A1.10}$$

$$v^*_{EF} = v^*_{FD} = 0.5\sqrt{2} \tag{A1.11}$$

$$v^*_{AE} = v^*_{BD} = \{(\frac{D}{d} - \frac{x}{d})^2 + (\frac{x}{d} - \frac{1}{2})^2\}^{1/2} \tag{A1.12}$$

$$v^*_{CE} = v^*_{CD} = \{(\frac{D}{d} - \frac{x}{d} - \frac{1}{2})^2 + (\frac{x}{d})^2\}^{1/2} \tag{A1.13}$$

Recall that the work rate is given by:

$$\dot{w} = k \Sigma S_i v^*_i \tag{A1.14}$$

Since the field is symemtric we can write

$$\dot{w} = 2k(AC.V^*_{AC} + EF.V^*_{EF} + AE.v^*_{AE} + CE\ v^*_{CE}) \tag{A1.15}$$

Considering each of the summations within Eqn. (A1.15) we have

$$AC.v^*_{AC} = \frac{d\sqrt{2}}{2} \cdot \frac{x\sqrt{2}}{2} = x \tag{A1.16}$$

$$EF.v^*_{EF} = x\sqrt{2} \cdot \frac{\sqrt{2}}{2} = x \tag{A1.17}$$

$$AE.v^*_{AE} = \frac{1}{d}\{(D-x)^2 + (x - \frac{d}{2})^2\} \tag{A1.18}$$

$$CE.v^*_{CE} = \frac{1}{d}\{(D - x - \frac{d}{2})^2 + x^2\} \tag{A1.19}$$

Summing these terms we obtain

$$\phi = 2x + \frac{1}{d}\{(D-x)^2 + (x - \frac{d}{2})^2 + (D - x - \frac{d}{2})^2 + x^2\} \tag{A1.20}$$

The minimum work rate is given by

$$\frac{d\dot{w}}{dx} = \frac{d\phi}{dx} = 0 \quad \text{if} \quad \frac{d^2\dot{w}}{dx^2} > 0 \tag{A1.21}$$

$$\frac{d\dot{w}}{dx} = 2 + \frac{1}{d}\left\{-2.(D-x)+2\left(x-\frac{d}{2}\right)-2\left(D-x-\frac{d}{2}\right)+2x\right\} \tag{A1.22}$$

and

$$\frac{d^2\dot{w}}{dx^2} = \frac{1}{d}\ \{8\} \tag{A1.23}$$

$$\frac{d^2\dot{w}}{dx} > 0$$

therefore

$$\frac{d\dot{w}}{dx} \quad \text{is a minimum}$$

Equating Eqn. (A1.22) to zero and simplifying we obtain

$$4x - 2D + d = 0$$

therefore

$$x = \frac{2D - d}{4} \tag{A1.24}$$

This is the optimum value of x to give a minimum work solution. Values of $(\bar{p}/2k)$ can now be generated using Eqns. (A1.16)→(A1.19).

APPENDIX 2

Algebraic expressions for velocity field and hodograph geoemtry; Model #2

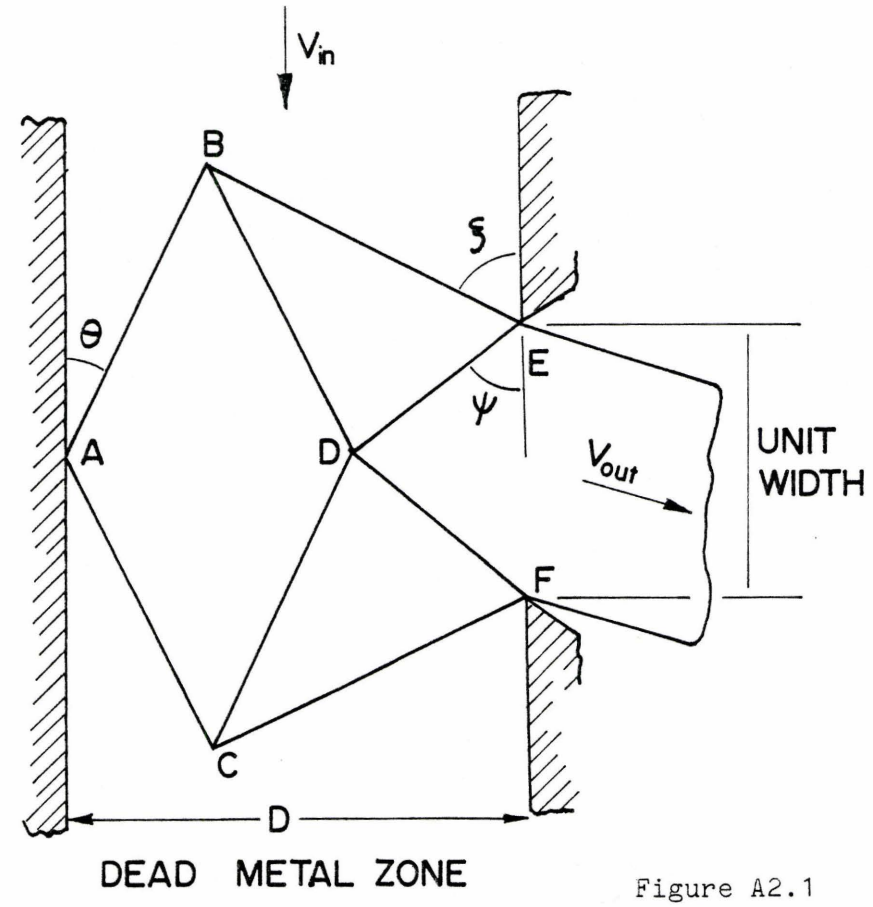

Figure A2.1

Physical Plane Diagram

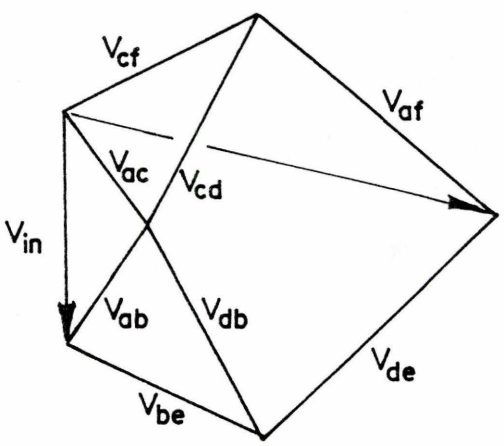

Figure A2.2

Hodograph

From Figure A2.1 for the physical plane diagram: Lengths of the discontinuities are given by:

$$AB = AC = \frac{D - \ell}{\sin \theta} \tag{A2.1}$$

$$BE = CF = \frac{\ell}{\sin \xi} \tag{A2.2}$$

$$BD = CD = \left(\frac{D - \ell}{\tan \theta}\right)^2 + (\ell - 0.5 \tan \psi)^{2\ 1/2} \tag{A2.3}$$

$$ED = DF = \frac{0.5}{\cos \psi} \tag{A2.4}$$

where D is the width of the die

and ℓ is defined in Figure A2.1.

If the ram speed is V_{in} then the lengths of the velocity vectors are given by

$$v^*_{AB} = v^*_{AC} = \frac{0.5\ V_{in}}{\cos \theta} \tag{A2.5}$$

$$v^*_{BE} = v^*_{CF} = \frac{x}{\sin \xi} \tag{A2.6}$$

$$v^*_{CD} = v^*_{BD} = \{(x - 0.5\ V_{in} \tan \theta)^2 + \{\frac{D - x}{\tan \psi}\}^2\}^{1/2} \tag{A2.7}$$

$$V^*_{ED} = V^*_{DF} = \frac{D - x}{\sin \psi} \tag{A2.8}$$

where D is the width of the die

and x is defined in Figure A2.2.

Relationship between x and the independent variables

From the geometry of the hodograph

$$\frac{D - x}{\tan \psi} = 0.5\ V_{in} + \frac{x}{\tan \xi}$$

$$(D-x)\tan \xi = 0.5\ V_{in} \tan \psi \tan \xi + x \tan \psi$$

$$x(\tan \xi + \tan \psi) = -0.5\ V_{in} \tan \psi \tan \xi + D \tan \xi$$

$$x \left\{\frac{\tan \psi}{\tan \xi} + 1\right\} = D - 0.5\ V_{in} \tan \psi$$

$$x = \frac{D - 0.5\ V_{in} \tan \psi}{\tan \psi/\tan \xi + 1} \qquad \text{(A2.9)}$$

Relationship between ℓ and the Independent Variables

From the geometry of the physical plane diagram

$$\frac{D - \ell}{\tan \theta} = \frac{\ell}{\tan \xi} + 0.5$$

$$\tan \xi\ (D-\ell) = \ell \tan \theta + 0.5 \tan \xi \tan \theta$$

$$\ell[\tan \theta + \tan \xi] = D \tan \xi - 0.5 \tan \xi \tan \theta$$

$$\ell = \frac{D - 0.5 \tan \theta}{(\tan \theta/\tan \xi) + 1} \qquad \text{(A2.10)}$$

APPENDIX 3

Algebraic expressions for velocity field and hodograph geometry; Model #3

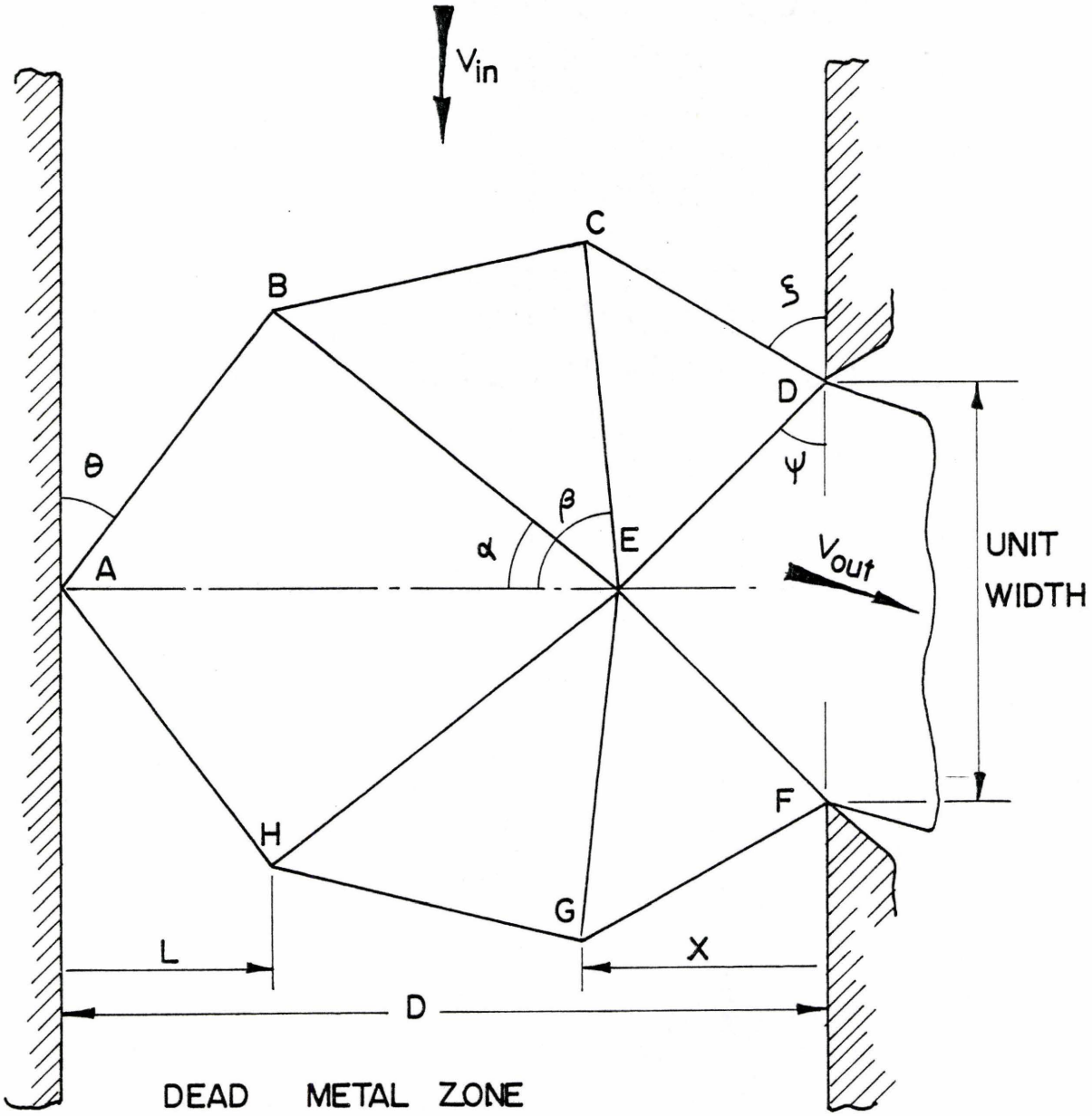

Figure A3.1

Physical Plane Diagram

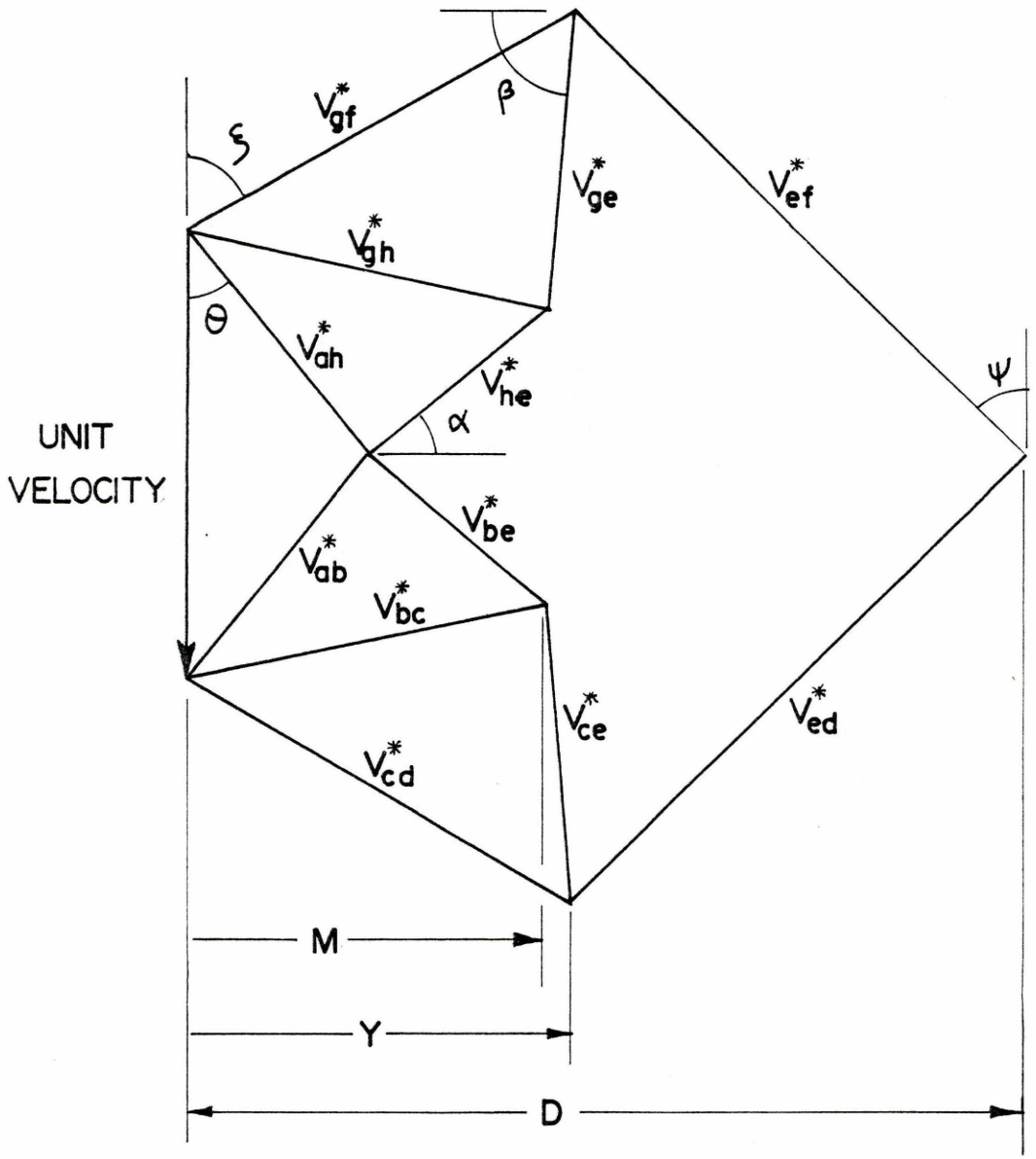

Figure A3.2

Hodograph

From the physical plane diagram Figure A3.1 the lengths of the discontinuities are given by:

$$AB = AH = \frac{\ell}{\sin \theta} \tag{A3.1}$$

$$BC = HG = \{[D-(\ell+x)]^2 + [0.5 + \frac{x}{\tan \xi} - \frac{\ell}{\tan \theta}]^2\}^{1/2} \tag{A3.2}$$

$$CD = GF = \frac{x}{\sin \xi} \tag{A3.3}$$

$$DE = EF = \frac{0.5}{\cos \psi} \tag{A3.4}$$

$$EC = EG = \{0.5 + \frac{x}{\tan \xi}\} \frac{1}{\sin \beta} \tag{A3.5}$$

$$EB = EH = \frac{D - (\ell + 0.5 \tan \psi)}{\cos \alpha} \tag{A3.6}$$

<u>To define x in terms of the variables</u>

From Figure A3.1

$$x = 0.5 \tan \psi + [0.5 + \frac{x}{\tan \xi}] \frac{1}{\tan \beta}$$

Simplifying

$$x = 0.5 \tan \xi \, [\frac{\tan \beta \tan \psi + 1}{\tan \beta \tan \xi - 1}] \tag{A3.7}$$

<u>To define ℓ in terms of the variables</u>

From Figure A3.1

$$\ell + \frac{\ell}{\tan \theta \tan \alpha} + 0.5 \tan \psi = D$$

therefore

$$\ell\left[1 + \frac{1}{\tan\theta \tan\alpha}\right] = D - 0.5 \tan\psi$$

Simplifying

$$\ell = \left[\frac{D - 0.5 \tan\psi}{1 + \tan\theta \tan\alpha}\right] \tan\theta \tan\alpha \qquad (A3.8)$$

From the hodograph Figure A3.2 the tangential velocities are given by:-

$$v^*_{AB} = v^*_{AH} = \frac{0.5}{\cos\theta} \qquad (A3.9)$$

$$v^*_{BC} = v^*_{HG} = [m^2 + (0.5 - (m - 0.5 \tan\theta) \tan\alpha)^2]^{1/2} \qquad (A3.10)$$

$$v^*_{CD} = v^*_{GF} = \frac{y}{\sin\xi} \qquad (A3.11)$$

$$v^*_{DE} = v^*_{EF} = \frac{D - y}{\sin\psi} \qquad (A3.12)$$

$$v^*_{EC} = v^*_{EG} = \frac{y - m}{\cos\beta} \qquad (A3.13)$$

$$v^*_{EB} = v^*_{EH} = \frac{m - 0.5 \tan\theta}{\cos\alpha} \qquad (A3.14)$$

<u>To define y in terms of the variables</u>

From Figure A3.2

$$\frac{y}{\tan\xi} + 0.5 = \frac{(D - y)}{\tan\psi}$$

therefore

$$y\left[\frac{1}{\tan\xi} + \frac{1}{\tan\psi}\right] = \frac{D}{\tan\psi} - 0.5$$

$$y = \left[\frac{D - 0.5 \tan\psi}{\tan\psi + \tan\xi}\right] \tan\xi \qquad (A3.15)$$

To define m in terms of the variables

From Figure A3.2, the hodogrpah

$$\frac{y}{\tan \xi} + 0.5 = \tan \alpha \, [m - 0.5 \tan \theta] + (y-m) \tan \beta$$

$$m(\tan \alpha - \tan \beta) = \frac{y}{\tan \xi} + 0.5 \, [1 + \tan \theta \tan \alpha] - y \tan \beta$$

$$m(\tan \alpha - \tan \beta) = y \, [\frac{1}{\tan \xi} - \tan \beta] + 0.5 \, (1 + \tan \theta \tan \alpha)$$

therefore

$$m = [\frac{1}{\tan \alpha - \tan \beta}][y \, (\frac{1}{\tan \xi} - \tan \beta) + 0.5 \, (1 + \tan \theta \tan \alpha)] \qquad (A3.16)$$

APPENDIX 4

Determination of relationship between strain rate coefficients σ_o and k'

where $\bar{\sigma} = \sigma_o \dot{\bar{\varepsilon}}^m$

and $\tau = k' \dot{\gamma}^m$

Relationship between materials parameters σ_o and k' as defined in the equations

$$\dot{\bar{\sigma}} = \sigma_o \dot{\bar{\varepsilon}}^m \tag{A4.1}$$

and

$$\tau = k' \dot{\gamma}^m \tag{A4.2}$$

Tensile and compressive test data are normally used to determine material parameters and it is thus necessary to determine the relationship between the two constant terms, σ_o and k'. Equation (A4.2) has been used in the derivation of the upper bound solution to the extrusion pressure and since there is no facility to measure the shear stress, shear strain rate properties it is necessary to deduce a relationship between these two parameters. For any general stress state the representative stress and strain are defined as

$$\bar{\sigma} = \{\frac{1}{2}[(\sigma_x-\sigma_y)^2 + (\sigma_y-\sigma_z)^2 + (\sigma_z-\sigma_x)^2] + 3[\tau_{xy}^2 + \tau_{yz}^2 + \tau_{zx}^2]\}^{1/2} \tag{A4.3}$$

$$\bar{\varepsilon} = \{\frac{2}{9}[(\varepsilon_x-\varepsilon_y)^2 + (\varepsilon_y-\varepsilon_z)^2 + (\varepsilon_z-\varepsilon_x)^2] + \frac{4}{3}[\gamma_{xy}^2 + \gamma_{yz}^2 + \gamma_{zx}^2]\}^{1/2} \tag{A4.4}$$

where γ_{xy}, γ_{yz}, and γ_{zx} are the engineering strains. Now in pure torsion $\tau_{yz} = \tau_{xz} = 0$

The representative stress is given by

$$\bar{\sigma} = \tau_{xy} \sqrt{3} \tag{A4.5}$$

In the pure torsion of an element we have

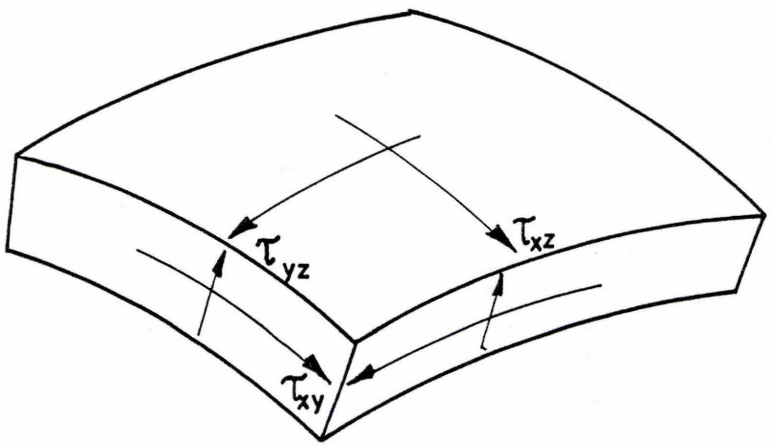

Since for pure torsion

$$\sigma_x = \sigma_y = \sigma_z = \tau_{yz} = \tau_{xz} = 0$$

the representative strain is given by

$$\bar{\varepsilon} = 2\,\gamma_{xy}/\sqrt{3} \qquad \text{(A4.6)}$$

Taking the derivative with respect to time we have

$$\dot{\bar{\varepsilon}} = 2\,\dot{\gamma}_{xy}/\sqrt{3} \qquad \text{(A4.7)}$$

For the tensile test we nave

$$\bar{\sigma} = \sigma_o\,\dot{\bar{\varepsilon}}^m$$

therefore substituting for $\bar{\sigma}$ and $\dot{\bar{\varepsilon}}$ with eqns. (A4.5) and (A4.7) we have

$$\tau\sqrt{3} = \sigma_o \left\{\frac{2\,\dot{\gamma}}{\sqrt{3}}\right\}^m \qquad \text{(A4.8)}$$

Now this is analogous to

$$\tau = k' \dot{\gamma}^m$$

where

$$k' = \frac{\sigma_o}{\sqrt{3}} \left\{\frac{2}{\sqrt{3}}\right\}^m \qquad \text{(A4.9)}$$

APPENDIX 5

OPTIMIZATION OF SIMPLE TWO LINES DISCONTINUITY MODEL

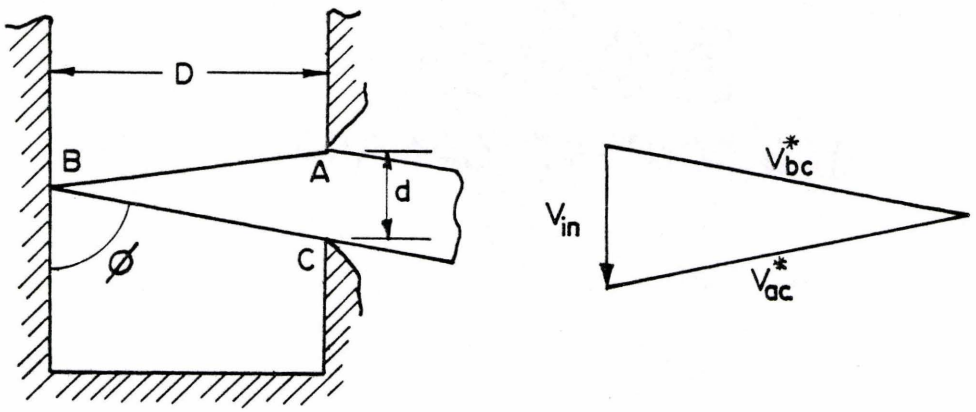

Figure A5.1

Physical plane diagram and associated hodograph

Lengths of Discontinuities

$$\ell_{AB} = \{D^2 + [d - \frac{D}{\tan \phi}]^2\}^{1/2} \qquad (A5.1)$$

$$\ell_{BC} = \frac{D}{\sin \phi} \qquad (A5.2)$$

Magnitude of Velocity Vectors

$$v_{AB} = \{[\frac{D}{d}]^2 + [1 - \frac{D}{d \tan \phi}]^2\}^{1/2} \qquad (A5.3)$$

$$v_{BC} = \frac{D}{d \sin \phi} \qquad (A5.4)$$

The Work Rate is given by

$$\dot{w} = \bar{P} V_{in} D$$

and also

$$\dot{w} = k \sum_{i=1}^{n} v_i^* S_i$$

For this example

$$\dot{w} = \ell_{AB}\, v^*_{AB} + v^*_{BC}\, \ell_{BC} \tag{A5.5}$$

$$\dot{w} = \{D^2 + [d - \frac{D}{\tan\phi}]^2\}^{1/2} \cdot \{(\frac{D}{d})^2 + [1 - \frac{D}{d \tan\phi}]^2\}^{1/2} + \frac{D}{d \sin\phi}\,\frac{D}{\sin\phi} \tag{A5.6}$$

$$\dot{w} = \{D^2 + [d - \frac{D}{\tan\phi}]^2\}\,\frac{1}{d} + \frac{D^2}{d \sin^2\phi} \tag{A5.7}$$

For a minimum $\quad \frac{d\dot{w}}{d\phi} = 0 \quad$ if $\frac{d^2\dot{w}}{d\phi^2} = +\text{ve}$

Differentiating Eqn. A5.7

$$\frac{d\dot{w}}{d\phi} = \frac{1}{d}[d - \frac{D}{\tan\phi}]\, 2D \operatorname{cosec}^2\phi + \frac{D^2 - 2\cos\phi}{d \sin^3\phi} \tag{A5.8}$$

$$= \frac{1}{d}\{d - \frac{D}{\tan\phi}\}\,\frac{2D}{\sin^2\phi} - \frac{2D^2\cos\phi}{d \sin^3\phi}$$

For a minimum $\quad \frac{2D}{d \sin^2\phi}[d - \frac{D}{\tan\phi} - \frac{D\cos\phi}{\sin\phi}] = 0$

Simplifying $\quad d = \frac{1}{\tan\phi}[D + D]$

$$\phi_{opt} = \tan^{-1}\{\frac{2D}{d}\} \tag{A5.9}$$

Hence the optimum field is a function of the die geometry - not just the extrusion ratio.

For the experimental set up D = 1.5

Extrusion Ratio	2	4	6	8	10	20
ϕ_{opt}	76.0	82.9	85.2	86.4	87.1	88.6
FR	0.5	0.75	.833	.875	0.9	.95

If we now substitute these values into Eqn. A5.7 the work rate can be evaluated.

Extrusion Ratio	2	4	6	8	10	20
p/2k	2.13	4.07	6.04	8.03	10.03	20.01

APPENDIX 6

SOLUTION TECHNIQUE FOR SIMPLE TWO LINE DISCONTINUITY MODEL - CURVED DISCONTINUITIES

Optimization of Curved Velocity Discontinuities

If curved velocity discontinuities are assumed and material exits with some constant angular velocity then there is a unique solution. This solution is a function of two independent variables R_1 and ξ, Figure A6.1, for a given geometry

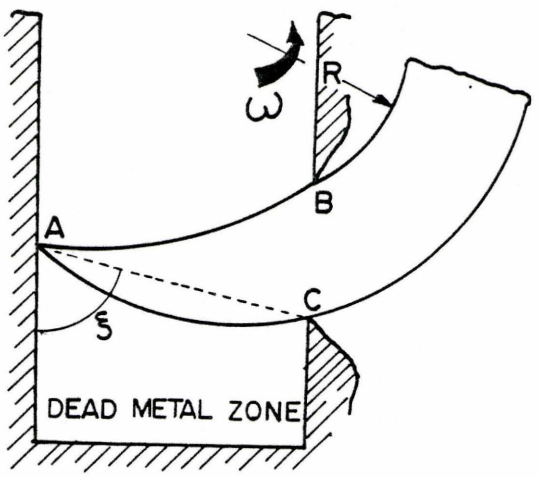

Figure A6.1

Physical plane diagram

For the solution to be compatible with the hodograph and for continuity to be satisfied the arc AB, radius R_2, must be obtained by trial and error from the hodograph.

Algebraic expression are evaluated below for the arc lengths A_{AB} and A_{CB} and the tangential velocity change across these discontinuities.

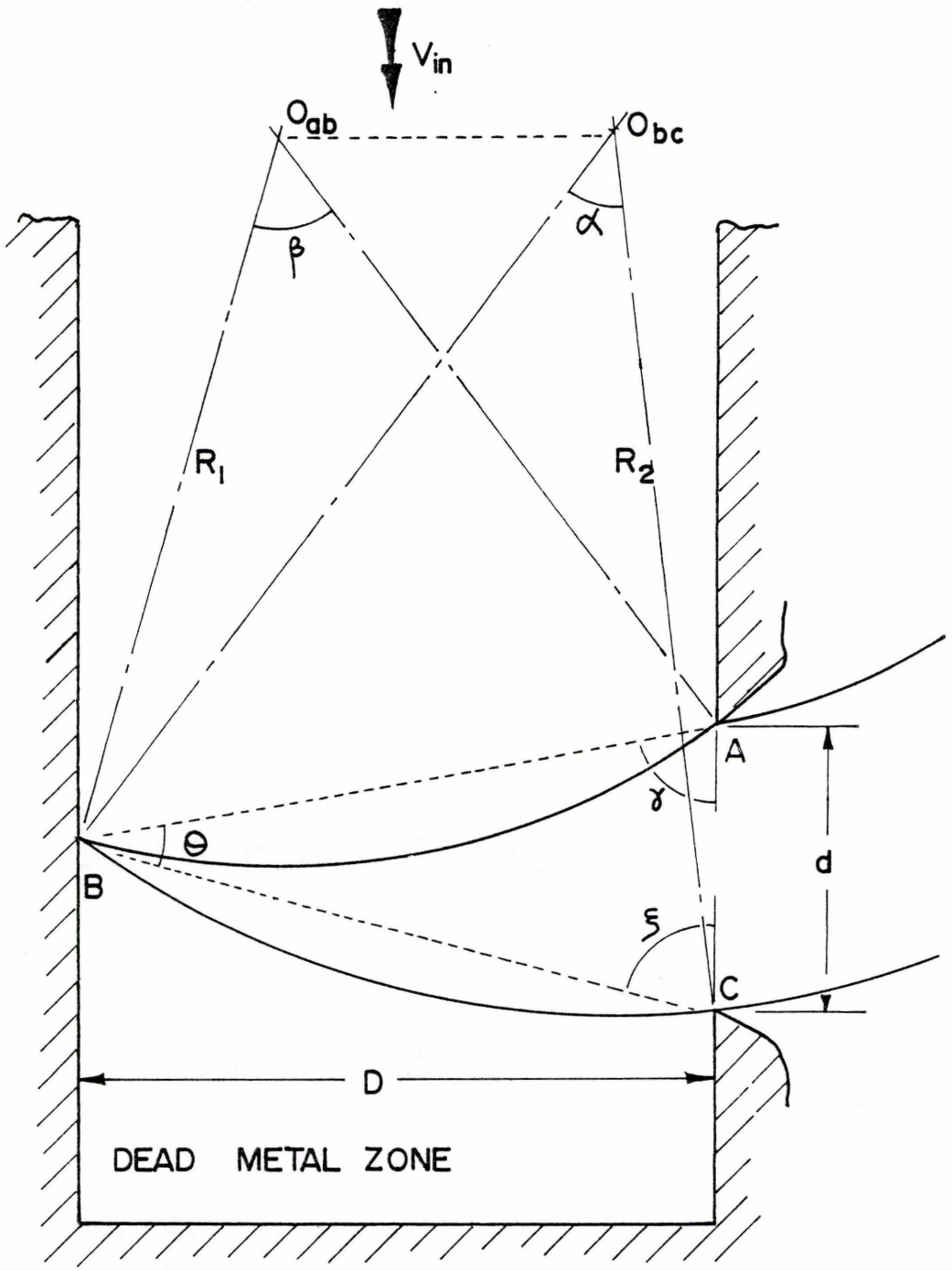

Figure A6.2

Detailed geometry of physical plane diagram

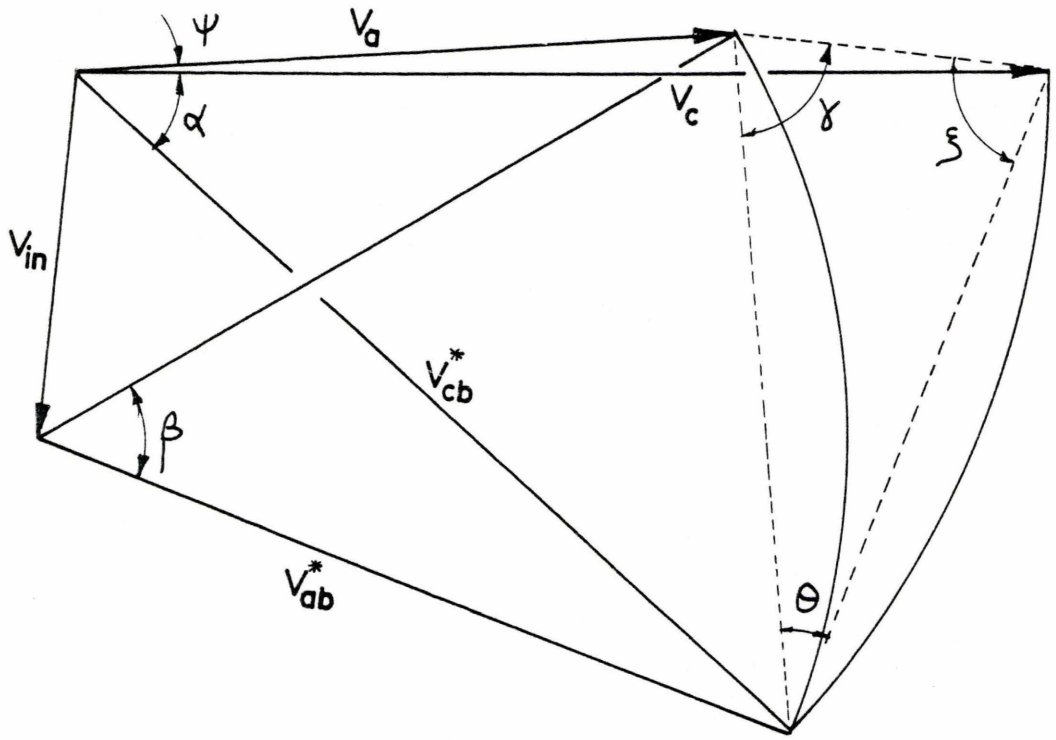

Figure A6.3

Detailed geometry of hodograph

It should be noted that the hodograph and the physical plane diagram are similar; the triangle 234 is similar to triangle ABC in the physical plane diagram.

From Figure A6.2

$$AB = \left[D^2 + \left\{d - \frac{D}{\tan \xi}\right\}^2\right]^{1/2} \tag{A6.1}$$

$$BC = \frac{D}{\sin \xi} \tag{A6.2}$$

$$AC = d \tag{A6.3}$$

Arc lengths

$$A_{AB} = R_2 \beta \tag{A6.4}$$

$$A_{BC} = R_1 \alpha \tag{A6.5}$$

Angle relationships

$$\frac{\sin \theta}{d} = \frac{\sin \xi}{AB} = \frac{\sin \gamma}{CB} \tag{A6.6}$$

$$\frac{\sin \alpha}{CB} = \frac{\sin (90 - \alpha/2)}{R_1} \tag{A6.7}$$

$$\sin \left(\frac{\alpha}{2}\right) = \frac{BC}{2 R_1} \tag{A6.8}$$

$$\sin \left(\frac{\beta}{2}\right) = \frac{AB}{2 R_2} \tag{A6.9}$$

$$\tan \psi = \frac{d \cos (\alpha/2 + \xi)}{R_1 - d \sin (\alpha/2 + \xi)} \tag{A6.10}$$

To obtain the constants of similarity between the hodograph and the physical plane diagram it is necessary to evaluate the velocity V_c -

which is also the tangential velocity discontinuity along CB.

Note $v = \omega R$

hence along any radius

$$v_{in}\, D = \int_{R_1}^{R_2} \omega R \, dr$$

therefore $$v_{in}\, D = \frac{\omega}{2} (R_2^2 - R_1^2).$$

If we travel along the radius through A then

$$v_{in}\, D = \frac{\omega}{2} [R_1^2 - R_a^2]$$

and

$$\omega = \frac{v_c}{R_1}$$

therefore $$v_c = \frac{2\, v_{in}\, D\, R_1}{[R_1^2 - R_a^2]} \qquad \text{(A6.11)}$$

Hence the proportionality between the hodograph and the discontinuity field is

$$\frac{v_c}{R_1} = \frac{2\, v_{in}\, D}{R_1^2 + R_a^2} \qquad \text{(A6.12)}$$

To evaluate this we must know R_a which is given by

$$\frac{\cos(\alpha/2 + \xi)}{R_A} = \frac{\cos(\psi - \alpha/2 - \xi)}{R_1} \qquad \text{(A6.13)}$$

where ψ is defined in equation (A6.10).

Alternatively

$$R_A = \frac{d \cos (\alpha/2 + \xi)}{\sin \psi} \qquad \text{(A6.14)}$$

From the geometry of the hodograph.

$$\tan \mu = \frac{v_c \, \text{Sin} \, (\xi - \alpha/2)}{v_c \, \text{Cos} \, (\xi - \alpha/2) - v_{in}} \qquad \text{(A6.15)}$$

but

$$\mu = \xi + \theta - \frac{\beta}{2}$$

Hence

$$\beta = 2 \, [\xi + \theta - \mu] \qquad \text{(A6.16)}$$